AD-A190 307

DTIC FILE COPY

DOCUMENTATION PAGE

1a. REPORT SECURITY CLASSIFICATION UNCLASSIFIED	1b. RESTRICTIVE MARKINGS NONE
2a. SECURITY CLASSIFICATION AUTHORITY	3. DISTRIBUTION/AVAILABILITY OF REPORT
2b. DECLASSIFICATION/DOWNGRADING SCHEDULE	Distribution unlimited; approved for public release

DTIC ELECTE JAN 1 9 1988 S D

4. PERFORMING ORGANIZATION REPORT NUMBER(S) 1-52097	5. MONITORING ORGANIZATION REPORT NUMBER(S) AFOSR·TR· 87-2012

6a. NAME OF PERFORMING ORGANIZATION Carnegie Mellon University Mechanical Engineering	6b. OFFICE SYMBOL (If applicable)	7a. NAME OF MONITORING ORGANIZATION AFOSR/NA
6c. ADDRESS (City, State, and ZIP Code) Schenley Park Pittsburgh, PA. 15213		7b. ADDRESS (City, State, and ZIP Code) Building 410 Bolling AFB, DC 20332-6448

8a. NAME OF FUNDING/SPONSORING ORGANIZATION AFOSR/NA	8b. OFFICE SYMBOL (If applicable)	9. PROCUREMENT INSTRUMENT IDENTIFICATION NUMBER AFSOR-83-0033

8c. ADDRESS (City, State, and ZIP Code) Bldg. 410 Bolling AFB, DC 20330-6448	10. SOURCE OF FUNDING NUMBERS			
	PROGRAM ELEMENT NO. 61102F	PROJECT NO. 2308	TASK NO. A1	WORK UNIT ACCESSION NO.

11. TITLE (Include Security Classification)
Final Scientific Progress Report on Fundamental Studies on MPD Thrusters

12. PERSONAL AUTHOR(S)
J. L. Lawless

13a. TYPE OF REPORT Final Scientific Report	13b. TIME COVERED FROM Apr.,'85 TO Dec.,'86	14. DATE OF REPORT (Year, Month, Day) 1987-Sept. 2	15. PAGE COUNT 259

16. SUPPLEMENTARY NOTATION

17. COSATI CODES			18. SUBJECT TERMS (Continue on reverse if necessary and identify by block number)
FIELD	GROUP	SUB-GROUP	MPD Thruster, Two-Temperature Flow, Electrode-Plasma Interactions

19. ABSTRACT (Continue on reverse if necessary and identify by block number)

1.0 Introduction

A theory has been developed which predicts onset and erosion in MPD thrusters. The theory predicts onset currents which are in quantitative agreement with experiment. Erosion rates are predicted for a steady-state hot cathode thruster. This theory is the first to model the viscous and thermal electrode boundary layers in MPD thrusters. Stability criteria for diffuse-mode electrode current conduction have been found.

This report, in conjunction with two earlier annual progress reports, summarizes progress made under grant AFOSR-83-0033.

20. DISTRIBUTION/AVAILABILITY OF ABSTRACT ☒ UNCLASSIFIED/UNLIMITED ☐ SAME AS RPT ☐ DTIC USERS	21. ABSTRACT SECURITY CLASSIFICATION UNCLASSIFIED
22a. NAME OF RESPONSIBLE INDIVIDUAL Mitat A. Birkan	22b. TELEPHONE (Include Area Code) 202/767-4938	22c. OFFICE SYMBOL AFOSR/NA

DD Form 1473, JUN 86 Previous editions are obsolete. SECURITY CLASSIFICATION OF THIS PAGE

UNCLASSIFIED

TABLE OF CONTENTS

DTIC
COPY
INSPECTED
6

88 1   6 013

A-1

Fundamental Studies On
MPD Thrusters

Final Technical Report

John L. Lawless
Space Power Inc.
1977 Concourse Drive
San Jose, CA 95131-1708

1.0 Introduction

A theory has been developed which predicts onset and erosion in MPD thrusters. The theory predicts onset currents which are in quantitative agreement with experiment. Erosion rates are predicted for a steady-state hot cathode thruster. This theory is the first to model the viscous and thermal electrode boundary layers in MPD thrusters. Stability criteria for diffuse-mode electrode current conduction have been found.

This report, in conjunction with two earlier annual progress reports, summarizes progress made under grant AFOSR-83-0033.

2.0 Research Objectives

The overall objectives of this work were to determine the erosion rates and limits of diffuse mode operation. To accomplish these overall objectives, the following objectives were set for the research effort: (1) to model the bulk flow in MPD thrusters, (2) to model the viscous and thermal boundary layers in MPD thrusters, (3) to model the sheath-boundary layer interactions, (4) to model the thermal response of the electrodes.

3.0 Status of the Research Effort

The discussion below summarizes the highlights of the research efforts under this grant. A more detailed discussion can be found in the appendices.

Previous work on frozen and equilibrium quasi one dimensional flow in plasma in MPD thrusters has been extended to include finite rate ionization, plasma boundary layers, and electrode sheath effects. The quasi one dimensional flow model with finite rate ionization mechanics can quantitively predict the occurence of onset. Combined with the boundary layer and sheath theories, electrode erosion rates can be predicted.

A comparison between predicted and experimental onset currents is shown in Table 1. The experimental results are from the 20 centimeter straight coaxial thruster of King. The theoretical prediction assumes a one dimensional channel flow and conserves mass momentum and energy. A rate equation for ionization is included.

MASS FLOW (g/s)	THEORY (kA)	EXPERIMENT (kA)
3	16.8	~16
6	25.2	~27

TABLE 1: Predicted and experimental onset currents are compared for two mass flows in King's 20 cm coaxial straight thruster.

Laboratory quasi-steady MPD thrusters typically conduct current through cathode spots. Spots tend to have very high erosion rates. These high erosion rates severely limit thruster lifetime. In actual space use, thruster will likely be run for long periods to time with hot electrodes. Hot electrodes permit defuse current conduction and much lower erosion rates. This study concentrates on the hot electrode case.

To understand the conditions at the plasma electrode interface, a study of the plasma boundary layer and plasma sheaths has been performed. The boundary layer theory uses a momentum integral method. Profiles of electron temperature, heavy particle temperature, density, and ionization fraction can be predicted. Sample profiles are shown in Fig. 1.

A major result of this theory is that the boundary layer thickness strongly depends on the ionization fraction near the wall. Electrons and ions recombine on the walls and this would tend to make the ionization fraction near the walls small. If it is small, the viscousity is large and the boundary layer grows rapidly and viscous flow losses can be expected to be important. If the ionization fraction is not very small, near the wall, the boundary layers grow slowly and viscous losses can be expected to be a small part.

Erosion from a hot cathode is largely by evaporation. From our boundary layer and sheath models, heat transfer to the cathode can be analysed and cathode temperature distributions predicted. From these predicted temperatures, the erosion rate by evaporation can be predicted. Sample predictions are shown in Fig. 2.

The stability of the diffuse mode MPD thruster has been analysed. It is found that, under some conditions, a thermal run away may occur in which the electrode regeneratively heats itself until it melts. This can be avoided by external cooling of the cathode. The external cooling rate, however, must be carefully chosen. If the cooling rate is too slow, thermal run-away will occur. If it is too fast, the arc will extinguish.
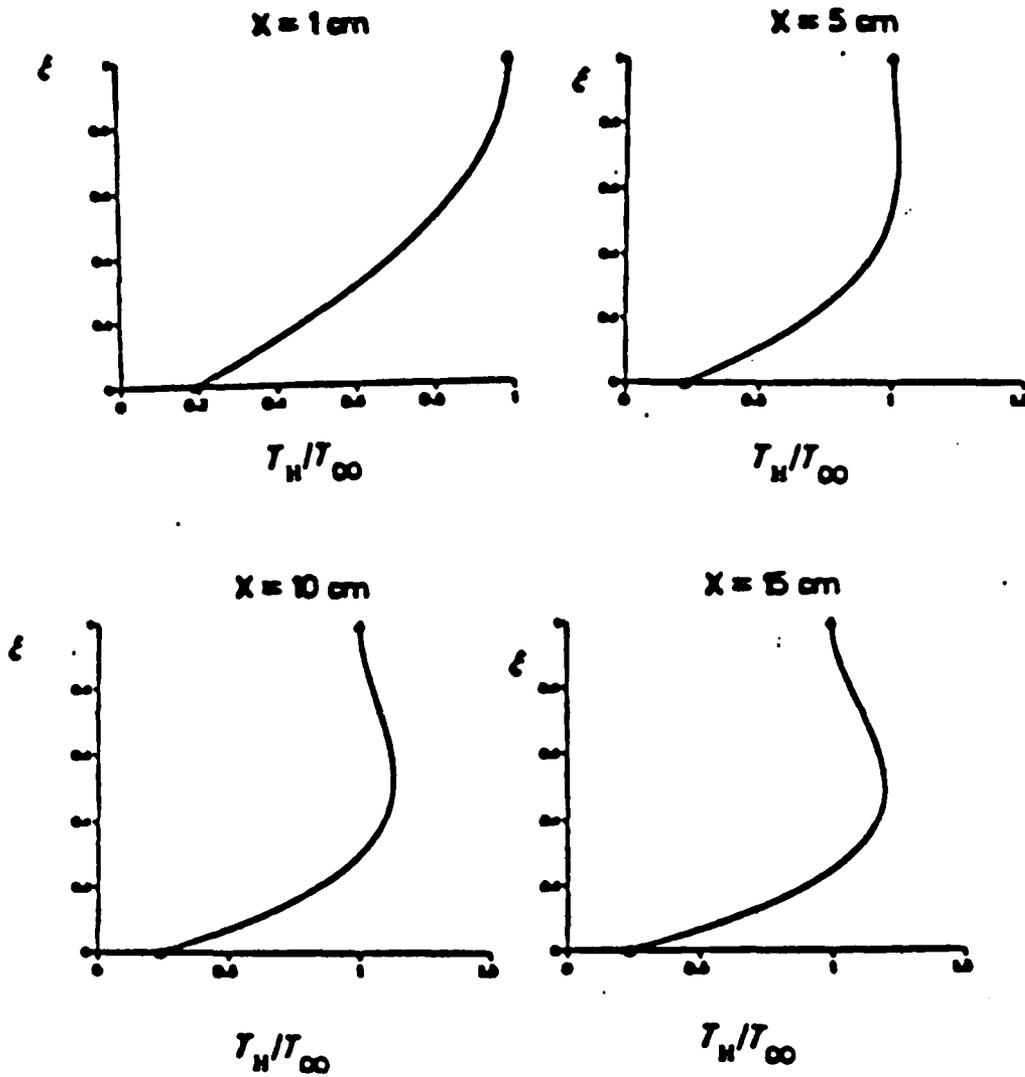
FIG. 1: The heavy particle temperature in the cathode boundary layer non-dimensionalized by the free stream temperature, has been plotted versus transverse coordinate at locations of 1 cm., 5cm., 10 cm., and 15 cm. from the leading edge for a straight co-axial thruster.
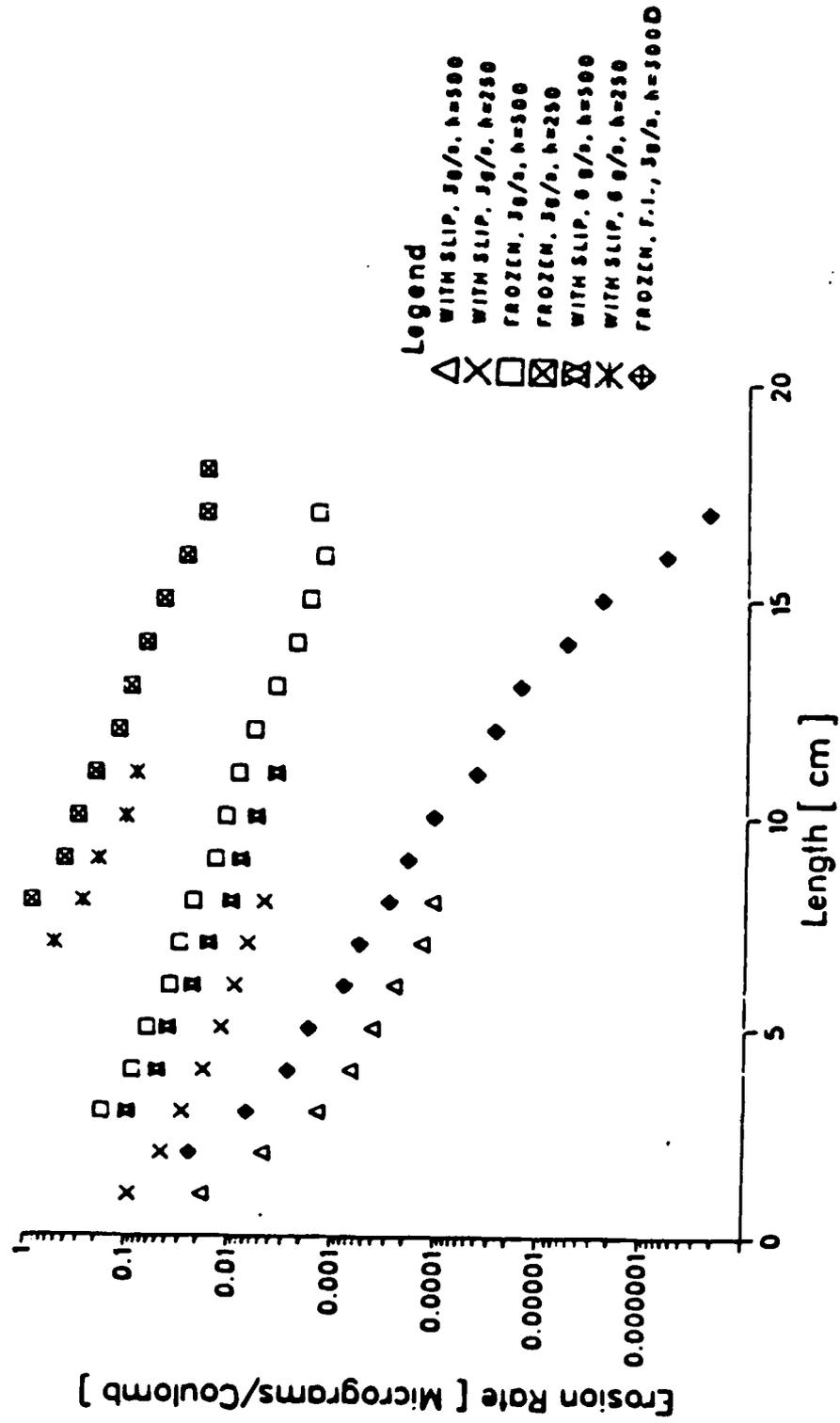
FIG. 2: Sample Predicted Evaporative Erosion Rates are Plotted versus Axial Distance for a Tungsten Cathode in a Straight Coaxial Thruster Under A Variety of Flow Assumptions.

Fig. #2

4.0 Personnel

John L. Lawless, Principal Investigator

Hamid Torab, Post Doctoral Research Assistant

Edward Richley, Graduate Student

Brian Sauk, Graduate Student

Viswanath Subramaniam, Graduate Student

Daniel Cox, Undergraduate Student

5.0 Interactions

In addition to those reported in previous Annual Reports, the following papers and publications resulted from this grant:

V. V. Subramanian and J. L. Lawless, "The Electrical Characteristics of MPD thrusters," IEEE Conference on Plasma Science, Pittsburgh, Pennsylvania, June 1985

V. V. Subramanian and J. L. Lawless, "An Integral method for Two-Temperature Ionizing Laminar Boundary Layers." accepted for publication in Physics of Fluids

V. V. Subramanian and J. L. Lawless, "Electrode-Adjacent Boundary Layer Flow in Magnetoplasmadynamic Thrusters," Submitted to Physics of Fluids

V. V. Subramanian and J. L. Lawless, "Onset in Magnetoplasmadynamic Thrusters," AIAA-87-1068, presented at the May 1987 AIAA EP conference, Colorado Springs, Colorado, also submitted to Journal of Propulsion and Power

J. L. Lawless and V. V. Subramanian, "Theory on Onset in Magnetoplasmadynamic Thrusters," AIAA-85-2039, presented at the AIAA EP Conference, October 1985, also published in Journal of Propulsion and Power, Vol. 3, No. 2, p121, March-April 1987

V. V. Subramanian and J. L. Lawless, "Thermal Instabilities of the Anode in an MPD Thruster," (in preparation)

E. Richley, H Torab, and J. L. Lawless, "Numerical Simulation of Two-Temperature MPD thruster Flow," (in preparation)

APPENDIX   A
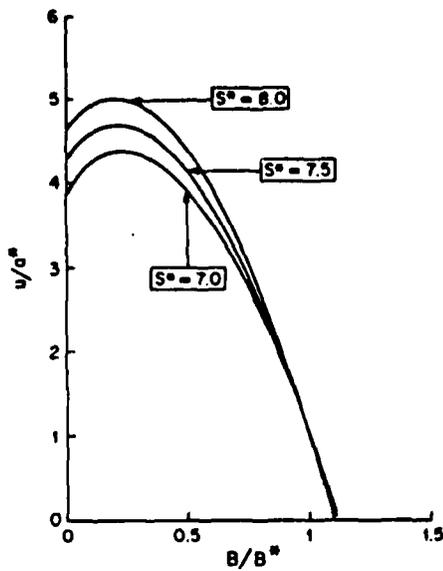
Fig. 2 The flow speed un plotted against the magnetic field B for three values of the magnetic force number S^*.

Fig. 4 The thrust efficiency η and Lorentz efficiency η_L plotted against the magnetic force number S^*.

To complete the problem description, boundary conditions are needed at the channel inlet, $x=0$, and exit, $x=L$. At $x=L$, we require $B=0$. At the inlet $x=0$, the flow speed is specified, $u=u_i$. The inlet flow speed, u_i is very small; and, for present purposes, it may be taken as approximately zero. The value of the magnetic field at the inlet $B=B_i$ is determined from the experimentally specified total current J by Ampere's law:

$$B_i = \mu_0 J / W \qquad (9)$$

The mass flux F is related to the total mass flow $\dot{m}$ by:

$$F = \dot{m}/(HW) \qquad (10)$$

The performance of the MPD thruster can be characterized by its efficiency. We will define two efficiencies. Although the definitions are different, they agree closely over the range of MPD operation. The first, inspired by thermodynamics, is the Lorentz efficiency, which is defined as the ratio of the work done by the electromagnetic force to the total electrical power in[7]

$$\eta_L = \int_0^L jBu\,dx \Big/ \int_0^L Ej\,dx \qquad (11)$$

When the integrand in Eq. (11) is rearranged, the Lorentz efficiency is seen to be the weighted average over the power of the ratio of the back-EMF to the electric field:

$$\eta_L = \int_0^L \left(\frac{uB}{E}\right) Ej\,dx \Big/ \int_0^L Ej\,dx \qquad (12)$$

$$= \left\langle\frac{uB}{E}\right\rangle \qquad (13)$$

It is then evident from Eq. (13) that for efficient thruster operation it is necessary to operate in a regime where the back-EMF is comparable to the electric field. This means that the back-EMF onset mechanism, discussed in Sec. V., is expected to be important in efficient thrusters.

The second type of efficiency is conventionally used to define overall propulsion system performance:

$$\eta = (T_A^2/2\dot{m})/(JV) \qquad (14)$$

where $T_A = (\dot{m}u + PHW)|_{x=L}$ is the total thrust. For a planar channel, $V=EH+V_s$ where V_s is the sum of the sheath voltage drops. By including the thrust due to pressure, η differs from η_L. For the normal operating regime of MPD thrusters, as opposed to electrothermal thrusters, the pressure component of thrust is small and the two efficiencies agree closely, as will be shown in Sec. IV.

The governing equations described in this section can be solved to determine the electrical characteristics and efficiency of the thruster. This will be done in the following sections.

III. Magnetogasdynamic Choking

The combined action of ohmic heating and Lorentz body force can cause a flow in a constant-area channel to accelerate from subsonic to supersonic. Since both of these effects are large in the MPD thruster, variation in the channel cross-sectional area may be unimportant even if it is present. This section will develop the condition for this choking to occur in the self-field flow of a nonideal gas obeying equation of state Eq. (4).

Rewriting Eqs. (1) and (4) in differential form, combining them with Eqs. (2) and (3) to eliminate dp and $d\rho$ using Eq. (5) to eliminate j, and solving for the velocity gradient yields

$$\frac{1}{u}\frac{du}{dx} = \frac{1}{M^2-1}\frac{1}{\rho\partial h/\partial\rho|_P}\left(\frac{B}{\mu_0}\frac{\partial h}{\partial P}\Big|_\rho - \frac{E}{\mu_0\rho u}\right)\frac{dB}{dx} \qquad (15)$$

where $M=u/a$ is the Mach number and a is given by[18]

$$a^2 = (\rho\partial h/\partial\rho|_P)/(1 - \rho\partial h/\partial P|_\rho) \qquad (16)$$

a is the acoustic speed of sound in a gas obeying equation of state Eq. (4).[18] For the special case of an ideal gas, Eq. (16) reduces to the conventional expression.

It is seen that Eq. (15) is singular at $M=1$. For continuous acceleration through $M=1$, it is required that

$$E = \rho^* a^* B^* \frac{\partial h}{\partial P}\Big|_{\rho^*} \qquad (17)$$

where * represents quantities evaluated at the sonic point, $M=1$. Equation (17) is the choking condition. It relates the

electric field E to the back-EMF at the choking point, a^*B^*. This will play a central role in the prediction of back-EMF induced onset discussed in Sec. V.

Equation (17) can be interpreted in terms of classical gasdynamics. Ohmic heating tends to drive a gas toward $M = 1$ and the magnetic body force tends to drive the flow away from $M = 1$.[17] Equation (17) determines the electric field necessary to provide the right amount of ohmic heating to drive the flow just to $M = 1$ where the body force can accelerate it to supersonic speeds.

This choking condition has been previously studied for the special case of an ideal gas. Resler and Sears[19,20] considered such choking for an applied-field calorically-perfect flow. King et al.[7] studied choking in self-field flow for the special case of a gas obeying the equation of state $h = h(P/\rho)$. The case of a self-field calorically-perfect flow will be considered in the next section, and the more general case of self-field choking in a nonideal gas will be addressed in Sec. VI.

IV. Frozen Flow Model

The concept of back-EMF onset is most easily understood in the special case of a constant-composition (frozen) calorically perfect plasma. In this section, the solution for the flow profiles for frozen flow is presented. The flow in this case is found to be characterized by a single nondimensional parameter. This parameter, the magnetic force number, is closely related to the experimental onset parameter $J^2/\dot{m}$.

The flow of a fully-ionized one-temperature plasma is modeled. Because ionization and recombination reaction rates are not considered in this section, this is called the frozen flow model. With electronic excitation neglected, this assumption of a fully ionized flow permits a simple expression for enthalpy:

$$h = \frac{5kT}{m_A} + \frac{\epsilon_i}{m_A} = \frac{5P}{2\rho} + \frac{\epsilon_i}{m_A} \tag{18}$$

Substituting this frozen flow enthalpy into the choking condition, Eq. (17), gives

$$E = \frac{5}{2}a^*B^* \tag{19}$$

This choking condition determines the electric field and defines the operating region.

To obtain an analytic solution, the conservation equations for mass [Eq. (1)], momentum [Eq. (7)], and energy [Eq. (8)] may be rewritten for frozen flow in terms of the sonic quantities:

$$\rho u = F = \rho^* a^* \tag{20}$$

$$P + Fu + \frac{B^2}{2\mu_0} = P^* + Fa^* + \frac{B^{*2}}{2\mu_0} \tag{21}$$

$$Fh + F\frac{u^2}{2} + \frac{EB}{\mu_0} = Fh^* + F\frac{a^{*2}}{2} + \frac{EB^*}{\mu_0} \tag{22}$$

Combining Eqs. (18–22), the following quadratic equation for u is obtained:

$$u^2 + \left(\frac{5}{8}S^*\left(\frac{B^2}{B^{*2}} - 2\right) - 2\right)a^*u$$

$$+ \left(\frac{5}{4}S^*\left(1 - \frac{B}{B^*}\right) + 1\right)a^{*2} = 0 \tag{23}$$

where

$$S^* = B^{*2}/(\mu_0 \rho^* a^{*2}) \tag{24}$$

The two solutions to quadratic Eq. (23) may be readily written in terms of B and the sonic quantities

$$u = a^*\left[-\frac{\zeta}{2} \pm \frac{(\zeta^2 - 4\xi)^{1/2}}{2}\right] \tag{25}$$

where

$$\zeta = \frac{5}{8}S^*\left(\frac{B^2}{B^{*2}} - 1\right) - 2, \qquad \xi = \frac{5}{4}S^*\left(1 - \frac{B}{B^*}\right) + 1$$

The upper sign in Eq. (25) represents the solution for supersonic flow and the lower sign is for subsonic flow. Eq. (25) shows that u/a^* is a function of B/B^* with S^* as a parameter. Combining Eq. (25) with conservation of mass Eq. (20), ρ can be found:

$$\rho = \rho^*\left[-\frac{\zeta}{2} \pm \frac{(\zeta^2 - 4\xi)^{1/2}}{2}\right]^{-1} \tag{26}$$

Eq. (26) determines ρ/ρ^* as a function of B/B^* with S^* as a parameter. Combining Eq. (25) with momentum conservation Eq. (21), the pressure P can be found:

$$P = Fa^*\left[\frac{8}{5} + \frac{\zeta}{2} \mp \frac{(\zeta^2 - 4\xi)^{1/2}}{2} + \frac{S^*}{2}\left(1 - \frac{B^2}{B^{*2}}\right)\right] \tag{27}$$

Eq. (27) determines P/Fa^* as a function of B/B^* with S^* as a parameter. The relationship between B and position x can be found by combining Ohm's law [Eq. (5)], Ampere's law [Eq. (6)], and choking condition [Eq. (19)]:

$$\frac{dB}{dx} = -\mu_0\sigma\left(\frac{5}{2}a^*B^* - uB\right) \tag{28}$$

From Eqs. (25–27), it is seen that S^*, defined by Eq. (24), is a very important parameter. S^* is the magnetic force number[21] evaluated at the choking point, and displays the relative importance of magnetic pressure and gas dynamic kinetic energy density:

$$S^* = \frac{B^{*2}/2\mu_0}{1/2\rho^*a^{*2}} = \frac{\text{magnetic pressure}}{\text{kinetic energy density}} \tag{29}$$

This magnetic force number S^* is very closely related to the onset parameter $J^2/\dot{m}$, which is used by experimentalists to correlate data. Using Ampere's law [Eq. (9)], mass flux definition [Eq. (10)], and the definition of S^*, [Eq. (24)] yields

$$\frac{J^2}{\dot{m}} = \left(\frac{\mathcal{R}a^*}{\mu_0\kappa^2}\right)S^* \tag{30}$$

where $\kappa = B_i/B^*$ is typically about 1.1.[7]

Limits on operating values of S^* can quickly be established. First, for Eq. (25) to have a real solution, it is necessary that $\zeta^2 > 4\xi$. This occurs for the trivial case of $S^* = 0$ or $S^* > 6.4$. For a physical solution, it is also necessary that $P > 0$. Examination of Eq. (27) shows that this limits S^* to values less than 14.0. In light of Eq. (30), this upper limit on S^* could signify onset. In the next section, however, a more severe limit than $S^* < 14.0$ will be found.

The behavior of these solutions is illustrated in several figures. Figure 2 shows the variation of the nondimensional exit speed (u_e/a^*) vs the parameter S^*. The top portion of the curve represents the supersonic branch of the solution, whereas the bottom portion gives the subsonic branch. The supersonic flow profiles for three values of S^* are shown in Fig. 3. The thruster efficiency for the supersonic flow branch

is shown in Fig. 4. This figure shows that the two definitions for efficiency presented in Sec. II are in close agreement.

In summary, analytical relations between u, ρ, P and B have been found. The solutions contained S^*, the magnetic force number evaluated at the choking point, as a parameter. The solution was found assuming a fully-ionized compositionally-frozen flow. Approximations such as isothermal flow or infinite magnetic Reynolds number have *not* been made. The next section reveals how this solution predicts a new mechanism of onset. In Sec. VI, how the solution is affected by ionization rates is discussed.

V. Onset

This section explains how the simple model of the previous section predicts onset. Onset appears as a limitation on the values S^*, as defined in Eq. (24) or Eq. (29), may assume in the supersonic mode. This limit is a consequence of combining Ohm's law with the flow solutions. The behavior of the back-EMF will be considered first. The effect of back-EMF on Ohm's law is then considered from mathematical and physical viewpoints.

The behavior of the back-EMF, uB, is considered first. Near the inlet, the flow speed u is very small, so uB is small. Near the exit, uB is again small because $B \to 0$. Somewhere near the middle of the thruster, the back-EMF, uB, peaks. This is shown in Fig. 5 for various values of S^*.

An important relationship between the electric field E and the back-EMF uB can be found if Ohm's law is considered. Combining Ohm's law [Eq. (5)] with Ampere's law [Eq. (6)] and integrating yields

$$L = \int_0^{B_i} \frac{dB}{\mu_0 \sigma (E - uB)} \tag{31}$$

where L is the thruster length, B_i the magnetic field at $x = 0$, and σ the plasma electrical conductivity. The relationship between u and B is given by Eq. (25). For frozen flow, the electric field E is given by the choking condition [Eq. (19)]. This is also plotted in Fig. 5. From Fig. 5, it is seen that as S^* increases from 7.0 to 8.5, the peak back-EMF approaches the electric field. This tends to make the denominator in Eq. (31) small. As the peak back-EMF reaches the electric field, the integral indicates that an infinite length thruster is necessary. This occurs at $S^* = 8.52$. For higher S^*, $E - uB$ changes sign

twice during the integral, which is hence singular and meaningless.

The physical significance of this limit can be found by returning to the governing equations, Eqs. (1-6). If at some location in the thruster $E = uB$, then from Ohm's law, [Eq. (5)] no current flows. If no current flows, no magnetic force acts on the plasma [see Eq. (7)] and no ohmic heating occurs [see Eq. (8)]. Consequently, the plasma flows at constant speed and temperature. Further, if no current flows, the magnetic field is constant [see Eq. (6)]. All this implies that if $E = uB$ somewhat in the channel, then it will be true that $E = uB$ at all points downstream. If this is so, the boundary condition of $B = 0$ at $x = L$ cannot be met no matter how long the thruster. Thus, it is necessary that $uB < E$ for all locations within the channel.

The limit of $uB < E$ for the analogous case of plasma accelerators with *applied* magnetic fields is well-known. It was first studied by Resler and Sears[19,20] and has since appeared in textbooks.[21,22]

This value of $S^* = 8.52$ at which $E = uB$ can therefore be considered as the onset limit, indicating a regime of operation beyond which the flow can no longer be supersonic. Using Eq. (30), this limit can be restated dimensionally:

$$\frac{J^2}{\dot{m}} \leq 8.52 \frac{\mathcal{R} a^*}{\mu_0 \kappa^2} \tag{32}$$

Eq. (32) correlates the experimental data of Malliaris et al.[5] very well. This is shown in Fig. 6. This success does not prove the existence of back-EMF onset, however, because the scaling laws for anode mass starvation onset[8,9] are similar.

The reason back-EMF should rise faster than the electric field can be explained with some scaling behavior. From Ampere's law [Eq. (6)] B scales directly with J. From the choking condition [Eq. (17)] E scales roughly with J, and from conservation of momentum [Eq. (2)], u scales roughly with $J^2/\dot{m}$. Thus, as one increases the current, the back-EMF, which scales as $J^3/\dot{m}$, increases faster than E, which scales as J. This leads ultimately to current blocking.

This paper does not attempt to establish the flow conditions after onset has occurred. For $S^* > 8.52$, the smoothly accelerating supersonic solution discussed in Sec. IV is not possible. Thus, some largely subsonic flow is expected. By energy conservation [Eq. (8)], a subsonic flow would likely
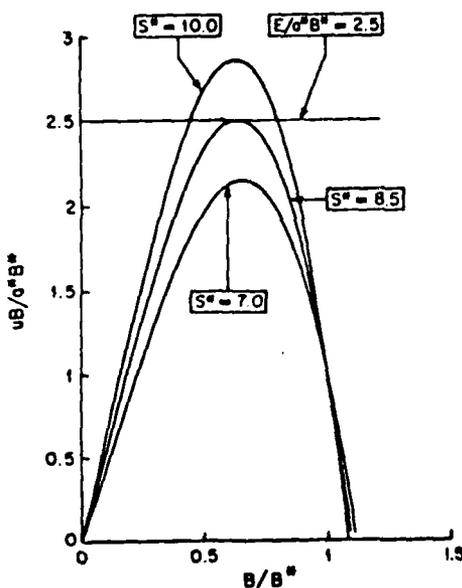
Fig. 5 The back-EMF uB plotted against the magnetic field B for three values of the magnetic force number S^* for supersonic flow.
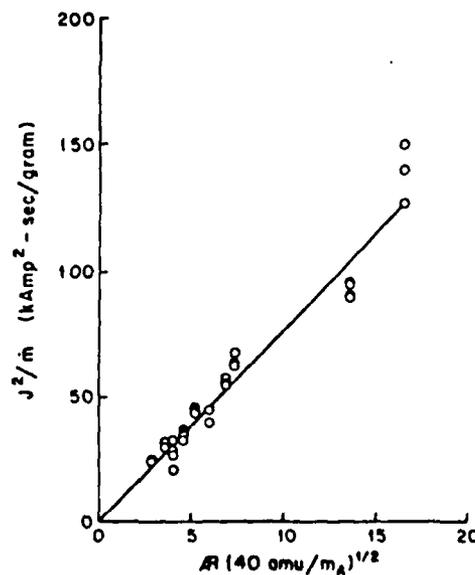
Fig. 6 The experimental data of Malliaris et al.[5] for onset conditions correlate as predicted by back-EMF onset theory.

have a higher temperature. Thus higher erosion rates, by evaporation as well as by sputtering, are expected.

Back-EMF onset also affects the efficiency. It was shown earlier in Eqs. (12) and (13) that for thruster operation with a high Lorentz efficiency, it is necessary to operate in a regime with a high average value of uB/E. Since back-EMF onset restricts the peak value of uB/E to one, its average must be much less (see Fig. 5). Thus, back-EMF onset restricts the efficiency as well as S^*.

VI.   Effect of Ionization

The previous section considered back-EMF onset quantitatively in the frozen flow model. In this section, the effect of non-zero ionization rates is included. This is done first under the equilibrium and secondly under the nonequilibrium assumptions. It is found that ionization rates have a strong effect on the choking condition and thus on the appearance of back-EMF onset.

For both the frozen flow and equilibrium flow limits, the magnetogasdynamic choking condition can be written as

$$\frac{E}{a^*B^*} = \rho^* \frac{\partial h}{\partial P}\bigg|_{\rho^*} \qquad (33)$$

For frozen flow of a monatomic gas, the right-hand side of Eq. (33) has the value of 5/2. The equilibrium calculation causes the right-hand side of Eq. (33) to be up to an order of magnitude larger. This is shown in Fig. 7. The major difference between the two limits is that an important part of the change in enthalpy in equilibrium is due to the change in the ionization fraction. The right-hand side of Eq. (33) oscillates in the equilibrium model as the plasma progresses through successive ionization stages.

The difference in thermodynamics has an important effect on back-EMF onset. Since the equilibrium model can predict large electric fields, the occurrence of back-EMF blocking is delayed. This is why King et al.[7] did not find evidence of onset over the range of parameters used in their numerical calculation.

The nature of the choking condition with nonequilibrium ionization can be analyzed as follows. A plasma composed of electrons, neutrals, and once-ionized ions is considered. In nonequilibrium, the equation of state [Eq. (4)] must be replaced by

$$h = h(P, \rho, \alpha) \qquad (34)$$

where α is the ionization fraction. Proceeding exactly as before, we can combine the governing equations in differential form with the new equation of state Eq. (34), solve for the velocity gradient, and obtain the following nonequilibrium choking condition:

$$E = \rho^* a^* B^* \frac{\partial h}{\partial P}\bigg|_{(\rho^*,a^*)} + \frac{\rho^* a^*}{j^*}\frac{\partial h}{\partial \alpha}\bigg|_{(P^*,\rho^*)}\frac{d\alpha}{dx}\bigg|_{x=x^*} \qquad (35)$$

where ( )* refers to quantities evaluated at the sonic point. The above shows the effect of ionization rates on the electric field explicitly.

Neglecting again electronic excitation, an analytic form for the equation of state can be found:

$$h = h(P, \rho, \alpha) = (5P/2\rho) + (\alpha\epsilon_i/m_A) \qquad (36)$$

Using Eq. (36), the choking condition Eq. (35) may be simplified to

$$E = \frac{5}{2}a^*B^* + \frac{\rho^* a^* \epsilon_i}{j^* m_A}\frac{d\alpha}{dx}\bigg|_{x=x^*}$$

Observe that the first term on the right-hand side is the electric field from the frozen flow theory and the second term
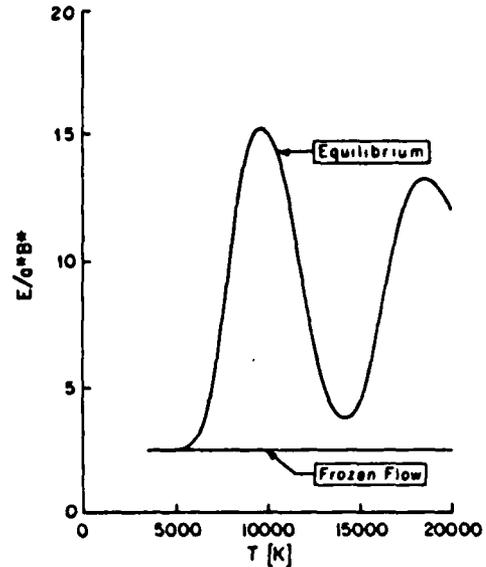
Fig. 7   The electric field determined by the choking condition, Eq. (17), plotted against temperature at the choking point for the two cases of equilibrium and frozen flow.

represents the dependence of the electric field on the ionization rate at the sonic point. The physical significance of the relative magnitude of these two terms can be found by rewriting the above equation in the following nondimensional form:

$$\frac{E}{a^*B^*} = \frac{5}{2} + \frac{\rho^* \epsilon_i}{j^* B^* m_A}\frac{d\alpha}{dx}\bigg|_{x=x^*} \qquad (37)$$

Consider a unit volume of the plasma as it travels a distance dx. $(\rho^*\epsilon_i/m_A)d\alpha$ is the energy added to ionization. $jBdx$ is the work done by the magnetic field to accelerate the plasma. Thus, the second term on the right of Eq. (37) measures the ratio of energy going into ionization to the work done in accelerating the plasma.

The ionization rate $d\alpha/dx$ is found in a nonequilibrium model from a rate equation:

$$\frac{d\alpha}{dx} = \frac{k_f \rho \alpha(1-\alpha)}{m_A u} - \frac{k_b \rho^2 \alpha^3}{m_A^2 u}$$

The frozen flow model is found as the limit in which k_f and k_b approach zero. If k_f and k_b approach infinity, the equilibrium model is recovered.

In this section, the choking condition for frozen and equilibrium flow have been compared. Fig. 7 showed a large quantitative difference between these two limits. Using a generalized equation of state [Eq. (34)], the magnetogasdynamics choking condition was extended to non-equilibrium flow in Eq. (35). It was shown that the importance of the ionization term in the choking condition was determined by the relative rate at which energy enters ionization to the rate at which work is done on the flow at the choking point.

VII.   Summary and Conclusions

A model of one-dimensional plasma flow in the MPD thruster has been presented. Three different thermodynamic models have been used: frozen flow, equilibrium flow, and nonequilibrium flow. Because of its simplicity, an analytical solution was found for the frozen flow case. A single parameter, S^*, governed the solution. S^* was shown to be proportional to the well-known experimental parameter $J^2/\dot{m}$. Onset appeared in this model through the nonintuitive result that, for a sufficiently large S^*, the electric field is insufficient

to draw the applied current in the supersonic mode. For frozen flow, the onset criterion was given by Eq. (32). When ionization occurs, such as in an equilibrium or nonequilibrium flow, onset is delayed because the choking condition predicts a larger electric field. This explains why, over the parameter range they studied, King et al.[7] did not observe back-EMF onset in their numerical results for equilibrium flow. No simple analytic solution was found when ionization occurs.

The cause of back-EMF onset can be traced to two physical phenomena. The first is magnetogasdynamic choking which relates the electric field to the back-EMF at the choking point. The second is the requirement that $E - uB$ not change sign in the thruster. If the latter is violated, it is not possible to draw all the current in a finite length thruster. Both these requirements are well-known for the case of applied-field accelerators.[19-22] This paper has shown that the combination of these two in a self-field flow limits the current that may be applied in one-dimensional supersonic flow.

The back-EMF mechanism of onset is distinctly different from the anode mass starvation hypothesis.[8-11,13] This is physically clear when considering injection of a small amount of mass through the downstream portion of the anode. Such mass injection could have a major effect on the possibility of anode mass starvation but no effect on the back-EMF onset mechanism.

This work, like that of King et al.,[7] shows the significance of considering conservation of energy, [Eq. (3)]. Without differential conservation of energy, as in the isothermal models, choking conditions such as Eq. (17) or Eq. (35) are not found. This changes the electrical characteristics of MPD thrusters. Further experimental information on the choking region would be valuable.

Acknowledgments

References

[1] Jahn, R.G., Physics of Electric Propulsion, McGraw-Hill Book Company, New York, 1968.

[2] Sherman, A., "Theoretical Performance of a Crossed Field MHD Accelerator," ARS Journal, Vol. 32, March 1962, pp. 414-420.

[3] Workman, J.B., "Arc Structure in a Magnetic Annular Discharge," AIAA Journal, Vol. 7, March 1969, pp. 512-519.

[4] Chubb, D.L., "Fully Ionized Quasi-One-Dimensional Magnetic Nozzle Flow," AIAA Journal, Vol. 10, Feb. 1972, pp. 113-114.

[5] Malliaris, A.C., John, R.R., Garrison, R.L., and Libby, D.R., "Performance of Quasi-Steady MPD Thrusters at High Powers," AIAA Journal, Vol. 10, Feb. 1972.

[6] King, D.Q., Smith, W.W., Jahn, R.G., and Clark, K.E., "Effect of Thrust Chamber Configuration on MPD Arcjet Performance," Proceedings of the Princeton/AIAA/DGLR 14th International Electric Propulsion Conference.

[7] King, D.Q., Clark, K.E., and Jahn, R.G., "Effect of Choked Flow on Terminal Characteristics of MPD Thrusters," AIAA Paper 81-0686, April 1981.

[8] Baksht, F.G., Moizhes, B. Ya., and Rybakov, A.B., "Critical Regime of a Plasma Accelerator," Soviet Physics Technical Physics, Vol. 18, No. 12, 1974, pp. 1613-1616.

[9] Heimerdinger, D.J., "An Approximate Two-Dimensional Analysis of an MPD Thruster," Master's Thesis, Massachusetts Institute of Technology, June 1984.

[10] Korsun, A.G., "Current Limiting by Self Magnetic Field in a Plasma Accelerator," Soviet Physics Technical Physics, Vol. 19, No. 1, 1974, pp. 124-126.

[11] Hugel, H. "Effect of Self-Magnetic Forces on the Anode Mechanism of a High Current Discharge," IEEE Transactions on Plasma Science, Vol. PS-8, No. 4, 1980, pp. 437-442.

[12] Kuriki K., Onishi, M., and Mormato, S., "Thrust Measurement of KIII MPD Arcjet," AIAA Journal, Vol. 20, 1982, pp. 1414-1419.

[13] Shubin, A.P., "Dynamic Nature of Critical Regimes in Steady-State High-Current Plasma Accelerators," Soviet Journal of Plasma Physics, Vol. 2, 1976, pp. 18-21.

[14] Schrade, H.O., Auweter-Kurtz, M., and Kurtz, H.L., "Stability Problems in Magnetoplasmadynamic Arc Thrusters," 18th Fluid Dynamics and Plasmadynamics and Laser Conference, Cincinnati, OH, 1985.

[15] Barnett, J., Operation of the MPD Thruster with Stepped Current Input, Ph.D. Dissertation, Princeton University, Princeton, NJ, 1985.

[16] Martinez-Sanchez, M., Heimerdinger, D.J., "Analysis of Performance Limiting Factors in MPD Thrusters," IEEE International Conference on Plasma Science, Pittsburgh, PA, 1985.

[17] Shapiro, A.H., The Dynamics and Thermodynamics of Compressible Fluid Flow, Ronald Press, New York, 1953.

[18] Vincenti, W.G., and Kruger, C.H., Introduction to Physical Gas Dynamics, John Wiley and Sons, New York, 1967.

[19] Resler, E.L. Jr., and Sears, W.R., "The Prospects for Magneto-Aerodynamics," Journal of the Aeronautical Sciences, Vol. 25 April 1958, pp. 235-245.

[20] Resler, E.L. Jr., and Sears, W.R., "Magneto-Gasdynamic Channel Flow," ZAMP, Vol. IXb, 1958, pp. 509-519.

[21] Sutton, G.W., and Sherman, A. Engineering Magnetohydrodynamics, McGraw-Hill Book Co., New York, 1965.

[22] Hughes, W.F., and Young, F.J., The Electromagnetodynamics of Fluids, John Wiley & Sons, Inc., New York, 1966.

APPENDIX   B

AIAA'87

AIAA-87-1068
Onset Magnetoplasmadynamic
Thrusters with Finite Rate Ionization
V.V. Subramaniam, Carnegie Mellon
Univ., Pittsburgh, PA; and J.L. Lawless,
Space Power Inst., San Jose, CA

19th AIAA/DGLR/JSASS International
Electric Propulsion Conference
May 11-13, 1987/Colorado Springs, Colorado

ONSET IN MAGNETOPLASMADYNAMIC THRUSTERS
WITH FINITE RATE IONIZATION*

V. V. Subramaniam**
J. L. Lawless[†]
Carnegie-Mellon University
Pittsburgh, Pennsylvania 15213

Abstract

Quasi one-dimensional self-field flow in a magnetoplasmadynamic thruster is analyzed including the effect of non-equilibrium ionization. This theory, like the frozen flow theory, predicts the occurrence of the destructive "onset" phenomenon due to an excessive back-EMF. Comparison between this theory and experiments on a straight coaxial thruster is given and shown to be good within the limits of quasi one-dimensionality. The back-EMF onset mechanism is also shown here to be influenced by wall friction and heat transfer, and a choking condition incorporating these effects is derived.

Nomenclature

a = Speed of sound

A = Cross-sectional area of channel

B = Magnetic field

$\bar{B} = B/B^*$ = Non-dimensionalized magnetic field

E = Electric field

$\bar{E} = E/a^*B^*$ = Non-dimensionalized electric field

$F = \rho u$ = Mass flux

h = Enthalpy per unit mass

j = Current density

k = Boltzmann's constant

L = Length of channel, or thruster length

$M = u/a$ = Mach number

P = Pressure

T = Temperature

$\bar{T} = T/T^*$ = Temperature non-dimensionalized by the temperature at the sonic point

u = Component of velocity along the channel, in the x direction

$\bar{u} = u/a^*$ = Component of velocity along the channel in the x direction, normalized by the speed of sound at the sonic point

x = Axial coordinate in the direction of the flow along the channel

α = Ionization fraction

ρ = Mass density

σ = Electrical conductivity

a^* = Speed of sound at the sonic point

B^* = Magnetic field at the sonic point

h^* = Enthalpy per unit mass at the sonic point

j^* = Current density at the sonic point

P^* = Pressure at the sonic point

S^* = Magnetic force number at the sonic point

T^* = Temperature at the sonic point

x^* = Position of the sonic point

α^* = Ionization fraction at the sonic point

ρ^* = Mass density at the sonic point

σ^* = Electrical conductivity at the sonic point

B_i = Magnetic field at the inlet, $x = 0$

C_D = Drag coefficient

D_H = Hydraulic diameter

h_c = Effective heat transfer coefficient

k_b = Three-body recombination rate constant

k_i = Ionization rate constant

m_A = Atomic mass

T_w = Wall temperature

ϵ_i = First ionization energy

μ_0 = Permeability of free space

I. Introduction

The performance of magnetoplasmadynamic (MPD) thrusters has primarily been limited by the onset phenomenon. This phenomenon collectively refers to increased erosion of

thruster components and large voltage oscillations, for steady operation at a critical current with fixed mass flow and geometry. Onset was first observed experimentally and since, there have been several theoretical attempts to understand and quantify it. Existing theories of onset[1, 2, 3, 4, 5, 6, 7] may be classified into three major categories. These are the anode starvation theories that partially account for the Hall effect[2, 3, 5]; those that account for the thermodynamics[1, 6, 7]; and those that consider the MPD discharge in the unsteady mode[3, 4].

Because of the complexity of the problem, several simplifying assumptions have been used in each of the theories. Bakshi *et al.*, Shubin, and Martinez *et al.* have assumed that the flow in the MPD thruster is isothermal and thereby eliminated the energy equation. In addition, Shubin and Martinez *et al.* have considered the magnetic Reynolds number to be infinite. The back-EMF theory[6, 7] made no such assumptions but considered the MPD flow to be fully ionized and frozen (i.e. zero ionization rate). The appearance of onset in this theory was found to be strongly affected by the assumptions regarding the thermodynamics. However, the Hall effect which was partially included in the anode starvation theories, was neglected in the back-EMF theory.

The back-EMF theory differs from the other theories. From the experimental results of Barnett[8], it is evident that the predictions of the anode starvation theories would be severely affected by the injection of a small amount of mass near the downstream end of the anode. This would have no effect on the back-EMF theory. The difference between the back-EMF theory and the unsteady (instability) theories is that onset by a dominant back-EMF appears in the steady state. The fact that the assumptions made in the back-EMF theory are different from the other theories indicates that the physical mechanisms responsible for onset are different. There is however insufficient experimental information on a uniform geometry at this time, to determine which of these different onset predictions occur first under which assumptions.

The back-EMF theory will now be summarized. King *et al.* and Lawless *et al.* have shown that the electric field

necessary to sustain supersonic flow in the MPD thruster, is determined by the requirement that the acceleration from subsonic to supersonic flow take place in a smooth fashion. This condition was known as the choking condition. Now, the electric field also had to satisfy the constraint imposed by Ohm's law which specified the magnitude of the field necessary to draw all the applied current. Lawless *et al.* also showed that frozen MPD flow was parametrized by the magnetic force number S^*, which then related to the onset parameter that is used by experimentalists to define the onset limit. Both constraints on the electric field could be satisfied for steady flow only for all values of S^* below a critical limit. This limit on S^* translated to a limit on the experimentally measured onset parameter and correlated well with the experimental data of Malliaris *et al.*[9]. This conflict between the electric field necessary to draw all the applied current and the electric field necessary for supersonic flow at a critical value of the current, is interpreted to be onset.

The effect of the ionization rate at the sonic point on the choking condition has been discussed by Lawless *et al.*. They showed that the electric field necessary for choking depends strongly on the ionization rate at the sonic point. The larger that rate, the larger the electric field must be in order to sustain a supersonic flow. Consequently, ionization rates control the terminal voltage. Another implication of this result is that the ionization rates may control the appearance of onset by the back-EMF mechanism. In this paper, the effect of realistic ionization rates on determining the electrical characteristics and on controlling the appearance of back-EMF onset will be examined using a quasi-1D non-equilibrium theory. This paper will underscore the importance of considering the detailed thermodynamics of MPD flow. Non-equilibrium ionization MPD flow with an externally applied magnetic field has been considered previously by Seals and Hassan[10]; However, they did not attempt an explanation of onset. Furthermore, their analysis was restricted to the operation of the thruster in the electrothermal mode. The non-equilibrium theory presented herein will be used specifically in order to predict and quantify onset in self-field MPD thrusters.

The governing equations of quasi-1D flow will be given

2

in section II, followed by a discussion of magnetoplasmadynamic choking in section III. Non-equilibrium flow is discussed in section IV and comparisons with the experiments of King *et al.*[1,11] are given in section V. The effects of wall friction and heat transfer on the magnetoplasmadynamic choking of quasi-1D non-equilibrium flow is discussed in section VI, followed by the summary and conclusions in section VII.

II. Governing Equations

The governing equations of quasi 1-D constant area channel flow under the assumptions of negligible viscous effect, Hall effect, and heat transfer have been previously described[1,6,7]. The only difference in the non-equilibrium case is that the equation of state is modified. Following the work of Lawless *et al.*[6], the conservation equations for a plasma consisting of neutral atoms, singly ionized atoms, and electrons is:

mass: $\qquad \rho u = F = constant \qquad$ (1)

Momentum: $\qquad P + Fu + \dfrac{B^2}{2\mu_o} = constant \qquad$ (2)

Energy: $\qquad Fh + \dfrac{Fu^2}{2} + \dfrac{EB}{\mu_o} = constant \qquad$ (3)

state: $\qquad h = h(P,\rho,\alpha) \qquad$ (4)

Ohm's law: $\qquad j = \sigma(E - uB) \qquad$ (5)

where σ is obtained from: $\qquad \sigma = \left(\dfrac{1}{\sigma_n} + \dfrac{1}{\sigma_c}\right)^{-1}$

where σ_n is the conductivity due to electron-neutral collisions and σ_c is the coulomb portion of the conductivity. The expressions for σ_c and σ_n have been summarized by King[11]. We also have:

Ampere's law $\qquad \dfrac{dB}{dx} = - \mu_o j \qquad$ (6)

The ionization and recombination processes are modelled according to : $\qquad Ar + e \rightleftharpoons A^+ + e + e$

where the left hand side represents ionization due to electron impact (e) with a neutral atom (Ar), and the right hand side represents three body recombination with two electrons and a singly ionized atom (A^+). This reaction is likely to be one of the dominant processes in the MPD thruster. The ionization

rate, $d\alpha/dx$ in the non-equilibrium theory is then found from the rate equation:

$$\dfrac{d\alpha}{dx} = \dfrac{k_i \rho \alpha(1-\alpha)}{m_A u} - \dfrac{k_b \rho^2 \alpha^3}{m_A^2 u} \qquad (7)$$

where α is the ionization fraction, and k_i and k_b are the ionization and recombination rate constants respectively. The frozen flow model is found as the limit in which k_i and k_b approach zero. If k_i and k_b approach infinity, the equilibrium model is recovered. The rate constants have been obtained from the work of Mansbach and Keck[12] for the non-equilibrium ionization case. These are:

$$k_i = \dfrac{48 \times 10^{-9}}{T^3 (5.556 \times 10^{-11})^{3/2}} exp\{- \epsilon_i/kT\}$$

$$k_b = \dfrac{4 \times 10^{-9}}{T^{9/2}}$$

where k_i is in cm^3/sec and k_b is in cm^6/sec

Normally, for equilibrium flow, two independent properties such as P and ρ are required to define a thermodynamic state. For non-equilibrium flow, a third independent property such as α is required to completely determine the thermodynamic state[13]. In order to complete the formulation of the problem, boundary conditions are required. This will be discussed in section IV where the simplified equations of non-equilibrium flow will be given. The introduction of the non-equilibrium equation of state, Eq. (4), and the rate equation, Eq. (7) modifies the magnetoplasmadynamic choking condition. This will be discussed next.

III. Magnetoplasmadynamic Choking

Magnetoplasmadynamic choking in the MPD thruster was first discussed by King *et al.*[1]. Subsequently, Lawless *et al.*[6] have examined the choking condition for frozen flow and equilibrium flow assumptions, and found that the ionization rate has a strong effect on the appearance of back-EMF onset. In this section, the effect of finite ionization rates on MPD choking will be discussed.

The nature of the choking condition with nonequilibrium ionization can be analyzed as follows. Consider a plasma composed of electrons, neutrals, and singly ionized atoms. In non-equilibrium, the equation of state is given by Eq. (4),

3

Proceeding exactly as Lawless et al., we can combine the governing equations in differential form with the new equation of state Eq. (4), solve for the velocity gradient, require smooth acceleration through the sonic point, and obtain the following non-equilibrium choking condition:

$$E = \rho^* a^* B^* \frac{\partial h}{\partial P}\Big|_{\rho^*,a^*} + \frac{\rho^* a^*}{j^*}\frac{\partial h}{\partial a}\Big|_{P^*,\rho^*}\frac{da}{dx}\Big|_{x=x^*} \quad (8)$$

where the superscript * refers to a quantity evaluated at the sonic point. Equation Eq. (8) shows the effect of ionization rates on the electric field explicitly. Neglecting again electronic excitation, an analytic form for the equation of state can be found:

$$h = h(P,\rho,a) = \frac{5P}{2\rho} + \frac{a\epsilon_i}{m_A} \quad (6)$$

where ϵ_i is the first ionization energy. Using Eq. (9), the choking condition Eq. (8) may be simplified to:

$$E = \frac{5}{2}a^* B^* + \frac{\rho^* a^* \epsilon_i}{j^* m_A}\frac{da}{dx}\Big|_{x=x^*}$$

Observe that the first term on the right hand side is the electric field from the frozen flow theory and the second term represents the dependence of the electric field on the ionization rate at the sonic point[6]. The frozen flow limit is recovered when the second term is set equal to zero, and the equilibrium flow limit is recovered when the second term is set equal to its maximum value at equilibrium.

In this section, the magnetoplasmadynamic choking condition for non-equilibrium flow with a generalized equation of state has been reviewed. This choking condition has incorporated in it, equilibrium and frozen flow limits as special cases. With the electric field determined by the choking condition given in this section, the solution of the governing equations will be discussed next.

IV. Non-Equilibrium Channel Flow

The governing equations for quasi-1D MPD flow have already been discussed in section II. In this section, II governing equations will be combined to give simpler non-dimensionalized equations which will then be solved numerically in section V. We begin by rewriting the equations of section II in terms of the respective quantities evaluated at the sonic point:

mass:
$$\rho u = F = \rho^* a^* \quad (10)$$

momentum:
$$P + Fu + \frac{B^2}{2\mu_0} = P^* + F_* a^* + \frac{B^{*2}}{2\mu_0} \quad (11)$$

energy:
$$h + \frac{u^2}{2} + \frac{EB}{\mu_0 F} = h^* + \frac{a^{*2}}{2} + \frac{EB^*}{\mu_0 F} \quad (12)$$

state:
$$P = (1+a)\frac{\rho kT}{m_A} \quad (13)$$

$$h = \frac{5}{2}(1+a)\frac{kT}{m_A} + \frac{a\epsilon_i}{m_A} \quad (14)$$

$$a^2 = \frac{5}{3}(1+a)\frac{kT}{m_A} \quad (15)$$

choking condition:
$$\frac{E}{a^* B^*} = \frac{5}{2} - \frac{\mu_0 F \epsilon_i}{a^* B^* m_A}\frac{da}{dB}\Big|_{x=x^*} \quad (16)$$

rate:
$$\frac{da}{dx} = \frac{k_f F a(1-a)}{m_A u^2} - \frac{k_b F^2 a^3}{m_A^2 u^3} \quad (17)$$

Ampere's & Ohm's laws:
$$j = -\frac{1}{\mu_0}\frac{dB}{dx} = \sigma(E - uB) \quad (18)$$

The pressure and enthalpy may be eliminated using Eq. (13) and Eq. (14). Equations Eq. (17) and Eq. (18) may also be combined to yield a single differential equation for da/dB. Thus, the equations Eq. (10) through Eq. (18) may be put into the following non-dimensional forms:

$$\frac{3(1+a)\bar{T}}{5(1+a^*)\bar{u}} + \bar{u} + \frac{S^* \bar{B}}{\cdot} = \frac{8}{5} + \frac{S^*}{2} \quad (19)$$

$$\frac{3(1+a)\bar{T}}{2(1+a^*)} + \frac{\bar{u}^2}{2} + \bar{E}S^* = 2 + \bar{E}S^* + \frac{(a^*-a)\epsilon_i}{m_A a^{*2}} \quad (20)$$

$$\bar{E} = \frac{5}{2} - \frac{\epsilon_i}{m_A a^{*2} S^*}\Big(\frac{da}{d\bar{B}}\Big)\Big|_. \quad (21)$$

$$\frac{da}{d\bar{B}} = \frac{k_b F^2 a^3 - m_A \bar{u} a^* k_f F a(1-a)}{\mu_0 \sigma m_A^2 \bar{u}^2 a^{*4}(\bar{E} - \bar{u}\bar{B})} \quad (22)$$

where k_f and k_b were given in section II, and the integral form of Ampere's law Eq. (18) when non-dimensionalized yields:

$$L = \int_0^{\bar{B}_i} \frac{d\bar{B}}{\mu_0 \sigma a^* [\bar{E} - \bar{u}\bar{B}]} \quad (23)$$

4

An interesting feature in these equations is the presence of the non-dimensional parameter, S^*. This S^* is the same magnetic force number that appears in the frozen flow theory of Lawless *et al*. However, the equations of non-equilibrium flow are sufficiently more complicated that limits on S^* may not be as easily established as in the frozen flow theory. Equations Eq. (19) through Eq. (23) must therefore be solved to calculate the onset limit.

To complete the description of quasi-1D non-equilibrium MPD channel flow, boundary conditions are required. In the quasi-steady operation of the MPD thruster[1], the weakly ionized flow enters the channel $x = 0$ at a slow speed and low temperature. Within a short distance of less than a centimeter, the plasma is accelerated to Mach 1 mainly due to ohmic heating. Beyond the sonic point, the electromagnetic force accelerates the plasma to supersonic speeds. At the exit $x = L$, the magnetic field, B is nearly zero.

The mathematical description of the flow is given by equations Eq. (19) through Eq. (23). The above set of equations Eq. (19) through Eq. (23) may be taken to constitute a system of five equations in the five unknowns u, T, e, E, and L with B^* and S^* as parameters. The independent variable is taken here to be the magnetic field, B. This formulation simplifies the system of equations but reduces the problem to a two-point boundary value problem. Therefore a manual shooting method is used. The mass flow rate is taken as given and constant. The channel cross sectional area is constant and fixed. The boundary conditions are as follows. The magnetic field B^*, the temperature T^*, and the ionization fraction e^* at the sonic point are specified as the boundary conditions at $x = x^*$. The integration of Eq. (23) is then performed in the two separate directions toward the inlet, and toward the exit. The sum of these lengths before and after the sonic point then is required to match the given length of the thruster, L. If the calculated length does not match the given length, then T^* and e^* are varied until the correct length has been calculated.

The physical significance of the manner in which the boundary conditions are specified will now be addressed. The total mass flow is fixed in the experiments. Hence it is natural to impose the same in this steady state theory. The total current to the thruster is also fixed. This implies from equation (6) of section II that at a given current level, the magnetic field at the inlet B_i is fixed. Thus, the magnetic field at the sonic point B^* would be fixed to within less than 10% of B_i. Hence, B^* may be specified as a boundary condition at $x = x^*$, and a reasonable initial guess is obtained from (6). Next, since the thruster length is fixed in the experiments, the parameters e^* and T^* are varied in a realistic fashion until the length calculated by Eq. (23) matches the length in the given experiment. In this manner, profiles of all the variables are computed for a given current and mass flow. The predictions of the non-equilibrium theory are then compared with experimentally measured values of electric fields and onset currents for a given mass flow rate.

This section has focused on the simplified governing equations of the quasi-1D non-equilibrium theory. In the next section, this theory will be used to predict electrical characteristics and onset. Comparisons will then be made with the experimental results of King[11] obtained from a 20 cm. long straight coaxial thruster. It will be shown that at a certain value of the current, the length constraint imposed by the integral form of Ampere's law Eq. (23) cannot be satisfied for steady flow. This is interpreted as onset in the non-equilibrium ionization theory, just as in the frozen flow and equilibrium flow theories.

V. Comparison with Experiment

A quasi-1D non-equilibrium MPD theory was developed in the previous sections. This section will focus on the solution of these equations, present some results, and compare these with the experiments of King[11]. Other experimental results exist, the most detailed of these having been obtained by Barnett[8] on plasma flow conditions at onset. However, these measurements were made on the "benchmark" thruster which is characterized by a protrusion at the anode (see Fig. 1). The theory developed in this paper considers a one-dimensional straight channel (see Fig. 2). For this reason, the data of King[11] which were taken from the straight channel coaxial 20 cm. long thruster, have been chosen for comparison.

The mathematical description along with the boundary conditions has been discussed in section IV. The numerical algorithm will now be summarized. Given the quantities B^*, T^*, and a^* at the sonic point, the mass flow $\dot{m}$, the channel width W, and the channel height H, the right hand side of the integral form of Ampere's law Eq. (23) is computed by integration from $B/B^* = 1$ to $B/B^* = 0$. The integrand of Eq. (23) depends on u, T, B, a, and the quantities at the sonic point. u and T can be obtained as a function of B, a, and the quantities at the sonic point by solving Eq. (19) and Eq. (20) simultaneously. This gives:

$$\bar{u} = -\frac{\gamma_1}{4} \pm \frac{1}{4}\left(\gamma_1^2 - \gamma_2 + \gamma_3\right)^{1/2} \quad (24)$$

where

$$\gamma_1 = 4 + \frac{5}{4}S^*\{1-\bar{B}\}, \qquad \gamma_2 = 16 + 8\bar{T}S^*\{1-\bar{B}\},$$

$$\gamma_3 = \frac{8(a-a^*)\epsilon}{m_A a^{*2}}, \qquad \text{and}$$

$$\bar{T} = -\frac{5}{3}\left(\frac{1+a^*}{1+a}\right)\bar{u} + \left(\frac{8}{3} + \frac{5}{6}S^*\{1-\bar{B}\}\right)\frac{(1+a^*)}{(1+a)}\bar{u} \quad (25)$$

Next, if the conditions at the sonic point are specified, the electric field may be calculated from equation Eq. (21) and Eq. (22). Then the differential equation Eq. (22) is integrated to obtain the ionization fraction a at any desired B. The integration of the differential equation is rather complicated by the fact that this equation is numerically "stiff". Consequently, an IMSL (International Mathematical Subroutine Library) routine DGEAR is employed. This routine uses the algorithm of Gear which is specially equipped to handle stiff systems. DGEAR is used to solve Eq. (22) and the result is used to evaluate the integrand in Eq. (23) at various stages of the numerical integration. In this manner, the thruster length from the sonic point to the exit is computed. In a similar manner, the length upstream of the sonic point is computed. As expected, the length between the inlet and the sonic point is found to be typically much smaller than 1 cm. The distance between the sonic point and the exit is to a very good approximation, the total length of the thruster. This calculated length is then compared to the length of 20 cm. used in King's experiments. If the lengths match, then a solution has been obtained for the current level corresponding to B_i. If the lengths do not match, then the inputs a^* and T^* are varied

until the computed length is ≈ 20 cm. In the results that have been obtained, a^* is kept constant at 0.001 until $T^* = 14000 K$. At $T^* = 14000 K$, a^* is varied from 0.001 to 1.0. Once $a^* = 1$, then T^* is allowed to increase beyond 14000 K. The limit of $T^* = 14000 K$ is chosen because at this temperature, the ionization rate begins to become large. In this way the parameters a^* and T^* are varied in a physically consistent manner. It is found that the solution was not very sensitive to the way in which a^* and T^* were increased.

Solutions to the quasi-1D non-equilibrium equations have thus been generated for mass flows of 3 g/sec and 6 g/sec of Argon propellant. The measured electric fields of King[11, 14] varied widely over the channel cross section as well as along the channel, due to non-uniform mass flow across the channel. Electric field measurements were taken near a location where the electric field was a maximum. Consequently, the data of King have been reduced by a factor of 0.53 in order to compare with the predictions of this quasi one-dimensional theory. The value of 0.53 was determined by comparing the electric field measured at a specific location to the value of the field averaged over the length of the thruster as well as over the cross section. The electric field versus current curves are shown in Fig. 3 for a mass flow of 3 g/sec, and in Fig. 4 for a mass flow of 6 g/sec. The continuous curve represents the results obtained from the non-equilibrium theory. The experimental data of King[11, 14] are plotted as discrete points.

It can be seen that on the basis of this comparison, the non-equilibrium theory predicts the shape of the electric field versus current curve very well. Furthermore, it is in quantitative agreement with experimental results within the bounds of deviation from quasi one-dimensionality. This is observed for both 3 g/sec and 6 g/sec experiments. The major accomplishments of the theory are the upper points in Fig. 3 and Fig. 4, where the calculated values end. These are the onset points in the theory. These are the currents at which no steady solutions could be found that would satisfy the length constraint dictated by Eq. (23). The current level where the discrete data points end signify the operating point

6

where onset was reached in the experiment. As can be seen from Fig. 3 and Fig. 4, the prediction of the onset current by the quasi-1D non-equilibrium theory is in excellent agreement with the experimental results. A numerical comparison of these theoretically predicted onset currents and King's experimentally measured onset currents are summarized in Table 1. Further, Barnett[8] has also observed that the back-EMF is very large near the onset limit for the "benchmark" thruster. This may be a further indication that the onset observed in the MPD thruster maybe due to the back-EMF current blocking mechanism presented in this paper.

In addition to giving the electrical characteristics, the quasi-1D theory also provides variations of various quantities along the length of the thruster. Typical profiles of velocity, temperature, ionization fraction, and current density are shown in Fig. 5, Fig. 6, Fig. 7, and Fig. 8. These were computed for a mass flow rate of 3 g/sec. Some of the features of the profiles require clarification. The velocity (Fig. 5) is seen to increase monotonically until near the exit, where it decreases. This is because ohmic heating is dominant near the exit and the addition of heat to a supersonic flow causes it to slow down. The temperature (Fig. 6) increases steadily until the sonic point, after which it decreases slightly and then increases sharply near the exit. The reason for the slight temperature decrease after the sonic point is that the supersonic flow is accelerating. It is well known that an accelerating supersonic flow cools[15]. Then near the exit, the temperature rises again due to ohmic heating. The temperature rise computed near the exit is unrealistically high. This is because only single ionization was considered in the theory. If the presence of second ions were considered, then this temperature rise at the exit would not be so dramatic. The ionization fraction profile (Fig. 7) requires little explanation. a increases sharply near the sonic point because the temperature rises sharply. It then becomes relatively constant since the temperature is nearly constant in the middle of the thruster. Near the exit, a rises sharply again because of the sharply increasing temperature. The current density (Fig. 8) starts out small near the inlet because the temperature is small (this makes the conductivity small) and then increases following the increasing temperature

and conductivity. Beyond the sonic point, the velocity is increasing and the magnetic field is decreasing. This causes the back-EMF to increase and reach a maximum somewhere in the middle of the thruster. This makes $E - uB$ decrease and reach a minimum somewhere in the middle. Consequently, the current density decreases and reaches a minimum in the center of the thruster, and then increases sharply near the exit because of the sharp increase in conductivity caused by the rising temperature. Thus far, quasi-1D MPD flow has been considered without friction and heat transfer. The effect of these on magnetoplasmadynamic choking will be examined in the next section.

VI. MPD Choking with Wall Friction and Heat Transfer

The previous sections of this chapter have considered quasi-1D MPD flow under the non-equilibrium assumption. However certain effects have been excluded in order to enable a simple solution to the problem. These include friction, heat transfer, and the Hall effect. In this section, friction and heat transfer will be partially included in the theory and their impact on MPD choking will be examined.

For a varying area quasi-1D MPD flow with wall friction and heat transfer, the equations of mass, momentum, and energy conservation yield:

$$\frac{1}{\rho}\frac{d\rho}{dx} + \frac{1}{u}\frac{du}{dx} + \frac{1}{A}\frac{dA}{dx} = 0 \qquad (26)$$

$$\frac{dP}{dx} + \rho u \frac{du}{dx} + \frac{B}{\mu_o}\frac{dB}{dx} + \frac{2C_D \rho u^2}{D_H} = 0 \qquad (27)$$

$$\rho u \frac{dh}{dx} + \rho u^2 \frac{du}{dx} + \frac{E}{\mu_o}\frac{dB}{dx} + 4\frac{h_c}{D_H}(T-T_w) = 0 \qquad (28)$$

where: $C_D = \dfrac{2\tau_w}{\rho u^2}$ is the drag coefficient,

$D_H = \dfrac{4A}{dA_w/dx}$

is the hydraulic diameter, and h_c is the effective heat transfer coefficient.

Following the earlier development, equations Eq. (26), Eq. (27), and Eq. (28) may be combined with Eq. (13), Eq. (14), Eq. (15), Eq. (17), and Eq. (18) to yield:

$$\frac{3}{2u}\frac{du}{dx} = \frac{\gamma_1 + \gamma_2 + \gamma_3 + \gamma_4 + \gamma_5}{(u^2 - a^2)} \qquad (29)$$

where

$$\gamma_1 = \frac{\epsilon_1}{m_A}\frac{da}{dx} \quad , \quad \gamma_2 = \frac{SP}{2\rho A}\frac{dA}{dx} \quad , \quad \gamma_3 = \frac{SC_D u^2}{D_H} \quad ,$$

$$\gamma_4 = \frac{4h_c(T-T_w)}{D_H \rho u} \quad , \quad \gamma_5 = \left(\frac{E}{\mu_o \rho u} - \frac{SB}{2\mu_o \rho}\right)\frac{dB}{dx}$$

For a constant area channel with no friction and no heat transfer, the above reduces to the same expression derived by Lawless et al. Using their same argument and requiring a smooth acceleration from subsonic flow to supersonic flow, gives 0 for the numerator of Eq. (29) when $u = a$. This gives the following choking condition for the electric field. Thus, for a constant area channel:

$$E = \frac{7}{4} a^* B^* + \frac{1}{2}\left(\beta_1 + \beta_2 - \beta_3 + \beta_4\right)^{1/2} \qquad (30)$$

where

$$\beta_1 = \frac{9}{4} a^{*2} B^{*2} \quad , \quad \beta_2 = \frac{16 h_c(T^* - T_w)}{D_H \sigma^*} \quad ,$$

$$\beta_3 = \frac{100 C_D F(1+\alpha^*) k T^*}{3 D_H m_A \sigma^*} \quad , \quad \beta_4 = \frac{4 \epsilon_1 F}{m_A \sigma^*}\frac{da}{dx}\Big|_{...}$$

From the above generalized choking condition, it can be seen that larger rates of heat transfer from the plasma to the wall near the choking point cause a larger electric field. Since a larger electric field permits a larger back-EMF, this may delay back-EMF onset in the same manner as larger ionization rates at the sonic point. The effect of wall friction may also be examined. It can be seen that friction actually causes a lower electric field. This in turn permits a smaller back-EMF, and could thus cause back-EMF onset to occur sooner. Wall friction and bulk heat transfer could thus have a significant effect on the lack of delay or delay of onset for non-equilibrium flow.

VII. Summary and Conclusions

The first non-equilibrium (finite rate ionization) self-field MPD theory to predict onset due to an excessive back-EMF at high currents, has been developed. The electric field dependence on the ionization rate (see section III) prompted the consideration of realistic ionization rates, under the non-equilibrium assumption. The governing equations of non-equilibrium MPD flow have been solved and the results have been compared with King's experiments on a straight coaxial

thruster[1, 11]. Back-EMF onset appears in this theory as the failure of a steady solution to exist at a critical value of the current, for a fixed mass flow. This onset is due to the conflict between the electric field required to sustain a supersonic flow in the thruster, and the electric field necessary to draw all the applied current.

It has been found that the non-equilibrium theory has not only predicted the onset limit, but has also predicted current versus voltage characteristics in agreement with the experiments of King within the limits of quasi-one dimensionality. More experimental data with a uniform mass flow is therefore needed for a more definitive comparison. Finally, non-equilibrium quasi-1D flow has been considered by partially including the effects of wall friction and heat transfer. It has been shown by examining the magnetoplasmadynamic choking condition, that heat transfer may delay back-EMF onset while wall friction may cause it to occur sooner.

References

1. D. Q. King, K. E. Clark, and R. G. Jahn, "Effect of Choked Flow on Terminal Characteristics of MPD Thrusters," AIAA-81-0686, 15th International Electric Propulsion Conference, April 1981, Las Vegas, Nevada.

2. F.G. Baksht, B. Ya. Moizhes, and A.B. Rybakov, "Critical Regime of a Plasma Accelerator," Sov. Phys Tech. Phys., Vol. 18, No. 12, 1974, pp. 1613-1616.

3. A.P. Shubin, "Dynamic Nature of Critical Regimes in Steady-State High-Current Plasma Accelerators," Sov. J. Plasma Phys., Vol. 2, No. 1, 1976, pp. 18-21.

4. H. O. Schrade, M. Auweter-Kurtz, and H. L. Kurtz, "Stability Problems in Magnetoplasmadynamic Arc Thrusters," AIAA 18th Fluid Dynamics and Plasmadynamics and Laser Conference, Cincinnati, Ohio, (1985).

5.   M. Martinez-Sanchez, D. J. Heimerdinger, "Analysis of Performance Limiting Factors in MPD Thrusters," IEEE International Conference on Plasma Science, Pittsburgh, Pennsylvania (1985).

6.   J. L. Lawless, and V. V. Subramaniam, "A Theory of Onset in Magnetoplasmadynamic Thrusters," AIAA/DGLR/JSASS 18th International Electric Propulsion Conference, Alexandria, Virginia (1985). To be published in AIAA Journal of Propulsion & Power.

7.   V. V. Subramaniam, and J. L. Lawless, "The Electrical Characteristics of Magnetoplasmadynamic Thrusters," IEEE International Conference on Plasma Science, Pittsburgh, Pennsylvania (1985).

8.   J. Barnett, *Operation of the MPD Thruster with Stepped Current Input*, PhD dissertation, Princeton University, 1985.

9.   A. C. Malliaris, R. R. John, R. L. Garrison, and D. R. Libby, "Performance of Quasi-Steady MPD Thrusters at High Powers," *AIAA Journal*, Vol. 10, No. 2, February 1972.

10. R. K. Seals Jr., and H. A. Hassan, "Analysis of MPD Arcs with Nonequilibrium Ionization," *AIAA Journal*, Vol. 6, No. 12, December 1968, pp. 2273-2278. .

11. D. Q. King, *Magnetoplasmadynamic Channel Flow for Design of Coaxial MPD Thrusters*, PhD dissertation, Princeton University, December 1981.

12. P. Mansbach and J. Keck, "Monte Carlo Trajectory Calculations of Atomic Excitation and Ionization by Thermal Electrons," *Physical Review*, Vol. 181, 1969, pp. 275. .

13. W. G. Vincenti and C. H. Kruger, *Introduction to Physical Gas Dynamics*, John Wiley and Sons, New York, 1967.

14. D. Q. King, "private communication".

15. A. H. Shapiro, *The Dynamics and Thermodynamics of Compressible Fluid Flow*, Ronald Press, New York, 1953.
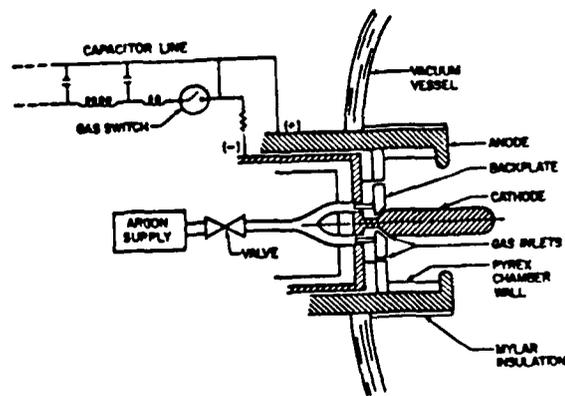
Fig. 1:   A schematic of an MPD thruster
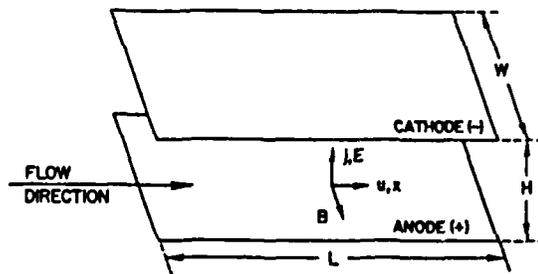
Fig. 2:   The plane-parallel electrode geometry studied in this paper is analogous to the co-axial geometry used in experiments. The above diagram shows the relative orientation of the flow velocity, u, the current, j, the electric field, E, and the magnetic field, B. The channel has a length L in the flow direction and a width W. The electrodes are separated by a distance H.
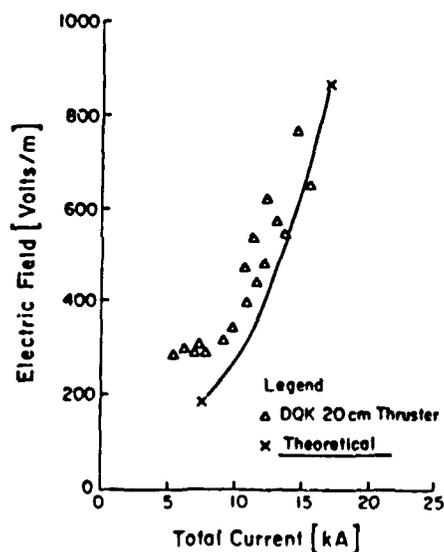
Fig. 3:   The variation of the electric field is shown

9

versus the total current. The experimental data of King[11] for a 20 cm. long straight coaxial thruster are plotted as discrete points, for a total mass flow of 3 g/sec. The solid curve represents the prediction of the non-equilibrium theory of section IV, corresponding to a uniform mass flow of 3 g/sec. The upper portion of the solid curve ends where no steady solution to the equations of section IV was found. This is interpreted as the theoretical onset point. As can be seen, this agrees well with the onset limit observed in the experiment, where the data is seen to be scattered. See section IV and section V for a detailed discussion.
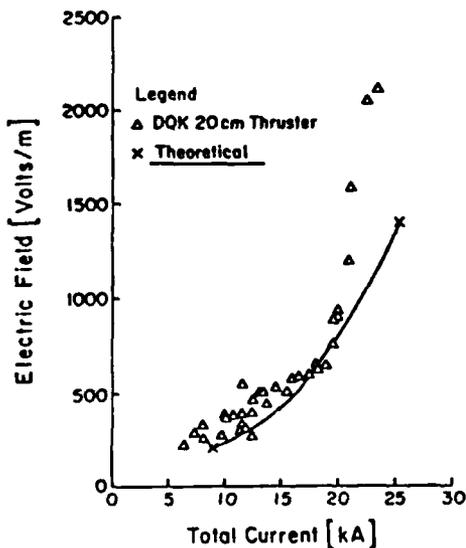
Fig. 4: The experimental data of King[11] for a 20 cm. long straight coaxial thruster are plotted as discrete points, for a total mass flow of 6 g/sec. The solid curve represents the theoretical predictions of the non-equilibrium theory of section IV for a uniform mass flow of 6 g/sec. The curve ends at the upper point where no steady solution could be found. This is the theoretical onset limit, which agrees well with the experimental onset limit of ≈ 26 kA.
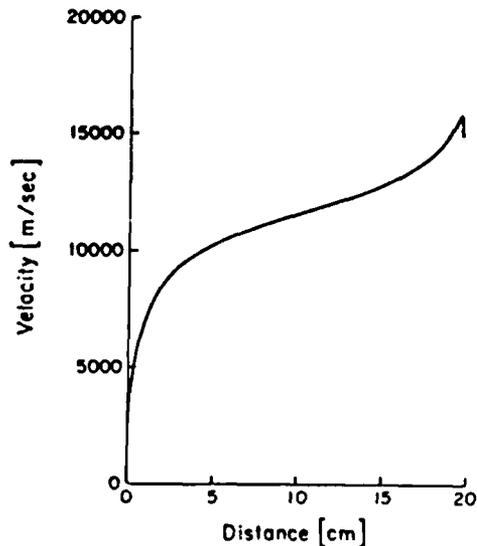
Fig. 5: The plasma flow speed is shown here as a function of distance along the thruster, for a uniform mass flow of 3 g/sec. This profile was obtained from the solutions to the quasi-1D non-equilibrium equations given in section IV and section V. It can be seen that the speed increases monotonically until near the exit, where it decreases. This is due to the dominance of ohmic heating near the exit which causes a supersonic flow to decelerate.
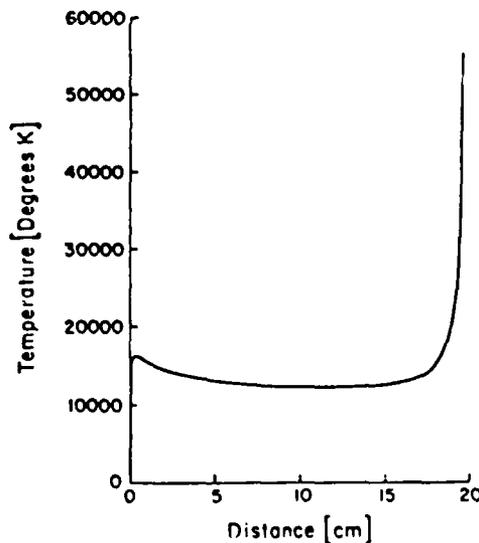
Fig. 6: The plasma temperature is shown in this figure versus distance along the length of the thruster, for a uniform mass flow of 3 g/sec. See section IV and section V for the solutions of the quasi-1D non-equilibrium theory, which were used to obtain the above profile. The temperature increases sharply from the inlet to the sonic point primarily due to

ohmic heating. Beyond the sonic point, there is a slight decrease because of the acceleration of the supersonic flow. Near the exit, the temperature rises again because of ohmic heating. This temperature rise near the exit is accompanied by the decreasing velocity shown earlier in Fig. 5. The unrealistically high exit temperatures are due to the fact that the presence of second ions were not considered in the non-equilibrium theory. See section V for details.
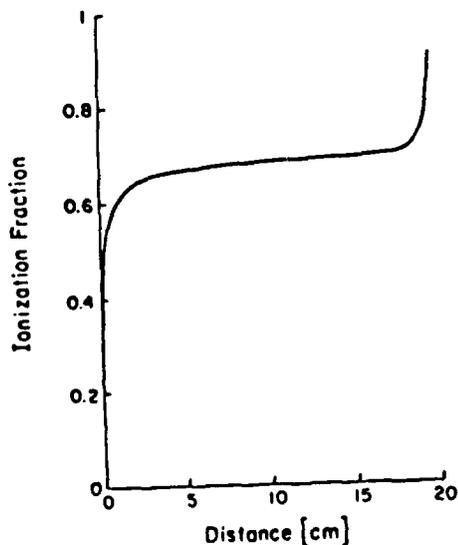
Fig. 7: The ionization fraction has been plotted here as function of the distance along the thruster. The ionization fraction shows marked increases near the entrance and near the exit, where the most drastic variations in temperature take place. This again, is from the solution of the non-equilibrium equations found in section IV and section V, for a uniform mass flow of 3 g/sec.
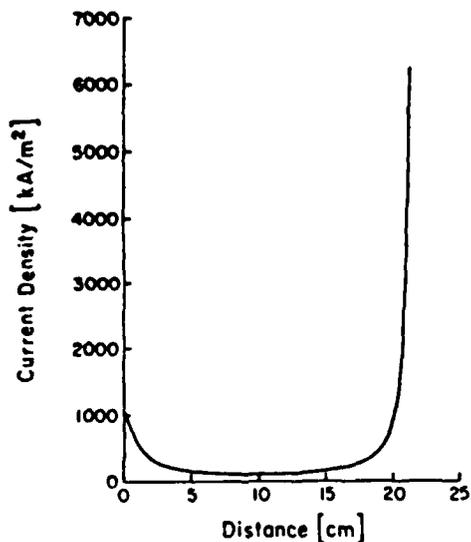
Fig. 8: The current density is shown here versus distance for a uniform mass flow of 3 g/sec. This is from the solutions of the governing equations given in section IV and section V. The current density is small near the entrance because the temperature is small which makes the conductivity small. Then, it increases as the temperature increases. Next, as the flow speed increases and the magnetic field decreases, the current density drops until a minimum is reached. This minimum current density corresponds to a maximum back-EMF. The current density then rises rapidly toward the exit because the rising temperature causes the conductivity to increase.

TABLE 1

MASS FLOW (g/sec)	ONSET LIMIT CURRENT (kA)	
	NON-EQUILIBRIUM THEORY	EXPERIMENT
3	16.8	16
6	25.2	26

APPENDIX   C

AN INTEGRAL METHOD FOR TWO-TEMPERATURE IONIZING LAMINAR BOUNDARY LAYERS

V. V. Subramaniam*
J. L. Lawless**
Carnegie-Mellon University
Pittsburgh, Pennsylvania 15213

Abstract

An integral method is developed in order to approximately solve the governing equations for a multi-temperature, non-equilibrium ionizing, compressible boundary layer. This method is based on classical momentum and energy integral methods which are used in conjunction with the Howarth-Dorodnitsyn transformation. A novel feature of this method is the separate treatment of the translational or sensible energy equations for each species. As an illustrative example, this method is applied to the problem of a shock-generated ionizing argon boundary layer on a flat surface at a uniform temperature. Reasonable agreement for this case is found between this approximate theory and existing experimental and numerical results.

*currently Post-Doctoral Scholar, Mechanical Engineering, Ohio State University, Columbus, Ohio 43210-1107

**currently Senior Physicist, Space Power Inc., 1977 Concourse Dr., San Jose, CA 95131.

I. Introduction

Recent research in the development of the National Aerospace Plane has aroused interest in supersonic and hypersonic ionizing boundary layers. A basic understanding of such flows is important for spacecraft reentry problems, interactions between solid surfaces and plasmas (such as in magnetoplasmadynamic thrusters), and possibly hypersonic or supersonic combustion. In addition to including the complications of classical compressible fluid boundary layers, ionizing boundary layers also include the effects of variable transport properties, plasma-wall electrical sheaths, atomic collision processes, chemical reactions, radiation transfer, and electromagnetic fields. The full boundary layer problem including all these effects is so complex that researchers have resorted to limited experimentation , extensive numerical computation, or approximate theories in order to understand and quantify the problem. This paper addresses the development of an integral method, and its contribution lies in the branch of approximate theories. The virtue of integral methods is in their simplicity, ease of implementation, and applicability to a number of situations and over a wide range of parameters.

In this paper, the boundary layer flow of an ionized gas adjacent to a cold flat plate at a constant temperature is discussed, and an approximate method of solution for the complete boundary layer problem is outlined. This theory may be quite easily generalized to other situations such as the flow over an adiabatic flat surface. An ionizing atomic gas (or plasma) generally consists of neutral atoms, ions, and electrons. The ions may be ionized to various degrees depending on the temperature. The ionization process usually takes place when an electron collides with a neutral atom (or ion) and causes a bound electron to be released. The reverse process known as three body recombination occurs when an electron collides with an ion and a third body (usually an electron) and is subsequently captured by the ion. When such a hot gas consisting of neutrals, ions, and electrons flows at high speeds and adjacent to a cold surface, it is often in a state of thermal and chemical non-equilibrium (i.e. electron, ion, and neutral temperatures are different from each other, and the ionization/recombination processes are determined by finite rate kinetics). Near the wall, the electrons are repelled by the negative electrical sheath. Consequently, they suffer elastic collisions with the sheath and retain most of their original kinetic energy. Therefore, the electron temperature does not vary significantly

across the boundary layer. The ions and neutrals on the other hand, exchange energy by colliding with each other and with the wall and therefore their temperatures are expected to vary appreciably across the boundary layer. In the absence of strong electric fields, the ion and neutral temperatures are approximately equal since the two species exchange energy efficiently due to their similar masses. When strong fields are present, the plasma is likely to be a three temperature fluid. In this paper, the case of weak or no electric fields will be considered and consequently the plasma is a two-temperature fluid. However, the method that is outlined herein can be extended to the case of a three-temperature fluid.

Existing work in ionizing boundary layers is either largely numerical, or experimental. A good review of numerical and experimental work on ionizing non-equilibrium boundary layers is given by Liu et al.[1, 2, 3] Ben-Dor et al.[4, 5] have considered plasma boundary layers under the assumption of frozen flow (i.e. zero ionization rate) . Though the assumption of frozen flow may be applicable in some situations, the more important problem of a reacting plasma boundary layer must be treated. The method presented in this paper is capable of handling a reacting plasma, and thus the frozen flow simply appears as a special case in this theory.

In this paper, a technique that uses integral methods will be outlined for a two-temperature plasma boundary layer in order to obtain an approximate solution. A review of the historical background of integral methods is given by Schlichting[6] and more recently by Subramaniam[7]. The proposed method may be summarized as follows. The conservation of mass and momentum are written for the combined two-temperature multi-species plasma, which are identical to the corresponding equations of classical boundary layer theory. However, instead of considering an energy equation for the combined fluid, we propose that separate equations for the transport of translational energy for each of the species be derived. These will be referred to in this paper as the species sensible energy equations. Finally, rate equations will be derived, describing any chemical processes that may occur in the plasma (such as ionization and recombination). We then propose applying integral methods to the above described set of equations, and seek polynomial expansions for the variables of interest (velocity, temperatures, and number densities) in terms of a transformed Howarth-Dorodnitsyn coordinate. This proposed method differs from other integral methods in two important respects that are responsible for its success in the case of

a compressible, ionizing, two-temperature plasma near a cold wall. The first is that the energy equations describing the transport of each mode of energy storage for each species is considered separately. The second is that self-similar solutions are sought in terms of a transformed Howarth-Dorodnitsyn coordinate.

Starting with non-equilibrium kinetic theory, the governing equations for a laminar, compressible, two-temperature boundary layer are derived in section II. Following some simplifying assumptions, these equations are rewritten in section III. The integral method is outlined in detail in section IV, and an illustrative example of a two-temperature ionizing boundary layer in argon generated by a shock wave is given in section V. A comparison with an existing numerical solution for a shock-generated ionizing argon boundary layer is also given in section V, and the contributions of this paper are summarized in section VI.

II. Governing Equations

For the purposes of this discussion, consider a monatomic gas that is partially ionized. In general, there may be external forces such as those caused by electric and magnetic fields. However, here we will consider no such external forces. If f_a is the distribution function for a species a, then the transport equation (Boltzmann equation) in cartesian tensor form is[1]:

$$\frac{\partial f_a}{\partial t} + C_i^{\ a} \frac{\partial f_a}{\partial x_i} + J_a = 0 \tag{1}$$

where x_i is the ith coordinate, t is time, $C_i^{\ a}$ is the ith component of the absolute velocity of a particle of species a, and J_a is the collision term. Before the macroscopic equations are derived, it is necessary to define the following :

$$v_i^{\ a} = C_i^{\ a} - c_{oi} \tag{2}$$

$$c_{oi} = \frac{1}{\rho} \sum_{a=1}^{3} \rho_a C_i^{\ a} \tag{3}$$

$$\rho = \sum_{a=1}^{3} \rho_a = \sum_{a=1}^{3} m_a n_a \tag{4}$$

$$n_a = \int f_a \, dC_i^a \tag{5}$$

$$<Q_j^a> = \frac{1}{n_a} \int f_a Q_j^a \, dC_i^a \tag{6}$$

where v_i^a is the ith component of the peculiar velocity of species a, c_{oi} is the local average mass velocity of the gas, ρ is the mass density, m_a is the mass of species a, n_a is the number density of species a, and $<Q_j^a>$ is the average over the distribution function of the jth component of a quantity Q of species a. In equation (1), the distribution function for species a is a function of x_i, C_i^a, and t. In order to correspond to macroscopic description, we must transform to a new coordinate system where the distribution function is a function of x_i, $v_i^a(x_i,t)$, and t. Therefore, using (2) we may rewrite (1) as :

$$\frac{Df_a}{Dt} + v_i^a \frac{\partial f_a}{\partial x_i} - \frac{Dc_{oi}}{Dt} \frac{\partial f_a}{\partial v_i^a} - v_i^a \frac{\partial c_{ok}}{\partial x_i} \frac{\partial f_a}{\partial v_k^a} + J_a = 0 \tag{7}$$

where

$$\frac{D}{Dt} = \frac{\partial}{\partial t} + c_{oi} \frac{\partial}{\partial x_i}$$

The conservation of mass for the ionizing plasma is obtained by multiplying (7) by unity, integrating over velocity space, and summing over a (i.e. summing each equation for the electrons, ions, and neutrals). This gives the well known classical compressible flow conservation of mass :

$$\frac{\partial \rho}{\partial t} + \frac{\partial}{\partial x_i} (\rho c_{oi}) = 0 \tag{8}$$

The conservation of momentum for the ionizing plasma is obtained by multiplying (7) by $m_a v_i^a$, integrating with respect to dC_1^a, and summing over a. This gives the classical conservation of momentum for a fluid :

$$\rho \frac{Dc_{oi}}{Dt} = -\frac{\partial \Pi_{ik}}{\partial x_k} \tag{9}$$

where the stress tensor is given by

$$\Pi_{ik} = \sum_{a=1}^{3} \Pi^a_{ik} = \sum_{a=1}^{3} n_a m_a <v_i^a v_k^a>$$

The development presented thus far is well known and not new. However, it is in the following treatment of the conservation of energy and species continuity equations that the present method will differ from already existing methods. The conservation of translational energy for each species a may be derived by multiplying (7) by $m_a v_a^2 / 2$ and integrating over velocity space. For the electrons this gives :

$$\frac{3}{2} k n_e \frac{DT_e}{Dt} + \frac{\partial q_i^e}{\partial x_i} + \Pi_{ik}^e \frac{\partial c_{oi}}{\partial x_k} = \frac{3}{2} kT_e \frac{\partial}{\partial x_i} \left(n_e <v_i^e> \right) - m_e n_e <v_i^e> \frac{Dc_{oi}}{Dt} - Q_e \tag{10}$$

where $\Pi_{ik}^e = m_e n_e <v_i^e v_k^e>$, $q_i^e = m_e n_e <v_a^2 v_i^e>/2$ is the heat flux, T_e is the electron temperature, k is Boltzmann's constant, and Q_e is the energy exchange between the electrons and other species. This Q_e may include both elastic and inelastic collisions. In a similar fashion, we may derive the energy equations for the neutrals and single ions. When strong electromagnetic fields are present, the ion and neutral translational energy equations must be treated separately. In the absence of strong electric fields, the neutrals and single ions may be assumed to have the same translational temperature T_H because of their similar masses. Then, adding the energy equations for the ions and neutrals gives the following heavy particle sensible (or translational) energy

equation :

$$\frac{3}{2}k(n_e + n_A)\frac{DT_H}{Dt} + \frac{\partial}{\partial x_i}(q_i^{atom} + q_i^{ion}) + \left(\Pi_{ik}^{ion} + \Pi_{ik}^{atom}\right)\frac{\partial c_{oi}}{\partial x_k}$$

$$= \frac{3}{2}kT_H\frac{\partial}{\partial x_i}\left(n_e<v_i^{ion}> + n_A<v_i^{atom}>\right)$$

$$- \left(m_{ion}n_e<v_i^{ion}> + m_A n_A<v_i^{atom}>\right)\frac{Dc_{oi}}{Dt} - Q_{ion} - Q_{atom} \qquad (11)$$

where Q_{ion} and Q_{atom} represent the energy exchange between the ions and other species, and between the neutrals and other species respectively. From the definition of a plasma, it has been assumed in (11) that any deviations from electrical quasi-neutrality are confined to dimensions of the order of the Debye length which is smaller than any macroscopic dimension. This means that the ion number density and electron number density are equal ($n_{ion} \approx n_e$).

A transport equation for each species a is obtained by integrating (7) over velocity space :

$$\frac{Dn_a}{Dt} + n_a\frac{\partial c_{oi}}{\partial x_i} + \frac{\partial}{\partial x_i}\left(n_a<v_i^a>\right) = \dot{n}_a \qquad (12)$$

where $\dot{n}_a$ is the net production of species a due to inelastic collisions resulting in chemical reaction (i.e. ionization and recombination in the case of a plasma). Equation (12) is the familiar species conservation equation which appears in classical chemically reacting flow theory[9].

The equations (10) and (11) are conservation equations for the transport of sensible or translational energy. Similar equations may be derived using this same procedure for other internal modes (i.e. electronic excitation or vibrational and rotational energies in the case of a molecular gas). However, if inelastic collisions are important, then there will be a more complex coupling between the various energy equations since energy may be exchanged between the many modes. For the purposes of illustration however, only elastic collisions will be considered in the

sensible energy equations and excited electronic states for the neutral atom and the single ion will not be considered. In the following section, the conservation equations will be simplified for the case of a boundary layer adjacent to a cold wall.

III. Simplified Boundary Layer Equations

The system of equations (8) through (12) is incomplete without the specification of the stress tensor $\Pi_{ik}{}^a$ and the heat flux vector $q_i{}^a$. In order to compute these quantities however, more information is needed about the distribution function f_a. By assuming that the distribution function is locally not too different from the Maxwell-Boltzmann distribution function, equation (7) may be solved by using perturbation theory in a fashion similar to the Chapman-Enskog expansion. The resulting expressions for $\Pi_{ik}{}^a$ and $q_i{}^a$ are summarized by Kalikhman[8].

The governing equations for a steady, laminar, two-dimensional, and two-temperature boundary layer may be written using equations (8) through (12) as[7]:

$$\frac{\partial(\rho u)}{\partial x} + \frac{\partial(\rho v)}{\partial y} = 0 \qquad (13)$$

where u is the component of the local mass average velocity in the x-direction or flow direction, and v is the y-component or transverse component. Conservation of x-momentum is given by

$$\rho u \frac{\partial u}{\partial x} + \rho v \frac{\partial u}{\partial y} = -\frac{\partial P}{\partial x} + \frac{\partial}{\partial y}\left(\eta_H \frac{\partial u}{\partial y}\right) \qquad (14)$$

and y-momentum is given by

$$\frac{\partial P}{\partial y} = 0 \qquad (15)$$

where P is the pressure and $\eta_H = \eta^{ion} + \eta^{atom}$ is the heavy particle dynamic viscosity. Considering

elastic collisions only, the energy equations for the translational mode are

$$\frac{3}{2} k n_e u_i \frac{\partial T_e}{\partial x_i} + \frac{\partial q_i^e}{\partial x_i} + \Pi_{ij}^e \frac{\partial u_i}{\partial x_j} = \frac{3}{2} k T_e \frac{\partial}{\partial x_i} \left(n_e U_i^e \right) - m_e n_e U_i^e u_k \frac{\partial u_i}{\partial x_k}$$
$$- \frac{3 m_e}{m_A} k n_e < v_{eH} > (T_e - T_H) \tag{16}$$

$$\frac{3}{2} k (n_e + n_A) u_i \frac{\partial T_H}{\partial x_i} + \frac{\partial}{\partial x_i} (q_i^{atom} + q_i^{ion}) + \left(\Pi_{ij}^{ion} + \Pi_{ij}^{atom} \right) \frac{\partial u_i}{\partial x_j}$$
$$= \frac{3}{2} k T_H \frac{\partial}{\partial x_i} \left(n_e U_i^{ion} + n_A U_i^{atom} \right)$$
$$- (m_{ion} n_e U_i^{ion} + m_A n_A U_i^{atom}) u_k \frac{\partial u_i}{\partial x_k}$$
$$+ \frac{3 m_e}{m_A} k n_e < v_{eH} > (T_e - T_H) \tag{17}$$

where repeated subscripts imply summation from 1 to 2 or over x and y, and $<v_{eH}>$ is the energy-weighted average momentum transfer elastic collision frequency between an electron and a heavy particle[10]. The species or rate equation reduces to

$$\rho u \frac{\partial a}{\partial x} + \rho v \frac{\partial a}{\partial y} + \frac{\partial}{\partial y} (m_A n_e V_{ion}) = \dot{n}_{ion} \tag{18}$$

where $a = n_e / (n_e + n_A)$ is the ionization fraction, V_{ion} is the transverse or y-component of the ion diffusion velocity, and axial diffusion is neglected.

The assumption of a two-temperature plasma was justified physically in section 1. This assumption may be quantified by comparing the heat conduction (contained in the second term on the left hand side of (16)) with the energy transfer by elastic collisions (third term on the right hand side of (16))[7]:

$$\frac{L_c^2}{\delta_T^2} \gg \frac{m_e}{m_A} \qquad (19)$$

where L_c is the electron mean free path and δ_T is the characteristic boundary layer thickness. It is also clear that for a continuum approximation to be valid, L_c must be much smaller than δ_T. Hence,

$$\left(\frac{m_e}{m_A}\right)^{1/2} \ll \left(\frac{L_c}{\delta_T}\right) \ll 1 \qquad (20)$$

With some additional simplifications and manipulations[7], equations (13) through (18) become :

Mass:

$$\frac{\partial(\rho u)}{\partial x} + \frac{\partial(\rho v)}{\partial y} = 0 \qquad (21)$$

Momentum:

$$\rho u \frac{\partial u}{\partial x} + \rho v \frac{\partial u}{\partial y} = -\frac{dP_\infty}{dx} + \frac{\partial}{\partial y}\left(\eta_H \frac{\partial u}{\partial y}\right) \qquad (22)$$

where P_∞ is the pressure in the free stream, outside the boundary layer;

Electron sensible energy:

$$\frac{\partial}{\partial y}\left(\lambda^{ec} \frac{\partial T_e}{\partial y} + \frac{5}{2} n_e k T_e V_e\right) \approx 0 \qquad (23)$$

where $\lambda^{\alpha\beta}$ is the thermal conductivity due to collisions between species α and β, and V_e is the transverse or y-component of the electron diffusion velocity. The heavy particle translational energy equation (17) may be combined with the momentum equation to give

Heavy particle sensible energy:

$$
\rho u \frac{\partial}{\partial x} \left(\frac{5kT_H}{2m_A} + \frac{u^2}{2} \right) + \rho v \frac{\partial}{\partial y} \left(\frac{5kT_H}{2m_A} + \frac{u^2}{2} \right)
$$
$$
- \frac{\partial}{\partial y} \left(\lambda_H \frac{\partial T_H}{\partial y} + (\lambda^{ie} + \lambda^{ae}) \frac{\partial T_e}{\partial y} + \eta_H \frac{\partial}{\partial y} (u^2/2) \right)
$$
$$
= 3 \left(\frac{m_e}{m_A} \right) kn_e < \nu_{eH} > (T_e - T_H) \tag{24}
$$

where $\lambda_H = \lambda^{ii} + \lambda^{ai}$ with λ^{ii} due to ion-ion collisions and λ^{ai} due to neutral-ion collisions. Assuming ionization and recombination according to the following process

$$
A + e === A^+ + e + e
$$
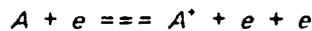
the rate equation (18) becomes

rate:

$$
\rho u \frac{\partial a}{\partial x} + \rho v \frac{\partial a}{\partial y} + \frac{\partial}{\partial y} (m_A n_e V_{ion}) = \frac{k_f a(1-a)\rho^2}{m_A} - \frac{k_b a^3 \rho^3}{m_A^2} \tag{25}
$$

where k_f is the ionization rate constant and k_b is the recombination rate constant. From a regular perturbation solution to (7), it can be shown that the ion and electron transverse diffusion velocities are given by[a]:

$$
V_e \approx -\frac{D_e}{n_e} \frac{\partial n_e}{\partial y}
$$

and

$$V_{ion} \approx -\frac{D_{ion}}{n_e}\frac{\partial n_e}{\partial y}$$

where D_e is the electron diffusion coefficient and D_{ion} is the ion diffusion coefficient.

A significant portion of this paper has been devoted to the derivation of the governing equations of an ionizing boundary layer. This has been done specifically in order to show that an essential feature of this approximate method, is the separate treatment of the translational energies of each specie instead of considering an overall energy equation for the ionizing plasma. In the next section, an approximate method of solution will be outlined.

IV. An Approximate Method

The proposed method consists of (a) integrating the system of equations (21) through (25) from the wall to the boundary layer edge; (b) applying the Howarth-Dorodnitsyn transformation; and (c) assuming polynomial forms for the dependent variables in terms of the transformed transverse coordinates ξ_i. This procedure reduces (21) through (25) to a system of ordinary differential equations that may then be integrated numerically. Numerical integration of ordinary differential equations is enormously easier than the numerical solution of the set of partial differential equations (21) through (25).

There are certain constraints that the quantities u, T_e, T_H, and a must obey. These are that $u=u_s$ at the wall ($y=0$) where u_s is the velocity slip; $u=u_\infty$ and $\partial u/\partial y = 0$ at the edge of the boundary layer; $T_e=T_{es}$ and $T_H=T_{Hs}$ at the wall where T_{es} and T_{Hs} are the electron and heavy particle temperature slip respectively; $T_e=T_H=T_\infty$ and $\partial T_H/\partial y = \partial T_e/\partial y = 0$ at the boundary layer edge; $a=a_w$ at the wall where a_w is the ionization slip; and $a=a_\infty$ and $\partial a/\partial y = 0$ at the boundary layer edge where a_∞ is the free stream ionization fraction. One may also require that the respective second derivatives be zero at the edge of the boundary layer in order to ensure that the solution is smooth. The aforementioned constraints dictate the minimum order of the chosen polynomials. For instance, the three constraints on the heavy particle temperature profile together

with the requirement that this profile satisfy equation (24) dictates that the heavy particle temperature profile is approximated by at least a cubic. Profiles for the outer variables may be chosen in a similar manner. It is possible to arrive at the minimum order of the polynomials by physical considerations. For instance, examination of equation (24) shows the presence of two opposing effects. These are viscous dissipation which tends to raise the temperature, and heat transfer to the relatively cold wall which tends to lower it. Consequently, an extremum value of the temperature may occur somewhere inside the boundary layer, and $\partial T_H/\partial y = 0$ at this location. However, $\partial T_H/\partial y$ must be zero at the boundary layer edge also, indicating that $\partial T_H/\partial y$ must be at least quadratic which means that T_H must be at least a cubic. Furthermore, it is necessary that the assumed polynomial forms be taken in terms of a transformed transverse coordinate ζ defined by

$$\zeta_i = \frac{\displaystyle\int_0^y \frac{\rho}{\rho_\infty}\,dy}{\displaystyle\int_0^{\delta_i} \frac{\rho}{\rho_\infty}\,dy} = \frac{1}{\Delta_i}\int_0^y \frac{\rho}{\rho_\infty}\,dy \qquad (26)$$

where $\Delta_i = \int_0^{\delta_i} \rho/\rho_\infty\,dy$ for $i = 1,2,3,4$, ρ_∞ is the free-stream mass density, and δ_i ($i = 1,2,3,4$) are the thicknesses of the boundary layers (velocity, electron temperature, heavy particle temperature, and concentration). The variables ζ_i (also for $i = 1,2,3,4$) are called Howarth-Dorodnitsyn coordinates because equation (26) closely resembles the Howarth-Dorodnitsyn transformation of classical compressible boundary layer theory.[9, 11]

The assumption of cubic profiles for u, T_e, T_H, and α yields four unknown coefficients for each variable. However, using the set of three constraints described earlier the number of unkowns reduces to one for each variable. In addition to these unknowns, we have ρ, v, the velocity boundary layer thickness δ_1, the electron thermal boundary layer thickness δ_2, the heavy particle thermal boundary layer thickness δ_3, and the ionization boundary layer thickness δ_4. The thicknesses δ_1, δ_2, δ_3, and δ_4 are the transverse distances away from the wall where $u = u_\infty$, $T_e = T_\infty$, $T_H = T_\infty$, and $\alpha = \alpha_\infty$. In addition to the five equations (21) through (25), we have

the following equation

$$P_\infty \approx P = \frac{\rho k}{m_A}(aT_c + T_H) \tag{27}$$

which is obtained by combining an equation of state $P(\rho, a, T_c, T_H)$ with equation (15). Therefore, there are a total of ten unknowns in the six equations (21), (22), (23), (24), (25), and (27). The remaining four equations may be obtained by :

multiplying equation (22) by u. (28)

multiplying equation (23) by T_c. (29)

multiplying equation (24) by $\left(\dfrac{5kT_H}{2m_A} + \dfrac{u^2}{2}\right)$. (30)

multiplying equation (25) by a. (31)

In this manner, enough equations are generated for the ten unknowns.

In summary, the integral method may be outlined as follows. (a) Integrate equation (21) from $y = 0$ to $y = \delta_1$. This gives v at $y = \delta_1$; (b) Integrate (22) and (28) from $y = 0$ to $y = \delta_1$, eliminating $v(y=\delta_1)$ using the result of (a); (c) Integrate (23) and (29) from $y = 0$ to $y = \delta_1$, eliminating $v(y=\delta_1)$ using the result of (a); (d) Integrate (24) and (30) from $y = 0$ to $y = \delta_1$, eliminating $v(y=\delta_1)$ using the result of (a); (e) Integrate (25) and (31) from $y = 0$ to $y = \delta_1$, eliminating $v(y=\delta_1)$ using the result of (a); (f) Assume cubic profiles for u, T_c, T_H, and a in terms of the variables ξ_1, ξ_2, ξ_3, ξ_4 defined by equation (26); (g) Apply the constraints discussed earlier in this section so as to leave only one undetermined coefficient for each variable; (h) Using the assumed polynomial forms, evaluate the integrals in (b) through (e) and express them in terms of the unknown coefficients.

Following the above procedure will result in nine first order quasi-linear ordinary

differential equations (including equation (27)) in the nine unknowns consisting of ρ, Δ_1, Δ_2, Δ_3, Δ_4, and the unknown coefficients for u, T_e, T_H, and α. This system can then be integrated numerically relatively easily using the stiff methods of Gear[12]. The next section will illustrate this procedure for the example of the ionizing argon boundary layer studied by Liu et al.[1]

V. An Illustrative Example

In this section, we consider a shock-generated ionizing boundary layer over a flat surface. The free stream is assumed to be constant, in order to be consistent with the assumptions of Liu et al.[1] We will begin by making some additional simplifications. The electron energy equation (23) will be replaced by

$$T_e \approx T_\infty \tag{32}$$

where T_∞ is the free stream temperature (the free stream is a single temperature plasma). This assumption is quite easily justified. The electrons being negative, are repelled by the electrical sheath at the wall and consequently retain their original kinetic energy (surfaces immersed in a plasma are bombarded by the greater random thermal flux of electrons and are thus enveloped by a negative charge layer). Therefore, the electron temperature is not expected to vary very much across the boundary layer. Next, only elastic collisions will be considered and radiation will be neglected (it should be pointed out however that Liu et al.[1] have partially considered plasma radiation in their numerical solution). Additionally, the velocity slip and temperature slip at the wall will be ignored. This means that $u_s = 0$ and $T_{Hs} = T_w$. As a final simplification, we will assume for illustrative purposes that all the boundary layer thicknesses are equal (i.e. $\delta_1 = \delta_2 = \delta_3 = \delta_4 = \delta_T$).

Following the procedure outlined in the previous section, for the case of constant free stream quantities considered by Liu et al.[1] the integro-differential equations are:

$$\frac{d\Theta}{dx} = \frac{\tau_w}{\rho_\infty u_\infty^2} \tag{33}$$

where τ_w is the wall shear defined by

$$\tau_w = \left(\eta_H \frac{\partial u}{\partial y} \right)_{y=0} \tag{34}$$

Θ is the momentum thickness defined by

$$\Theta = \int_0^{\delta_T} \frac{\rho u}{\rho_\infty u_\infty} \left(1 - \frac{u}{u_\infty} \right) dy \tag{35}$$

and the subscript ∞ refers to free stream quantities. Integration of the heavy particle sensible energy equation gives:

$$\frac{d\Theta_H}{dx} = \frac{q_{wH}}{\rho_\infty u_\infty (C_{pa} T_\infty + u_\infty^2/2)}$$
$$+ \frac{3 m_e k a_\infty}{m_A^2 u_\infty (C_{pa} T_\infty + u_\infty^2/2)} \int_0^{\delta_T} \frac{\rho a}{\rho_\infty a_\infty} < \nu_{eH} > (T_\infty - T_H) \, dy \tag{36}$$

where Θ_H is the enthalpy thickness defined by

$$\Theta_H = \int_0^{\delta_T} \frac{\rho u}{\rho_\infty u_\infty} \left(\frac{C_{pa} T_H + u^2/2}{C_{pa} T_\infty + u_\infty^2/2} - 1 \right) dy \tag{37}$$

where $C_{pa} = 5k/2m_A$ is the specific heat, and q_{wH} is the heavy particle conductive wall heat flux given by

$$q_{wH} = -\left(\lambda_H \frac{\partial T_H}{\partial y} \right)_{y=0} \tag{38}$$

The integrated rate equation gives:

$$\frac{dI^*}{dx} - \frac{m_A}{\rho_\infty u_\infty a_\infty}(n_{cw}V_{iw}) = \frac{a_\infty k_i \rho_\infty}{m_A u_\infty}\int_0^{\delta_T}\frac{a}{a_\infty}\left(\frac{1}{a_\infty}-\frac{a}{a_\infty}\right)\frac{\rho^2}{\rho_\infty{}^2}dy$$

$$-\frac{k_b a_\infty{}^2 \rho_\infty{}^2}{m_A{}^2 u_\infty}\int_0^{\delta_T}\frac{a^3\rho^3}{a_\infty{}^3\rho_\infty{}^3}dy \qquad (39)$$

where I^* is the ionization thickness defined by:

$$I^* = \int_0^{\delta_T}\frac{\rho u}{\rho_\infty u_\infty}\left(\frac{a}{a_\infty}-1\right)dy \qquad (40)$$

and n_{cw} and V_{iw} are the number density and transverse diffusion velocity of the ions evaluated at the wall. An expression for V_{ion} was given in section III.

The ionization slip a_w from which n_{cw} may be obtained, must be supplied in order to solve equation (39). This is obtained by considering the edge of the boundary layer near the wall. In this region is a collisionless layer known as the Knudsen layer where all the slip in the various quantities is confined. Thus, by setting the macroscopic diffusive ion flux (from the continuum boundary layer side) equal to the random thermal flux of ions (from the rarefied Knudsen layer side), we get :

$$D_w{}^{ion}\left(\frac{\partial n_c}{\partial y}\right)_{y=0} = \frac{n_{cw}<C_H>}{4} \qquad (41)$$

where $D_w{}^{ion}$ is the ion diffusion coefficient evaluated at the wall, and C_H is the heavy particle mean thermal speed at the wall. Next, if

$$\xi = \frac{1}{\Delta}\int_0^y\frac{\rho}{\rho_\infty}dy \qquad (42)$$

where

$$\Delta = \int_0^{\delta_T} \frac{\rho}{\rho_\infty} d\gamma$$

then (35) reduces to

$$\frac{\Theta}{\Delta} = \int_0^1 \frac{u}{u_\infty} \left(1 - \frac{u}{u_\infty} \right) d\xi \tag{43}$$

and similarly, the other quantities that appear in terms of derivatives of y or in terms of integrals over y may be transformed into derivatives and integrals in ξ. Before these various integrals are evaluated, polynomial forms are assumed for the variation of the velocity, heavy particle temperature, and the ionization fraction across the boundary layer. For the purposes of illustration, we will assume that the velocity is quadratic in ξ and is therefore completely determined by the constraints $u = 0$ at $\xi = 0$, $u = u_\infty$ at $\xi = 1$, and $\partial u / \partial \xi = 0$ at $\xi = 1$:

$$\frac{u}{u_\infty} = 2\xi - \xi^2 \tag{44}$$

Similarly, assuming cubic profiles and using the constraints $T_H = T_w$ at $\xi = 0$, $T_H = T_\infty$ at $\xi = 1$, $\partial T_H / \partial \xi = 0$ at $\xi = 1$, $a = a_w$ at $\xi = 0$, $a = a_\infty$ at $\xi = 1$, and $\partial a / \partial \xi = 0$ at $\xi = 1$ gives

$$\frac{T_H}{T_\infty} = \frac{T_w}{T_\infty} + \left(2 - \frac{2T_w}{T_\infty} + b_4 \right) \xi + \left(\frac{T_w}{T_\infty} - 1 - 2b_4 \right) \xi^2 + b_4 \xi^3 \tag{45}$$

and

$$\frac{a}{a_\infty} = \frac{a_w}{a_\infty} + \left(2 - \frac{2a_w}{a_\infty} + c_4 \right) \xi + \left(\frac{a_w}{a_\infty} - 1 - 2c_4 \right) \xi^2 + c_4 \xi^3 \tag{46}$$

where b_4 and c_4 are coefficients yet to be determined. With these polynomial forms, the integrated form of the momentum equation (33) is a differential equation for Δ, the integrated form of the energy equation (36) is a differential equation for the unknown coefficient b_4, and the integrated form of the rate equation (39) is a differential equation for the coefficient c_4. Thus, the original system of non-linear partial differential equations are reduced to a system of quasi-linear ordinary differential equations. To complete the formulation, conditions must be prescribed at $\zeta = 0$, the leading edge of the boundary layer. These are that the thicknesses Δ, Θ, Θ_H, and I^* are zero at the leading edge. This gives $c_4 = 1$ and $b_4 = 1 - (T_w/T_\infty)$ at the leading edge. These approximate equations describing the ionizing boundary layer flow considered by Liu et al.[1] are then solved by using the stiff methods of Gear[12].

The case chosen here is that labeled as "case 1" by Liu et al.[1] where the free stream conditions are $\rho_\infty = 0.125 \; Kg/m^3$, $u_\infty = 4860 \; m/s$, $T_\infty = 10490 \; °K$, $a_\infty = 0.021$, and the surface is 14 cm. long. The transport properties, cross sections, and rate constants are those given by Liu et al.[1] The results of the present calculation are summarized in Fig. 1 through Fig. 4. The boundary layer thickness as a function of distance is shown in Fig. 1, and this computed thickness is less than twice the thicknesses computed by Liu et al.'s finite difference scheme. In view of the approximations that have been made in this illustrative example (i.e. all the boundary layer thicknesses are equal; radiative heat transfer is neglected; and temperature slip at the wall is neglected), the predictions using the present integral method seem quite reasonable. A major factor influencing the accuracy of the results is the precise knowledge of the wall surface temperature. Since there is bound to be some heating, the temperature at the wall edge of the boundary layer should be significantly higher than the initial wall temperature of $296 \, °K$ which has been used in the present calculation. This should therefore lead to a lower mass density and a lower electron number density near the wall, than those predicted here. The ionization fraction non-dimensionalized by the free stream ionization fraction versus distance across the boundary layer at an axial position of 14 cm. downstream from the leading edge is shown in Fig. 2. Also shown in this figure are the measured data of Liu et al.[1] Interestingly enough, a slight bulge is present in our approximate solution which was observed in the experimental data and which did not appear in the numerical results of Liu et al. The bulge is

characteristic of the opposing effects of ionization and recombination in the boundary layer. The high electron temperature tends to ionize the plasma while the presence of the cold wall drives the plasma to recombine. Consequently, the ionization fraction profile achieves its maximum somewhere inside the boundary layer. Finally, it is worth noting that the numerical computations of Liu et al.[1] exhibit a weakly varying electron temperature across the boundary layer, in accord with the assumption given by equation (32). Since the purpose of boundary layer analysis is to estimate the heat transfer to the wall and to estimate the viscous drag, these cannot go without mention. Fig. 3 and Fig. 4 show the variation of the heavy particle conductive wall heat flux and the variation of the wall shear versus distance downstream from the leading edge. These exhibit classical behaviour, being large near the leading edge where the boundary layer thickness is small and decreasing with increasing boundary layer thickness.

This section has focused on an example that illustrates the integral method described in section IV. The results obtained with relative quickness and ease, compare reasonably well with the numerical computation and experiment of Liu et al.[1] A number of assumptions have been made in this example that may be quite easily removed, and the success of the present method does not depend on these assumptions. For instance, this method is sufficiently robust that plasma radiation could be included as well as unequal boundary layer thicknesses (i.e. $\delta_1 \neq \delta_2 \neq \delta_3 \neq \delta_4 \neq \delta_1$), temperature slip at the wall, velocity slip at the wall, mass injection at the wall, additional chemical reactions, and even electromagnetic effects.

VI. Summary and Conclusions

An integral method has been developed which is capable of handling multi-temperature, multi-specie, ionizing, laminar boundary layers. Effects of plasma radiation and electromagnetics may also be incorporated in the method. A unique feature of the method is the separate treatment of the electrons and heavy particles. The two-temperature ionizing boundary layer equations have been simplified for the example of a shock-generated ionizing argon boundary layer. The simplified equations have been solved using the integral method described in section IV for this case, in order to illustrate this method. This integral method appears to be a powerful tool in providing solutions to the non-equilibrium boundary layer equations relatively easily and quickly. Moreover, the method is sufficiently robust that it can be extended to

incorporate non-equilibrium chemical reactions and electromagnetic effects. It can therefore be used to validate and be an integral part of multidimensional numerical computations.

Several important characteristics of high speed ionizing boundary layers near cold surfaces are evident from the illustrative example of section V. First, the thickness of the boundary layer by virtue of its dependence on the wall shear stress, is significantly affected by the viscosity near the wall. The viscosity depends strongly on the ionization fraction near the wall and may therefore vary considerably[7]. This implies that boundary layers in ionizing channel flows may be appreciably thick and may even merge if the density is low enough. Second, the ionization fraction profile across the boundary layer may exhibit a bulge due to the opposing effects of ionization and recombination. The hot electrons tend to ionize the plasma in the boundary layer, while the cold wall tends to drive the plasma to recombine. A similar behaviour may be observed in the profile for the heavy particle temperature, if the flow speed is high enough[7]. In this case, viscous dissipation in the boundary layer can heat the flow while heat transfer to the wall can cool it. In the specific example of the shock-generated boundary layer considered here, a bulge was not observed in the heavy particle temperature profile.

In spite of the simplicity and elegance of the integral method, a number of weaknesses exist. For instance, the inclusion of excited states for the atom and the ion which is important for the consideration of plasma radiation may render this integral method ineffective. However, useful information may still be obtained using this integral method by considering the plasma to be optically thin or thick. Weaknesses also exist in terms of the boundary conditions for the ionization fraction and heavy particle temperature near the wall, and the neglect of the electrical sheath region near the wall. All four effects could affect the value of the ionization fraction at the boundary layer-Knudsen layer edge near the wall, and consequently affect the viscosity and the boundary layer thickness. Nevertheless, use of this integral method provides a reasonable means of estimating channel entry lengths, heat transfer, and viscous drag for high speed reacting flows. Finally, this method may be most useful for studying the effects of non-equilibrium processes (i.e. rate kinetics) on boundary layer growth, heat transfer, and viscous drag.

22

References

1. W. S. Liu, B. T. Whitten, and I. I. Glass, "Ionizing argon boundary layers. Part 1. Quasi-steady flat-plate laminar boundary-layer flows," *J. Fluid Mech.*, Vol. 87, No. 4, 1978, pp. 609-642. .

2. W. S. Liu and I. I. Glass, "Ionizing argon boundary layers. Part 2. Shock-tube side-wall boundary-layer flows," *J. Fluid Mech.*, Vol. 91, No. 4, 1979, pp. 679-696. .

3. W. S. Liu, K. Takayama, and I. I. Glass, "Coupled interactions of shock-wave structure with laminar boundary layers in ionizing-argon flows," *J. Fluid Mech.*, Vol. 97, No. 3, 1980, pp. 513-530. .

4. G. Ben-Dor, Z. Rakib, and O. Igra, "Frozen Plasma Boundary-Layer Flows over Isothermal Flat Plates-Parametric Study," *AIAA Journal*, Vol. 22, No. 2, February 1984, pp. 299-301. .

5. G. Ben-Dor, Z. Rakib, and O. Igra, "Frozen-Plasma Boundary-Layer Flows over Adiabatic Flat Plates," *AIAA Journal*, Vol. 22, No. 7, July 1984, pp. 1005-1007. .

6. H. Schlichting, *Boundary-Layer Theory*, McGraw-Hill,Inc., New York, NY, 1968.

7. V. V. Subramaniam, *On the Phenomenon of Onset in Magnetoplasmadynamic Thrusters*, PhD dissertation, Carnegie-Mellon University, August 1986.

8. L. E. Kalikhman, *Elements of Magnetogasdynamics*, W. B. Saunders Co., Philadelphia, PA, 1967.

9. F. A. Williams, *Combustion Theory*, Addison-Wesley, 1965.

10. M. Mitchner and C.H. Kruger, Jr., *Partially Ionized Gases*, John Wiley & Sons, New York, 1973.

11. F. D. Hains, "Heat Transfer and Skin Friction in Magneto-Gas Dynamic Channel Flow," Tech. report D1-82-0047, No. 26, Boeing Scientific Research Laboratories, May 1960.

12. C. W. Gear, *Numerical Initial Value Problems in Ordinary Differential Equations*, Prentice-Hall, Englewood Cliffs, New Jersey, 1971.

Fig. 1: Boundary layer thickness versus distance.

Fig. 2: The ionization fraction non-dimensionalized by its free stream value is shown here versus transverse distance, at an axial location of 14 cm. The scattered data are the experimental values of Liu *et al.*[1]

Fig. 3: Heavy particle conductive wall heat flux versus distance.

Fig. 4: Wall shear stress versus distance.
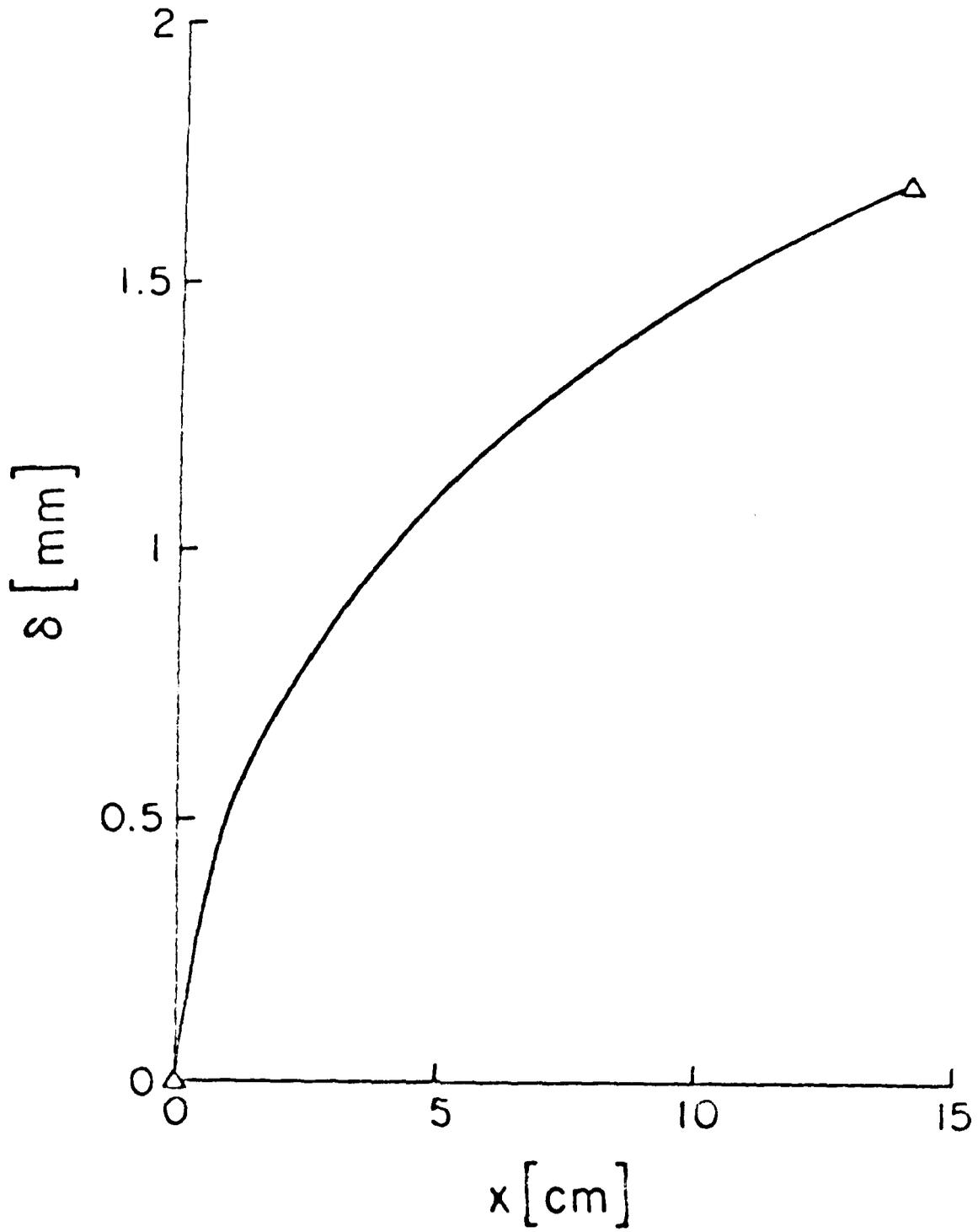
FIG. 1
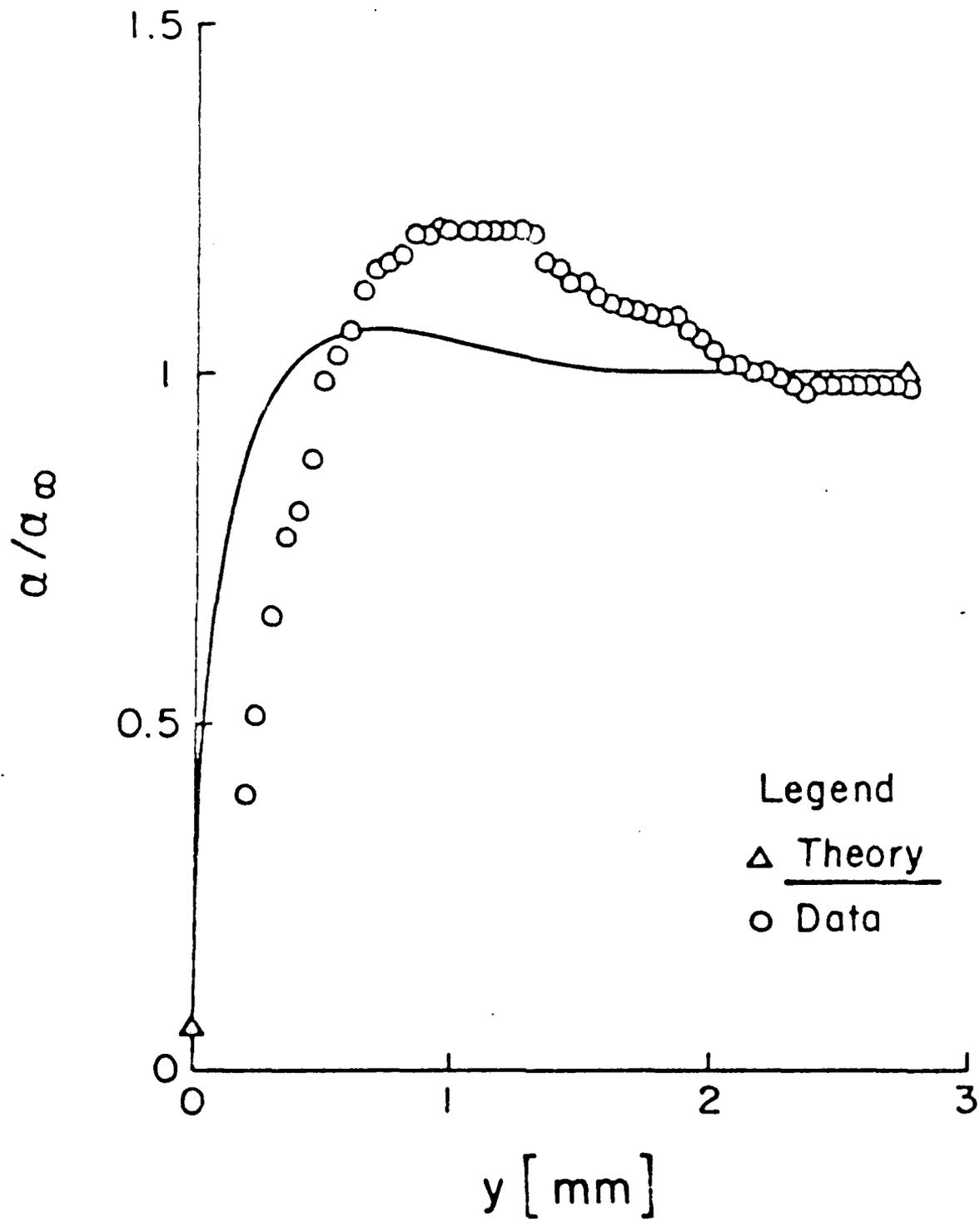
FIG. 2:
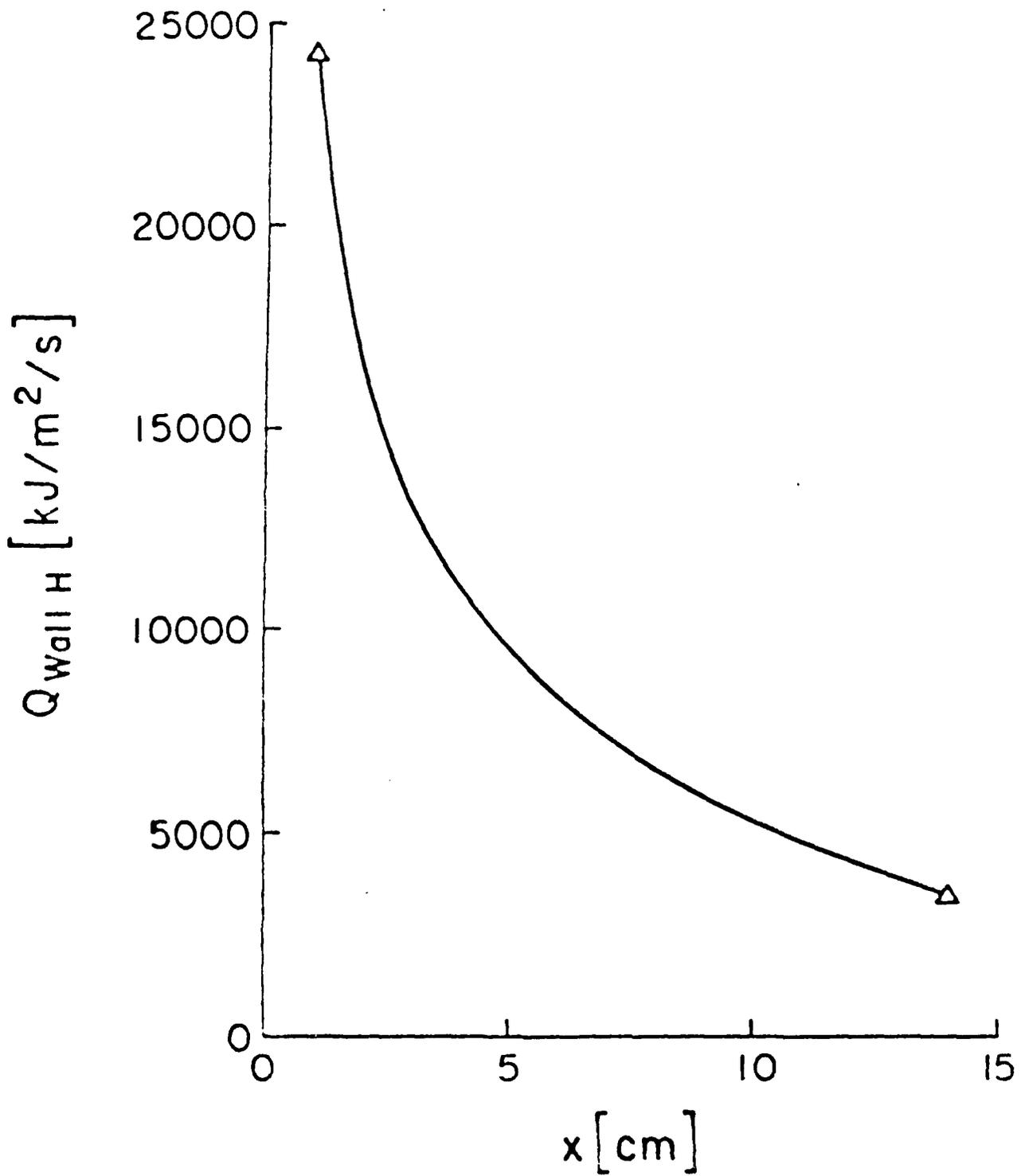
FIG. 3:
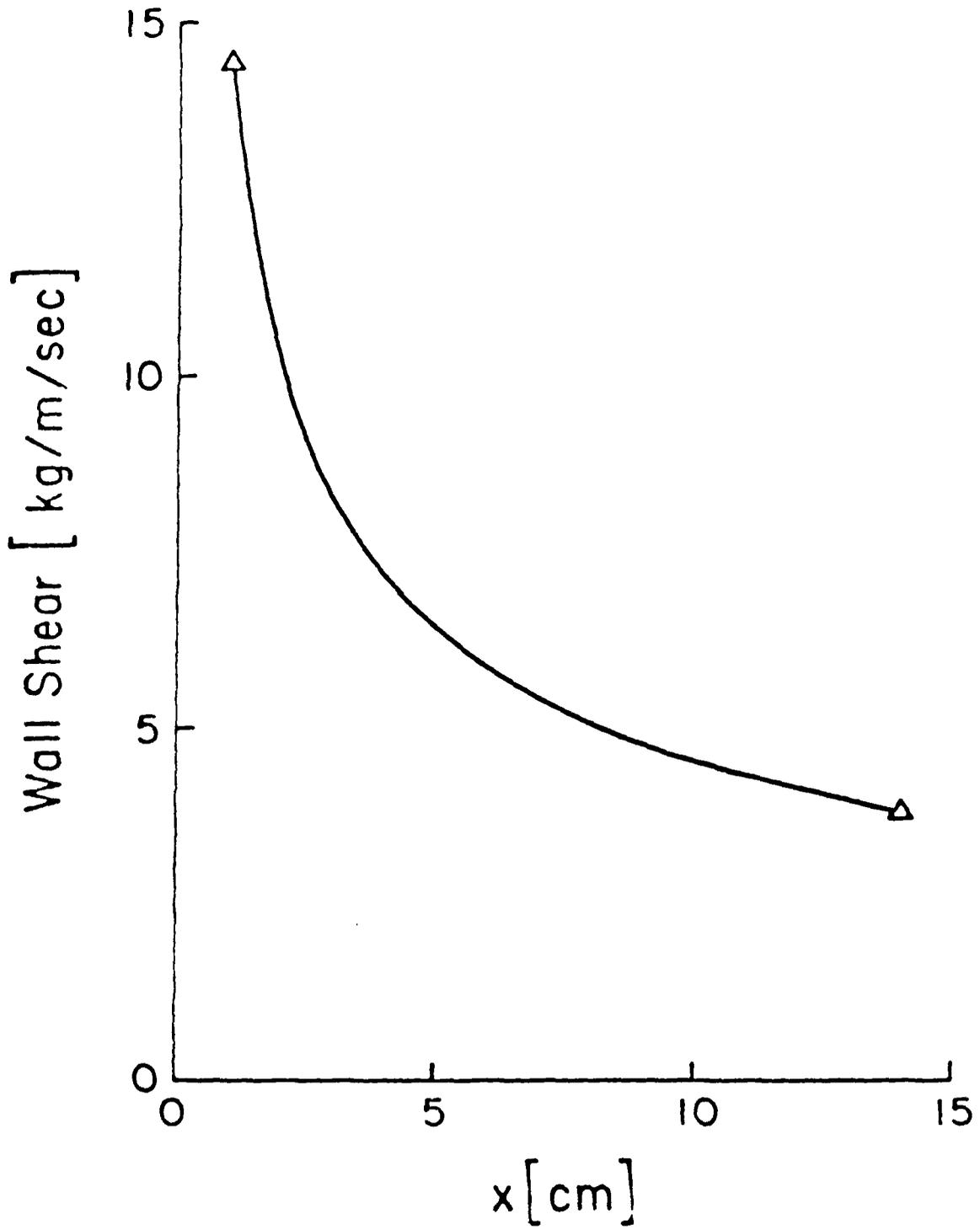
FIG. 4:

ELECTRODE-ADJACENT BOUNDARY LAYER FLOW IN MAGNETOPLASMADYNAMIC THRUSTERS

V. V. Subramaniam*
J. L. Lawless**
Carnegie-Mellon University
Pittsburgh, Pennsylvania 15213

Abstract

The steady boundary layer flow of a two-temperature plasma adjacent to the electrode in a self-field magnetoplasmadynamic (MPD) thruster is analyzed for frozen (zero ionization rate) flow and non-equilibrium (finite ionization rate) flow. The free stream boundary conditions for this analysis are obtained from the results of an earlier quasi one-dimensional non-equilibrium theory. The ionizing, two-temperature, compressible boundary layer equations are derived from first principles and are solved using momentum and energy integral methods. This enables an approximate calculation of the wall shear and the heat transfer to the electrode. The most significant result of the two-temperature boundary layer theory presented herein is to show the strong dependence of the viscosity on the ionization slip (i.e. ionization fraction at the wall). This affects such relevant quantities as boundary layer thickness, wall shear, and wall heat flux which in turn influence viscous drag and electrode erosion.

I. Introduction

Previous works have focused on the development of a new theory of the life-limiting phenomenon known as "onset" in magnetoplasmadynamic (MPD) thrusters[1, 2]. The predictions of this new back-EMF theory correlated well with measured electrical characteristics as well as with experimentally determined onset limits[3, 4, 5]. However, in order to quantify onset further and estimate electrode erosion rates, it is necessary to consider the electrode-adjacent boundary layer in detail. It is the study of this boundary layer that is discussed in this paper and represents the first such study for the MPD thruster.

Some important characteristics of the boundary layer in the MPD thruster will be described first. The MPD boundary layer is compressible because of density variation caused by a temperature that varies from above about 1 eV ($\sim$ 12000 K) in the free stream to less than 3500 K near the wall (i.e. the electrode). A further complication is that because of the presence of a cold wall and the difference in the masses of the various particles (ions, neutral atoms, and electrons), the plasma is expected to be a two-temperature fluid. The ions and neutrals being very similar in mass, would tend to exchange *translational energy by elastic collisions* more readily amongst themselves than with the electrons. The presence of the cold wall implies that the heavier particles would, by colliding with the wall tend to assume the wall temperature. Therefore, the heavy particle temperature varies significantly across the boundary layer from the free stream to the wall. But, the electrons being negative, are repelled by the negative electrical sheath at the wall and consequently retain their original kinetic energy. Therefore, their temperature is not expected to vary very much across the boundary layer. Hence, it is expected that the heavy particles (ions and neutrals) would have a temperature different from the lighter particles (electrons). For quasi-steady operation of the MPD thruster, the electrode temperature is fairly constant over the entire length. Therefore, the MPD boundary layer flow may be treated as a boundary layer with a constant wall temperature and a varying free stream. In summary, the MPD boundary layer is compressible, ionizing, two-temperature, and is adjacent to a cold wall at a constant temperature.

Laminar, compressible boundary layer theory for a single temperature fluid in the absence of any electromagnetic effects has been summarized by Schlichting[6] and studied by several other

authors[7, 8, 9, 10, 11]. However, these are not applicable for a two-temperature fluid. A detailed finite difference solution to the compressible two-temperature equations for a boundary layer adjacent to a non-current conducting surface has been given by Liu et al.[12]. Their solution considers an ionizing argon boundary layer in a supersonic flow over a wing. However the complexity of Liu et al.'s numerical solution does not permit ease of applicability to design situations. A similar finite difference calculation has been performed by Doss et al.[13], which deals with the non-equilibrium, compressible boundary layer in a subsonic MHD flow with an applied and constant magnetic field. Again, the numerical computation is tedious. This paper will focus on the development of a theory that preserves the physics of the results of Liu et al. but is mathematically much simpler. This theory further differs from Liu et al. in that it includes electromagnetic effects. Nageswara Rao[14] has recently studied the incompressible momentum boundary layer in an MHD channel and has included the Hall effect. However, he has neglected the energy equation and the thermodynamics. These assumptions along with the effect of ionization will be shown to be crucial in the case of the MPD thruster.

A novel feature of the two-temperature boundary layer that will be considered here is the important role played by ionization on the growth of the boundary layer. It will be shown in this paper that the strong dependence of the viscosity on the ionization fraction and the subsequent control of boundary layer growth by the viscosity, affect such important quantities as the wall heat flux and the wall shear. This in turn affects the skin drag and the heat transfer to the electrode, which has an important effect on electrode erosion.

The governing equations of the two-temperature MPD compressible boundary layer are solved by means of an approximate method. The approximate method which will be outlined here, is based on the use of the Howarth-Dorodnitsyn transformation in conjunction with the momentum and energy integral method. The momentum integral equation of boundary layer theory was first derived by von Karman[15]. The modern form of this equation was first given by Gruschwitz[16] and finds its applications in the approximate theories for both laminar and turbulent boundary layers. Since then, Wieghardt[17] has deduced an energy integral equation by a similar approach. This approach will be used in this paper to reduce the original partial differential equations to ordinary differential equations. The success of using this integral method depends

largely on finding self-similar profiles for the velocity, heavy particle temperature, and ionization fraction. The presence of the cold wall often destroys the applicability of this approach to compressible, chemically reacting, supersonic boundary layers. For this reason, the integral method is adapted and is used here in conjunction with a two-temperature plasma assumption and the Howarth-Dorodnitsyn transformation. Self-similar profiles are then sought in terms of *the transformed Howarth-Dorodnitsyn transverse coordinate.* The assumption of the two-temperature plasma besides being realistic, enables the heavy particle fluid to be treated in a fashion similar to the treatment of constant Prandtl number fluids of classical boundary layer theory. This is what allows the use of the momentum and energy integral methods.

The derivation of the two temperature, non-equilibrium, compressible boundary layer equations from first principles for the MPD channel flow, will be summarized in section II. The important assumptions required to simplify these equations will also be discussed. An approximate method of solving these equations will be outlined in section III and the results will be given in section IV. Finally a summary will be given in section V, along with the conclusions.

II. Governing Equations

This section will focus on the development of the boundary layer equations for the plasma in the MPD thruster. Using the standard boundary layer assumptions, the boundary layer equations for a steady, two-temperature, non-equilibrium, compressible plasma will be derived from the general equations of two temperature magnetoplasmadynamics. These have been described in some detail by Kalikhman[18]. Kalikhman's approach has been followed to derive the general equations for MPD flow, since it is important to recognize these equations prior to making the boundary layer assumptions. These have been rigorously developed from the successive moments of the generalized Boltzmann equation (i.e. the conservation of mass, momentum, and energy)[2]. However, only a summary will be given here. Since the development of these equations is long and tedious, the interested reader is referred to the development found in detail elsewhere[2, 18, 19, 20].

The plasma of the MPD thruster is assumed to consist of neutral atoms, single ions, and

electrons. As a first approach, the sheaths will be ignored, and the condition of local quasi-neutrality (i.e. the ion and electron number densities are equal) will be assumed to hold everywhere in the boundary layer. The electrical resistance of the boundary layer is assumed to be small compared to the free stream, so that the electrical characteristics are determined by the free stream. Then, the governing equations for two dimensional steady flow may be summarized as follows in cartesian tensor notation, with the repeated subscripts denoting summation from 1 to 2 which are the x and y directions respectively:

Mass :

$$\frac{\partial}{\partial x}(\rho u) + \frac{\partial}{\partial y}(\rho v) = 0 \tag{1}$$

x-Momentum :

$$\rho u \frac{\partial u}{\partial x} + \rho v \frac{\partial u}{\partial y} = -\frac{\partial P}{\partial x} - \frac{\partial}{\partial x}\left(\frac{B^2}{2\mu_o}\right) + \frac{\partial}{\partial y}\left(\eta_H \frac{\partial u}{\partial y}\right) \tag{2}$$

y-Momentum :

$$\frac{\partial P}{\partial y} = 0 \qquad\qquad \textit{for negligible Hall parameter} \tag{3}$$

$$\frac{\partial P}{\partial y} = -\frac{\partial}{\partial y}\left(\frac{B^2}{2\mu_o}\right) \qquad\qquad \textit{for significant Hall parameter} \tag{4}$$

Electron sensible energy : (translational mode only)

$$\frac{3}{2}kn_e u_i \frac{\partial T_e}{\partial x_i} + \frac{\partial q_i^e}{\partial x_i} + \Pi_{ij}^e \frac{\partial u_i}{\partial x_j} = j_k^e (E_k - \epsilon_{kpq} u_p B_q)$$

$$+ \frac{3}{2}kT_e \frac{\partial}{\partial x_i}\left(n_e U_i^e\right) - m_e n_e U_i^e u_k \frac{\partial u_i}{\partial x_k}$$

$$- \frac{3m_e}{m_A}kn_e <v_{eH}>(T_e - T_H) \tag{5}$$

Heavy particle sensible energy : (translational mode only)

$$\frac{3}{2}k(n_e+n_A)u_i\frac{\partial T_H}{\partial x_i} + \frac{\partial}{\partial x_i}(q_i^{atom}+q_i^{ion}) + \left(\Pi_{ij}^{ion}+\Pi_{ij}^{atom}\right)\frac{\partial u_i}{\partial x_j}$$
$$= j_k^{ion}(E_k - \epsilon_{kpq}u_p B_q)$$
$$+ \frac{3}{2}kT_H\frac{\partial}{\partial x_i}\left(n_e U_i^{ion} + n_A U_i^{atom}\right)$$
$$- (m_{ion}n_e U_i^{ion} + m_A n_A U_i^{atom})u_k\frac{\partial u_i}{\partial x_k}$$
$$+ \frac{3m_e}{m_A}kn_e < \nu_{eH} > (T_e - T_H) \tag{6}$$

Rate :

$$\rho u_i\frac{\partial}{\partial x_i}(n_e/\rho) + \frac{\partial}{\partial x_i}(n_e U_i^{ion}) = \dot{n}_{ion} \tag{7}$$

State :

$$P = n_e kT_e + (n_e+n_A)kT_H \tag{8}$$

where $\dot{n}_{ion}$ is the net production of ions by inelastic collisions; ρ is the mass density; P is the pressure; B is the magnetic field; $\eta_H = \eta^{ion} + \eta^{atom}$ is the heavy particle dynamic viscosity; μ_o is the permeability of free space; k is Boltzmann's constant; n_e is the electron number density which is equal to the ion number density because of the quasi-neutrality assumption; T_e is the electron temperature; m_e is the mass of an electron; m_A is the mass of an atom; j_k^a is the kth component of the current density vector of the species a; q_i^a is the ith component of the heat flux vector of species a; ϵ_{kpq} is the cartesian permutation tensor; E_k is the kth component of the electric field vector; B_q is the qth component of the magnetic field vector; u_i is the ith component of the mass weighted local average plasma velocity; $u = u_1$ is the velocity component in the x-direction or the flow direction; $v = u_2$ is the velocity component in the y-direction normal to the electrode and transverse to the flow; U_i^a is the ith component of the diffusion

velocity or the average peculiar or thermal velocity of species a; n_A is the neutral atom number density; T_H is the temperature of the heavy particles (ions and neutrals); $\langle \nu_{eH} \rangle$ is the energy-weighted average momentum transfer elastic collision frequency between an electron and a heavy particle[21]; and the stress tensor $\Pi_{ij}{}^a$ is given by:

$$\Pi_{ik}{}^a = -\eta^a{}_{ikpq}\frac{\partial u_p}{\partial x_q} + P_a \delta_{ik} \tag{9}$$

where $\eta^a{}_{ikpq}$ is the viscosity tensor for species a, P_a is the partial pressure of species a, and δ_{ik} is the Kronecker delta. In order to calculate the transport properties and obtain the diffusion velocity, it is necessary to solve the full Boltzmann equation for the velocity distribution function[22, 20, 19, 18]. The flow is assumed to deviate slightly away from equilibrium, so that the velocity distribution function is the sum of the Maxwell-Boltzmann distribution function and a perturbation. This regular perturbation solution has been summarized by Kalikhman[18] for the case where electromagnetic effects are present. However, in this paper the transport properties are calculated from kinetic theory. Equations (1) through (8) constitute a system of 6 equations in the 6 unknowns ρ, u, v, T_e, T_H, and the ionization fraction $a = n_e/(n_e + n_A)$. Before proceeding with any further simplifications or with the solution of the above equations, it is necessary to summarize the assumptions that lead to these simplifications:

- **The boundary layer flow is laminar, steady, and two dimensional.**

- **The Hall effect is neglected.**

- **The electrical characteristics of the boundary layer are determined by the free stream.** Therefore, $E = constant$; $B = B_\infty(x)$; and $j = j_\infty(x)$; where B_∞ and j_∞ are the free stream magnetic field and current density respectively.

- **Radiative heat transfer is neglected in this first approach.**

- **Axial diffusion is neglected.**

- **The plasma is a two-temperature plasma.** A quantitative statement of this assumption is obtained from the electron energy equation (5) by comparing the heat conduction (the second term on the left hand side of (5)) to the energy transfer by elastic collisions (the fourth term on the right hand side of (5)). This gives the condition[2]:

$$\left(\frac{m_A}{m_e}\right)\left(\frac{L_e^2}{\delta_T^2}\right) \gg 1 \tag{10}$$

where L_e is the mean free path of the electron, and δ_T is the boundary layer thickness. For a two temperature approach to be valid therefore, we must have:

$$\frac{L_e^2}{\delta_T^2} \gg \frac{m_e}{m_A} \tag{11}$$

Simultaneously, for the continuum approximation to be valid, we require that $L_e/\delta_T \ll 1$. Thus,

$$\left(\frac{m_e}{m_A}\right)^{1/2} \ll \left(\frac{L_e}{\delta_T}\right) \ll 1 \tag{12}$$

With these assumptions and some additional manipulation[2], equations (1) through (7) become:

Mass:

$$\frac{\partial(\rho u)}{\partial x} + \frac{\partial(\rho v)}{\partial y} = 0 \tag{13}$$

Momentum:

$$\rho u \frac{\partial u}{\partial x} + \rho v \frac{\partial u}{\partial y} = -\frac{dP}{dx} - \frac{d}{dx}(B^2/2\mu_o) + \frac{\partial}{\partial y}\left(\eta_H \frac{\partial u}{\partial y}\right) \tag{14}$$

Electron sensible energy:

$$\frac{\partial}{\partial y}\left(\lambda^{ee}\frac{\partial T_e}{\partial y} + \frac{5}{2}n_e k T_e V_e\right) = e n_e V_e (E - uB) \tag{15}$$

Heavy particle sensible energy:

$$\rho u \frac{\partial}{\partial x}\left(\frac{5kT_H}{2m_A}+\frac{u^2}{2}\right) + \rho v \frac{\partial}{\partial y}\left(\frac{5kT_H}{2m_A}+\frac{u^2}{2}\right)$$

$$- \frac{\partial}{\partial y}\left((\lambda^{ii}+\lambda^{ai})\frac{\partial T_H}{\partial y}+(\lambda^{ie}+\lambda^{ae})\frac{\partial T_e}{\partial y}+\eta_H\frac{\partial}{\partial y}(u^2/2)\right)$$

$$= en_e V_i E + 3\left(\frac{m_e}{m_A}\right)kn_e<\nu_{eH}>(T_e-T_H) \tag{16}$$

Rate:

$$\rho u \frac{\partial a}{\partial x} + \rho v \frac{\partial a}{\partial y} + \frac{\partial}{\partial y}(m_A n_e V_i) = \frac{k_f a(1-a)\rho^2}{m_A} - \frac{k_b a^3 \rho^3}{m_A^2} \tag{17}$$

where $a = n_e/(n_e+n_A)$; k_f is the ionization rate constant; k_b is the recombination rate constant; $\lambda^{a\beta}$ is the thermal conductivity due to collisions between species a and β; V_e is the electron diffusion velocity in the y direction, given by[2, 18]:

$$V_e \approx \frac{eD^e(E-uB)}{kT_H} - \frac{D^e}{n_e}\frac{\partial n_e}{\partial y} \tag{18}$$

and D^e is the electron diffusion coefficient. The ionization and recombination processes are modelled according to:

$$Ar + e \ === \ A^+ + e + e$$

where the left hand side represents ionization due to electron impact (e) with a neutral atom (Ar), and the right hand side represents three body recombination with two electrons and a singly ionized atom (A^+). This reaction is likely to be one of the dominant processes in the MPD thruster. Finally, the ion diffusion velocity in the y direction, V_i is given by[2, 18]:

$$V_i \approx \frac{eD^i(E-uB)}{kT_H} - \frac{D^i}{n_e}\frac{\partial n_e}{\partial y} \tag{19}$$

where D^i is the ion diffusion coefficient and e is the electronic charge. In equation (19), the neutral concentration gradient term and the effects of thermal diffusion have been ignored in

order to simplify the equations. Thus, equation (19) resembles Fick's law with an additional term that is present because there is a current being driven through the plasma.

The equations (15) and (16) may be simplified further with the following additional assumptions:

- **The electron temperature, T_e is assumed to be fairly uniform across the boundary layer.** This is a reasonable approximation and is supported by the work of Liu et al[12]. This means that $T_e \approx T_\infty(x)$ throughout the boundary layer, where T_∞ represents the free stream temperature.

- **The ion ohmic heating is assumed to be negligible.** This means that the first term on the right hand side of the heavy particle sensible heat equation (16), is neglected.

The final form of the governing equations is then:

Mass:

$$\frac{\partial(\rho u)}{\partial x} + \frac{\partial(\rho v)}{\partial y} = 0 \tag{20}$$

Momentum:

$$\rho u \frac{\partial u}{\partial x} + \rho v \frac{\partial u}{\partial y} = -\frac{dP}{dx} - \frac{d}{dx}(B^2/2\mu_o) + \frac{\partial}{\partial y}\left(\eta_H \frac{\partial u}{\partial y}\right) \tag{21}$$

Electron sensible energy:

$$T_e \approx T_\infty(x) \tag{22}$$

Heavy particle sensible energy:

$$\rho u \frac{\partial}{\partial x}\left(\frac{5kT_H}{2m_A} + \frac{u^2}{2}\right) + \rho v \frac{\partial}{\partial y}\left(\frac{5kT_H}{2m_A} + \frac{u^2}{2}\right)$$
$$- \frac{\partial}{\partial y}\left(\lambda_H \frac{\partial T_H}{\partial y} + \eta_H \frac{\partial}{\partial y}(u^2/2)\right) = 3\left(\frac{m_e}{m_A}\right)kn_e < v_{eH} > (T_e - T_H) \tag{23}$$

Rate:

$$\rho u \frac{\partial a}{\partial x} + \rho v \frac{\partial a}{\partial y} + \frac{\partial}{\partial y}(m_A n_e V_i) = \frac{k_i a(1-a)\rho^2}{m_A} - \frac{k_b a^3 \rho^3}{m_A^2} \qquad (24)$$

The equations (19) through (24) have been obtained after a lengthy derivation and after making several assumptions. These equations will be discussed next. Equation (20) is the equation of mass continuity encountered in standard compressible boundary layer theory[6]. Equation (21) is the conservation of momentum. It resembles the usual form except for the presence of the electromagnetic body force which appears as a gradient of the magnetic pressure (see the second term on the right hand side of (21)). Mathematically, this should pose no additional trouble since it has the same form as the hydrodynamic pressure gradient. It is the sensible energy equations (22) and (23) that require some explanation. These equations have been referred to in this paper as the sensible energy equations, because they include only the translational part of the total energy of the particles. The energy in translation is therefore the "sensible" heat while any internal mode such as electronic excitation is referred to as "latent" heat. Hence, equation (23) would resemble the standard energy equation written in terms of enthalpy if the particles had no other modes of energy storage except in translation. This is clear since in the presence of pure translation, the enthalpy is $h = 5kT/2m_A$ which appears on the left hand side of (23). Equation (23) therefore resembles the classical compressible boundary layer equations with heat conduction and viscous dissipation (the third term on the left hand side of (23)), but for the presence of a source term on the right hand side. This source term is present because the electron fluid and heavy particle fluid have been treated separately. Consequently, there appears a term that couples the two energy equations together. This term which represents the transfer of energy by elastic collisions between the electron gas and the heavy particle gas, appears as the source term on the right hand side of (23). Equation (24) is the familiar species conservation equation encountered in the field of combustion[20, 22, 19]. The only differences are in the expressions for the diffusion velocities, equations (18) and (19) which contain additional terms due to the presence of a current in the plasma. Equations (20) through (24) represent the approximate boundary layer equations for the electrodes in the MPD thruster. This section has focused on a summary of a derivation of these equations which are given in detail elsewhere[18, 2].

The next section will focus on an approximate solution of these governing equations.

III. An Approximate Method of Solution

This section will focus on the description of an approximate method of solution to the governing equations presented in section II. A brief review of existing approximate methods will be given first. Then, the complications of the electrode-adjacent boundary layer in the MPD thruster will be briefly mentioned, followed by a detailed description of the approximate method proposed herein.

A system of equations similar to those presented in section II have been solved by Liu et al.[12] by the use of a finite difference technique. In this section, a simpler but approximate solution technique will be developed in order to solve equations (20) through (24). Several authors have solved systems of equations that are similar to the governing equations of section II. These will be reviewed briefly. The equations are particularly easier to solve if the Prandtl number is either one or constant. Emmons and Brainerd[10] have developed a similarity solution for a compressible boundary layer over an insulated plate at arbitrary Prandtl numbers. For a Prandtl number of unity, Poots[8] has studied heat transfer in laminar boundary layers with an adverse pressure gradient and an adiabatic wall. Poots uses the Illingworth-Stewartson transformation to reduce the compressible flow equations to incompressible form. Curle[7] has extended the work of Poots to the case of a constant wall temperature and an arbitrary but constant Prandtl number greater than 0.5. Such a similarity solution fails in the case of a reacting supersonic boundary layer with a constant wall temperature. Nageswara Rao[14] has recently studied the compressible boundary layer in a magnetohydrodynamic channel, but has altogether neglected the energy equation and the thermodynamics. These will be shown to be crucial for the MPD thruster. The method presented herein differs from all the above in that a relatively easy approximate solution is found by reducing the original partial differential equations to ordinary differential equations, and then solving by using a momentum integral method. An integral method has been successfully used by Chan[9] who does not consider a reacting boundary layer. None of these authors with the exception of Nageswara Rao[14] have considered electromagnetic effects. Hains[23] has considered electromagnetic effects in a constant conductivity, non-reacting compressible boundary layer. He too has successfully used an integral method.

The problem of the electrode boundary layer in the MPD thruster includes all the complications of a classical compressible boundary layer and more. It includes the additional effects of electromagnetics, chemical reaction (ionization and recombination), variable flow properties, and a constant wall temperature. The constant wall temperature, together with chemical reaction often destroy the simplicity of the integral method because unlike the case of the adiabatic wall, the temperature may not achieve its maximum at either the wall or the free stream. This makes approximate solutions very tricky. The method proposed herein addresses all these complications.

Simply stated, the present integral method begins by integrating the partial differential equations (20) through (24) from $y = 0$ to $y = \delta_T$ in order to eliminate the dependence on the transverse coordinate y. The result is a set of ordinary differential equations in the axial coordinate x for certain dependent variables that appear as integrals over the transverse coordinate y. Next, the Howarth-Dorodnitsyn transformation[20] is used to transform the integration variable from y to a variable ξ which varies from 0 at the wall to 1 at the edge of the boundary layer. This is done in order to eliminate the density dependence in compressible flow. Then, the integrands in the integrals are assumed to be polynomial functions of this variable ξ. The choice of the order of these polynomials is not obvious but will be discussed in detail later in this section. The differential equations are then simultaneously integrated from the leading edge of the boundary layer to any desired downstream location. The details of this scheme have been outlined by Hains[23] and Subramaniam[2].

Let us now examine the integro-differential equations obtained by integrating equations (21), (23), and (24). Integrating these equations and rearranging, we obtain:

$$\frac{d\Theta}{dx} + \frac{\Theta}{\rho_\infty u^2_\infty} \frac{d}{dx}(\rho_\infty u^2_\infty) + \frac{\delta^*}{u_\infty} \frac{du_\infty}{dx} = \frac{\tau_w}{\rho_\infty u_\infty^2} \tag{25}$$

where τ_w is the wall shear defined by:

$$\tau_w = \left\langle \eta_H \frac{\partial u}{\partial y} \right\rangle_{y=0} \tag{26}$$

Θ is the momentum thickness defined by:

14

$$\Theta = \int_0^{\delta_T} \frac{\rho u}{\rho_\infty u_\infty} \left(1 - \frac{u}{u_\infty} \right) dy \tag{27}$$

δ^* is given by:

$$\delta^* = \int_0^{\delta_T} \left(1 - \frac{\rho u}{\rho_\infty u_\infty} \right) dy \tag{28}$$

and the subscript ∞ refers to free stream quantities. Integration of the heavy particle sensible energy equation (23) gives

$$\frac{d\Theta_H}{dx} + \frac{\Theta_H}{\rho_\infty u_\infty (C_{pa} T_\infty + u_\infty^2/2)} \frac{d}{dx} \left(\rho_\infty u_\infty [C_{pa} T_\infty + u_\infty^2/2] \right)$$

$$+ \frac{\phi^*}{(C_{pa} T_\infty + u_\infty^2/2)} \frac{d}{dx} (C_{pa} T_\infty + u_\infty^2/2)$$

$$= \frac{q_{wH} - u_s \tau_w}{\rho_\infty u_\infty (C_{pa} T_\infty + u_\infty^2/2)}$$

$$+ \frac{3 m_e k a_\infty}{m_A^2 u_\infty (C_{pa} T_\infty + u_\infty^2/2)} \int_0^{\delta_T} \frac{\rho a}{\rho_\infty a_\infty} < \nu_{eH} > (T_\infty - T_H) \, dy \tag{29}$$

where u_s is the slip velocity at the wall, Θ_H is the enthalpy thickness defined by

$$\Theta_H = \int_0^{\delta_T} \frac{\rho u}{\rho_\infty u_\infty} \left(\frac{C_{pa} T_H + u^2/2}{C_{pa} T_\infty + u_\infty^2/2} - 1 \right) dy \tag{30}$$

ϕ^* is defined by

$$\phi^* = \int_0^{\delta_T} \frac{\rho u}{\rho_\infty u_\infty} dy \tag{31}$$

and q_{wH} is the heavy particle wall heat flux given by

$$q_{wH} = - \left(\lambda_H \frac{\partial T_H}{\partial y} \right) \Big|_{y=0} \tag{32}$$

where $\lambda_H = \lambda^{ion} + \lambda^{atom}$ is the heavy particle thermal conductivity. The integrated rate equation is:

$$
\frac{dI^*}{dx} + \frac{I^*}{\rho_\infty u_\infty a_\infty} \frac{d}{dx}(\rho_\infty u_\infty a_\infty) + \frac{\psi^*}{a_\infty} \frac{da_\infty}{dx}
$$

$$
- \frac{m_A}{\rho_\infty u_\infty a_\infty}(n_{cw}V_{iw}) = \frac{a_\infty k_i \rho_\infty}{m_A u_\infty} \int_0^{\delta_T} \frac{a}{a_\infty}\left(\frac{1}{a_\infty} - \frac{a}{a_\infty}\right)\frac{\rho^2}{\rho_\infty^2} dy
$$

$$
- \frac{k_b a_\infty^2 \rho_\infty^2}{m_A^2 u_\infty} \int_0^{\delta_T} \frac{a^3 \rho^3}{a_\infty^3 \rho_\infty^3} dy \tag{33}
$$

where n_{cw} and V_{iw} are the number density and y-component of the diffusion velocity of the ions evaluated at the wall, and I^* is the ionization thickness defined by:

$$
I^* = \int_0^{\delta_T} \frac{\rho u}{\rho_\infty u_\infty}\left(\frac{a}{a_\infty} - 1\right) dy \tag{34}
$$

The general case of velocity slip $u_s \neq 0$ (where u_s is the plasma velocity at the wall), temperature slip $T_s \neq T_w$ (where T_w is the wall or electrode temperature and T_s is the plasma temperature at the wall), and ionization or concentration slip at the wall, have been treated by Subramaniam[2]. However, in this paper only ionization slip will be considered. This means that $u_s = 0$ and $T_s = T_w$. The ionization slip a_w which must be supplied for the rate equation (33), is obtained by setting the macroscopic diffusive mass flux at the wall equal to the random thermal mass flux at the wall[2]:

$$
D_w'\left(\frac{\partial n_e}{\partial y}\right)_{y=0} - \frac{n_{cw}D_w^i e E_w}{kT_w} = \frac{n_{cw}<C_H>}{4} \tag{35}
$$

where D_w^i is the ion diffusion coefficient at the wall, E_w is the electric field at the wall which is determined from overall current conservation, and $<C_H>$ is the mean heavy particle thermal speed at the wall. The application of the Howarth-Dorodnitsyn transformation to the integrals enables the elimination of density from the integrand. Thus, if

$$\xi = \frac{1}{\Delta} \int_0^y \frac{\rho}{\rho_\infty} dy \tag{36}$$

where Δ is given by

$$\Delta = \int_0^{\delta_T} \frac{\rho}{\rho_\infty} dy \tag{37}$$

then (27) reduces to:

$$\frac{\Theta}{\Delta} = \int_0^1 \frac{u}{u_\infty} \left(1 - \frac{u}{u_\infty} \right) d\xi \tag{38}$$

Similarly, the other quantities that appear in terms of derivatives with respect to y or in terms of integrals over y may be transformed into derivatives and integrals in ξ.

Before the various integrals can be evaluated, it is necessary to assume profiles for the variation of the velocity, heavy particle temperature, and the ionization fraction across the boundary layer. A quadratic profile for u and cubic profiles for T_H and a in terms of ξ are assumed. Cubic profiles for T_H and a are assumed because the maximum temperature and maximum ionization fraction could occur somewhere inside the boundary layer, and not necessarily at the wall as in the case of an adiabatic wall. The velocity profile is then completely determined by the following constraints:

$$u(\xi = 0) = 0$$

$$u(\xi = 1) = u_\infty$$

$$\frac{\partial u}{\partial y}(\xi = 1) = 0$$

which give

$$\frac{u}{u_\infty} = 2\xi - \xi^2 \tag{39}$$

Analogously, for the temperature and ionization fraction

$$T_H(\xi=0) = T_w \qquad a(\xi=0) = a_w$$

$$T_H(\xi=1) = T_\infty \qquad a(\xi=1) = a_\infty$$

$$\frac{\partial T_H}{\partial \xi}(\xi=1) = 0 \qquad \frac{\partial a}{\partial \xi}(\xi=1) = 0$$

Thus, the temperature and ionization profiles are:

$$\frac{T_H}{T_\infty} = \frac{T_w}{T_\infty} + \left(2 - \frac{2T_w}{T_\infty} + b_4\right)\xi + \left(\frac{T_w}{T_\infty} - 1 - 2b_4\right)\xi^2 + b_4\xi^3 \tag{40}$$

and

$$\frac{a}{a_\infty} = \frac{a_w}{a_\infty} + \left(2 - \frac{2a_w}{a_\infty} + c_4\right)\xi + \left(\frac{a_w}{a_\infty} - 1 - 2c_4\right)\xi^2 + c_4\xi^3 \tag{41}$$

where b_4 and c_4 are coefficients yet to be determined, the subscript ∞ refers to free stream quantities, and the subscript W refers to quantities evaluated at the wall. Using these polynomial forms, the integrated form of the momentum equation (25) is a differential equation for Δ, the integrated form of the energy equation (29) is a differential equation for the unknown coefficient b_4, and the integrated form of the rate equation (33) is a differential equation for the coefficient c_4. Thus, the original system of non-linear partial differential equations have been reduced to a system of quasi-linear ordinary differential equations. To complete the formulation, conditions must be prescribed at $x = 0$, the leading edge of the boundary layer. These are that the thicknesses, Δ, Θ, Θ_H, and I^* are zero at the leading edge. Further, starting conditions must be specified for b_4 and c_4. This can be obtained by requiring that the second derivatives of T_H and a with respect to ξ be zero at the leading edge. This gives $c_4 = 1$ and $b_4 = 1 - (T_w/T_\infty)$ at the leading edge. These approximate equations describing boundary layer flow have been

integrated using the Gear method[24]. The Gear algorithm is used because of the "stiffness" of the system of ordinary differential equations.

In summary, an approximate solution to the two temperature boundary layer theory of section II has been outlined. This approximate solution uses the Howarth-Dorodnitsyn transformation and reduces the complicated system of non-linear partial differential equations to a relatively simpler set of quasi-linear ordinary differential equations. In the next section, the solution to these equations will be given for various conditions that arise in the electrode-adjacent boundary layer of the MPD thruster.

IV. Results of Boundary Layer Theory

The boundary layer equations have been solved by the integral method outlined in the previous section, near the onset condition predicted by the quasi one-dimensional non-equilibrium theory of back-EMF onset[1,2]. The results of this analysis are presented in this section. The results focus primarily on a mass flow rate of 3 g/sec of argon propellant, but results for a mass flow of 6 g/sec are also mentioned. The free stream conditions at onset for a given mass flow rate, have been obtained from the results of quasi-1D non-equilibrium theory[1,2]. A constant wall temperature of 3000 K is assumed, and the heavy particle Prandtl number is taken to be ≈ 0.7. Since boundary layers usually begin at stagnation points or at sharp edges, the starting point or leading edge must be specified. The entrance region of the MPD thruster is not well understood, and it is not clear what the flow pattern is in this region. Therefore, for the purposes of this analysis, the boundary layer is assumed to begin at the inlet. Since the sonic point ($M = 1$, where M is the Mach number) is very close to the inlet, the calculation is simpler if the leading edge defined by $x = 0$ is taken to be at the sonic point.

The governing equations (20) through (24) are then simultaneously integrated from $x = 0$ to $x = L$. This is done for several different cases in order to examine the effect of ionization on the boundary layer growth. The case of a non-equilibrium boundary layer with ionization slip (i.e. a_w is determined from (35)) with a non-equilibrium free stream will be considered first. Next, the ionizing free stream with a frozen boundary layer (i.e. $a = a_\infty(x)$) will be considered. Finally, the case of a fully ionized, frozen free stream with a frozen boundary layer (i.e. $a = 1$

all across the boundary layer) will be addressed. The mass flow of 3 g/sec will be considered first.

The results of the non-equilibrium theory are summarized in Fig. 1, Fig. 2, Fig. 3, Fig. 4, Fig. 5, and Fig. 6. Fig. 1 shows the growth of the boundary layer at the cathode. The boundary layer at the anode is assumed to be similar to the cathode, and is plotted assuming this symmetry for the 5 cm. high straight coaxial thruster of King[4]. It is found that the boundary layers are relatively thick and actually merge at an axial distance of approximately 4 cm. from the leading edge. This surprising fact will be discussed at length, later in this section. The ionization fraction at the wall is shown in Fig. 2 as a function of distance. This ionization slip decreases with distance as expected, since the diffusion time increases as the boundary layer thickness increases with distance along the thruster. Thus, though the free stream ionization fraction increases, it takes longer for ions to diffuse to the wall in order to replenish those that are lost due to recombination. The ionization fraction non-dimensionalized by the free stream ionization fraction is shown in Fig. 3 versus distance, at a location of 1 cm. from the leading edge. The bulge in the profile is characteristic of hot, high speed flows in contact with a cold wall. The constant electron temperature in the boundary layer tends to ionize the plasma, whereas the presence of the cold wall drives the plasma to recombine. These two opposing effects cause the maximum ionization fraction to occur somewhere in the middle of the boundary layer as shown in the figure. The non-dimensional temperature profile is shown in Fig. 4. A bulge analogous to the one observed in Fig. 3 is not apparent, because the plasma flow velocity is not high enough for the viscous dissipation to be comparable with the heat transfer to the wall. Another source of heating is the energy transfer from elastic collisions with the hot electrons. This too is not comparable with the conductive heat transfer to the wall. Fig. 5 and Fig. 6 show the variation of the heavy particle wall heat flux and the wall shear stress respectively. The heat flux is large near the leading edge of the boundary layer ($x = 0$) because the boundary layer thickness is small. In fact, the heat flux is infinite exactly at the leading edge, because of the singularity at $x = 0$. This is of course non-physical, because the boundary layer becomes free-molecular very close to the leading edge. Thus, the leading edge is a singularity only in the continuum theory. The wall shear is large when the boundary layer thickness is small (since this

means that the velocity gradient at the wall is large), and then decreases as the boundary layer grows to be thicker. The heavy particle wall heat flux exhibits a similar behaviour. From classical boundary layer theory, both the wall shear and the wall heat flux would be expected to decrease with increasing boundary layer thickness.

The case of the frozen boundary layer with an ionizing free stream will be considered next. Again, the free stream conditions are obtained from quasi-1D non-equilibrium theory[1,2] since the free stream is assumed to be ionizing. However, since the boundary layer is chemically frozen, the ionization fraction in the boundary layer is the same as in the free stream (i.e. $a = a_{\infty}$ throughout the boundary layer). This means that there is no ionization or recombination in the boundary layer. The motivation for studying this case, is to examine the effect of varying ionization fraction at the wall (i. e. a_w) on the viscosity. The boundary layers in the thruster for this case are shown in Fig. 7. This case differs from the non-equilibrium case with ionization slip in that the boundary layers do not merge, though they are appreciably thick. The boundary layer thickness is seen to decrease near the exit of the thruster, due to the drastic variation of the free stream conditions near the exit[2]. The heavy particle temperature profile is shown in Fig. 8 at four different locations, 1 cm., 5 cm., 10 cm., and 15 cm. from the leading edge. The noticeable bulge in the profiles far from the leading edge exists, because of the opposing effects of viscous dissipation and heat transfer to the cold wall. This bulge does not appear near the leading edge because the plasma flow velocity is small and therefore the viscous dissipation is small. Fig. 9 and Fig. 10 depict the variation of the heavy particle wall heat flux, and the wall shear respectively. The heat flux and wall shear are seen to decrease with increasing boundary layer thickness, as expected. The magnitudes of the heat flux and the wall shear are lower in the frozen boundary layer as opposed to the non-equilibrium boundary layer with ionization slip, because of the smaller thermal conductivity and smaller viscosity. The viscosity is smaller, because the frozen boundary layer has a greater ionization fraction than in the non-equilibrium case. The thermal conductivity is smaller because the viscosity is smaller, and the heavy particle Prandtl number is fixed. It is evident by comparing these cases, that the amount of ionization at the wall is extremely important in determining the heat transfer and the wall shear because of its effect on boundary layer growth.

A more dramatic illustration of the effect of ionization is enabled by studying the case of the fully ionized frozen boundary layer. In this instance, the fully ionized, frozen, quasi-1D flow described by Lawless *et al.*[1] is used to provide the free stream boundary conditions, and the boundary layer is treated as being fully ionized and chemically frozen. The results of this calculation are shown in Fig. 11, Fig. 12, Fig. 13, and Fig. 14. The qualitative behaviour of the various quantities (i.e. heavy particle temperature, heavy particle wall heat flux, and wall shear) are the same as before, and have been explained in the other cases that were considered. The magnitudes of the quantities are lower in this fully ionized case, again because of the lower viscosity and thermal conductivity. This will be addressed in detail next.

The heavy particle Prandtl number has been fixed at 0.7 in the boundary layer calculations. Thus, if the viscosity is known, the thermal conductivity may be calculated using the definition of the Prandtl number. The viscosity of the plasma is primarily due to the heavy particles. Since the electrons have a significantly smaller mass than the ions and neutrals, their contribution to the viscosity is negligible[21]. The heavy particle dynamic viscosity is the sum of the ion viscosity and the neutral viscosity. Since the mass of the ion differs from that of a neutral only by the mass of the electron, the ions and neutrals are treated as having the same mass in this two-temperature theory. Therefore, at a given heavy particle temperature, the mean thermal speed of the ions is approximately the same as that of the neutrals. The viscosity may then be obtained from kinetic theory[22, 21]:

$$\eta_H = \eta^{ion} + \eta^{atom} = m_A <C_H> (n_e L_{iH} + n_A L_{AH}) \tag{42}$$

where $<C_H>$ is the mean thermal speed of the heavy particles, L_{iH} is the mean free path for an ion colliding with other heavy particles, and L_{AH} is the mean free path for a neutral colliding with other heavy particles. The mean free paths for the ions and neutrals are given by[21]:

$$L_{iH} = \frac{1}{n_e O_{ii} + n_A O_{iA}}$$

$$L_{AH} = \frac{1}{n_A O_{AA} + n_e O_{iA}}$$

where the Q's denote energy-averaged momentum transfer collision cross sections between the various species (the subscript i refers to ions and A refers to neutral atoms). Using these, the definition of the ionization fraction $a = n_i/(n_i + n_A)$, and quasi-neutrality $n_i = n_e$ gives the following expression for viscosity in terms of the ionization fraction:

$$\eta_H = m_A <C_H> \left(\frac{a}{aQ_{ii} + (1-a)Q_{iA}} + \frac{1-a}{(1-a)Q_{AA} + aQ_{iA}} \right) \qquad (43)$$

where Q_{ii} denotes the coulombic ion-ion cross section, Q_{iA} denotes the ion-neutral cross section, and Q_{AA} denotes the neutral-neutral cross section. Typically for argon, $Q_{AA} \approx 10^{-19} m^2$, $Q_{iA} \approx 10^{-18} m^2$, and $Q_{ii} \approx 10^{-16} m^2$. It can be seen from (43) that when $a = 0$, the viscosity is determined by Q_{AA}. If $a = 1$, then the viscosity is determined by Q_{ii}, which is three orders of magnitude bigger than Q_{AA}. Further, if $a < 0.9$, the viscosity is primarily determined by Q_{iA}, which is only about an order of magnitude bigger than Q_{AA}. This indicates that in order to have very small boundary layer thicknesses, the boundary layer flow must be very nearly fully ionized. In fact, it is this dependence of the viscosity on the degree of ionization that has resulted in the relatively large boundary layer thicknesses that have been computed. This explains why the non-equilibrium boundary layer grew so quickly as to merge in the middle of the thruster. The straight coaxial thruster of King[4] has been described by experimentalists as being "lossy" compared to the shorter "benchmark" thruster (the "benchmark" thruster was less than 10 cm. long whereas King's coaxial thruster was 20 cm. long). The non-equilibrium boundary layer theory presented in this paper explains why this is so. The resulting dependence of the viscosity on the ionization fraction also causes the heavy particle thermal conductivity to depend on the ionization fraction as well (this is because the heavy particle Prandtl number is roughly constant). Consequently, this affects the heat transfer to the electrode.

Thus far, MPD boundary layer flow has been discussed under the non-equilibrium, frozen, and fully ionized assumptions, for a uniform mass flow of 3 g/sec. A calculation of the non-equilibrium boundary layer has also been performed for a uniform mass flow of 6 g/sec. For this mass flow, the boundary layers merged at approximately 6 cm., as opposed to 4 cm. from

the leading edge for a mass flow of 3 g/sec. This is to be expected, since the density is higher in the higher mass flow case which in turn, gives smaller boundary layer thicknesses.

The boundary layer solutions presented in this section may be used to estimate the drag as well as the heat transfer. The heavy particle heat flux that has been calculated in this section, gives an idea of how much heat is transferred from the hot flowing plasma to the wall by thermal conduction. The results of this section may be used to determine electrode surface temperatures which determine erosion rates.

V. Summary and Conclusions

The electrode-adjacent boundary layer in an MPD thruster has been analyzed for the first time. The governing equations for a two-temperature, laminar, compressible, plasma boundary layer have been derived from first principles. Approximate solutions to these equations have been obtained for the MPD thruster operating at steady state under near-onset conditions, under various assumptions regarding the rate kinetics. The approximate solutions have been obtained by the Howarth-Dorodnitsyn transformation used in conjunction with energy and momentum integral methods. Thus, the effects of wall friction and heat transfer to the wall have been quantified.

The boundary layer theory presented in this paper provides a means of estimating viscous drag, heat transfer, and has underscored the importance of ionization and recombination rate kinetics. Three cases have been considered. The first is a non-equilibrium boundary layer with ionization slip, the second is a frozen boundary layer with a non-equilibrium ionizing free-stream, and the third is a fully ionized frozen boundary layer with a fully ionized frozen free-stream. The three different assumptions about the rate kinetics have yielded significantly different boundary layer thicknesses. This has important consequences for viscous drag and heat transfer to the electrode. The case of the non-equilibrium boundary layer with realistic ionization slip has yielded a large boundary layer thickness. This implies that the anode and cathode boundary layers merge in the channel, leading to a fully developed flow.

The strength of this boundary layer theory lies in its assumption of a two-temperature plasma. However, two weak assumptions namely that of scalar electrical conductivity and that of negligible radiative heat transfer, must be addressed. These assumptions have been made in order

to simplify an otherwise complicated problem. Inclusion of the Hall effect (tensor electrical conductivity) would render the free stream flow two-dimensional. Further, it would render the assumption of negligible ion ohmic heating in the heavy particle sensible energy equation (see section II) invalid. Radiation from the hot plasma to the wall may also be important for determining the heat transfer to the electrode. The inclusion of radiation could lead to higher ionization fractions near the wall, and therefore possibly reduce the wall shear and wall conductive heat flux by lowering the viscosity and the thermal conductivity. However, there would be additional heat transfer to the wall because of the radiative interaction between the plasma and the wall and this is expected to be the dominant effect. Also, the increased ionization fraction near the wall will lead to higher ion bombardment. Plasma radiation may therefore enhance the overall electrode erosion rate.

This work has demonstrated the importance of ionization and recombination in the electrode-adjacent boundary layer of the MPD thruster. The results of the boundary layer analysis has indicated that the MPD boundary layer may be appreciably thick and therefore may have important consequences for the viscous drag and electrode erosion. Further experimental information on temperatures and concentrations near the electrodes would therefore be invaluable.

Acknowledgements

References

1. J. L. Lawless, and V. V. Subramaniam, "A Theory of Onset in Magnetoplasmadynamic Thrusters," AIAA/DGLR/JSASS 18th International Electric Propulsion Conference, Alexandria, Virginia (1985). To be published in AIAA Journal of Propulsion & Power.

2. V. V. Subramaniam, *On the Phenomenon of Onset in Magnetoplasmadynamic Thrusters,* PhD dissertation, Carnegie-Mellon University, August 1986.

3. D. Q. King, K. E. Clark, and R. G. Jahn, "Effect of Choked Flow on Terminal Characteristics of MPD Thrusters," AIAA-81-0686, 15th International Electric Propulsion Conference, April 1981, Las Vegas, Nevada.

4. D. Q. King, *Magnetoplasmadynamic Channel Flow for Design of Coaxial MPD*

Thrusters, PhD dissertation, Princeton University, December 1981.

5. A. C. Malliaris, R. R. John, R. L. Garrison, and D. R. Libby, "Performance of Quasi-Steady MPD Thrusters at High Powers," *AIAA Journal*, Vol. 10, No. 2, February 1972.

6. H. Schlichting, *Boundary-Layer Theory*, McGraw-Hill,Inc., New York, NY, 1968.

7. N. Curle, "Heat Transfer Through a Compressible Laminar Boundary Layer," The Aeronautical Quarterly, May 1962, pp. 255-270.

8. G. Poots, "A Solution of the Compressible Laminar Boundary Layer Equations with Heat Transfer and Adverse Pressure Gradient," *Quart. Journ. Mech. and Applied Math.*, Vol. XIII, No. 1, 1960, pp. 57-84. .

9. Y. Y. Chan, "Integral Method in Compressible Laminar Boundary Layers and its Application," *The Physics of Fluids*, Vol. 9, No. 2, February 1966, pp. 350-358. .

10. H. W. Emmons and J. G. Brainerd, "Temperature Effects in a Laminar Compressible-Fluid Boundary layer along a Flat Plate," Journal of Applied Mechanics, No. A, September 1941, pp 105-110.

11. H. Blasius, "Grenzschichten in Flussigkeiten mit kleiner Reibung," Z. Math. u. Phys. 56, 1-37 (1908). Engl. transl. NACA TM 1256.

12. W. S. Liu, B. T. Whitten, and I. I. Glass, "Ionizing argon boundary layers. Part 1. Quasi-steady flat-plate laminar boundary-layer flows," *J. Fluid Mech.*, Vol. 87, No. 4, 1978, pp. 609-642. .

13. E. D. Doss, H. A. Dwyer, and M. A. Hoffman, "Influence of Segmentation and Ambipolar Diffusion on MHD Nonequilibrium Boundary Layers," *AIAA Journal*, Vol. 12, No. 2, February 1974, pp. 155-162. .

14. B. Nageswara Rao, "Boundary-layer flow in a magnetohydrodynamic channel," *J. Appl. Phys.*, Vol. 58, No. 7, October 1985, pp. 2516-2518. .

15. Th. von Karman, "Uber laminare und turbulente Reibung," ZAMM 1, 233-253 (1912). Engl. transl. in NACA TM 1092. Also Coll. Works vol. 2. 70-97 London 1956.

16. E. Gruschwitz, "Die tubulente Reibungsschicht in ebener Stroemung bei Druckabfall und Druckanstieg," Ing. Arch. 2, 321-346 (1931).

17. K. Wieghardt, "Ueber einen Energiesatz zur Berechnung laminarer Grenzschichten," Ing.

Arch. 16, 231-242 (1948).

18. L. E. Kalikhman, *Elements of Magnetogasdynamics*, W. B. Saunders Co., Philadelphia, PA, 1967.

19. S. Chapman, and T. G. Cowling, *The Mathematical Theory of Non-Uniform Gases*, Cambridge University Press, Cambridge, England, 1952.

20. F. A. Williams, *Combustion Theory*, Addison-Wesley, 1965.

21. M. Mitchner and C.H. Kruger, Jr., *Partially Ionized Gases*, John Wiley & Sons, New York, 1973.

22. W. G. Vincenti and C. H. Kruger, *Introduction to Physical Gas Dynamics*, John Wiley and Sons, New York, 1967.

23. F. D. Hains, "Heat Transfer and Skin Friction in Magneto-Gas Dynamic Channel Flow," Tech. report D1-82-0047, No. 26, Boeing Scientific Research Laboratories, May 1960.

24. C. W. Gear, *Numerical Initial Value Problems in Ordinary Differential Equations*, Prentice-Hall, Englewood Cliffs, New Jersey, 1971.

Fig. 1: Non-equilibrium boundary layer growth for a total mass flow of 3 g/s.

Fig. 2: Ionization fraction at the wall (i.e. ionization slip) versus distance along the electrode, for a total mass flow of 3 g/s.

Fig. 3: Profile of non-dimensionalized ionization fraction across the boundary layer, at a location of 1 cm. downstream from the leading edge. The case shown here is that of a non-equilibrium boundary layer for a mass flow of 3 g/s.

Fig. 4: Profile of the heavy particle temperature across the boundary layer at 1 cm. from the leading edge. The case shown here is that of a non-equilibrium boundary layer for a mass flow of 3 g/s.

Fig. 5: Variation of heavy particle wall conductive heat flux versus distance. The case shown here is that of a non-equilibrium boundary layer for a mass flow of 3 g/s.

Fig. 6: Variation of wall shear versus distance for a mass flow of 3 g/s. The case shown here is that of a non-equilibrium boundary layer.

Fig. 7: Frozen boundary layer growth for a mass flow of 3 g/s. In this case, the free stream is a non-equilibrium ionizing flow.

Fig. 8: Heavy particle temperature profiles at various locations downstream from the leading edge for a mass flow of 3 g/s. The case shown here is that of a frozen boundary layer with a non-equilibrium ionizing free stream.

Fig. 9: Variation of the heavy particle wall conductive heat flux versus distance for a mass flow of 3 g/s. The case shown here is that of a frozen boundary layer with a non-equilibrium ionizing free stream.

Fig 10 Variation of the wall shear versus distance for a mass flow of 3 g/s. The case here is that of a chemically frozen boundary layer and a non-equilibrium ionizing free

Fig 11 Fully ionized boundary layer growth for a total mass flow of 3 g/s. The case of a fully ionized and frozen boundary layer, with a fully ionized and frozen

free stream.

Fig. 12: Profiles of the heavy particle temperature across the boundary layer at various locations downstream from the leading edge, for a mass flow of 3 g/s. The case shown here is that of a fully ionized and frozen boundary layer, with a fully ionized and frozen free stream.

Fig. 13: Variation of the heavy particle wall conductive heat flux versus distance, for a mass flow of 3 g/s. The case shown here is that of a fully ionized and frozen boundary layer, with a fully ionized and frozen free stream.

Fig. 14: Variation of the wall shear versus distance, for a mass flow of 3 g/s. The case shown here is that of a fully ionized and frozen boundary layer, with a fully ionized and frozen free stream.

FIG 1

FIG. 2

FIG. 3:

FIG. 4:

FIG 5

FIG. 6

ANODE BOUNDARY LAYER

CATHODE BOUNDARY LAYER

5 cm.

X [cm]
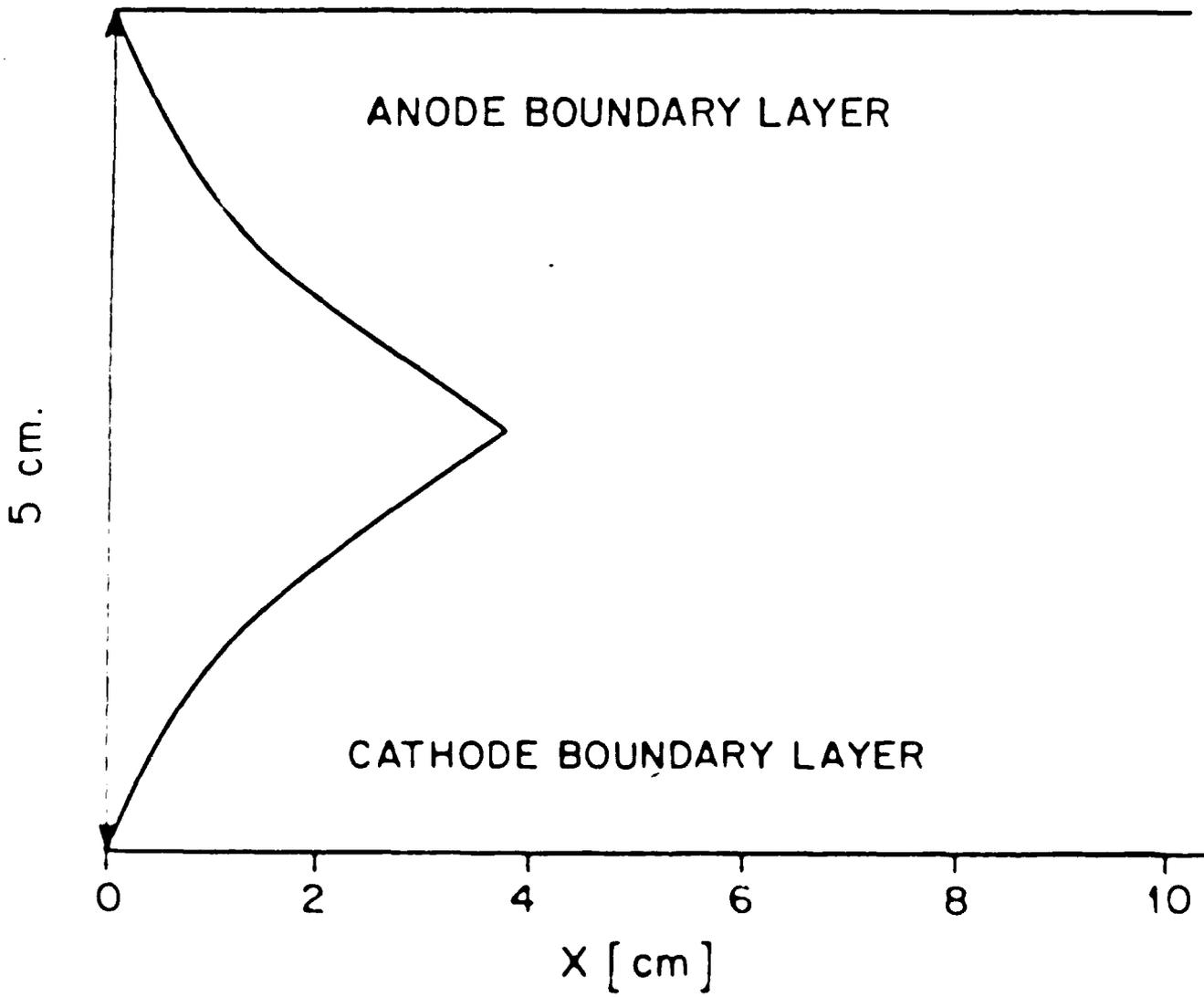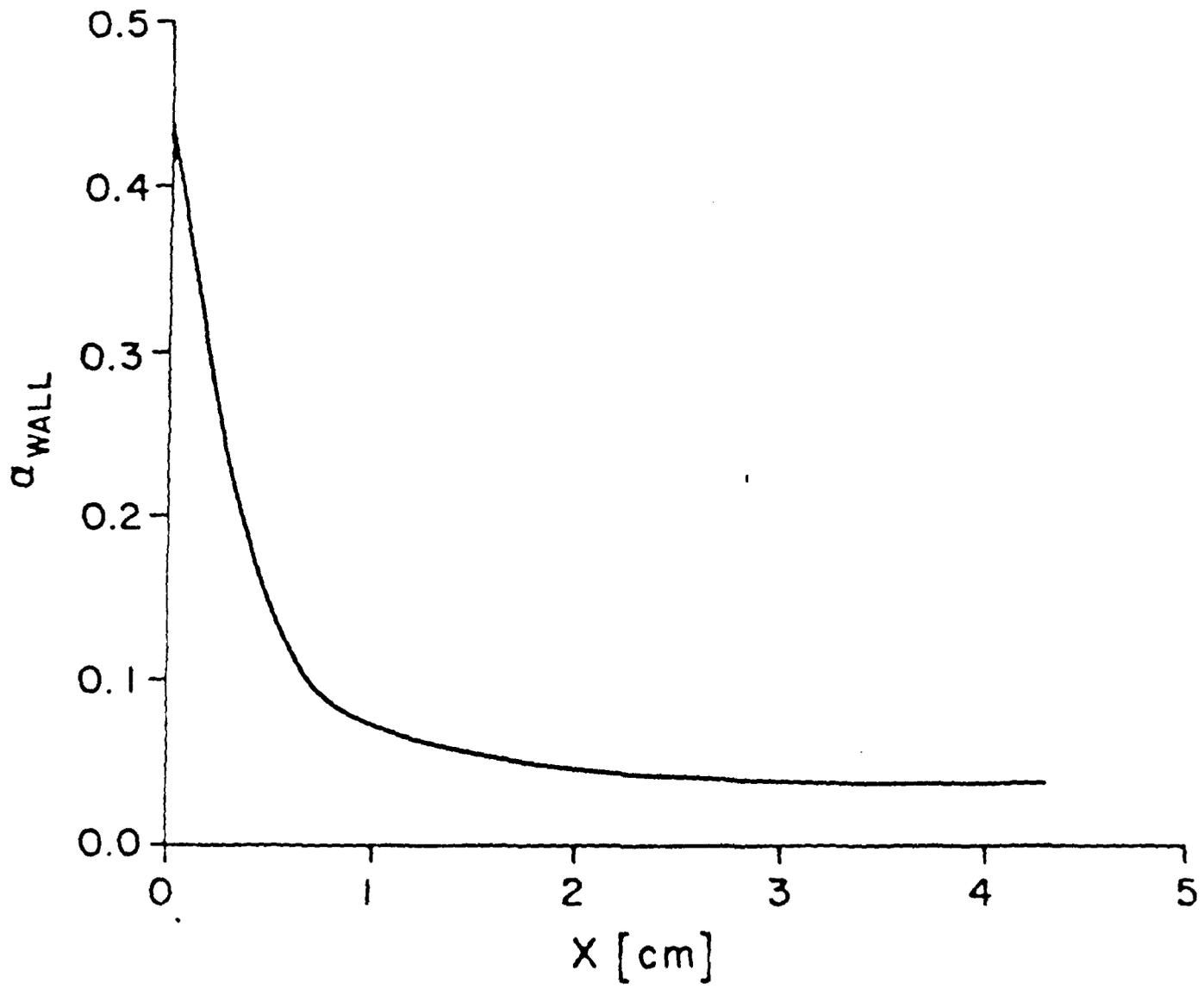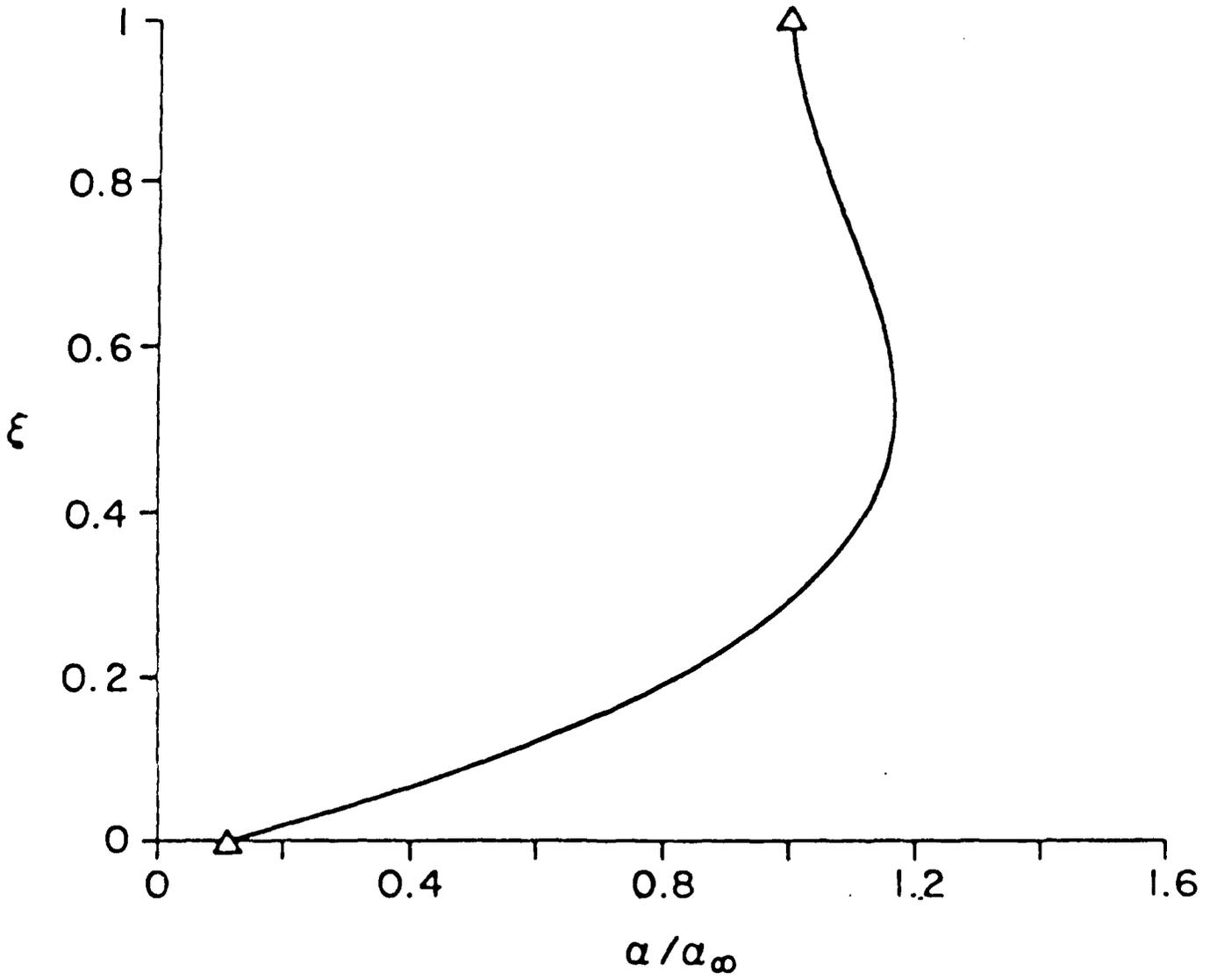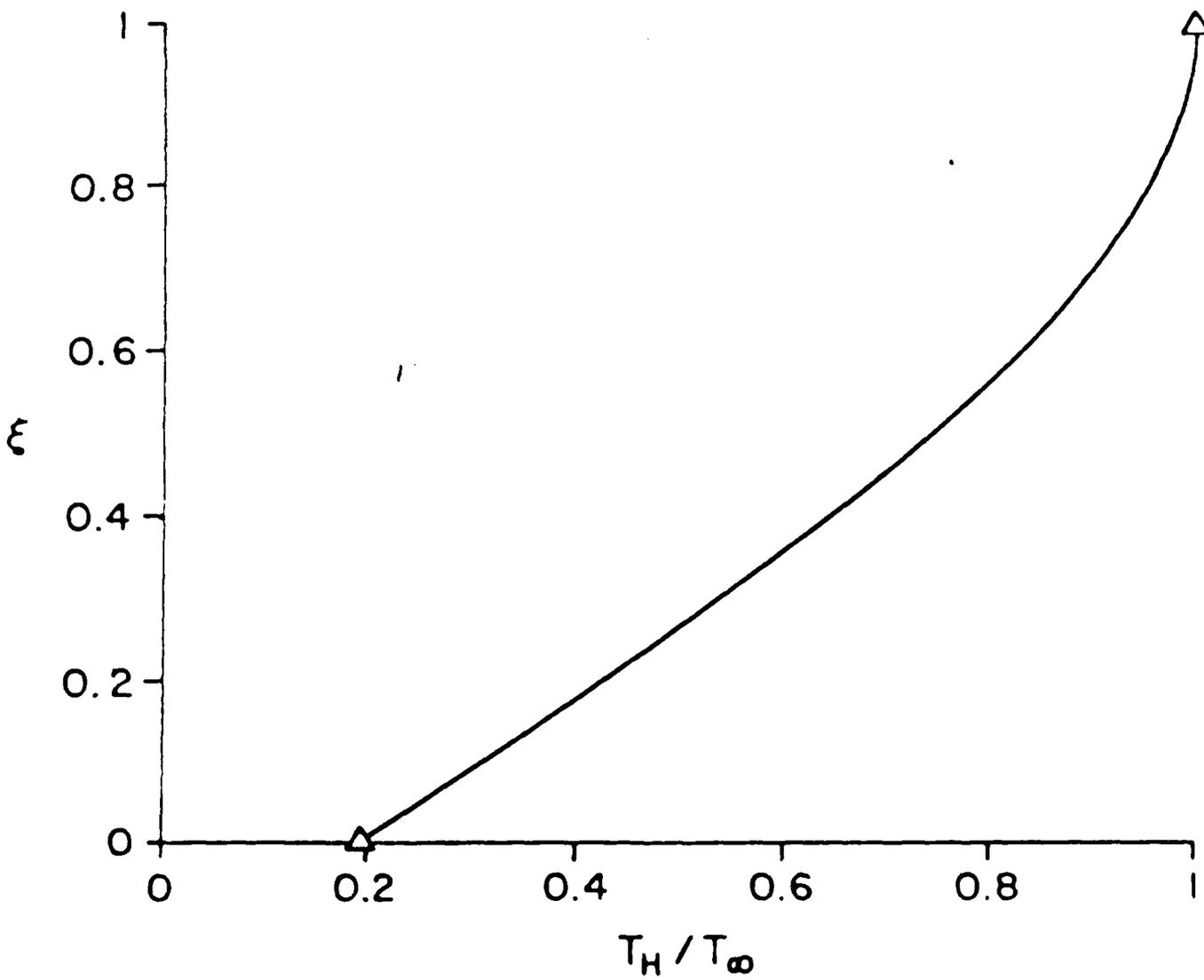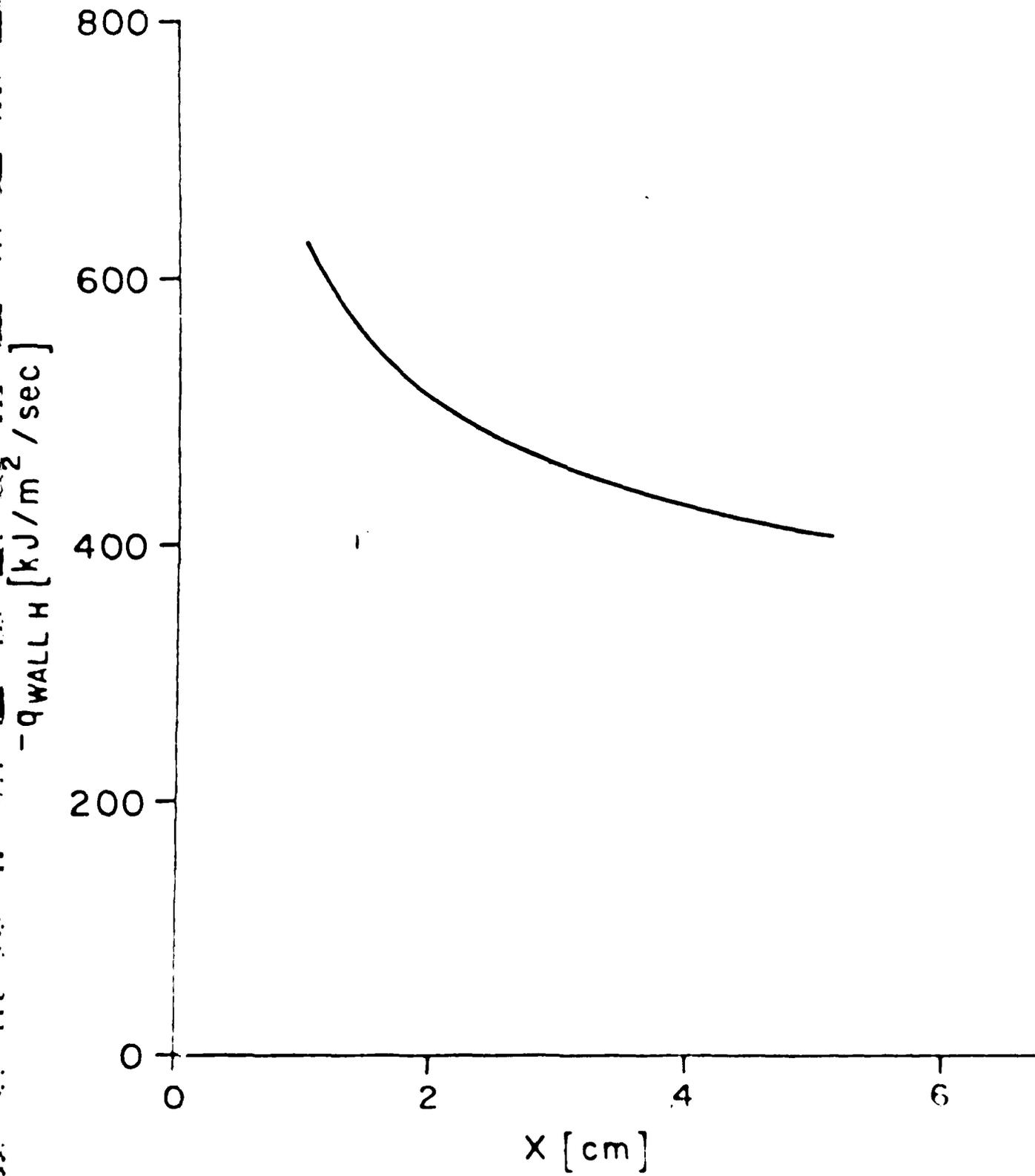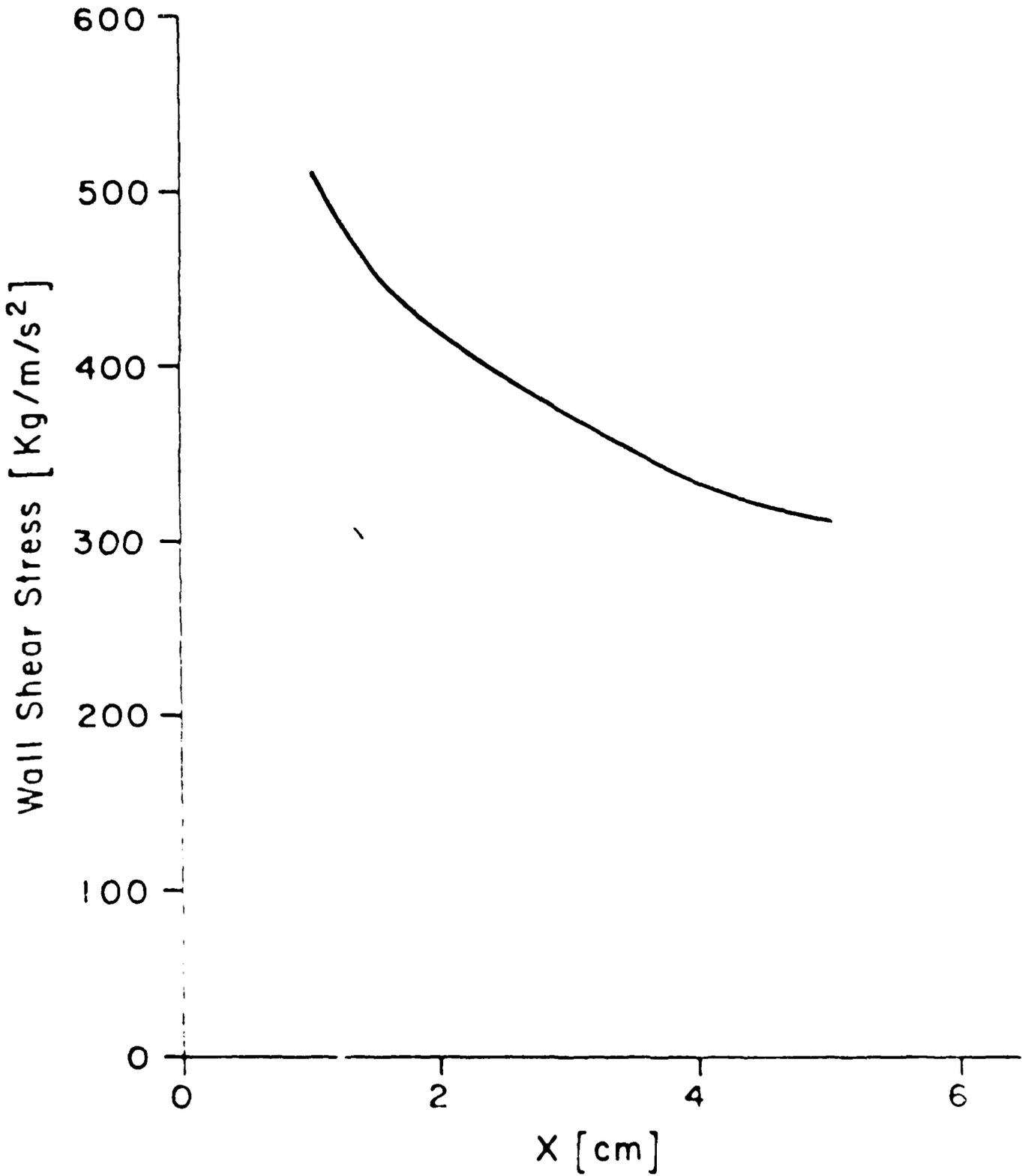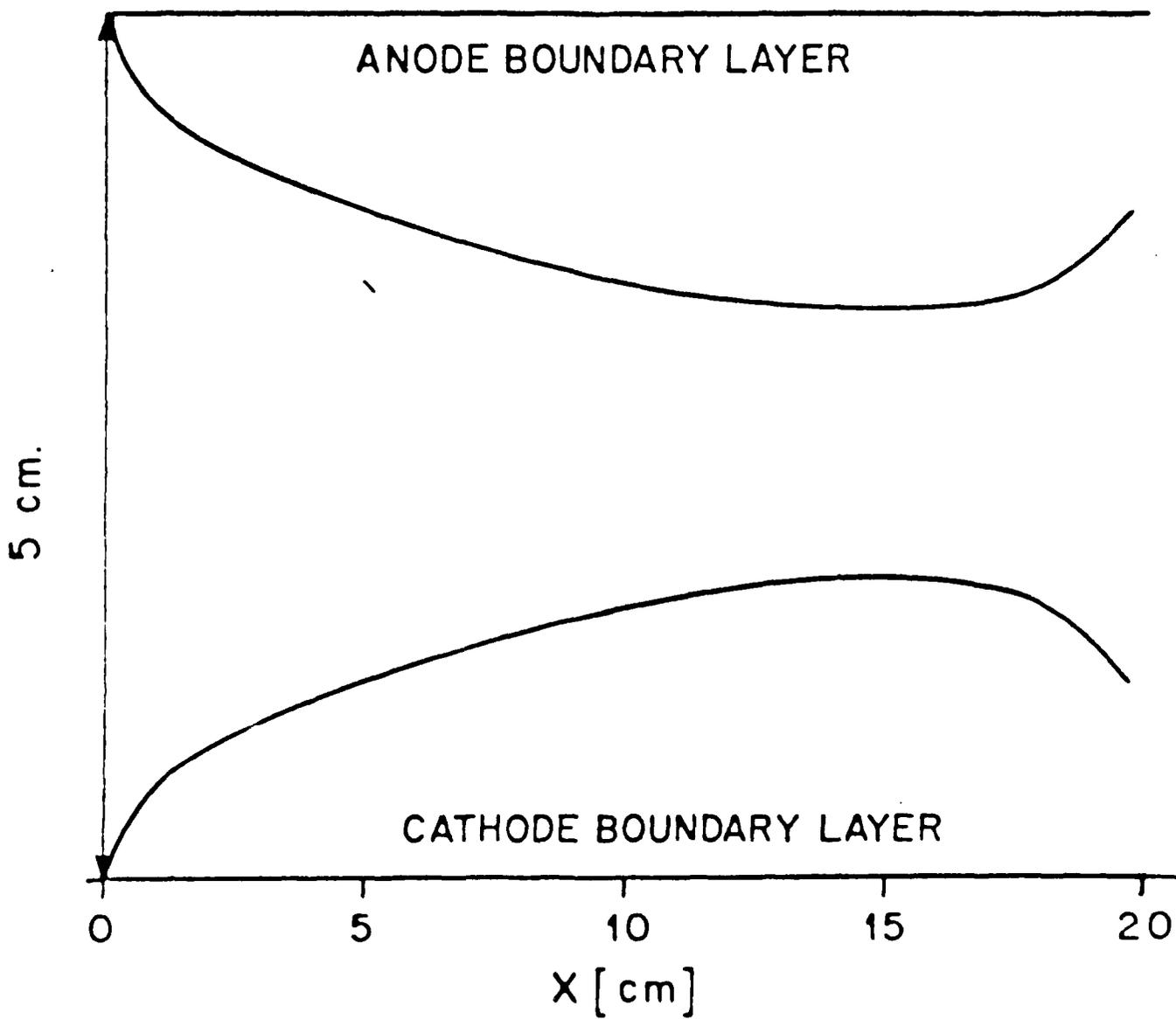
FIG. 7:
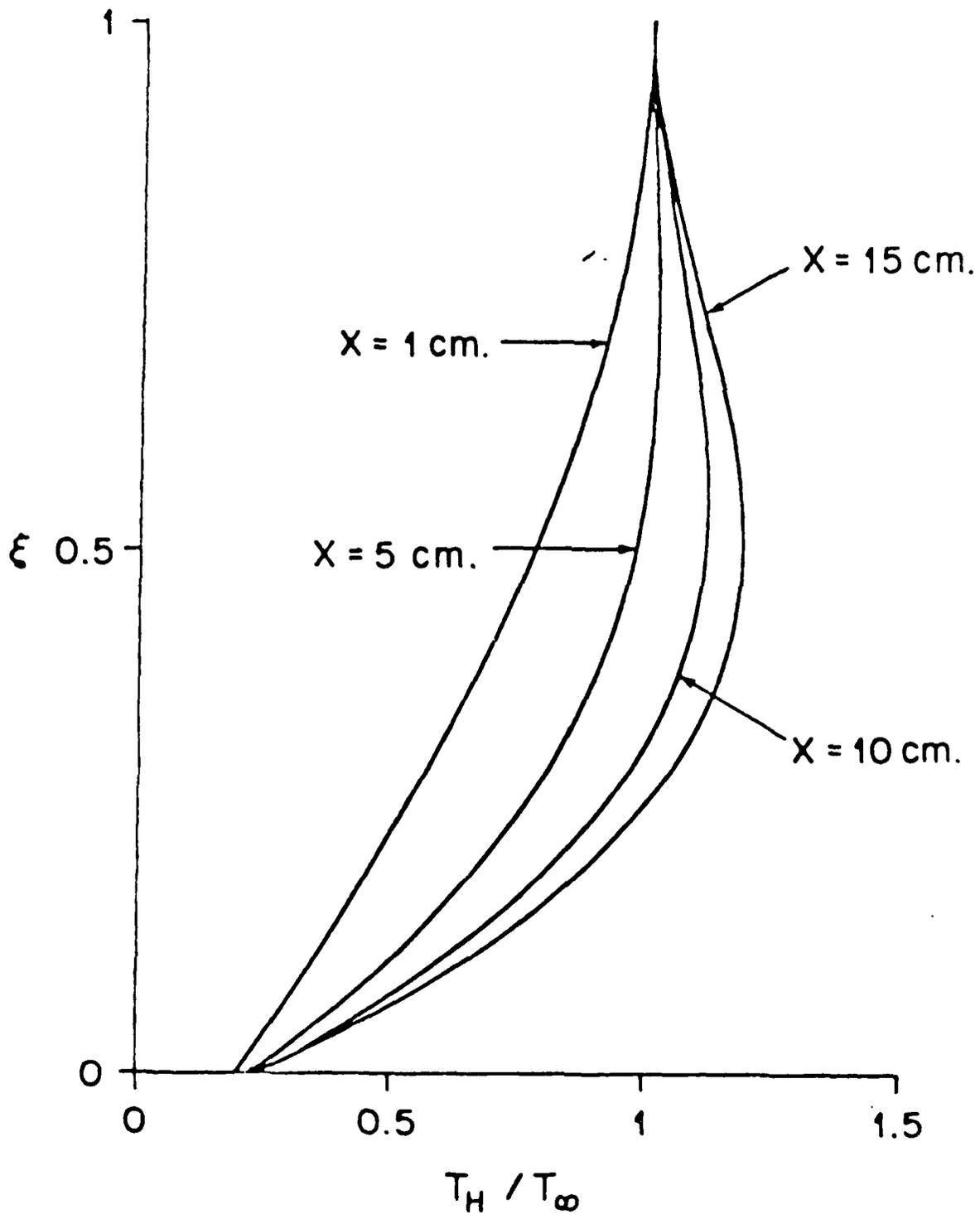
FIG. 8:
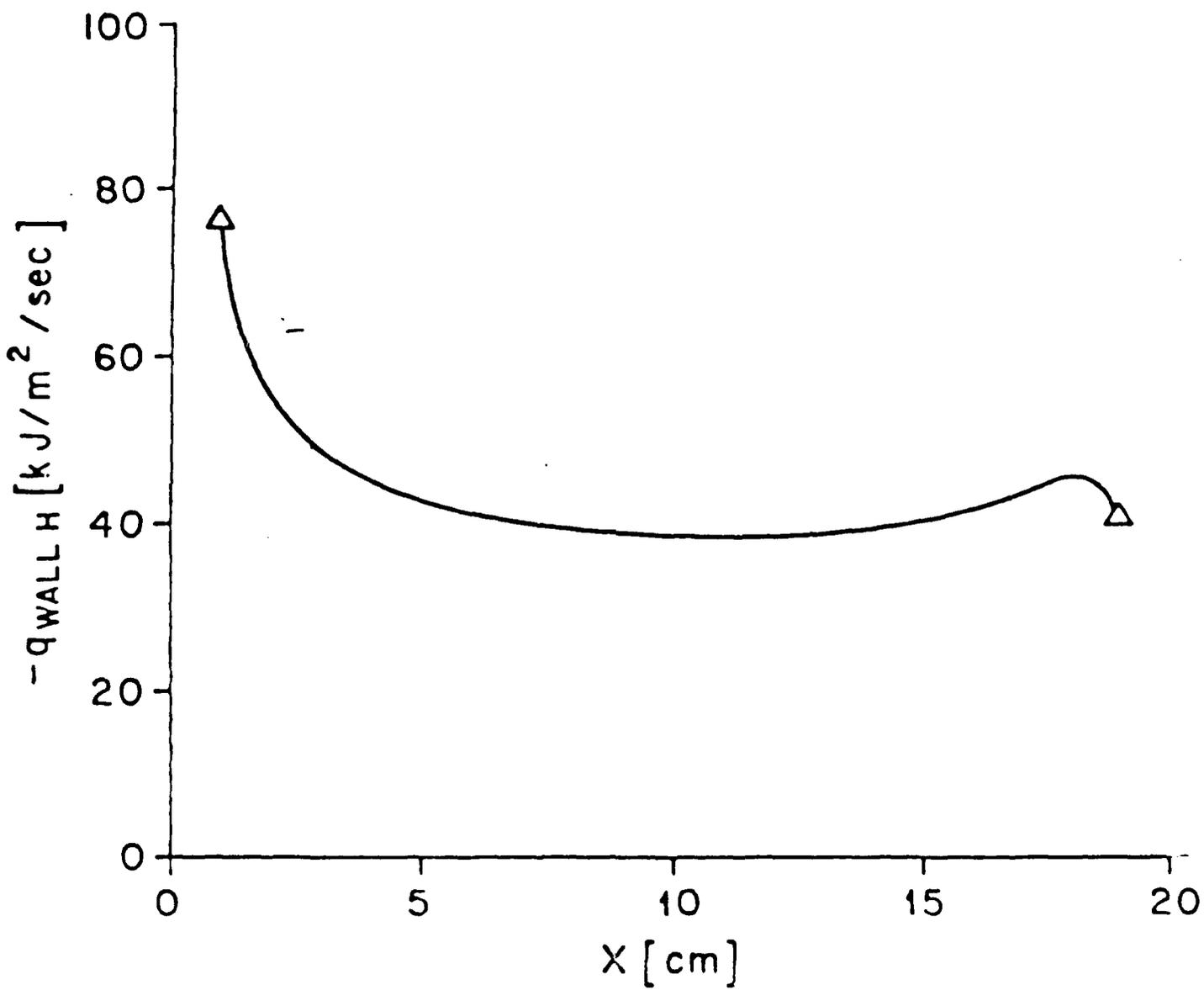
FIG. 9:
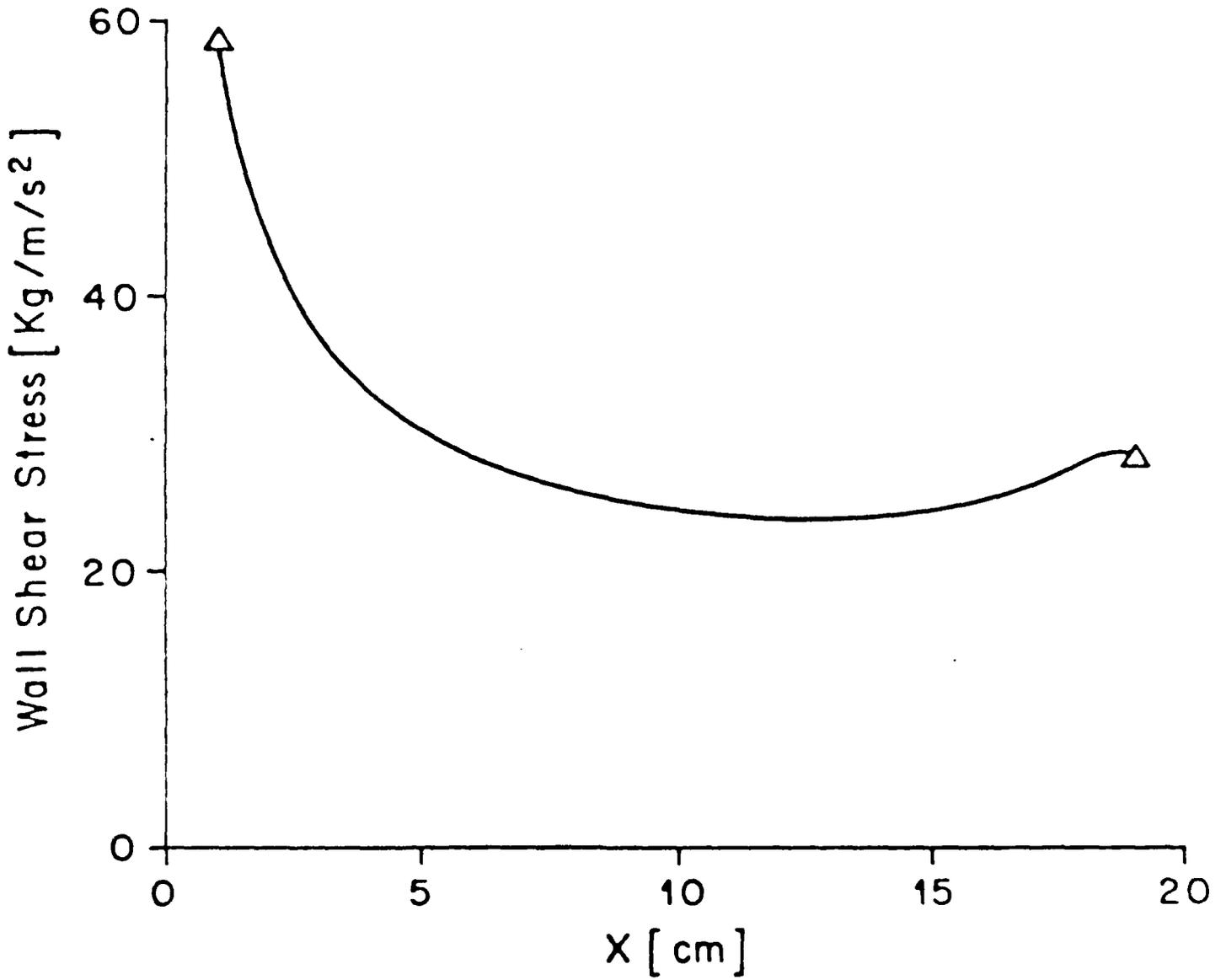
FIG. 10:
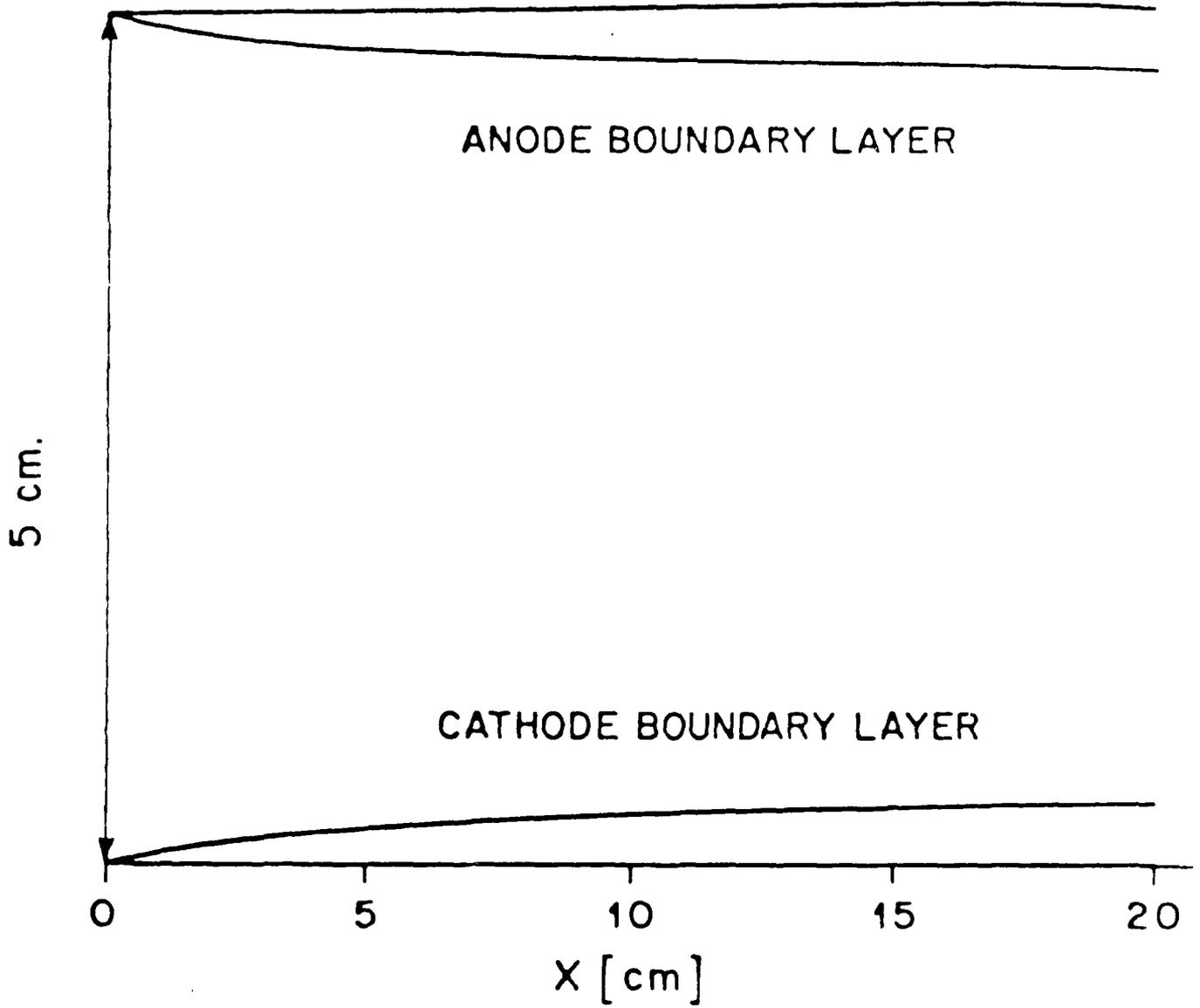
FIG. 11:
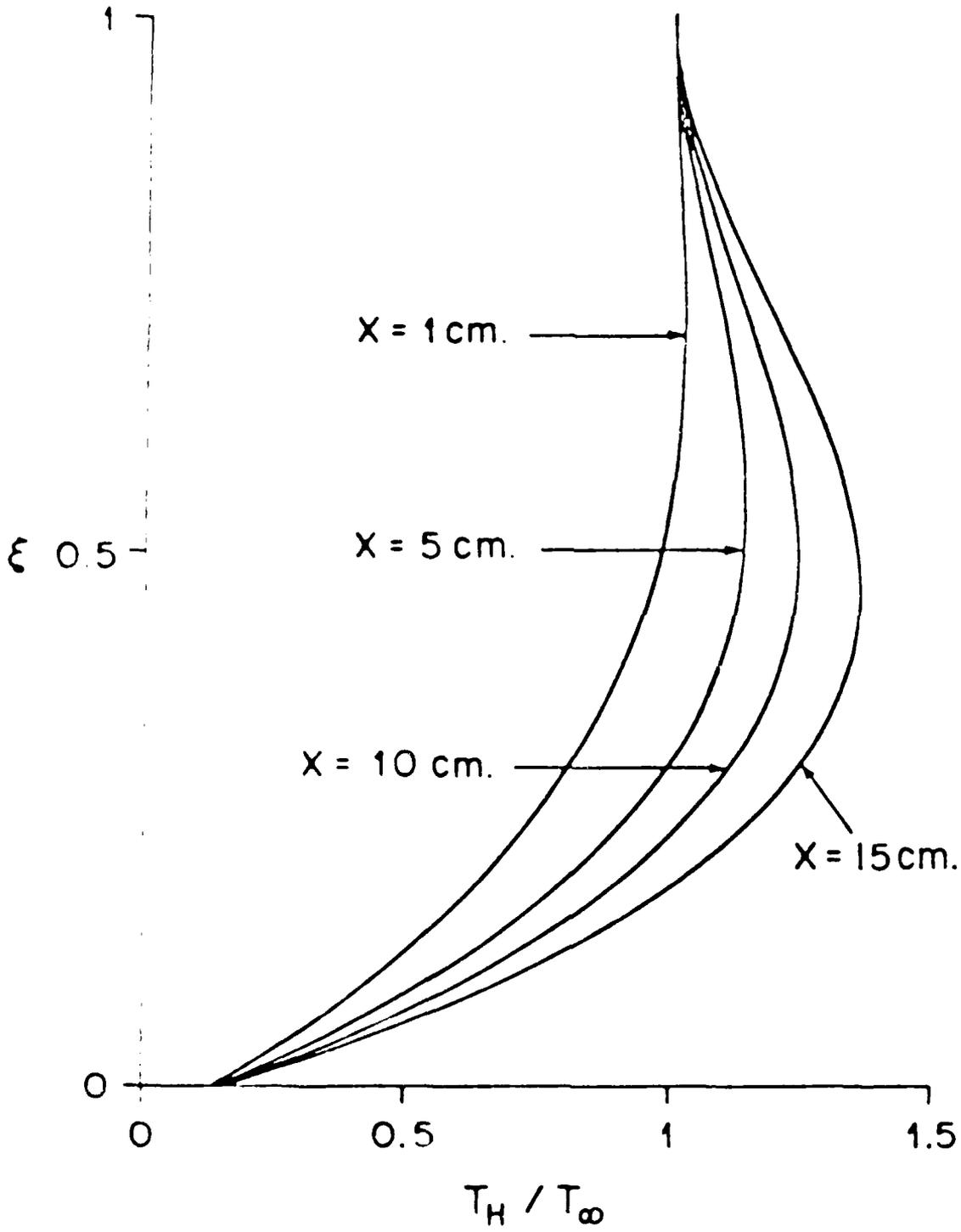
FIG. 12:
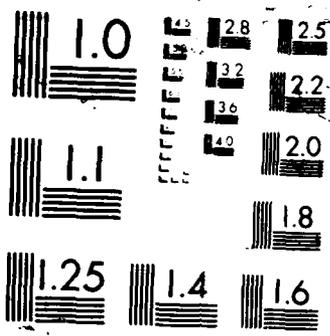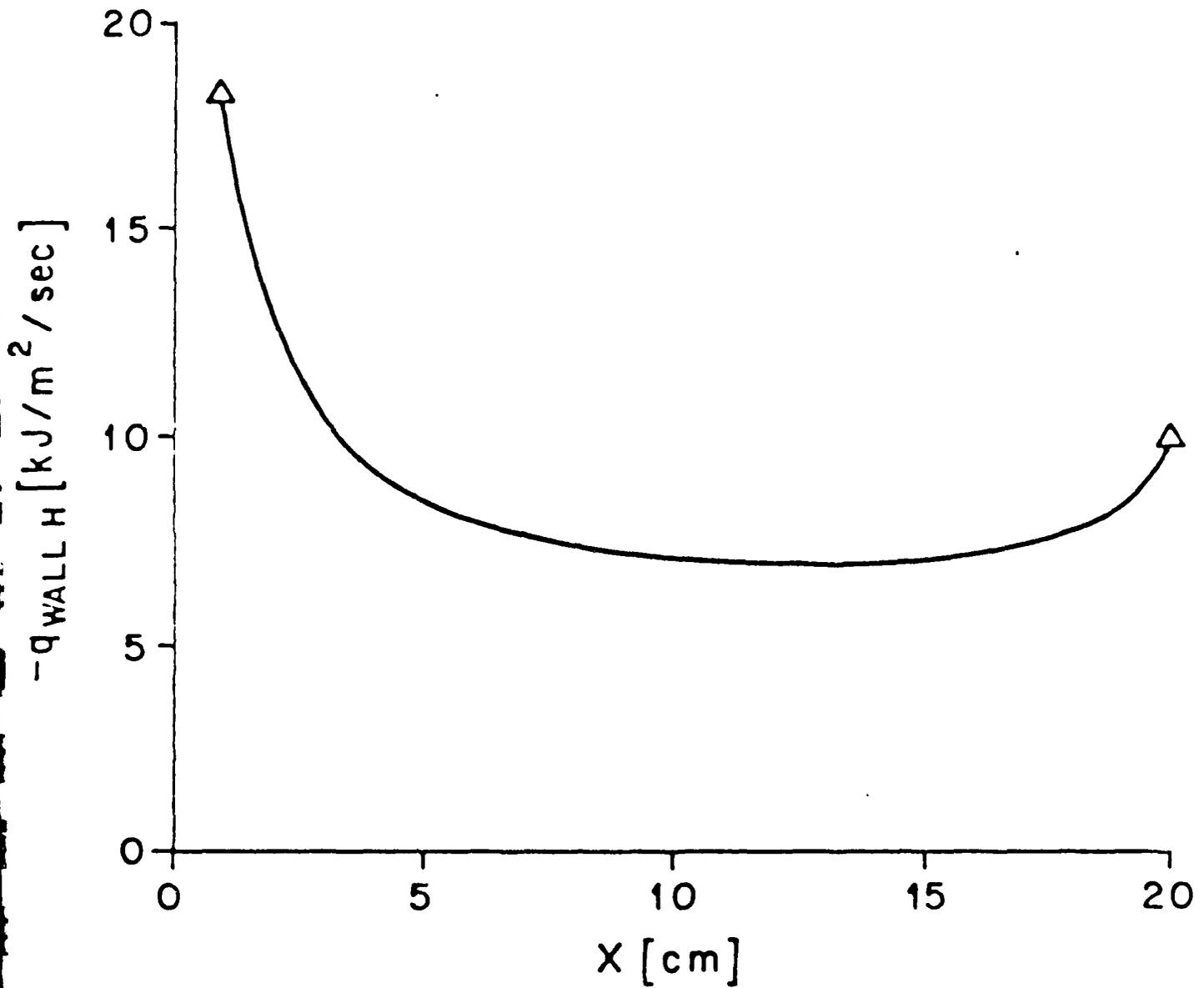
FIG. 13:
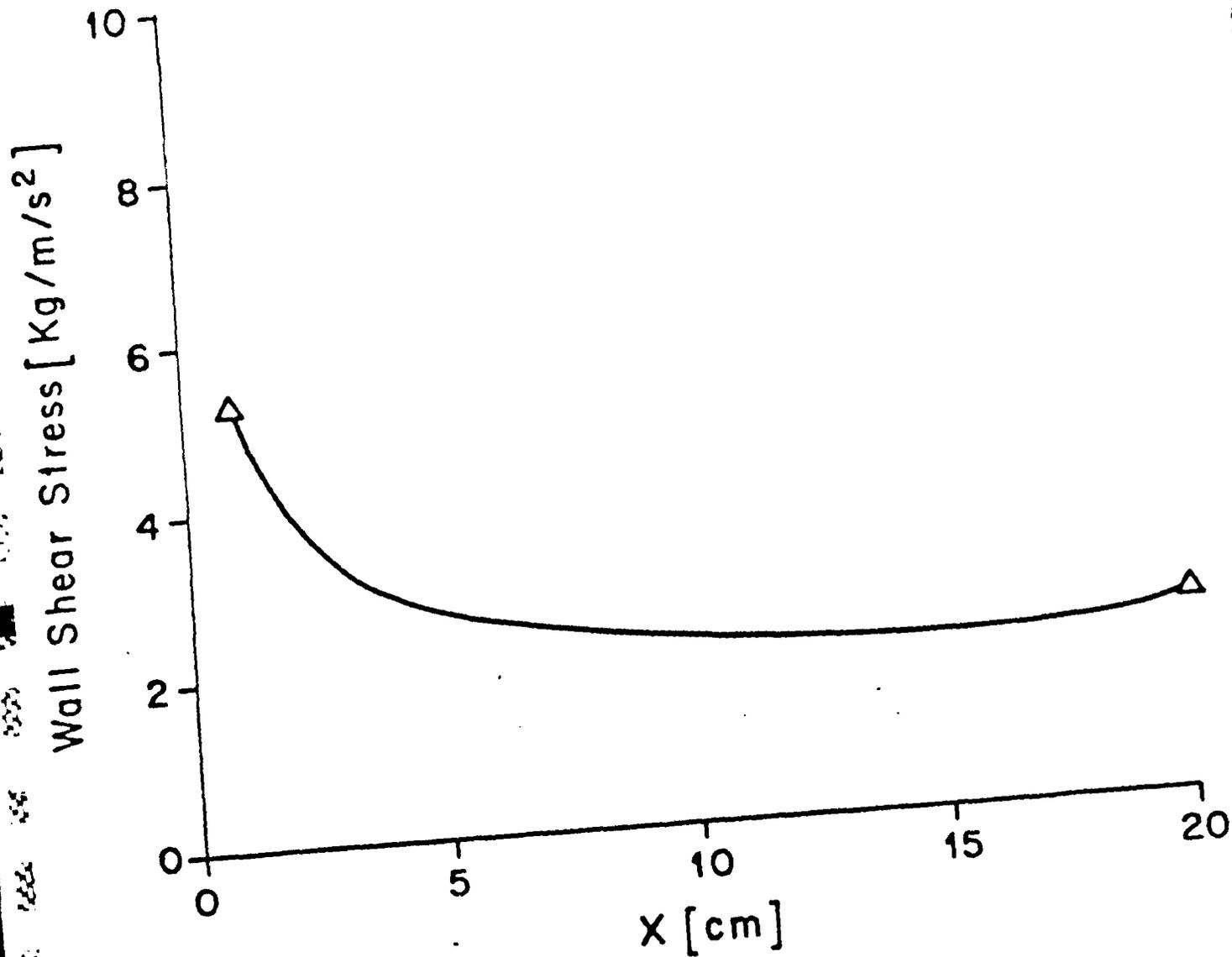
FIG. 14:

APPENDIX   E

Carnegie-Mellon University

CARNEGIE INSTITUTE OF TECHNOLOGY

THESIS

SUBMITTED IN PARTIAL FULFILLMENT OF THE REQUIREMENTS

FOR THE DEGREE OF DOCTOR OF PHILOSOPHY

TITLE ON THE PHENOMENON OF ONSET IN MAGNETOPLASMADYNAMIC THRUSTERS

PRESENTED BY VISHWANATH VENKATESWARAN SUBRAMANIAM

ACCEPTED BY THE DEPARTMENT OF MECHANICAL ENGINEERING
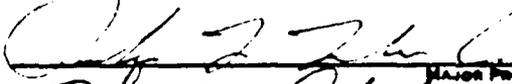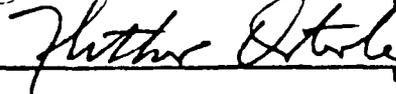
_____ MAJOR PROFESSOR   7/1/86 DATE

_____ DEPARTMENT HEAD   21 Aug 86 DATE

APPROVED BY THE COLLEGE COUNCIL

_____ DEAN   Aug 25, 1986 DATE

CARNEGIE-MELLON UNIVERSITY

ON THE PHENOMENON OF ONSET IN
MAGNETOPLASMADYNAMIC THRUSTERS[1]

A DISSERTATION

SUBMITTED TO THE GRADUATE SCHOOL

IN PARTIAL FULFILLMENT OF THE REQUIREMENTS

for the degree

DOCTOR OF PHILOSOPHY

in

MECHANICAL ENGINEERING

by

Vishwanath Venkateswaran Subramaniam

Pittsburgh, Pennsylvania

June , 1986

ABSTRACT

The performance of Magnetoplasmadynamic (MPD) thrusters has been severely limited by 'onset'. The destructive onset phenomenon refers to the abrupt increase in voltage oscillations accompanied by severe electrode erosion which occurs at a critical value of the current for a given mass flow rate. This research is aimed at explaining and quantifying onset.

The steady, one-dimensional, self-field flow in the MPD thruster is first analyzed for frozen flow, equilibrium flow, and non-equilibrium flow. This quasi one-dimensional theory explains the behaviour of efficiency and predicts a new mechanism for the onset phenomenon. This model predicts that smoothly accelerating supersonic flow can exist only below a critical current level because of increasing back-EMF. This limit is interpreted as onset and correlates with the experimentally observed $J^2/\dot{m}$ onset parameter.

In order to quantify electrode erosion rates, the electrode-adjacent boundary layer is analyzed using the results of the quasi one-dimensional theory. The free stream boundary conditions for the steady boundary layer flow analysis are obtained from the results of the quasi one-dimensional theory. Since the electrode wall is relatively cold compared to the flow, and since relatively fewer collisions are required for the heavier particles to equilibrate, an approximate two temperature boundary layer theory is developed. The two temperature compressible non-equilibrium ionization equations are then solved using momentum integral and energy integral methods. Wall shear stress, wall heat flux, temperature, density, and

ionization fraction profiles are then calculated. These results of the two temperature theory may then be used to estimate rates of erosion by evaporation and due to sputtering.

The major accomplishments of this thesis include the development of a new theory that for the first time, predicts onset due to an excessive back-EMF at high currents, the establishment of the importance of ionization and recombination, and the first study of an electrode-adjacent boundary layer in MPD flow.

This thesis addresses steady flow only. Thus, only the conditions leading upto onset are considered. No attempt is made to study any phenomena beyond the limit of onset. Such a theory would have to take into consideration the unsteady nature of the flow beyond onset. However, this research provides. the basis for a more comprehensive approach to understanding and quantifying the phenomenon of onset and electrode erosion in MPD thrusters. Such a theory may prove to be valuable in the design and perhaps future design of MPD thrusters.

ACKNOWLEDGEMENTS

My sincerest gratitude is extended to my advisor, Dr. J. L. Lawless, whose scientific expertise requires no further acknowledgement. Here, I wish to bring attention to his special talents of teaching through patience, understanding, and guidance that are vital during the sometimes frustrating moments that accompany independent research and learning; for this I will always be grateful.

My special thanks are also extended to my committee members, Prof. J. F. Osterle, Prof. W. F. Hughes, Dr. D. Q. King, and Dr. H. Torab. I am especially grateful to Dr. King of the Jet Propulsion Laboratory, and Dr. Torab of Gannon University for making special visits for my thesis proposal and defense.

To my dear friends, Francis Stefani, Bob Sturges, and Katherine Nelson, thank you for all the inspiration, encouragement, support, and love they provided during every phase of this dissertation. I thank Kathie also for being a special kind of teacher (at W.P.S.B.C.) who has helped me to understand a little better what life is all about.

To Medini Singh, Dr. Paul Steif, Dr. T. R. Viswanathan, Tony Rosato, P. K. Mozumder, Brian Sauk, Bob Gubernat, Paco Ruiz, a special note of thanks for all the necessary encouragement and diversion that they provided throughout the doctoral research. Most of all, I am grateful to them for beginning with me what promises to be truly great friendships.

Finally, I would like to extend the simplest but most special gratitude to my father, mother, Sunder, and Sheila for their constant love and support throughout my educational career. I dedicate this work to them.

NOMENCLATURE

$a =$ Acoustic speed of sound

$a^* =$ Acoustic speed of sound at the sonic point

$A =$ Cross sectional channel area

$Æ = W/H =$, Aspect ratio

$B =$ Magnetic field

$B^* =$ Magnetic field at the sonic point

$B_i =$ Magnetic field at the inlet, $x = 0$

$C_D =$ Drag coefficient

$C_e =$ Mean thermal speed of electrons at the sheath-boundary layer edge

$<C_H> =$ Mean thermal speed of the heavy particles

$C_i =$ Mean thermal speed of ions at the sheath-boundary layer edge

$C_{pe} = 5k/2m_A =$ Specific heat at constant pressure

$C_v =$ Specific heat at constant volume

$D^e =$ Electron diffusion coefficient

$D^i =$ Ion diffusion coefficient

$D_w^i =$ Ion diffusion coefficient evaluated at the wall

$D_H =$ Hydraulic diameter

$e =$ Electronic charge

$e_{int} =$ Specific internal energy

$e_c =$ Specific internal energy at cutoff temperature, $T = T_c$

$E =$ Electric field

$E_w =$ Electric field at the wall, evaluated from overall current conservation

$F = \rho u =$ Mass flux

$F_H =$ Helmholtz free energy

$H =$ Interelectrode distance

H_e = Total enthalpy

h = Specific enthalpy

h^* = Specific enthalpy at the sonic point

h_c = Effective heat transfer coefficient

h_e = Electron enthalpy

h_{EFF} = Heat transfer coefficient between cathode and external coolant

l^* = Ionization thickness

J = Total current

j = Current density

j^* = Current density at the sonic point

$\cdot j_\infty$ = Free stream current density

j_{TE} = Current density due to thermionic emission

k = Boltzmann's constant

k_b = Recombination rate constant

k_i = Ionization rate constant

K_1, K_2, K_3 = Equilibrium constants for first, second, and third ionization-recombination reactions

L = Thruster length

L_e = Mean free path of the electron

L_{AH} = Mean free path for neutral atom colliding with other heavy particles

L_{IH} = Mean free path for ion colliding with other heavy particles

$M = u/a$ = Mach number

$\dot{m}$ = Mass flow rate

m_A = Atomic mass

m_e = Mass of electron

n = Electron or ion number density at the sheath-boundary layer edge

n_A = Neutral atom number density

n_e = Electron number density

n_{ew} = Electron number density at the wall

$n_+ = n_i$ = Single ion number density

n_{++} = Double ion number density

n_{+++} = Triple ion number density

$\dot{n}_{ion}$ = Net production rate of ions by inelastic collisions

n_o = Total number density of heavy particles

P = Pressure

P^* = Pressure at the sonic point

Q_{AA} = Total momentum transfer atom-atom cross section

Q_{ea} = Total momentum transfer electron-atom cross section

Q_{ei} = Total momentum transfer electron-ion cross section

Q_{iA} = Total momentum transfer ion-atom cross section

Q_{ii} = Total momentum transfer ion-ion cross section

q_H = Heavy particle conductive heat flux

q_{wH} = Heavy particle conductive heat flux at the wall

S = Entropy

S^* = Magnetic force number at the sonic point

T = Temperature

T^* = Temperature at the sonic point

T_c = Cutoff temperature in the piecewise linear model

T_e = Electron temperature

T_{EC} = Effective cathode surface temperature

T_H = Heavy particle temperature

T_h = Total thrust at the exit, $x = L$

T_s = Wall slip temperature, in general $\neq T_w$

T_w = Wall or electrode temperature

T_∞ = Free stream temperature

u = Component of local average plasma velocity in x direction

U = Internal energy

u_i = Local average plasma velocity vector

u_{in} = Inlet flow speed

u_s = x component of slip velocity at the wall, in general $\neq 0$

$v =$ Component of local average plasma velocity in y direction

$V =$ Voltage drop across the thruster

$V_c =$ Cathode sheath voltage drop

$V_e =$ y component of electron diffusion velocity

$V_i =$ y component of ion diffusion velocity

$V_{iw} =$ y component of the ion diffusion velocity at the wall

$V_s =$ Sum of the sheath voltage drops

$W =$ Width of the electrode transverse to the flow

$x =$ Axial coordinate in direction of flow

$x^* =$ Position of the sonic point

$x_o^{21}, x_o^{11} =$ Sonine coefficients

$y =$ Transverse coordinate perpendicular to the flow

$Z_A, Z_e, Z_i, Z_{ii}, Z_{iii} =$ Total partition functions of neutral atom, electron, single ion, double ion, and triple ion

$a =$ Ionization fraction

$a_w =$ Ionization fraction at the wall

$a^* =$ Ionization fraction at the sonic point

$\Gamma =$ Evaporative mass flux

$\Delta =$ Transformed boundary layer thickness

$\delta_T =$ Boundary layer thickness

$\epsilon_i =$ First ionization energy

$\eta =$ Overall performance efficiency

$\eta_H =$ Heavy particle dynamic viscosity

$\eta_i =$ Ion dynamic viscosity

$\eta_A =$ Neutral atom dynamic viscosity

$\eta_L =$ Lorentz efficiency

$\Theta =$ Momentum thickness

$\Theta_H =$ Enthalpy thickness

$\kappa = B_i/B^*$

$\Lambda =$ Specific heat of sublimation of cathode

λ_H = Heavy particle heat conductivity

μ_0 = Permeability of free space

$<v_{eH}>$ = Energy-weighted average momentum transfer elastic collision frequency

ξ = Howarth-Dorodnitsyn transform variable

ρ = Mass density

ρ^* = Mass density at the sonic point

σ = Electrical conductivity

σ_c = Electrical conductivity due to electron-ion collisions

σ_n = Electrical conductivity due to electron-neutral collisions

σ_{SB} = Stefan-Boltzmann constant

σ^* = Electrical conductivity evaluated at the sonic point

TABLE OF CONTENTS

LIST OF FIGURES

CHAPTER 1

INTRODUCTION

Space missions require fuel efficient thrusters in order to transport greater amounts of payload. Therefore, given a particular thrust level $T = \dot{m} u_{exit}$, it is desirable to maximize the exit speed so that the mass flow rate (i.e. fuel consumption) is minimized. Magnetoplasmadynamic (MPD) thrusters use electric and magnetic fields to accelerate a plasma to high speeds. MPD thrusters, as distinguished from other electric propulsion devices, derive most of their thrust from $\vec{j} \times \vec{B}$ body forces in a steady flow[1]. The magnetic field may be externally applied as in some early work on the subject[2, 3, 4]. During the past ten years, work has concentrated on self-field thrusters. Operating at current levels of tens of kiloamps, self-field MPD thrusters have experimentally demonstrated exhaust speeds of 15000 to 40000 m/s and thrusts of the order of 100 Newtons. By contrast, the most exotic chemical propellants provide maximum exit speeds of about 6000 m/s. This fuel efficiency is the primary advantage that MPD thrusters have over conventional chemical thrusters. This thesis studies self-field thrusters.

MPD thrusters have been shown to achieve efficiencies of ~50%, but are limited by a destructive phenomenon known as 'onset'. This thesis theoretically examines the plasma flow in a one-dimensional self-field thruster. The behaviour of efficiency and its relationship to onset are considered. This theory predicts a new mechanism of onset related to the back-EMF. In this theory, onset appears as a conflict between the electric field required for magnetogasdynamic choking and the electric field necessary to draw all the

applied current. For a given mass flow and geometry, it is experimentally known that efficiency increases rapidly as the current increases. This increase is limited by the rapid erosion which begins to occur at some current level. This limit, also typically associated with voltage oscillations, is known as 'onset'. For a given geometry and varying mass flow, this limit correlates with $J^2/\dot{m}$ where J is the total current and $\dot{m}$ is the mass flow. This limit has been observed to vary with geometry[5, 6] but this variation is not understood.

Equilibrium flow in an MPD thruster has been modeled by King et al.[7] They assume a one-dimensional, local equilibrium, continuum flow with a uniform and constant electric field. The fluid enters the thruster at a slow speed and low temperature, whereupon the speed increases to sonic primarily due to ohmic heating. The fluid is then accelerated to supersonic speeds primarily by the magnetic body force. The electric field is determined by the choking condition that permits a transition from subsonic to supersonic speeds. In this thesis, the model of King et al.[7] will be considered for frozen and nonequilibrium flow. In a non-intuitive result, it will be found that the electric field required by the choking condition can be insufficient to draw all the applied current. This occurs at high values of $J^2/\dot{m}$ and is interpreted as onset.

Among the contributions of this thesis to the understanding and quantification of onset are:

- The first non-equilibrium self-field MPD theory to predict onset due to an excessive back-EMF at high currents has been developed.

- For the first time, the electrode-adjacent boundary layer in MPD flow has been studied.

- The importance of non-equilibrium ionization in controlling the appearance of back-EMF onset, and in determining boundary layer growth has been established.

- The Howarth-Dorodnitsyn transformation in conjunction with the momentum integral method, has been applied successfully for the first time in the case of a two-temperature, non-equilibrium, plasma boundary layer. The approximate solution has been used to compute the wall shear and the wall heat flux.

Several previous explanations for onset have been advanced. In addition to the back-EMF theory presented herein, there are two other approaches. One deals with anode mass starvation and the second with current channel instability. Each will be reviewed.

The first approach, anode mass starvation, was first analyzed by Baksht et al.[8] Because of flow acceleration and the Hall effect, they predicted that the plasma density near the downstream portion of the anode would decline as total current increased. Consequently as current increases, the anode sheath voltage will eventually shift signs, from electron-retaining to ion-retaining polarities. Baksht et al. took this sign change as their onset criterion[8]. This work has been refined by Heimerdinger.[9] Korsun considered a similar mass starvation effect in a two-dimensional model[10]. The anode mass starvation hypothesis has experimental support from Hugel.[11] The reason why a change in sign of the anode sheath voltage should cause onset is not clear because many discharges operate in steady state with anode sheaths of both signs. Two hypotheses exist: (i) Kuriki and Onishi[12] suggest that, when the anode fall is positive, ions accelerated in the sheath may produce sputtering, and (ii) Shubin[13] has found that anode mass starvation is associated not just with anode sheath reversal but also with plasma instabilities and has suggested that these may cause onset.

The second approach to onset is being developed by Schrade et al.[14] They analyze the stability of current tubes to fluctuations in the magnetic field distribution. This is a volume rather than an electrode phenomenon.

The back-EMF theory presented herein differs fundamentally from these other two approaches. For one, the injection of a small amount of mass near the downstream end of the anode would have a major effect on the onset predictions of the anode mass starvation theories[8, 9, 10, 13] but no effect on the back-EMF mechanism. A fundamental difference between the back-EMF limit and the instability theories[13, 14] is that the former appears in a steady-state model. Further, the magneto-gas-dynamic choking condition plays an essential role in the back-EMF mechanism but not in the other two. These differences indicate that the physical mechanisms for these approaches are different. It is not yet known which mechanism occurs first under which experimental conditions.

The most detailed experimental data on plasma flow conditions at onset are due to Barnett.[15] These experiments were conducted in what has become known as the "benchmark" thruster which is characterized by a lip on the anode which protrudes into the flow channel (see Fig.1) . His experiments found instabilities associated with low density regions. Unlike Baksht et al.'s theory,[8] the low density region was not necessarily near the anode. These results have not yet been repeated in a thruster with a smoothly shaped flow channel.

The complexity of this problem has prompted the use of some simplifying assumptions. Baksht et al.[8], Shubin[13], and Martinez et al.[16] have used the isothermal assumption. Shubin[13] and Martinez et al.[16] have used the infinite magnetic Reynolds number assumption. Neither approximation is used herein. However, the Hall effect, which was partially included in the above models, will be neglected herein. This work, an extension of King et al.[7], uses conservation of mass, momentum, and energy for a one-dimensional plasma flow. Unlike King et al.[7] who assume equilibrium thermodynamics, this work will also consider frozen-flow and non-equilibrium models. The choking condition is found to be strongly affected by these assumptions.

The approach to understanding and quantifying the phenomenon of onset in this thesis, is in two phases. The first phase is devoted to the development of a quasi one-dimensional theory that explains the behaviour of efficiency and predicts a new mechanism for onset. This is described in chapters 2 and 3.

The second phase is devoted to the development of a boundary layer theory that will enable calculation of erosion rates at onset. This is described in chapter 4. This two temperature non-equilibrium ionization boundary layer theory is developed in Sec. 4.2. The free stream conditions for the boundary layer analysis are obtained from the quasi one- dimensional theory developed in Sec. 3.5. A two temperature fluid model is used because of two reasons. Firstly, the presence of a relatively cold electrode and the relatively fewer number of collisions required for the heavier particles to equilibrate would cause the heavier particles (ions and neutrals) to have a temperature different from the lighter particles (electrons). Secondly, the Prandtl number for the heavy particles is ~ 1 and constant throughout the boundary layer. This would not be the case if a one temperature approach were taken for the combined fluid consisting of ions, neutrals, and electrons. Next, the boundary layer equations are solved approximately by using momentum integral and energy integral methods. This is discussed in Sec.4.3, and the results are given in Sec.4.4. A discussion of the cathode sheath is given in Sec.4.5. In this section, a description of how the boundary layer theory of Sec.4.2 may be used in calculating erosion rates by evaporation, is given. Finally, the results of this two step approach are summarized in chapter 5 along with the conclusions and recommendations for future work.

CHAPTER 2

QUASI 1-D FROZEN MPD CHANNEL FLOW

2.1. INTRODUCTION

The back-EMF onset theory has its beginings in the frozen flow theory that will be discussed in this chapter. Frozen flow refers to flow of a fixed chemical composition, such as fully ionized flow . The governing equations of a steady, one-dimensional, constant area, frozen MPD channel flow will be discussed in section 2, and magnetogasdynamic choking will be found in section 3. The solution of the frozen flow equations is derived in section 4. The culmination of this chapter is section 5 which uses the results of the frozen flow model to find a new mechanism for onset.

2.2. GOVERNING EQUATIONS

A steady, one-dimensional, constant-area MPD channel flow will be considered. The geometry is as shown in Fig.2. Viscous effects, Hall effects, and heat transfer will be neglected. The governing equations can be written:

mass:

$$\rho u = F = constant \tag{2.2.1}$$

momentum:

$$dP + Fdu = jBdx \tag{2.2.2}$$

energy:

$$Fdh + Fudu = jEdx \tag{2.2.3}$$

state:

$$h = h(P,\rho) \tag{2.2.4}$$

Ohm's law:

$$j = \sigma (E - uB) \tag{2.2.5}$$

Ampere's law:

$$\frac{dB}{dx} = - \mu_o j \tag{2.2.6}$$

These can be understood as the equations of classical gas dynamics with the inclusion of ohmic heating in the energy (2.2.3) and a magnetic body force in the momentum (2.2.2).[17] The equation of state, (2.2.4), applies to non-ideal as well as ideal gases. It will be generalized to non-equilibrium flow in Sec. 3.2 and Sec. 3.5.

First integrals can be found for both the momentum and energy equations. Using Ampere's law, (2.2.6), momentum conservation, (2.2.2), and energy conservation, (2.2.3), become:

Momentum:

$$P + Fu + \frac{B^2}{2\mu_o} = constant \tag{2.2.7}$$

Energy:

$$Fh + \frac{Fu^2}{2} + \frac{EB}{\mu_o} = constant \tag{2.2.8}$$

To complete the problem description, boundary conditions are needed at the channel inlet, $x=0$, and exit, $x=L$. At $x=L$, we require $B=0$. At the inlet,

$x=0$, the flow speed is specified, $u=u_{in}$. The inlet flow speed, u_i, is very small and, for present purposes, it may be taken as approximately zero. The value of the magnetic field at the inlet, $B=B_i$, is determined by the experimentally specified total current, J, by Ampere's law:

$$B_i = \mu_o J / W \tag{2.2.9}$$

The mass flux, F, is related to the total mass flow, $\dot{m}$, by:

$$F = \dot{m} / (HW) \tag{2.2.10}$$

The performance of the MPD thruster can be characterized by efficiency. Two efficiencies will be defined. Although the definitions are different, they agree closely over the range of MPD operation. The first, inspired by thermodynamics, is the Lorentz efficiency which is defined as the ratio of the work done by the electromagnetic force to the total electrical power in[7]:

$$\eta_L = \frac{\int_0^L jBu\, dx}{\int_0^L Ej\, dx} \tag{2.2.11}$$

When the integrand in (2.2.11) is rearranged, the Lorentz efficiency is seen to be the weighted average over the power, of the ratio of the back-EMF to the electric field:

$$\eta_L = \frac{\int_0^L \left(\frac{uB}{E}\right) Ej\, dx}{\int_0^L Ej\, dx} \tag{2.2.12}$$

or,

$$\eta_L = < \frac{uB}{E} > \qquad (2.2.13)$$

It is then evident from (2.2.13) that for efficient thruster operation, it is necessary to operate in a regime where the back-EMF is comparable to the electric field. This means that the back-EMF onset mechanism, to be discussed in Sec. 2.5, is expected to be important in efficient thrusters.

The second type of efficiency to be defined is conventionally used to define overall propulsion system performance:

$$\eta = \frac{T_h^2 / 2\dot{m}}{JV} \qquad (2.2.14)$$

where $T_h = (\dot{m}u + PHW)|_{x=L}$ is the total thrust. For a planar channel, $V = EH + V_s$, where V_s is the sum of the sheath voltage drops. η differs from η_L by including the thrust due to pressure. For the normal operating regime of MPD thrusters, as opposed to electrothermal thrusters, the pressure component of thrust is small and the two efficiencies agree closely, as will be shown in Sec. 2.4.

The governing equations described in this section can be solved to determine the electrical characteristics and efficiency of the thruster. This will be done in the following sections.

2.3. MAGNETOGASDYNAMIC CHOKING

The combined action of ohmic heating and Lorentz body force can cause a flow in a constant-area channel to accelerate from subsonic to supersonic. Since both of these effects are large in the MPD thruster, variation in the channel cross-sectional area may be unimportant even if it is present. This section will develop the condition for this choking to occur in the self-field flow of a non-ideal gas obeying equation of state (2.2.4).

Rewriting (2.2.1) and (2.2.4) in differential form, combining with (2.2.2) and (2.2.3) to eliminate dp and $d\rho$, using (2.2.5) to eliminate j, and solving for the velocity gradient yields:

$$\frac{1}{u}\frac{du}{dx} = \frac{1}{M^2-1}\frac{1}{\left(\rho\frac{\partial h}{\partial \rho}\big|_P\right)}\left(\frac{B}{\mu_o}\frac{\partial h}{\partial P}\big|_\rho - \frac{E}{\mu_o\rho u}\right)\frac{dB}{dx} \qquad (2.3.1)$$

where a is given by[18]:

$$a^2 = \frac{\rho\frac{\partial h}{\partial \rho}\big|_P}{1 - \rho\frac{\partial h}{\partial P}\big|_\rho} \qquad (2.3.2)$$

For the special case of an ideal gas, (2.3.2) reduces to the conventional expression.

It is seen that (2.3.1) is singular at $M=1$. For continuous acceleration through $M=1$, it is required that:

$$E = \rho^*a^*B^*\frac{\partial h}{\partial P}\big|_{\rho^*} \qquad (2.3.3)$$

where the asterisks represent quantities evaluated at the sonic point, $M=1$. (2.3.3) is the choking condition. It relates the electric field, E, to the back-EMF at the choking point, a^*B^*. This will play a central role in the prediction of back-EMF induced onset to be discussed in Sec. 2.5.

(2.3.3) can be interpreted in terms of classical gas dynamics. Ohmic heating tends to drive a gas toward $M=1$ and the magnetic body force tends to drive the flow away from $M=1$.[17] (2.3.3) determines the electric field

necessary to provide the right amount of ohmic heating to drive the flow just to $M=1$ where the body force can accelerate it to supersonic speeds.

This choking condition has been previously studied for the special case of an ideal gas. Resler and Sears[19, 20] considered such choking for an applied-field calorically-perfect flow. King et al.[7] studied choking in self-field flow for the special case of a gas obeying the equation of state $h=HP/\rho$). The case of a self-field calorically-perfect flow will be considered in the next section. The more general case of self-field choking in a non-ideal gas will be addressed in Sec. 3.3 and Sec. 3.5.

2.4. FROZEN FLOW

The concept of back-EMF onset is most easily understood in the special case of a constant-composition (frozen) calorically perfect plasma. In this section, the solution for the flow profiles for frozen flow will be presented. *It will be found that the flow in this case is characterized by a single non-dimensional parameter.* This parameter, S^*, the magnetic force number, is closely related to the experimental onset parameter, $J^2/\dot{m}$.

The flow of a fully ionized one-temperature plasma will be modeled. Because ionization and recombination will not be considered in this section, this will be called the frozen flow model. With electronic excitation neglected, this assumption of a fully ionized flow permits a simple expression for enthalpy:

$$h = \frac{5kT}{m_A} + \frac{\epsilon_i}{m_A} = \frac{5P}{2\rho} + \frac{\epsilon_i}{m_A} \qquad (2.4.1)$$

Substituting this frozen flow enthalpy into the choking condition, (2.3.3), gives:

$$E = \frac{5}{2} a^* B^* \tag{2.4.2}$$

This choking condition determines the electric field and defines the operating region.

To obtain an analytic solution, the conservation equations for mass (2.2.1), momentum (2.2.7), and energy (2.2.8) may be rewritten for frozen flow in terms of the sonic quantities:

$$\rho u = F = \rho^* a^* \tag{2.4.3}$$

$$P + Fu + \frac{B^2}{2\mu_o} = P^* + Fa^* + \frac{B^{*2}}{2\mu_o} \tag{2.4.4}$$

$$Fh + F\frac{u^2}{2} + \frac{EB}{\mu_o} = Fh^* + F\frac{a^{*2}}{2} + \frac{EB^*}{\mu_o} \tag{2.4.5}$$

Combining (2.4.1) through (2.4.5), the following quadratic equation for u is obtained:

$$u^2 + \left(\frac{5}{8} S^* \left(\frac{B^2}{B^{*2}} - 1 \right) - 2 \right) a^* u$$
$$+ \left(\frac{5}{4} S^* \left(1 - \frac{B}{B^*} \right) + 1 \right) a^{*2} = 0 \tag{2.4.6}$$

where:

$$S^* = \frac{B^{*2}}{\mu_o \rho^* a^{*2}} \tag{2.4.7}$$

The two solutions to quadratic (2.4.6) may be readily written in terms of B and the sonic quantities:

$$u = a^* \left(-\frac{\zeta_1}{2} \pm \frac{(\zeta_1{}^2 - 4\zeta_2)^{1/2}}{2} \right) \qquad (2.4.8)$$

where:

$$\zeta_1 = \frac{5}{8}S^*\left(\frac{B^2}{B^{*2}} - 1\right) - 2$$

$$\zeta_2 = \frac{5}{4}S^*\left(1 - \frac{B}{B^*}\right) + 1$$

The upper sign in (2.4.8) represents the solution for supersonic flow and the lower sign is for subsonic flow. (2.4.8) shows that u/a^* is a function of B/B^* with S^* as a parameter. Combining (2.4.8) with (2.4.3), ρ can be found:

$$\rho = \rho^* \left(-\frac{\zeta_1}{2} \pm \frac{(\zeta_1{}^2 - 4\zeta_2)^{1/2}}{2} \right)^{-1} \qquad (2.4.9)$$

(2.4.9) determines ρ/ρ^* as a function of B/B^* with S^* as a parameter. Combining (2.4.8) with (2.4.4), P can be found:

$$P = Fa^* \left[\frac{8}{5} + \frac{\zeta_1}{2} \mp \frac{(\zeta_1{}^2 - 4\zeta_2)^{1/2}}{2} + \frac{S^*}{2}\left(1 - \frac{B^2}{B^{*2}}\right) \right] \qquad (2.4.10)$$

(2.4.10) determines P/Fa^* as a function of B/B^* with S^* as a parameter. The relationship between B and position x can be found by combining (2.2.5), (2.2.6), and (2.4.2):

$$\frac{dB}{dx} = -\mu_o \sigma \left(\frac{5}{2}a^*B^* - uB \right) \qquad (2.4.11)$$

From (2.4.8) through (2.4.10), it is seen that S^*, defined by (2.4.7), is a very important parameter. S^* is the magnetic force number[21] evaluated at the choking point. S^* displays the relative importance of magnetic pressure and gas dynamic kinetic energy density:

choking point, as a parameter. The solution was found assuming a fully-ionized compositionally-frozen flow. Approximations such as isothermal flow or infinite magnetic Reynolds number have not been made. The next section will show how this solution predicts a new mechanism of onset. Sec. 3.5 will discuss how the solution is affected by ionization rates.

2.5. A THEORY OF ONSET

This section will explain how the simple model of the previous section predicts onset. Onset appears as a limitation on the values S^*, as defined in (2.4.7) or (2.4.12), may assume in the supersonic mode. This limit is a consequence of combining Ohm's law with the flow solutions. The behavior of the back-EMF will be considered first. The effect of back-EMF on Ohm's law will then be considered from mathematical and physical viewpoints.

The behavior of the back-EMF, uB, will be considered first. Near the inlet, the flow speed u is very small so that uB is small. Near the exit, uB is small again because $B \to 0$. Somewhere near the middle of the thruster, the back-EMF, uB, peaks. This is shown in Fig.6 for various values of S^*.

An important relationship between E, and the back-EMF, uB, can be found from considering Ohm's law. Combining Ohm's law, (2.2.5), with Ampere's law, (2.2.6), and integrating yields:

$$L = \int_0^{B_i} \frac{dB}{\mu_o \sigma(E - uB)} \qquad (2.5.1)$$

The relationship between u and B is given by (2.4.8). For frozen flow, E is given by the choking condition, (2.4.2). This is also plotted in Fig.6. From Fig.6, it is seen that as S^* increases from 7.0 to 8.5, the peak back-EMF approaches the electric field. This tends to make the denominator in (2.5.1)

small. As the peak back-EMF reaches the electric field, the integral indicates that an infinite length thruster is necessary. This occurs at $S^*=8.52$. For higher S^*, $E-uB$ changes sign twice during the integral which is hence singular and meaningless.

The physical significance of this limit can be found by returning to the governing equations, (2.2.1) to (2.2.6). If, at some location in the thruster, $E=uB$ then from Ohm's law, (2.2.5), no current flows. If no current flows, no magnetic force acts on the plasma, see (2.2.7), and no ohmic heating occurs, see (2.2.8). Consequently, the plasma flows at constant speed and temperature. Further, if no current flows, the magnetic field is constant, see (2.2.6). All this implies that if $E=uB$ somewhere in the channel, then it will be true that $E=uB$ at all points downstream. If this is true, the boundary condition of $B=0$ at $x=L$ cannot be met no matter how long the thruster. Thus, it is necessary that $uB<E$ for all locations within the channel.

The limit of $uB<E$ for the analogous case of plasma accelerators with *applied* magnetic fields is well-known. It was first studied by Resler and Sears[19, 20] and has since appeared in textbooks.[21, 22]

This value of $S^* = 8.52$ at which $E=uB$ can therefore be considered as the onset limit, indicating a regime of operation beyond which the flow can no longer be supersonic. Using (2.4.13), this limit can be restated dimensionally:

$$\frac{J^2}{\dot{m}} \leq 8.52 \frac{\mathcal{R} a^*}{\mu_0 \kappa^2} \qquad (2.5.2)$$

(2.5.2) correlates the experimental data of Malliaris et al.[5] very well. This is shown in Fig.7. This success does not prove the existence of back-EMF onset, however, because the scaling laws for anode mass starvation onset[8, 9] are similar.

The reason why back-EMF should rise faster than the electric field can be explained with some scaling behavior. From Ampere's law (2.2.6), B scales directly with J. From the choking condition (2.3.3), E scales roughly with J, and from conservation of momentum (2.2.2), u scales roughly with $J^2/\dot{m}$. Thus, as one increases the current, the back-EMF, which scales as $J^3/\dot{m}$, increases faster than E, which scales as J, and thereby leads ultimately to current blocking.

This research does not attempt to establish the flow conditions after onset has occurred. For $S^*>8.52$, the smoothly accelerating supersonic solution discussed in Sec. 2.4 is not possible. Thus, some largely subsonic flow is expected. A subsonic flow would, by energy conservation (2.2.8), likely have a higher temperature. Thus higher erosion rates by evaporation as well as by sputtering are expected.

Back-EMF onset also affects the efficiency. It was shown earlier in (2.2.12) and (2.2.13) that for thruster operation with a high Lorentz efficiency, it is necessary to operate in a regime with a high average value of uB/E. Since back-EMF onset restricts the peak value of uB/E to one, its average must be much less (see Fig.6). Thus, back-EMF onset restricts the efficiency as well as S^*.

CHAPTER 3

QUASI 1-D EQUILIBRIUM AND
NON-EQUILIBRIUM FLOWS

3.1. INTRODUCTION

In the previous chapter, the frozen flow theory was described which culminated in a new mechanism for onset known as back-EMF onset. The effect of non-zero ionization rates on back-EMF onset will be investigated in this chapter. The governing equations for equilibrium and non-equilibrium flows will be discussed in Sec. 3.2, and the effect of non-zero ionization rates on magnetogasdynamic choking will be analyzed in Sec. 3.3. The equilibrium model of King et al.[7] will be discussed using a simpler, piecewise linear model in Sec. 3.4. This simplification to the equilibrium relationship between enthalpy, h and temperature, T is made in order to explain why back-EMF onset was not observed in the numerical results of King et al.[7]. Although this piecewise linear model is a somewhat drastic approximation to their equilibrium flow theory, it preserves the necessary physics and enables a qualitative understanding of quasi 1-D equilibrium flow. Next, non-equilibrium flow is discussed in Sec. 3.5 and comparisons with the experiments of King et al.[7] are given in Sec. 3.6. The effects of wall friction and bulk heat transfer on the magnetogasdynamic choking of quasi-1D non-equilibrium flow is discussed in Sec. 3.7. Finally, a summary of quasi 1-D flow under the assumptions of frozen, equilibrium, and non-equilibrium flows is given in Sec. 3.8.

3.2. GOVERNING EQUATIONS

The governing equations of quasi 1-D flow under the assumptions of negligible viscous effects, Hall effects, and heat transfer have been previously described in Sec. 2.2. The only difference in the equilibrium and non-equilibrium cases is that the equation of state (2.2.4) is modified. Thus, the conservation equations may be rewritten as follows:

mass:

$$\rho u = F = constant \tag{3.2.1}$$

Momentum:

$$P + Fu + \frac{B^2}{2\mu_0} = constant \tag{3.2.2}$$

Energy:

$$Fh + \frac{Fu^2}{2} + \frac{EB}{\mu_0} = constant \tag{3.2.3}$$

state:

$$h = h(P,\rho,a) \qquad for\ non\text{-}equilibrium \tag{3.2.4}$$

$$h = h(P,\rho) \qquad for\ equilibrium \tag{3.2.5}$$

Ohm's law:

$$j = \sigma(E - uB) \tag{3.2.6}$$

where σ is obtained from:

$$\sigma = \left(\frac{1}{\sigma_n} + \frac{1}{\sigma_c}\right)^{-1}$$

where σ_n is the conductivity due to electron-neutral collisions and σ_c is the

coulomb portion of the conductivity. The expressions for σ_c and σ_n have been summarized by King[23]. Ampere's law:

$$\frac{dB}{dx} = - \mu_o j \qquad (3.2.7)$$

The ionization rate, $d\alpha/dx$ in the non-equilibrium theory is found from the rate equation:

$$\frac{d\alpha}{dx} = \frac{k_i \rho \alpha (1 - \alpha)}{m_A u} - \frac{k_b \rho^2 \alpha^3}{m_A^2 u} \qquad (3.2.8)$$

where α is the ionization fraction, and k_i and k_b are the ionization and recombination rate constants respectively. The frozen flow model is found as the limit in which k_i and k_b approach zero. If k_i and k_b approach infinity, the equilibrium model is recovered. The rate constants have been obtained from the work of Mansbach and Keck[24] for the non-equilibrium ionization case. These are:

$$k_i \, [cm^3/sec] = \frac{48.10^{-9}}{T^3(5.556.10^{-11})^{3/2}} exp\{ - \epsilon_i /kT \}$$

$$k_b \, [cm^6/sec] = \frac{4.10^{-9}}{T^{9/2}}$$

Normally, for equilibrium flow, two independent properties are required to define a thermodynamic state such as P and ρ. For non-equilibrium flow, a third independent property such as α is required to completely determine the thermodynamic state[18]. The boundary conditions necessary to complete the problem description have been discussed in Sec. 2.2. In addition to these, a boundary condition for α must be specified. This is that the gas be weakly

ionized at the entrance. The details of this will be discussed in Sec. 3.6 where the solution to the non-equilibrium flow equations will be given. The introduction of the non-equilibrium equation of state, (3.2.4), and the rate equation, (3.2.8) modifies the magnetogasdynamic choking condition. This will be discussed next.

3.3. MAGNETOPLASMADYNAMIC CHOKING

In this section, the effect of non-zero ionization rates on magnetogasdynamic choking will be studied. This will be done first under the equilibrium and then under the nonequilibrium assumptions. It is found that ionization rates have a strong effect on the choking condition and hence on the appearance of back-EMF onset.

For both the frozen flow and equilibrium flow limits, the magneto-gas dynamic choking condition can be written as:

$$\frac{E}{a^{\cdot}B^{\cdot}} = \rho^{\cdot}\frac{\partial h}{\partial P}\Big|_{\rho^{\cdot}} \qquad (3.3.1)$$

For frozen flow of a monatomic gas, the right hand side of (3.3.1) has the value of 5/2. The equilibrium calculation causes the right hand side of (3.3.1) to be up to an order of magnitude larger. This is shown in Fig.8. This will be evident in the results of the piecewise linear model that will be discussed in Sec. 3.4. The major difference between the two limits is that an important part of the change in enthalpy in equilibrium is due to the change in the ionization fraction. The right hand side of (3.3.1) oscillates in the equilibrium theory as the plasma progresses through successive stages of ionization.

The difference in thermodynamics has an important effect on back-EMF onset. Since the equilibrium theory can predict large electric fields, the

occurrence of back-EMF blocking is delayed. This is why King *et al.*[7] did not find evidence of onset over the range of parameters used in their numerical calculation.

The nature of the choking condition with nonequilibrium ionization can be analyzed as follows. Consider a plasma composed of electrons, neutrals, and singly ionized ions. In non-equilibrium, the equation of state is given by (3.2.4). Proceeding exactly as before (see Sec. 2.3), we can combine the governing equations in differential form with the new equation of state (3.2.4), solve for the velocity gradient, require smooth acceleration through the sonic point, and obtain the following non-equilibrium choking condition:

$$E = \rho^* a^* B^* \frac{\partial h}{\partial P}\Big|_{(\rho^*, a^*)} + \frac{\rho^* a^*}{j^*} \frac{\partial h}{\partial a}\Big|_{(P^*, \rho^*)} \frac{da}{dx}\Big|_{x = x^*} \tag{3.3.2}$$

where the superscript * refers to a quantity evaluated at the sonic point.

The above equation (3.3.2) shows the effect of ionization rates on the electric field explicitly.

Neglecting again electronic excitation, an analytic form for the equation of state can be found:

$$h = h(P, \rho, a) = \frac{5P}{2\rho} + \frac{a \epsilon_i}{m_A} \tag{3.3.3}$$

where ϵ_i is the first ionization energy. Using (3.3.3), the choking condition (3.3.2) may be simplified to:

$$E = \frac{5}{2} a^* B^* + \frac{\rho^* a^* \epsilon_i}{j^* m_A} \frac{da}{dx}\Big|_{x = x^*}$$

occurrence of back-EMF blocking is delayed. This is why King *et al.*[7] did not find evidence of onset over the range of parameters used in their numerical calculation.

The nature of the choking condition with nonequilibrium ionization can be analyzed as follows. Consider a plasma composed of electrons, neutrals, and singly ionized ions. In non-equilibrium, the equation of state is given by (3.2.4). Proceeding exactly as before (see Sec. 2.3), we can combine the governing equations in differential form with the new equation of state (3.2.4), solve for the velocity gradient, require smooth acceleration through the sonic point, and obtain the following non-equilibrium choking condition:

$$E = \rho^* a^* B^* \frac{\partial h}{\partial P}\Big|_{(\rho^*,a^*)} + \frac{\rho^* a^*}{j^*} \frac{\partial h}{\partial a}\Big|_{P^*,\rho^*} \frac{da}{dx}\Big|_{x=x^*} \tag{3.3.2}$$

where the superscript * refers to a quantity evaluated at the sonic point.

The above equation (3.3.2) shows the effect of ionization rates on the electric field explicitly.

Neglecting again electronic excitation, an analytic form for the equation of state can be found:

$$h = h(P,\rho,a) = \frac{5P}{2\rho} + \frac{a\,\epsilon_i}{m_A} \tag{3.3.3}$$

where ϵ_i is the first ionization energy. Using (3.3.3), the choking condition (3.3.2) may be simplified to:

$$E = \frac{5}{2} a^* B^* + \frac{\rho^* a^* \epsilon_i}{j^* m_A} \frac{da}{dx}\Big|_{x=x^*}$$

Observe that the first term on the right hand side is the electric field from the frozen flow theory and the second term represents the dependence of the electric field on the ionization rate at the sonic point. The physical significance of the relative magnitude of these two terms can be found by rewriting the above equation in the following non-dimensional form:

$$\frac{E}{a^*B^*} = \frac{5}{2} + \frac{\rho^*\epsilon_i}{j^*B^*m_A}\frac{d\alpha}{dx}\Big|_{x=x^*}.$$ (3.3.4)

Consider a unit volume of the plasma as it travels a distance dx. $\frac{\rho^*\epsilon_i}{m_A}d\alpha$ is the energy added to ionization. $jBdx$ is the work done by the magnetic field to accelerate the plasma. Thus, the second term on the right of (3.3.4) measures the ratio of energy going into ionization to the work done in accelerating the plasma.

In this section, the choking condition for frozen and equilibrium flow have been compared. The equilibrium values were computed using statistical thermodynamics. This will be discussed in the next section. Fig.8 shows a large quantitative difference between these frozen and equilibrium flow limits. Using a generalized equation of state, (3.2.4), the magneto-gas dynamic choking condition was extended to non-equilibrium flow in (3.3.2). It was shown that the importance of the ionization term in the choking condition was determined by the relative rate at which energy enters ionization to the rate at which work is done on the flow at the choking point. The piecewise linear model will be discussed in the next section. This will further illustrate the effect of equilibrium ionization rates at the choking point on the back-EMF onset.

3.4. EQUILIBRIUM MPD CHANNEL FLOW

It was shown in the last section that the electric field in quasi 1-D MPD flow is strongly determined by the ionization rate at the sonic point. The largest ionization rates occur for equilibrium flow. Equilibrium flow was first studied by King et al.[7] who found no evidence of back-EMF onset over the range of parameters they studied. In this section, their equilibrium theory is approximately modeled using a piecewise linear profile for enthalpy. It is shown that the equilibrium ionization rates yield much larger electric fields than zero ionization rates (i.e. frozen flow). it will also be shown that this may delay back-EMF onset by increasing the limit on S^* found in Sec.2.5. The equilibrium flow will only be qualitatively addressed here since the subject is dealt with at greater length by King et al.[7]. The motivation behind this section is to discuss the equilibrium flow assumption on the delaying of back-EMF onset which was first mentioned in Sec. 3.3.

The governing equations of equilibrium flow have already been stated in Sec. 3.2. The primary difference between equilibrium and frozen flows was the variation of enthalpy, h versus temperature, T. For fully ionized frozen flow (i.e. $\alpha = 1$), the relationship is:

$$h = \frac{5kT}{m_A} + \frac{\epsilon_i}{m_A} \qquad (3.4.1)$$

For equilibrium flow, the variation of enthalpy with temperature may be obtained by using statistical thermodynamics. These methods have been described by various authors[18, 25, 26]. Argon will be used as an example. Consider a fixed volume V_{box}, of stationary gas at a given temperature consisting of neutral atoms, single ions, double ions, triple ions, and electrons. Suppose further that the total number of nuclei is fixed. This therefore

corresponds to a mixture of A, A+, A++, A+++, and e- at a given density and temperature. From the law of mass action[18], we find:

$$\frac{n_+ n_e}{n_A} = \frac{Z_+ Z_e}{Z_A} = K_1 \tag{3.4.2}$$

$$\frac{n_{++} n_e}{n_+} = \frac{Z_{++} Z_e}{Z_+} = K_2 \tag{3.4.3}$$

$$\frac{n_{+++} n_e}{n_{++}} = \frac{Z_{+++} Z_e}{Z_{++}} = K_3 \tag{3.4.4}$$

where $Z_A, Z_+, Z_{++}, Z_{+++}$, and Z_e are the total partition functions of the neutrals, single ions, double ions, triple ions, and electrons respectively, and K_1, K_1, and K_3 are the equilibrium constants. The partition function is so named because it expresses the partition or distribution of energies over various energy levels[25]. Since the discussion here is restricted to atoms and not molecules, the partition function involves only the translational and electronic parts. Since a density is given, the total number of nuclei that is initially specified is constant:

$$n_o = n_A + n_+ + n_{++} + n_{+++} \tag{3.4.5}$$

In addition, we have a statement of conservation of charge:

$$n_e = n_+ + 2n_{++} + 3n_{+++} \tag{3.4.6}$$

The system of equations (3.4.2) through (3.4.6) are complete in the five unknowns n_A, n_e, n_+, n_{++}, and n_{+++}. This system can be reduced to a single fourth order equation in n_e:

$$n_e^4 + K_1 n_e^3 + (K_1 K_2 - K_1 n_o) n_e^2 + (K_1 K_2 K_3 - 2K_1 K_2 n_o) n_e$$
$$- 3K_1 K_2 K_3 n_o = 0 \tag{3.4.7}$$

Given the temperature, all the equilibrium number densities can be calculated by solving for the roots of (3.4.7). Quantum mechanical data on atomic energy levels[27] and electronic partition functions are calculated assuming the ground state of the atom as the datum. The electronic partition functions of the other species are then suitably corrected to ensure consistency. Translational partition functions are calculated assuming that each particle behaves quantum mechanically in the same manner as a free particle translating in a box. After using Sterling's approximation for a large number of particles[25], the thermodynamic properties, total partition function, Helmholtz free energy, entropy, internal energy, pressure, enthalpy, and specific heat at constant volume can be calculated using the following identities:

$$\frac{Z_j}{V_{box}} = \left(2\pi m_j kT / h^2 \right)^{3/2} \sum_{i=1}^{M} g_{ij} exp\{E_{ij}/kT\} \tag{3.4.8}$$

where Z_j is the total partition function of the jth species.

$$F_H = -kT \sum_{j=1}^{5} n_j \left(ln(Z_j) - ln(n_j) + 1 \right) \tag{3.4.9}$$

$$S = -\frac{\partial F}{\partial T}\Big|_{V_{box}} \tag{3.4.10}$$

$$U = F + TS \tag{3.4.11}$$

$$P = kT \sum_{j=1}^{5} n_j \tag{3.4.12}$$

$$H_e = U + PV \tag{3.4.13}$$

$$C_v = \frac{\partial U}{\partial T}\Big|_{V_{box}} \tag{3.4.14}$$

where the respective variables have been defined in the nomenclature. With a little extra computation, one may also compute the speed of sound, a from[18]:

$$a^2 = \frac{-\rho \frac{\partial h}{\partial \rho}\big|_P}{\left(\rho \frac{\partial h}{\partial P}\big|_\rho - 1 \right)} \qquad (3.4.15)$$

A numerical calculation has been performed using the method outlined above. The results were compared with existing published results[28] and are summarized in table 1 and table 2. It is seen from these tables that the numerical results are quite good. This calculation was used to compute the electric field from the choking condition of Sec. 3.3, and is shown in Fig.8. This equilibrium calculation also forms the basis for the piecewise linear model, which will be discussed next.

The statistical thermodynamics calculation that has just been discussed yielded the variation of enthalpy as a function of temperature that is depicted in Fig.9. For the purposes of qualitatively examining the equilibrium flow model of King et al.[7], the exact variation of enthalpy shown in Fig.9 will be replaced by the piecewise continuous profile shown in Fig.10. In this piecewise linear model, the enthalpy varies linearly until a cutoff temperature , T_c . This means that until this cutoff .temperature is reached, any energy added to the plasma will go primarily into the translational mode. After this cutoff temperature is reached, the temperature remains at $T = T_c$, and thereafter enthalpy continues to increase. This signifies that at this cutoff temperature, any energy that is added to the plasma goes into electronic excitation, with none going into the translational mode. This in a very rough way, simulates the behaviour of the enthalpy of a plasma in thermodynamic equilibrium. This

piecewise linear model thus qualitatively represents the equilibrium behavior of the plasma.

The approximate equation of state for equilibrium flow will now be derived. In the vertical branch of Fig.10, the internal energy consists of the energy per unit mass of the excited states. Thus,

$$e_{int} = e_c + \frac{a \epsilon_i}{m_A} \tag{3.4.16}$$

where e_c is the specific internal energy at $T = T_c$.

The enthalpy and pressure are given by:

$$h = e_{int} + \frac{P}{\rho} \tag{3.4.17}$$

$$P = \frac{(1 + a) \rho k T}{m_A} \tag{3.4.18}$$

Combining (3.4.16), (3.4.17), and (3.4.18), the following expression is obtained for the enthalpy in the vertical branch of Fig.10:

$$h = e_c - \frac{\epsilon_i}{m_A} + \frac{P}{\rho} \left(1 + \frac{\epsilon_i}{k T_c} \right) \tag{3.4.19}$$

The governing equations for mass, momentum, and energy are the same as in Sec.2.2. The equations for enthalpy and pressure are replaced with (3.4.18) and (3.4.19). The choking condition (3.3.2) for the piecewise linear model reduces to:

$$E = \frac{5}{2} u' B^* \qquad \text{if } T < T_c \tag{3.4.20}$$

$$E = \left(1 + \frac{\epsilon_i}{kT_c} \right) a^* B^* \qquad \text{if } T^* = T_c \qquad (3.4.21)$$

Examination of the actual variation of enthalpy from Fig.9 shows that the cutoff temperature for Argon in the piecewise linear model may be taken to be about 7000 K. The temperature at the sonic point is typically higher[7]. The sonic point thus occurs on the vertical branch of Fig.10. The electric field in the piecewise linear model is larger than in the frozen flow case by a factor of $(1 + \epsilon_i/kT_c)/2.5$. For a cutoff temperature of 7000 K for argon, the piecewise linear model gives an electric field of $E \approx 27.12\, a^* B^*$. This is about an order of magnitude bigger than in the frozen flow case.

Though (3.4.20) and (3.4.21) imply a discontinuous jump in the electric field, it is clear that this is due to the drastic approximation of the piecewise linear model. Thus, in the equilibrium flow case, the electric field will vary *continuously* from the lower to the upper values given by (3.4.20) and (3.4.21). The consequences of this on onset will now be summarized.

During quasi-steady operation of the thruster, an increase in the total current corresponds to an increase in T^*. As T^* increases from some value below T_c upto T_c. The electric field varies continously from $2.5\, a^* B^*$ to $\approx 27.12\, a^* B^*$ (if the cutoff is taken to be at roughly 7000 K for argon). It may then be seen by an analysis identical to the one outlined in Sec.2.4, that this corresponds to an *increase in the upper limit of the magnetic force number, S^*.* This is illustrated in table 3 for the case of $h^* = h_c$. It was shown earlier in chapter 2 that back-EMF onset manifested itself in the form of an upper limit on S^*. It is evident from this model based on a piecewise linear approximation to the equilibrium enthalpy, that back-EMF onset could be delayed. This may explain why back-EMF onset was not observed by King *et al.*[7].

In this section, the equilibrium flow in the MPD thruster has been qualitatively studied by approximating the equilibrium variation of enthalpy with temperature, in a piecewise linear fashion. The form of the piecewise linear enthalpy profile and the cutoff temperature were determined from a rather precise statistical thermodynamics calculation. Based on this theory, it was shown that the electric field could be upto an order of magnitude higher for equilibrium flow when compared to frozen flow. This qualitatively explains why back-EMF onset was not found by King et al.[7] over the range of parameters they considered. Furthermore, the strong relationship of the electric field to the ionization rate at the sonic point has been established. In the next section, the effect of more realistic ionization rates will be studied, and a new theory of non-equilibrium MPD flow will be developed.

3.5. NON-EQUILIBRIUM MPD CHANNEL FLOW

The importance of non-equilibrium ionization on the choking condition has been discussed in chapter 2 and Sec.3.3. It was shown that the electrical characteristics are determined by the dynamics at the choking point, i.e., the transition from subsonic to supersonic flow. It was shown in Sec.2.3 and Sec.3.3 that the electric field necessary for choking depends strongly on the ionization rate at the sonic point. The larger that rate, the larger the electric field must be in order to sustain a supersonic flow. This was shown in the equilibrium model of Sec.3.4. Consequently, ionization rates may control the terminal voltage. Another implication of this result is that the ionization rates may control the appearance of onset by the back-EMF current blocking mechanism. In this section, the effect of realistic ionization rates on determining the electrical characteristics and on controlling the appearance of back-EMF onset will be examined using a quasi-1D non-equilibrium theory. Non-equilibrium ionization MPD flow with an externally applied magnetic field has been considered previously by Seals and Hassan[29]; However, they did not

attempt an explanation of onset. Furthermore, their analysis was restricted to the operation of the thruster in the electrothermal mode. The non-equilibrium theory presented herein will be used specifically in order to predict and quantify onset in self-field MPD thrusters.

The objective of the non-equilibrium ionization theory in this thesis is three-fold. Firstly, it will be used to estimate electric field versus current characteristics. Next, the theory will provide an explanation of onset and be able to predict the level of total current at which this occurs. Finally, this theory will provide the free stream boundary conditions for a boundary layer analysis that will be used to quantify erosion rates by evaporation when onset is reached.

The governing equations for quasi-1D MPD flow have already been discussed in Sec.3.2. For the non-equilibrium theory, the same assumptions of negligible viscous, Hall, and heat transfer effects are made. Though these effects are ultimately important and probably should be included in a complete model, they are ignored at this moment. Whether these effects should be included or not will be addressed later in chapter 5. Thus, using these assumptions together with a constant channel area, the governing equations of Sec.3.2 may be written as follows: mass:

$$\rho u = F = \rho^* a^* \tag{3.5.1}$$

momentum:

$$P + Fu + \frac{B^2}{2\mu_0} = P^* + Fa^* + \frac{B^{*2}}{2\mu_0} \tag{3.5.2}$$

energy:

$$h + \frac{u^2}{2} + \frac{EB}{\mu_0 F} = h^* + \frac{a^{*2}}{2} + \frac{EB^*}{\mu_0 F} \tag{3.5.3}$$

state:

$$P = (1+a)\frac{\rho kT}{m_A} \tag{3.5.4}$$

$$h = \frac{5}{2}(1+a)\frac{kT}{m_A} + \frac{a\,\epsilon_i}{m_A} \tag{3.5.5}$$

$$a^2 = \frac{5}{3}(1+a)\frac{kT}{m_A} \tag{3.5.6}$$

choking condition:

$$\frac{E}{a^*B^*} = \frac{5}{2} - \frac{\mu_0 F \epsilon_i}{a^*B^* m_A}\frac{da}{dB}\Big|_{x \cdot x^*} \tag{3.5.7}$$

rate:

$$\frac{da}{dx} = \frac{k_i F a(1-a)}{m_A u^2} - \frac{k_b F^2 a^3}{m_A^2 u^3} \tag{3.5.8}$$

Ampere's & Ohm's laws:

$$\cdot j = -\frac{1}{\mu_0}\frac{dB}{dx} = \sigma(E - uB) \tag{3.5.9}$$

where σ was given in Sec.3.2.

The pressure and enthalpy may be eliminated using (3.5.4) and (3.5.5). Equations (3.5.8) and (3.5.9) may also be combined to yield a single differential equation for da/dB. In this way, the equations (3.5.1) through (3.5.9) may be put into the following non-dimensional forms:

$$\frac{3(1+a)T}{5(1+a^*)u}\Big(\frac{a^*}{T^*}\Big) + \Big(\frac{u}{a^*}\Big) + \frac{S^*}{2}\Big(\frac{B}{B^*}\Big)^2 = \frac{8}{5} + \frac{S^*}{2} \tag{3.5.10}$$

$$\frac{3(1+a)T}{2(1+a^*)T^*} + \frac{1}{2}\Big(\frac{u}{a^*}\Big)^2 + \frac{EBS^*}{a^*B^{*2}} = 2 + \frac{ES^*}{a^*B^*} + \frac{(a^*-a)\epsilon_i}{m_A a^{*2}} \tag{3.5.11}$$

$$\frac{E}{a^*B^*} = \frac{5}{2} - \frac{\epsilon_i}{m_A a^{*2} S^*}\Big(\frac{da}{d(B/B^*)}\Big)\Big|_{x \cdot x^*} \tag{3.5.12}$$

$$\frac{da}{d(B/B^*)} = \frac{k_b F^2 a^3 - m_A(u/a^*)a^* k_i F a(1-a)}{\mu_0 \sigma m_A^2 (u/a^*)^3 a^{*4}\{(E/a^*B^*) - (uB/a^*B^*)\}} \tag{3.5.13}$$

where k_i and k_b were given in Sec.3.2,

and the integral form of Ampere's law (3.5.9) when non-dimensionalized yields:

$$L = \int_0^{B_i/B^*} \frac{d(B/B^*)}{\mu_o \sigma a^* [(E/a^*B^*) - (uB/a^*B^*)]} \qquad (3.5.14)$$

To complete the description of quasi-1D non-equilibrium MPD channel flow, boundary conditions are required. In the quasi-steady operation of the MPD thruster[7], the weakly ionized flow enters the channel $x = 0$ at a slow speed and low temperature. Within a short distance of less than a centimeter, the plasma is accelerated to Mach 1 mainly due to ohmic heating. Beyond the sonic point, the electromagnetic force accelerates the plasma to supersonic speeds. At the exit $x = L$, the magnetic field, B is nearly zero.

The mathematical description of the flow is given by equations (3.5.10) through (3.5.14). The above set of equations (3.5.10) through (3.5.14) may be taken to constitute a system of five equations in the five unknowns u, T, a, E, and L with B^* and S^* as parameters. The independent variable is taken here to be the magnetic field, B. This formulation simplifies the system of equations but reduces the problem to a two-point boundary value problem. Therefore a manual shooting method is used. The boundary conditions are as follows. The mass flow rate is taken as given and constant. The channel cross sectional area is constant and fixed. The magnetic field B^*, the temperature T^*, and the ionization fraction a^* at the sonic point are specified as the boundary conditions at $x = x^*$. The integration of (3.5.14) is then performed in the two separate directions toward the inlet, and toward the exit. The sum of these lengths before and after the sonic point then is required to

match the given length of the thruster. If the calculated length does not match the given length, then T^* and a^* are varied until the correct length has been calculated. This will be discussed in greater detail in the next section, Sec.3.6.

The physical significance of the manner in which the boundary conditions are specified will now be addressed. The total mass flow is fixed in the experiments. Hence it is natural to impose the same in this steady state theory. The total current to the thruster is also fixed. This implies from equation (2.2.9) of Sec.2.2 that at a given current level, the magnetic field at the inlet B_i is fixed. Thus, the magnetic field at the sonic point B^* would be fixed to within less than 10% of B_i. Hence, B^* may be specified as a boundary condition at $x = x^*$, and a reasonable initial guess is obtained from (2.2.9). Next, since the thruster length is fixed in the experiments, the parameters a^* and T^* are varied in a realistic fashion until the length calculated by (3.5.14) matches *the length in the given experiment*. In this manner, profiles of all the variables are computed for a given current and mass flow. The predictions of the non-equilibrium theory can then be compared with experimentally measured values of electric fields and onset currents for some given mass flow rate.

This section has focused on the development of the quasi-1D non-equilibrium theory. In the next section, this theory will be used to predict electrical characteristics and onset. Comparisons will then be made with the experimental results of King[23] obtained from the 20 cm. straight coaxial thruster. It will be shown that at a certain value of the current, the length constraint imposed by the integral form of Ampere's law (3.5.14) cannot be satisfied for steady flow. This is interpreted as onset in the non-equilibrium ionization theory.

3.6. COMPARISONS WITH EXPERIMENT

The quasi-1D non-equilibrium MPD theory was developed in the previous section. This section will focus on the solution of these equations, present some results, and compare these with the experiments of King[23]. Other experimental results exist, the most detailed of these having been obtained by Barnett[15] on plasma flow conditions at onset. However, these measurements were made on the "benchmark" thruster which is characterized by a protrusion at the anode (see Fig.1). The theory developed in this thesis considers a one-dimensional straight channel. For this reason, the data of King[23] which were taken from the straight channel coaxial 20 cm. long thruster, have been chosen for comparison.

The mathematical description along with the boundary conditions has been discussed in Sec.3.5. The numerical algorithm will now be described. Given the quantities B^*, T^*, and a^* at the sonic point, the mass flow $\dot{m}$, the channel width W, and the channel height H, the right hand side of the integral form of Ampere's law (3.5.14) is computed by integration from $B/B^* = 1$ to $B/B^* = 0$. The integrand of (3.5.14) depends on u, T, B, a, and the quantities at the sonic point. u and T can be obtained as a function of B, a, and the quantities at the sonic point by solving (3.5.10) and (3.5.11) simultaneously. This gives:

$$\frac{u}{a^*} = -\frac{\gamma_1}{4} \pm \frac{1}{4}\left(\gamma_1^2 - \gamma_2 + \gamma_3\right)^{1/2} \tag{3.6.1}$$

where

$$\gamma_1 = 4 + \frac{5}{4}S^* \{1-(B/B^*)^2\}$$

$$\gamma_2 = 16 + \frac{8ES^*\{1-(B/B^*)\}}{a^*B^*}$$

$$\gamma_3 = \frac{8(a-a^\bullet)\epsilon_1}{m_A a^{\bullet 2}}$$

and

$$\frac{T}{T^\bullet} = -\frac{5}{3}\left(\frac{1+a^\bullet}{1+a}\right)\left(\frac{u^2}{a^{\bullet 2}}\right)$$
$$+ \left(\frac{8}{3} + \frac{5}{6}S^\bullet\{1-(B/B^\bullet)^2\}\right)\left(\frac{(1+a^\bullet)u}{(1+a)a^\bullet}\right) \tag{3.6.2}$$

Next, if the conditions at the sonic point are specified, the electric field may be calculated from equation (3.5.12) and (3.5.13). Then the differential equation (3.5.13) is integrated to obtain the ionization fraction a at any desired B. The integration of the differential equation is rather complicated by the fact that this equation is numerically "stiff". Consequently, an IMSL (International Mathematical Subroutine Library) routine DGEAR was employed. This routine uses the algorithm of Gear which is specially equipped to handle stiff systems. DGEAR is used to solve (3.5.13) and the result is used to evaluate the integrand in (3.5.14) at various stages of the numerical integration. In this manner, the thruster length from the sonic point to the exit is computed. In a similar manner, the length upstream of the sonic point is computed. As expected, the length between the inlet and the sonic point is found to be typically much smaller than 1 cm. The distance between the sonic point and the exit is to a very good approximation, the total length of the thruster. This calculated length is then compared to the length of 20 cm. used in King's experiments. If the lengths match, then a solution has been obtained for the current level corresponding to B_i. If the lengths do not match, then the inputs $a^\bullet$ and $T^\bullet$ are varied until the computed length is $\sim$ 20 cm. In the results that have been obtained, $a^\bullet$ is kept constant at 0.001 until $T^\bullet = 14000\,K$. At $T^\bullet = 14000\,K$, $a^\bullet$ is varied from 0.001 to 1.0. Once $a^\bullet = 1$, then $T^\bullet$ is allowed to increase beyond 14000 K. The limit of $T^\bullet = 14000\,K$ is chosen because at this

temperature, the ionization rate begins to become large. In this way the parameters a^* and T^* are varied in a physically consistent manner. It was found that the solution was not very sensitive to the way in which a^* and T^* were increased.

Solutions to the quasi-1D non-equilibrium equations have thus been generated for mass flows of 3 g/sec and 6 g/sec. The electric field versus current curves are shown in Fig. 11 for a mass flow of 3 g/sec, and in Fig. 12 for a mass flow of 6 g/sec. The continuous curve represents the results obtained from the non-equilibrium theory. The experimental data are plotted as discrete points. It must be pointed out that *the bars on the experimental points are not error bars.* The bars represent the deviation of the measured values from quasi one dimensionality. The reason the bars indicate such a large variation is that the mass flow in the experiment was not uniform across the channel. The magnitude of these bars were based on across-the-channel measurements of the electric field made by King[30].

It can be seen that on the basis of this comparison, the non-equilibrium theory predicts the shape of the electric field vs. current curve very well. Furthermore, it is in quantitative agreement with experimental results within the bounds of deviation from quasi one dimensionality. This is observed for both 3 g/sec and 6 g/sec experiments. The major accomplishment of the theory are the upper points in Fig.11 and Fig. 12 where the calculated values end. This is the onset point in the theory. This is the current at which no steady solution could be found that would satisfy the length constraint dictated by (3.5.14). The stage where the discrete data points end signify the point where onset was reached in the experiment. As can be seen from Fig.11 and Fig.12, the prediction of the onset current is in excellent agreement with the quasi-1D non-equilibrium theory. Further, Barnett[15] has also observed that the back-EMF is very large near the onset limit for the "benchmark" thruster. This may be

a further indication that the onset observed in the MPD thruster maybe due to the back-EMF current blocking mechanism presented in this thesis.

In addition to giving the electrical characteristics, the quasi-1D theory also provides variations of various quantities along the length of the thruster. Typical profiles of velocity, temperature, ionization fraction, and current density are shown in Fig.13, Fig.14, Fig.15, and Fig.16. These were computed for a mass flow rate of 3 g/sec. Some of the features of the profiles require clarification. The velocity is seen to increase monotonically until near the exit, where it decreases. This is because ohmic heating is dominant near the exit and the addition of heat to a supersonic flow causes it to slow down. The temperature increases steadily until the sonic point, after which it decreases slightly and then increases sharply near the exit. The reason for the slight temperature decrease after the sonic point is that the supersonic flow is accelerating. It is well known that an accelerating supersonic flow cools[17]. Then near the exit, the temperature rises again due to ohmic heating. The temperature rise computed near the exit is unrealistically high. This is because only single ionization was considered in the theory. If the presence of second ions were considered, then this temperature rise at the exit would not be so dramatic. The ionization fraction profile requires little explanation. a increases sharply near the sonic point because the temperature rises sharply. It then becomes relatively constant since the temperature is fairly constant in the middle of the thruster. Near the exit, a rises sharply again because of the sharply increasing temperature. The current density starts out small near the inlet because the temperature is small (this makes the conductivity small) and then increases following the increasing temperature and conductivity. Beyond the sonic point, the velocity is increasing and the magnetic field is decreasing. This causes the back-EMF to increase and reach a maximum somewhere in the middle of the thruster. This makes $E - uB$ decrease and reach a minimum

somewhere in the middle. Consequently, the current density decreases and reaches a minimum in the center of the thruster, and then increases sharply near the exit because of the sharp increase in conductivity caused by the rising temperature. These profiles will be useful in providing the free stream boundary conditions for the boundary layer analysis that will be discussed in chapter 4.

Thus far, quasi-1D MPD flow has been considered without friction and heat transfer. The effect of these on magnetoplasmadynamic choking will be addressed in the next section. Finally the quasi-1D MPD flow theory will be summarized in Sec.3.8.

3.7. EFFECT OF WALL FRICTION AND HEAT TRANSFER ON MPD CHOKING

The previous sections of this chapter have considered quasi-1D MPD flow under the equilibrium and non-equilibrium assumptions. However certain effects have been excluded in order to enable a simple solution to the problem. These include friction, heat transfer, and the Hall effect. In this section, friction and heat transfer will be partially accounted for and their impact on MPD choking will be examined.

For a varying area quasi-1D MPD flow with wall friction and heat transfer, the equations of mass, momentum, and energy conservation yield:

$$\frac{1}{\rho}\frac{d\rho}{dx} + \frac{1}{u}\frac{du}{dx} + \frac{1}{A}\frac{dA}{dx} = 0 \qquad (3.7.1)$$

$$\frac{dP}{dx} + \rho u \frac{du}{dx} + \frac{B}{\mu_o}\frac{dB}{dx} + \frac{2C_D \rho u^2}{D_H} = 0 \qquad (3.7.2)$$

$$\rho u \frac{dh}{dx} + \rho u^2 \frac{du}{dx} + \frac{E}{\mu_o}\frac{dB}{dx} + 4\frac{h_c}{D_H}(T-T_w) = 0 \qquad (3.7.3)$$

where:

$$C_D = \frac{2\tau_w}{\rho u^2}$$

is the drag coefficient,

$$D_H = \frac{4A}{dA_w/dx}$$

is the hydraulic diameter,

and h_c is the effective heat transfer coefficient. Following the development of Sec.2.3, equations (3.7.1), (3.7.2), and (3.7.3) may be combined with (3.5.4), (3.5.5), (3.5.6), (3.5.8), and (3.5.9) to yield:

$$\frac{3}{2u}\frac{du}{dx} = \frac{\gamma_1 + \gamma_2 + \gamma_3 + \gamma_4 + \gamma_5}{(u^2 - a^2)} \tag{3.7.4}$$

where

$$\gamma_1 = \frac{\epsilon_1}{m_A}\frac{da}{dx}$$

$$\gamma_2 = -\frac{5P}{2\rho A}\frac{dA}{dx}$$

$$\gamma_3 = \frac{5C_D u^2}{D_H}$$

$$\gamma_4 = \frac{4h_c(T-T_w)}{D_H \rho u}$$

$$\gamma_5 = \left(\frac{E}{\mu_o \rho u} - \frac{5B}{2\mu_o \rho}\right)\frac{dB}{dx}$$

It can be seen that for a constant area channel with no friction or heat transfer, the above reduces to (2.3.1). Again using the same argument as in Sec.2.3 and requiring a smooth acceleration from subsonic flow to supersonic flow, gives 0 for the numerator of (3.7.4) when $u = a$. This gives the following choking condition for the electric field. Thus, for a constant area channel:

$$E = \frac{7}{4} a^* B^* + \frac{1}{2} \left(\beta_1 + \beta_2 - \beta_3 + \beta_4 \right)^{1/2} \qquad (3.7.5)$$

where

$$\beta_1 = \frac{9}{4} a^{*2} B^{*2}$$

$$\beta_2 = \frac{16 h_c (T^* - T_w)}{D_H \sigma^*}$$

$$\beta_3 = \frac{100 C_D F (1 + a^*) k T^*}{3 D_H m_A \sigma^*}$$

$$\beta_4 = \frac{4 \epsilon_i F}{m_A \sigma^*} \frac{da}{dx} \Big|_{x=x^*}$$

From the above generalized choking condition, it can be seen that larger rates of heat transfer from the plasma to the wall near the choking point cause a larger electric field. Since a larger electric field permits a larger back-EMF, this may delay back-EMF onset in the same manner as larger ionization rates at the sonic point. The effect of wall friction may also be examined. It can be seen that friction actually causes a lower electric field. This in turn permits a smaller back-EMF, and could thus cause back-EMF onset to occur sooner. However, the presence of the ionization rate (in the last term in (3.7.5)) is dominant in determining the electric field for equilibrium flow.

Wall friction and bulk heat transfer could have a significant effect on the lack of delay or delay of onset for non-equilibrium flow. The inclusion of friction and heat transfer further complicates the solution of the equations in Sec.3.5. Therefore, these will not be included in the calculation of the free stream boundary conditions that are used in chapter 4. This is deemed as a necessary first approach. Chapter 4 will focus on the development of a two temperature boundary layer theory which will be used to calculate the wall

shear and the wall heat flux. But before proceeding to the boundary layer theory, the quasi-1D theory will be summarized in the following section.

3.8. SUMMARY OF QUASI-1D MPD THEORY

This section will serve to unify the ideas that have been presented in chapter 2 and this chapter. However, before this is accomplished, a brief summary of existing theories and their assumptions will be given. Existing theories[7, 8, 9, 13, 14, 16, 31, 32] of onset may be classified into three major approaches. These are the theories that partially account for the Hall effect[8, 13, 16]; those that account for the thermodynamics[7, 31, 32]; and those that consider the MPD discharge in the unsteady mode[13, 14].

Because of the complexity of the problem several simplifying assumptions have been used in each of the theories. Baksht et al.[8], Shubin[13], and Martinez et al.[16] have assumed that the flow in the MPD thruster is isothermal and thereby eliminated the energy equation. In addition, Schubin[13] and Martinez et al.[16] have considered the magnetic Reynolds number to be infinite. However, these models do account partially for the Hall effect.

The back-EMF theory presented in this thesis[31, 32] is an extension of the theory of King et al.[7]. King et al.[7, 23] however assume equilibrium thermodynamics. The back-EMF theory that has been presented in this thesis includes the conservation of mass, momentum, and energy, and examines the MPD flow under the assumptions of frozen flow and non-equilibrium flow. The appearance of onset by the back-EMF mechanism is found to be strongly affected by these assumptions. However, the Hall effect which was partially included in the anode starvation theories, is neglected in this back-EMF theory. The back-EMF theory differs from the other theories. From the experimental results of Barnett[15], It is evident that the predictions of the anode starvation theories would be severely affected by the injection of a small amount of

mass near the downstream end of the anode. This would have no effect on the back-EMF theory. The difference between the back-EMF theory and the unsteady (instability) theories is that onset by a dominant back-EMF appears in the steady-state. The fact that the assumptions made in the back-EMF theory are different from the other theories indicates that the physical mechanisms responsible for onset are different. Further experimental information on a uniform geometry would be valuable in determining which of these different onset predictions occur first under which assumptions.

The back-EMF theory will now be summarized. It was first shown in Sec.2.3 that the electric field necessary to sustain a supersonic flow in the MPD thruster is determined by the requirement that the acceleration from subsonic to supersonic flow take place in a smooth fashion. Next, the electric field also had to satisfy the constraint imposed by Ohm's law which specified the magnitude of the field necessary to draw all the applied current. It was also shown in Sec.2.4 that frozen flow (zero ionization rates) was parametrized by the magnetic force number, S^*. S^* was then related to the onset parameter that is used by experimentalists to define the onset limit. Both constraints on the electric field could be satisfied for steady flow only for all values of S^* below a critical limit. This limit on S^* translated to a limit on the experimentally measured onset parameter and correlated well with the experimental data of Malliaris et al.[5]. This conflict between the electric field necessary to draw all the applied current and the field necessary for choking at a critical value of the current is interpreted to be onset in the theory.

Quasi-1D MPD flow was then considered in chapter 3 under the equilibrium assumption of King et al.[7]. The magnetoplasmadynamic choking condition was then considered in Sec.3.3. It was shown that the electric field from the choking condition was strongly dependent on the ionization rate at the sonic point. King et al. did not find back-EMF onset over the range of

parameters they studied. In order to understand why, the equilibrium equation of state was replaced with a piecewise linear model. In this way King's equilibrium theory could be qualitatively studied in the light of the back-EMF theory presented in chapter 2. The basis for the equilibrium equation of state was a statistical thermodynamics calculation of the properties of argon. This piecewise linear theory showed that the equilibrium ionization rates are large and this yielded a large electric field. This in turn would permit large back-EMF's and delay back-EMF onset. This explains why back-EMF onset was not observed in the equilibrium theory of King.

The quasi-1D theory was then studied with realistic ionization rates in Sec.3.5. The non-equilibrium theory showed that since the realistic ionization rates were smaller than equilibrium ionization rates, onset by an excessive back-EMF would occur more readily in the non-equilibrium case than in the equilibrium case. The equations of non-equilibrium MPD flow were solved and the results were compared with the straight *coaxial channel thruster of King*[23]. It was found that the non-equilibrium theory predicted the shape of the electric field versus current characteristics and the onset limit, in agreement with experiment. Exact quantitative agreement was not obtained because the experiment did not have a uniform mass flow. However, fairly good quantitative agreement was found within the expected deviations from quasi-one dimensionality. More experimental data with a uniform mass flow is needed for a more definitive comparison.

The non-equilibrium equations presented in this thesis are general enough that they could include the effects of wall friction and heat transfer. However, since the solution of the equations becomes much more difficult, these have been omitted as a first approach. These results without wall friction or heat transfer will be used as the free stream boundary conditions for the boundary layer analysis in the next chapter. The boundary layer theory

will be used to estimate wall shear and wall heat flux. This can not only be used to calculate the drag force and the total heat transferred to the walls, but will also indicate the importance of including the wall friction and heat transfer in quasi-1D flow. These will be discussed further in chapters 4 and 5.

CHAPTER 4

BOUNDARY LAYER FLOW

4.1. INTRODUCTION

The previous chapters have focused on the development of a new theory of onset. The predictions of this theory correlated well with the measured -electrical characteristics as well as the prediction of the onset limit. However, in order to quantify onset further, it is necessary to estimate the erosion rate. Erosion of the electrodes may occur by means of either evaporation or sputtering. In order to estimate the erosion rate however, it is necessary to consider the boundary layer in detail. To the best of this author's knowledge, boundary layer flow in the MPD thruster has not been studied until now and this work represents the first such attempt.

For quasi-steady operation in the MPD thruster, the electrode temperature is fairly constant over the entire length. For all practical purposes therefore, the MPD boundary layer flow may be treated as a boundary layer with a constant wall temperature and a varying free-stream. The electrodes are at some temperature below the melting point ($\approx 3650\,K$) and this is presumed to be fixed. Across the boundary layer the temperature can vary from above 1 ev in the free-stream to less than $\approx 3650\,K$ near the wall. Furthermore, the boundary layer is compressible because the density varies considerably across the boundary layer due to the temperature variation. A further complication is that because of the presence of a cold wall and the difference in the masses of various particles (ions, atoms, and electrons), the plasma is expected to be

a two temperature fluid. The ions and neutrals being very similar in mass, would tend to exchange translational energy by elastic collisions more readily amongst themselves than with the electrons. The presence of the cold wall implies that the heavier particles would, by colliding with the wall tend to assume the wall temperature. Therefore, the heavy particle temperature varies significantly across the boundary layer from the free stream to the wall. But the electrons being negative, are repelled by the cathode sheath and consequently retain their original kinetic energy. Therefore, their temperature is not expected to vary very much across the boundary layer. Hence, it is expected that the heavy particles (ions and atoms) would have a temperature different from the lighter particles (electrons).

The problem of calculating the heat transfer rate and wall shear in a laminar boundary layer in a compressible flow is by no means easy. Mathematically the problem of solving the governing equations of Sec.4.2 reduces to the solution of simultaneous non-linear partial differential equations. Physically the reason for the complexity lies in the fact that the temperature appearing in the energy equation influences the density which in turn affects the momentum equation. Thus, unlike the low speed incompressible case, it is not possible to uncouple these equations[33].

Laminar compressible boundary layer theory for a single temperature fluid, in the absence of any electromagnetic effects has been summarized by Schlichting[33] and studied by several other authors[34, 35, 36, 37]. The similarity behaviour of incompressible boundary layers was first investigated by Blasius[38]. Poots[35] has extended this similarity method to study heat transfer in compressible laminar boundary layers with an adverse pressure gradient and an adiabatic wall for a Prandtl number of unity. Poots uses the Illingworth-Stewartson transformation to reduce the compressible flow equations to incompressible form. Curle[34] has extended the work of Poots to the case of

a fluid with a constant Prandtl number greater than 0.5 and in contact with a wall of constant temperature. However, these are not applicable for a two temperature fluid. A detailed finite difference solution to the compressible two temperature equations for a boundary layer adjacent to a non-current conducting surface has been given by Liu *et al.*[39]. Their solution considers an ionizing argon boundary layer in a supersonic flow over a wing. However the complexity of Liu *et al.*'s numerical solution does not permit ease of applicability to design situations. A similar finite difference calculation has been performed by Doss *et al.*[40], which deals with the non-equilibrium, compressible boundary layer in a subsonic MHD flow with an applied and constant magnetic field. Again, the numerical computation is tedious. Throughout this thesis, the spirit of the research has been to develop approximate theories that permit ease of solution while retaining the important physics. This chapter will focus therefore on the development of a theory that preserves the physics of the results of Liu *et al.* but is mathematically much simpler. This theory further differs from Liu *et al.* in that it includes electromagnetic effects. Nageswara Rao[41] has recently studied the incompressible momentum boundary layer in an MHD channel and has included the Hall effect. However, he has neglected the energy equation and the thermodynamics. These assumptions along with the effect of ionization will be shown to be crucial in the case of the MPD thruster.

A novel feature of the two-temperature boundary layer that will be considered here is the important role played by ionization on the growth of the boundary layer. It will be shown in Sec.4.4 that the strong dependence of the viscosity on the ionization fraction and the subsequent control of boundary layer growth by the viscosity, affect such important quantities as the wall heat flux and the wall shear. This in turn affects the skin drag and the heat transfer to the electrode, which could have an important effect on electrode erosion.

The governing equations of the two-temperature MPD compressible boundary layer are solved by means of an approximate method. The approximate method which will be outlined in Sec.4.3, is based on the use of the Howarth-Dorodnitsyn transformation in conjunction with the momentum and energy integral method. The momentum integral equation of boundary layer theory was first derived by von Karman[42]. The modern form of this equation was first given by Gruschwitz[43] and finds its applications in the approximate theories for both laminar and turbulent boundary layers. Since then, Wieghardt[44] has deduced an energy integral equation by a similar approach. This approach will be used in this thesis to reduce the original partial differential equations to ordinary differential equations. The success of using this scheme depends largely on finding self-similar profiles for the velocity, heavy particle temperature, and ionization fraction. The presence of the cold wall often destroys the applicability of this approach to compressible, chemically reacting, supersonic boundary layers. For this reason, this approach is used in conjunction with a two-temperature plasma assumption, and the use of the Howarth-Dorodnitsyn transformation. Self-similar profiles are then sought in terms of *the transformed Howarth-Dorodnitsyn transverse coordinate*. The assumption of the two-temperature plasma besides being realistic, enables the heavy particle fluid to be treated in a fashion similar to the treatment of constant Prandtl number fluids of classical boundary layer theory. This allows the use of the momentum and energy integral methods.

The derivation of the two temperature, non-equilibrium, compressible boundary layer equations from first principles for the MPD channel flow, will be summarized in Sec.4.2. The important assumptions required to simplify these equations will also be discussed. Sec.4.3 will outline an approximate method of solving these equations and the results will be given in Sec.4.4. Sec.4.5 will focus on a discussion of the electrical sheath near the cathode.

A study of the cathode sheath is important in determining the erosion rate by evaporation, which is the prime motivation for considering the boundary layer in detail.

4.2. GOVERNING EQUATIONS

This section will focus on the development of the boundary layer equations for the plasma in the MPD thruster. Using the standard boundary layer assumptions, the boundary layer equations for a steady, two-temperature, non-equilibrium, compressible plasma will be derived from the general equations of two temperature magnetoplasmadynamics. These have been described in some detail by Kalikhman[45]. Kalikhman's approach has been followed to derive the general equations for MPD flow, since it is important to recognize these equations prior to making the boundary layer assumptions. These have been rigorously developed by this author[46] from the successive moments of the generalized Boltzmann equation (i.e. the conservation of mass, momentum, and energy). However, only a summary will be given here. Since the development of these equations is long and tedious, the interested reader is referred to the development found in detail elsewhere[46, 45, 47, 48].

The plasma is assumed to consist of neutral atoms, single ions, and electrons. As a first approach, the sheaths will be ignored, and the condition of local quasi-neutrality $(n_{ion} = n_e)$ will be assumed to hold everywhere in the boundary layer. The electrical resistance of the boundary layer is assumed to be small compared to the free stream, so that the electrical characteristics are determined by the free stream. Then, the governing equations for two dimensional steady flow may be summarized as follows in cartesian tensor notation, with the repeated subscripts denoting summation from 1 to 2:

mass :

$$\frac{\partial}{\partial x}(\rho u) + \frac{\partial}{\partial y}(\rho v) = 0 \tag{4.2.1}$$

x-momentum :

$$\rho u \frac{\partial u}{\partial x} + \rho v \frac{\partial u}{\partial y} = -\frac{\partial P}{\partial x} - \frac{\partial}{\partial x}\left(\frac{B^2}{2\mu_o}\right) + \frac{\partial}{\partial y}\left(\eta_H \frac{\partial u}{\partial y}\right) \tag{4.2.2}$$

where $\eta_H = \eta^{ion} + \eta^{atom}$ is the heavy particle dynamic viscosity;

y-momentum :

$$\frac{\partial P}{\partial y} = 0 \qquad \textit{for negligible Hall parameter} \tag{4.2.3}$$

$$\frac{\partial P}{\partial y} = -\frac{\partial}{\partial y}\left(\frac{B^2}{2\mu_o}\right) \qquad \textit{for significant Hall parameter} \tag{4.2.4}$$

electron sensible energy : (translational mode only)

$$\frac{3}{2}kn_e u_i \frac{\partial T_e}{\partial x_i} + \frac{\partial q_i^e}{\partial x_i} + \Pi_{ij}^e \frac{\partial u_i}{\partial x_j} = j_k^e(E_k - \epsilon_{kpq}u_p B_q)$$

$$+ \frac{3}{2}kT_e \frac{\partial}{\partial x_i}\left(n_e U_i^e\right) - m_e n_e U_i^e u_k \frac{\partial u_i}{\partial x_k}$$

$$- \frac{3m_e}{m_A}kn_e <\nu_{eH}>(T_e - T_H) \tag{4.2.5}$$

where $<\nu_{eH}>$ is the energy-weighted average momentum transfer elastic collision frequency between an electron and a heavy particle[49].

heavy particle sensible energy : (translational mode only)

$$\frac{3}{2}k(n_e+n_A)u_i\frac{\partial T_H}{\partial x_i} + \frac{\partial}{\partial x_i}(q_i^{atom} + q_i^{ion}) + \left(\Pi_{ij}^{ion} + \Pi_{ij}^{atom}\right)\frac{\partial u_i}{\partial x_j}$$

$$= j_k^{ion}(E_k - \epsilon_{kpq}u_pB_q)$$

$$+ \frac{3}{2}kT_H\frac{\partial}{\partial x_i}\left(n_eU_i^{ion} + n_AU_i^{atom}\right)$$

$$- (m_{ion}n_eU_i^{ion} + m_An_AU_i^{atom})u_k\frac{\partial u_i}{\partial x_k}$$

$$+ \frac{3m_e}{m_A}kn_e<\nu_{eH}>(T_e-T_H) \tag{4.2.6}$$

rate :

$$\rho u_i\frac{\partial}{\partial x_i}(n_e/\rho) + \frac{\partial}{\partial x_i}(n_eU_i^{ion}) = \dot{n}_{ion} \tag{4.2.7}$$

where $\dot{n}_{ion}$ = net production of ions by inelastic collisions,

state :

$$P = n_ekT_e + (n_e+n_A)kT_H \tag{4.2.8}$$

where j_k^{α} is the kth component of the current density vector of the species α, q_i^{α} is the ith component of the heat flux vector of species α, ϵ_{kpq} is the cartesian permutation tensor, E_k is the kth component of the electric field vector, B_q is the qth component of the magnetic field vector, u_i is the ith component of the mass weighted local average plasma velocity, $u = u_1$ is the velocity in the x-direction or the flow direction, $v = u_2$ is the velocity in the y-direction normal to the electrode and transverse to the flow, U_i^{α} is the ith component of the diffusion velocity or the average peculiar or thermal velocity of species α, and the stress tensor Π_{ij}^{α} is given by:

$$\Pi_{ik}^{\alpha} = -\eta^{\alpha}_{ikpq}\frac{\partial u_p}{\partial x_q} + P_{\alpha}\delta_{ik} \tag{4.2.9}$$

where η^{a}_{ikpq} is the viscosity tensor for species a, P_a is the partial pressure of species a, and δ_{ik} is the Kronecker delta. In order to calculate the transport properties and obtain the diffusion velocity, it is necessary to solve the full Boltzmann equation for the velocity distribution function[18, 48, 47, 45]. The flow is assumed to deviate slightly away from equilibrium, so that the velocity distribution function is the sum of the Maxwell–Boltzmann distribution function and a perturbation. This regular perturbation solution has been summarized by Kalikhman[45] for the case where electromagnetic effects are present. Equations (4.2.1) through (4.2.8) constitute a system of 6 equations in the 6 unknowns ρ, u, v, T_e, T_H, and $a = n_e/(n_e+n_A)$. Before proceeding with any further simplifications or with the solution of the above equations, it is necessary to summarize the assumptions that lead to these simplifications:

- The boundary layer flow is laminar, steady, and two dimensional.

- The Hall effect is neglected.

- The electrical characteristics of the boundary layer are determined by the free stream. Therefore, $E = constant$, $B = B_\infty(x)$, and $j = j_\infty(x)$.

- Radiative heat transfer will be neglected in this first approach. It may ultimately be important to include radiation effects as will be shown later in Sec.4.4.

- The plasma is a two-temperature plasma. The quantitative statement of this is obtained from the electron energy equation (4.2.5) by comparing the ratio of the heat conduction (the second term on the left hand side of (4.2.5)) to the energy transfer by elastic collisions (the fourth term on the right hand side of (4.2.5)). This gives the condition[46]:

$$\left(\frac{m_A}{m_e}\right)\left(\frac{L_e^2}{\delta_T^2}\right) \gg 1 \tag{4.2.10}$$

where L_e is the mean free path of the electron, and δ_T is the boundary layer thickness. For a two temperature approach to be valid therefore, we must have:

$$\frac{L_\bullet^2}{\delta_\tau^2} \gg \frac{m_\bullet}{m_A} \approx 10^{-5} \tag{4.2.11}$$

Simultaneously, for a continuum approximation to be valid, we require that $L_\bullet/\delta_\tau \ll 1$. Thus,

$$\left(\frac{m_\bullet}{m_A}\right)^{1/2} \ll \left(\frac{L_\bullet}{\delta_\tau}\right) \ll 1 \tag{4.2.12}$$

- Axial diffusion is neglected.

. With these assumptions and some additional manipulation[46], equations (4.2.1) through (4.2.7) become:

mass:

$$\frac{\partial(\rho u)}{\partial x} + \frac{\partial(\rho v)}{\partial y} = 0 \tag{4.2.13}$$

momentum:

$$\rho u \frac{\partial u}{\partial x} + \rho v \frac{\partial u}{\partial y} = -\frac{dP}{dx} - \frac{d}{dx}(B^2/2\mu_0) + \frac{\partial}{\partial y}\left(\eta_H \frac{\partial u}{\partial y}\right) \tag{4.2.14}$$

electron sensible energy:

$$\frac{\partial}{\partial y}\left(\lambda^{\bullet\bullet}\frac{\partial T_\bullet}{\partial y} + \frac{5}{2}n_\bullet kT_\bullet V_\bullet\right) = en_\bullet V_\bullet(E - uB) \tag{4.2.15}$$

where the electron diffusion velocity in the y direction, $V_\bullet$ is given by[46, 45]:

$$V_\bullet \approx \frac{eD^\bullet(E - uB)}{kT_H} - \frac{D^\bullet}{n_\bullet}\frac{\partial n_\bullet}{\partial y} \tag{4.2.16}$$

and $D^\bullet$ is the electron diffusion coefficient.

heavy particle sensible energy:

$$\rho u \frac{\partial}{\partial x}\left(\frac{5kT_H}{2m_A}+\frac{u^2}{2}\right) + \rho v \frac{\partial}{\partial y}\left(\frac{5kT_H}{2m_A}+\frac{u^2}{2}\right)$$

$$- \frac{\partial}{\partial y}\left((\lambda^{ii}+\lambda^{ei})\frac{\partial T_H}{\partial y}+(\lambda^{ie}+\lambda^{ee})\frac{\partial T_e}{\partial y}+\eta_H\frac{\partial}{\partial y}(u^2/2)\right)$$

$$= en_e V_i E + 3\left(\frac{m_e}{m_A}\right)kn_e<v_{eH}>(T_e-T_H) \tag{4.2.17}$$

rate:

$$\rho u \frac{\partial a}{\partial x} + \rho v \frac{\partial a}{\partial y} + \frac{\partial}{\partial y}(m_A n_e V_i) = \frac{k_f a(1-a)\rho^2}{m_A} - \frac{k_b a^3 \rho^3}{m_A^2} \tag{4.2.18}$$

where $a = n_e/(n_e+n_A)$. Also, the ion diffusion velocity in the y direction, V_i is given by[40, 45]:

$$V_i \approx \frac{eD^i(E-uB)}{kT_H} - \frac{D^i}{n_e}\frac{\partial n_e}{\partial y} \tag{4.2.19}$$

where D^i is the ion diffusion coefficient.

In equation (4.2.19), the neutral concentration gradient term and the effects of thermal diffusion have been ignored in order to simplify the equations. Thus, (4.2.19) resembles Fick's law with an additional term that is present because there is a current being driven through the plasma.

The equations (4.2.15) and (4.2.17) may be simplified further with the following additional assumptions:

- The electron temperature, T_e is assumed to be fairly uniform across the boundary layer. This is a reasonable approximation and is supported by the work of Liu et al[39]. This means that $T_e \approx T_\infty(x)$ throughout the boundary layer.

- The ion ohmic heating is assumed to be negligible. This means that the first term on the right hand side of the heavy particle sensible heat equation, (4.2.17) is neglected.

The final form of the governing equations is then:

mass:

$$\frac{\partial(\rho u)}{\partial x} + \frac{\partial(\rho v)}{\partial y} = 0 \tag{4.2.20}$$

momentum:

$$\rho u \frac{\partial u}{\partial x} + \rho v \frac{\partial u}{\partial y} = -\frac{dP}{dx} - \frac{d}{dx}(B^2/2\mu_o) + \frac{\partial}{\partial y}\left(\eta_H \frac{\partial u}{\partial y}\right) \tag{4.2.21}$$

electron sensible energy:

$$T_e \approx T_\infty(x) \tag{4.2.22}$$

heavy particle sensible energy:

$$\rho u \frac{\partial}{\partial x}\left(\frac{5kT_H}{2m_A} + \frac{u^2}{2}\right) + \rho v \frac{\partial}{\partial y}\left(\frac{5kT_H}{2m_A} + \frac{u^2}{2}\right)$$

$$- \frac{\partial}{\partial y}\left(\lambda_H \frac{\partial T_H}{\partial y} + \eta_H \frac{\partial}{\partial y}(u^2/2)\right) = 3\left(\frac{m_e}{m_A}\right)kn_e < v_{eH} > (T_e - T_H) \tag{4.2.23}$$

rate:

$$\rho u \frac{\partial a}{\partial x} + \rho v \frac{\partial a}{\partial y} + \frac{\partial}{\partial y}(m_A n_e V_i) = \frac{k_f a(1-a)\rho^2}{m_A} - \frac{k_b a^3 \rho^3}{m_A^2} \tag{4.2.24}$$

where $a = n_e/(n_e + n_A)$, and the ion diffusion velocity in the y direction, V_i is given by (4.2.19).

The equations (4.2.19) through (4.2.24) have been obtained after a lengthy derivation and after making several assumptions. These equations will be discussed next. A detailed critique of this boundary layer theory will be given in chapter 5.

Equation (4.2.20) is the equation of mass continuity encountered in standard compressible boundary layer theory[33]. Equation (4.2.21) is the

conservation of momentum. It resembles the usual form except for the presence of the electromagnetic body force which appears as a gradient of the magnetic pressure (see the second term on the right hand side of (4.2.21)). Mathematically, this should pose no additional trouble since it has the same form as the hydrodynamic pressure gradient. It is the sensible energy equations (4.2.22) and (4.2.23) that require some clarification. These equations have been referred to as the sensible energy equations because they include only the translational part of the total energy of the particles. The energy in translation is therefore the "sensible" heat while any internal mode such as electronic excitation is referred to as "latent" heat. Hence, equation (4.2.23) would resemble the standard energy equation written in terms of enthalpy if the particles had no other modes of energy storage. This is clear since in the presence of pure translation, the enthalpy is $h = 5kT/2m_A$ which appears on the left hand side of (4.2.23). Equation (4.2.23) therefore resembles the classical compressible boundary layer equations with heat conduction and viscous dissipation (the third term on the left hand side of (4.2.23)), but for the presence of a source term on the right hand side. This source term is present because the electron fluid and heavy particle fluid have been treated separately. Consequently, there appears a term that couples the two energy equations together. This term which represents the transfer of energy by elastic collisions between the electron gas and the heavy particle gas, appears as the source term on the right hand side of (4.2.23). Equation (4.2.24) is the familiar species conservation equation encountered in the field of combustion[48, 18, 47]. The only difference is in the expression for the diffusion velocities (4.2.16) and (4.2.19) which contain additional terms due to the presence of a current in the plasma. The source term on the right hand side of (4.2.24) represents the production of ions due to the following reaction:

$$A + e^- \rightleftharpoons e^- + e^- + A^+ \qquad (4.2.25)$$

The equations (4.2.20) through (4.2.24) represent the approximate boundary layer equations for the electrodes in the MPD thruster. This section has focused on a summary of a derivation of these equations which are given in detail elsewhere[45, 46]. The next section will focus on an approximate solution of these governing equations.

4.3. AN APPROXIMATE METHOD OF SOLUTION

This section focuses on the description of an approximate method of solution to the governing equations presented in Sec.4.2. A brief review of existing approximate methods will be given first. Then, the complications of the electrode-adjacent boundary layer in the MPD thruster are briefly mentioned, followed by a detailed description of the approximate method proposed herein.

A system of equations *similar* to those presented in Sec.4.2 have been solved by Liu *et al.*[39] by the use of a finite difference technique. In this section, a simpler but approximate sol 'ion technique will be developed in order to solve equations (4.2.20) through (4.2.24). Several authors have solved systems of equations that are similar to the governing equations of Sec.4.2. These will be described briefly. The equations are particularly easier to solve if the Prandtl number is either one or constant. For a Prandtl number of unity, Poots[35] has studied heat transfer in laminar boundary layers with an adverse pressure gradient and an adiabatic wall. Poots uses the Illingworth-Stewartson transformation to reduce the compressible flow equations to incompressible form. Curle[34] has extended the work of Poots to the case of a constant wall temperature and an arbitrary but constant Prandtl number greater than 0.5. Emmons and Brainerd[37] have developed a similarity solution for a compressible boundary layer over an insulated plate at arbitrary Prandtl

numbers. Such a similarity solution often fails in the case of a reacting supersonic boundary layer with a constant wall temperature. Nageswara Rao[41] has recently studied the compressible boundary layer in a magnetohydrodynamic channel, but has altogether neglected the energy equation and the thermodynamics. These will be shown to be crucial for the MPD thruster. The method presented herein differs from all the above in that a relatively easy approximate solution is found by reducing the original partial differential equations to ordinary differential equations, and is then solved by using a momentum integral method. The integral method has been successfully used by Chan[36] who does not consider a reacting boundary layer. None of these authors with the exception of Nageswara Rao[41] have considered electromagnetic effects. Hains[50] has considered electromagnetic effects in a constant conductivity, non-reacting compressible boundary layer. He too has successfully used the integral method.

The problem of the electrode boundary layer in the MPD thruster includes all the complications of a classical compressible boundary layer and more. It includes the additional effects of electromagnetics, chemical reaction (ionization and recombination), variable flow properties, and a constant wall temperature. The constant wall temperature, together with chemical reaction often destroy the simplicity of the integral method because unlike the case of the adiabatic wall, the temperature may not achieve its maximum at either the wall or the free stream. This makes approximate solutions very tricky. The method proposed herein addresses all these complications.

Simply stated, the integral method proposed here begins by integrating the partial differential equations (4.2.20) through (4.2.24) from $y = 0$ to $y = \delta_T$ in order to eliminate the dependence on the transverse coordinate y. The result is an ordinary differential equation in the axial coordinate x for certain dependent variables that appear as integrals over the transverse coordinate y.

Next, the Howarth-Dorodnitsyn transformation[49] is used to transform the integration variable from y to a variable ξ which varies from 0 at the wall to 1 at the edge of the boundary layer. This is done in order to eliminate the density dependence in compressible flow. Then, the integrands in the integrals are assumed to be polynomial functions in terms of this variable ξ. The choice of the order of these polynomials is not obvious but will be discussed in detail later in this section. The differential equations are then simultaneously integrated from the leading edge of the boundary layer to any desired downstream location. The details of this scheme are outlined by Hains[50] and this author[46].

Let us now examine the integro-differential equations obtained by integrating (4.2.21), (4.2.23), and (4.2.24). Integrating these equations and rearranging, we obtain[46]:

$$\frac{d\Theta}{dx} + \frac{\Theta}{\rho_\infty u^2_\infty} \frac{d}{dx}(\rho_\infty u^2_\infty)$$
$$+ \frac{\delta^*}{u_\infty} \frac{du_\infty}{dx} = \frac{\tau_w}{\rho_\infty u_\infty^2} \qquad (4.3.1)$$

where τ_w is the wall shear defined by:

$$\tau_w = \left(\eta_H \frac{\partial u}{\partial y} \right)_{y=0} \qquad (4.3.2)$$

Θ is the momentum thickness defined by:

$$\Theta = \int_0^{\delta_T} \frac{\rho u}{\rho_\infty u_\infty}\left(1 - \frac{u}{u_\infty} \right) dy \qquad (4.3.3)$$

δ^* is given by:

$$\delta^* = \int_0^{\delta_T} \left(1 - \frac{\rho u}{\rho_\infty u_\infty} \right) dy \qquad (4.3.4)$$

Next, the Howarth-Dorodnitsyn transformation[48] is used to transform the integration variable from y to a variable ζ which varies from 0 at the wall to 1 at the edge of the boundary layer. This is done in order to eliminate the density dependence in compressible flow. Then, the integrands in the integrals are assumed to be polynomial functions in terms of this variable ζ. The choice of the order of these polynomials is not obvious but will be discussed in detail later in this section. The differential equations are then simultaneously integrated from the leading edge of the boundary layer to any desired downstream location. The details of this scheme are outlined by Hains[50] and this author[46].

Let us now examine the integro-differential equations obtained by integrating (4.2.21), (4.2.23), and (4.2.24). Integrating these equations and rearranging, we obtain[46]:

$$\frac{d\Theta}{dx} + \frac{\Theta}{\rho_\infty u^2_\infty}\frac{d}{dx}(\rho_\infty u^2_\infty)$$
$$+ \frac{\delta^*}{u_\infty}\frac{du_\infty}{dx} = \frac{\tau_w}{\rho_\infty u_\infty^2} \tag{4.3.1}$$

where τ_w is the wall shear defined by:

$$\tau_w = \left(\eta_H\frac{\partial u}{\partial y}\right)_{y=0} \tag{4.3.2}$$

Θ is the momentum thickness defined by:

$$\Theta = \int_0^{\delta_T} \frac{\rho u}{\rho_\infty u_\infty}\left(1 - \frac{u}{u_\infty}\right)dy \tag{4.3.3}$$

δ^* is given by:

$$\delta^* = \int_0^{\delta_T}\left(1 - \frac{\rho u}{\rho_\infty u_\infty}\right)dy \tag{4.3.4}$$

and the subscript ∞ refers to free stream quantities. Integration of the heavy particle sensible energy equation (4.2.23) gives:

$$\frac{d\Theta_H}{dx} + \frac{\Theta_H}{\rho_\infty u_\infty (C_{pe}T_\infty + u_\infty{}^2/2)} \frac{d}{dx}(\rho_\infty u_\infty [C_{pe}T_\infty + u_\infty{}^2/2]$$

$$+ \frac{\phi^*}{(C_{pe}T_\infty + u_\infty{}^2/2)} \frac{d}{dx}(C_{pe}T_\infty + u_\infty{}^2/2)$$

$$= \frac{q_{wH} - u_s \tau_w}{\rho_\infty u_\infty (C_{pe}T_\infty + u_\infty{}^2/2)}$$

$$+ \frac{3m_e k a_\infty}{m_A{}^2 u_\infty (C_{pe}T_\infty + u_\infty{}^2/2)} \int_0^{\delta_T} \frac{\rho a}{\rho_\infty a_\infty} < \nu_{eH} > (T_\infty - T_H)\, dy \qquad (4.3.5)$$

where Θ_H is the enthalpy thickness defined by:

$$\Theta_H = \int_0^{\delta_T} \frac{\rho u}{\rho_\infty u_\infty} \left(\frac{C_{pe}T_H + u^2/2}{C_{pe}T_\infty + u_\infty{}^2/2} - 1 \right) dy \qquad (4.3.6)$$

$$\phi^* = \int_0^{\delta_T} \frac{\rho u}{\rho_\infty u_\infty} dy \qquad (4.3.7)$$

where u_s is the slip velocity at the wall, $< \nu_{eH} >$ is the energy-weighted average momentum transfer electron-heavy particle collision frequency, and q_{wH} is the heavy particle wall heat flux given by:

$$q_{wH} = - \left(\lambda_H \frac{\partial T_H}{\partial y} \right) \Big|_{y=0} \qquad (4.3.8)$$

where $\lambda_H = \lambda^{ion} + \lambda^{atom}$ is the heavy particle thermal conductivity. The integrated rate equation is:

$$\frac{dl^*}{dx} + \frac{l^*}{\rho_\infty u_\infty \alpha_\infty} \frac{d}{dx}(\rho_\infty u_\infty \alpha_\infty) + \frac{\phi^*}{\alpha_\infty}\frac{d\alpha_\infty}{dx}$$

$$- \frac{m_A}{\rho_\infty u_\infty \alpha_\infty}(n_{ew}V_{iw}) = \frac{\alpha_\infty k_i \rho_\infty}{m_A u_\infty}\int_0^{\delta_T} \frac{\alpha}{\alpha_\infty}\left(\frac{1}{\alpha_\infty} - \frac{\alpha}{\alpha_\infty}\right)\frac{\rho^2}{\rho_\infty^2}dy$$

$$- \frac{k_b \alpha_\infty^2 \rho_\infty^2}{m_A^2 u_\infty}\int_0^{\delta_T} \frac{\alpha^3 \rho^3}{\alpha_\infty^3 \rho_\infty^3}dy \qquad (4.3.9)$$

where l^* is the ionization thickness defined by:

$$l^* = \int_0^{\delta_T} \frac{\rho u}{\rho_\infty u_\infty}\left(\frac{\alpha}{\alpha_\infty} - 1\right)dy \qquad (4.3.10)$$

and n_{ew} and V_{iw} are the number density and transverse diffusion velocity of the ions evaluated at the wall.

The general case of velocity slip, temperature slip, and ionization or concentration slip at the wall have been treated[46]. However, in this chapter only ionization slip will be considered. This means that $u_s = 0$ and $T_s = T_w$. The ionization slip α_w which must be supplied for the rate equation (4.3.9), is obtained[46] by setting the macroscopic diffusive mass flux at the wall to the random thermal mass flux at the wall:

$$D_w^i \frac{\partial n_e}{\partial y}\Big|_{y=0} - \frac{n_{ew}D_w^i eE_w}{kT_w} = \frac{n_{ew}<C_H>}{4} \qquad (4.3.11)$$

where D_w^i is the ion diffusion coefficient at the wall, E_w is the electric field at the wall which is determined from overall current conservation, and $<C_H>$ is the mean heavy particle thermal speed at the wall. The application of the Howarth-Dorodnitsyn transformation to the integrals enables the elimination of density from the integrand. Thus, if

$$\xi = \frac{1}{\Delta} \int_0^y \frac{\rho}{\rho_\infty} dy \qquad (4.3.12)$$

where Δ is given by:

$$\Delta = \int_0^{\delta_T} \frac{\rho}{\rho_\infty} dy \qquad (4.3.13)$$

then, (4.3.3) reduces to:

$$\frac{\Theta}{\Delta} = \int_0^1 \frac{u}{u_\infty} \left(1 - \frac{u}{u_\infty} \right) d\xi \qquad (4.3.14)$$

similarly, the other quantities that appear in terms of derivatives of y or in terms of integrals over y may be transformed into derivatives and integrals in ξ. These have been summarized elsewhere[46].

Before the various integrals can be evaluated, it is necessary to assume profiles for the variation of the velocity, heavy particle temperature, and the ionization fraction across the boundary layer. A quadratic profile for u and cubic profiles for T_H and α in terms of ξ are assumed. Cubic profiles for T_H and α are assumed because the maximum temperature could occur somewhere inside the boundary layer, and not necessarily at the wall as in the case of an adiabatic wall. The velocity profile is then completely determined by the following constraints:

$$u(\xi = 0) = 0$$

$$u(\xi = 1) = u_\infty$$

$$\frac{\partial u}{\partial y}(\xi = 1) = 0$$

This gives:

$$\frac{u}{u_\infty} = 2\xi - \xi^2 \; . \tag{4.3.15}$$

Analogously, for the temperature and ionization fraction:

$$T_H(\xi=0) = T_w \qquad a(\xi=0) = a_w$$

$$T_H(\xi=1) = T_\infty \qquad a(\xi=1) = a_\infty$$

$$\frac{\partial T_H}{\partial \xi}(\xi=1) = 0 \qquad \frac{\partial a}{\partial \xi}(\xi=1) = 0$$

Thus, the temperature and ionization profiles are:

$$\frac{T_H}{T_\infty} = \frac{T_w}{T_\infty} + \left(2 - \frac{2T_w}{T_\infty} + b_4 \right) \xi$$
$$+ \left(\frac{T_w}{T_\infty} - 1 - 2b_4 \right) \xi^2 + b_4 \xi^3 \tag{4.3.16}$$

and

$$\frac{a}{a_\infty} = \frac{a_w}{a_\infty} + \left(2 - \frac{2a_w}{a_\infty} + c_4 \right) \xi$$
$$+ \left(\frac{a_w}{a_\infty} - 1 - 2c_4 \right) \xi^2 + c_4 \xi^3 \tag{4.3.17}$$

where b_4 and c_4 are coefficients yet to be determined. Using these polynomial forms, the integrated form of the momentum equation (4.3.1) is a differential equation for Δ, the integrated form of the energy equation (4.3.5) is a differential equation for the unknown coefficient b_4, and the integrated form of the rate equation (4.3.9) is a differential equation for the coefficient c_4. Thus, the original system of non-linear partial differential equations have

been reduced to a system of quasi-linear ordinary differential equations. To complete the formulation, conditions must be prescribed at $x = 0$, the leading edge of the boundary layer. These are that the thicknesses, Δ, Θ, Θ_H, and I^* are zero at the leading edge. Further, starting conditions must be specified for b_4 and c_4. This can be obtained by requiring the second derivatives of T_H and a with respect to ξ to be zero at the leading edge. This gives $c_4 = 1$ and $b_4 = 1 - (T_w/T_\infty)$ at the leading edge. These approximate equations describing boundary layer flow have been integrated using the IMSL subroutine DGEAR which has already been discussed in chapter 3. The Gear algorithm is used because of the "stiffness" of the system of ordinary differential equations. The results of applying this boundary layer theory to the electrodes in the MPD thruster will be discussed in the next section.

In summary, an approximate solution to the two temperature boundary layer theory of Sec.4.2 has been outlined. This approximate solution uses the Howarth-Dorodnitsyn transformation and reduces the complicated system of non-linear partial differential equations to a relatively simpler set of quasi-linear ordinary differential equations. In the next section, the solution to these equations will be given for various conditions that may arise in the MPD thruster.

4.4. RESULTS OF BOUNDARY LAYER THEORY

The boundary layer equations have been solved by the integral method outlined in the previous section, near the onset condition predicted by the non-equilibrium theory of Sec.3.5. The results of this analysis are presented in this section. The results focus primarily on a mass flow rate of 3 g/sec, but results for a mass flow of 6 g/sec are also mentioned. The wall heat flux computed in this section, will then be used to estimate the erosion rate due to evaporation at onset. The free stream conditions at onset for a given

mass flow rate, have been obtained from the results of quasi-1D non-equilibrium theory. A constant wall temperature of 3000 K is assumed, and the heavy particle Prandtl number is taken to be $\approx$ 0.7. Since boundary layers usually begin at stagnation points or at sharp edges, the starting point or leading edge must be specified. The entrance region of the MPD thruster is not well understood, and it is not clear what the flow pattern is in this region. Therefore, for the purposes of this analysis, the boundary layer is assumed to begin at the inlet. Since the sonic point is very close to the inlet, the calculation is simpler if the leading edge, $x = 0$ is taken to be at the sonic point.

The governing equations (4.2.20) through (4.2.24) are then simultaneously integrated from $x = 0$ to $x = L$. This is done for several different cases in order to examine the effect of ionization on the boundary layer growth. The case of a non-equilibrium boundary layer with ionization slip (i.e. a_w is determined from (4.3.11)) with a non-equilibrium free stream will be considered first. Next, the ionizing free stream with a frozen boundary layer (i.e. $a = a_\infty(x)$) will be considered. Finally, the case of a fully ionized, frozen free stream with a frozen boundary layer (i.e. $a = 1$ all across the boundary layer) will be addressed. The mass flow of 3 g/sec will be considered first.

The results of the non-equilibrium theory are summarized in Fig.17, Fig.18, Fig.19, Fig.20, Fig.21, and Fig.22. Fig.17 shows the growth of the boundary layer at the cathode. The boundary layer at the anode is assumed to be similar to the cathode, and is plotted assuming this symmetry for the 5 cm. wide straight coaxial thruster of King[23]. It is found that the boundary layers are relatively thick and actually merge at an axial distance of approximately 4 cm. from the leading edge. This surprising fact will be discussed at length, later in this section. The ionization fraction at the wall is shown in Fig.18 as a function of distance. This ionization slip decreases with

distance as expected, since the diffusion time increases as the boundary layer thickness increases with distance along the thruster. Thus, though the free stream ionization fraction increases, it takes longer for ions to diffuse to the wall in order to replenish those that are lost due to recombination. The ionization fraction, non-dimensionalized by the free stream ionization fraction is shown in Fig.19 versus distance, at a location of 1 cm. from the leading edge. The bulge in the profile is characteristic of hot, high speed flows in contact with a cold wall. The constant electron temperature in the boundary layer tends to ionize the plasma, whereas the presence of the cold wall drives the plasma to recombine. These two opposing effects cause the maximum *ionization fraction to occur somewhere in the middle of the boundary layer as* shown in the figure. The non-dimensional temperature profile is shown in Fig.20. A bulge analogous to the one observed in Fig.19 is not present 1 cm. downstream from the leading edge, because the plasma flow velocity is not high enough for the viscous dissipation to be comparable with the heat transfer to the wall. Another source of heating is the energy transfer from elastic collisions with the hot electrons. This too is not comparable with the conductive heat transfer to the wall. Fig.21 and Fig.22 show the variation of the heavy particle wall heat flux and the wall shear stress respectively. The heat flux is large near the leading edge of the boundary layer ($x = 0$) because the boundary layer thickness is small. In fact, the heat flux is infinite exactly at the leading edge, because of the singularity at $x = 0$. This is of course non-physical, because the boundary layer becomes free-molecular very close to the leading edge. Thus, the leading edge is a singularity only in the continuum theory. The wall shear is large when the boundary layer thickness is small (since this means that the velocity gradient at the wall is large), and then decreases as the boundary layer grows to be thicker. The heavy particle wall heat flux exhibits a similar behaviour. From classical boundary layer theory, both the wall shear and the wall heat flux would be expected to decrease with increasing boundary layer thickness.

The case of the frozen boundary layer with an ionizing free stream will be considered next. Again, the free stream conditions are obtained from the quasi-1D non-equilibrium theory presented earlier in Sec.3.5 since the free stream is assumed to be ionizing. However, since the boundary layer is chemically frozen, the ionization fraction in the boundary layer is the same as in the free stream (i.e. $a = a_w$ throughout the boundary layer). Furthermore, there is no ionization or recombination in the boundary layer. The motivation for studying this case, is to examine the effect of varying ionization at the wall (a_w) on the viscosity. The boundary layers in the thruster for this case are shown in Fig.23. This case differs from the non-equilibrium case with real ionization slip in that the boundary layers do not merge, though they are appreciably thick. The boundary layer thickness is seen to decrease near the exit of the thruster, due to the drastic variation of the free stream conditions near the exit (see Sec.3.6). The ionization fraction is identical to the free stream ionization fraction, and has already been shown in Fig.15. The heavy particle temperature profile is shown in Fig.24 at four different locations, 1 cm., 5 cm., 10 cm., and 15 cm. from the leading edge. The noticeable bulge in the profiles far from the leading edge exists, because of the opposing effects of viscous dissipation and heat transfer to the cold wall. This bulge does not appear near the leading edge because the plasma flow velocity is small and therefore the viscous dissipation is small. Fig.25 and Fig.26 depict the variation of the heavy particle wall heat flux, and the wall shear respectively. The heat flux and wall shear are seen to decrease with increasing boundary layer thickness, as expected. The magnitudes of the heat flux and the wall shear are lower in the frozen boundary layer as opposed to the non-equilibrium boundary layer with ionization slip, because of the smaller thermal conductivity and smaller viscosity. The viscosity is smaller, because the frozen boundary layer has a greater ionization fraction than in the non-equilibrium case. The thermal conductivity is smaller because the viscosity is

smaller, and the heavy particle Prandtl number is fixed. It is evident by comparing these cases, that the amount of ionization at the wall is extremely important in determining the heat transfer and the wall shear because of its effect on boundary layer growth.

A more dramatic illustration of the effect of ionization is enabled by studying the case of the fully ionized frozen boundary layer. In this instance, the fully ionized, frozen, quasi-1D flow of chapter 2 is used to provide the free stream boundary conditions, and the boundary layer is treated as being fully ionized and chemically frozen. The results of this calculation are shown in Fig.27, Fig.28, Fig.29, and Fig.30. The characteristic behaviour of the various quantities (i.e. heavy particle temperature, heavy particle wall heat flux, and wall shear) is the same as before, and has been explained in the other cases that were considered. The magnitudes of the quantities is lower in this fully ionized case, again because of the lower viscosity and thermal conductivity. This will be addressed in detail next.

The heavy particle Prandtl number has been fixed at 0.7 in the boundary layer calculations. Thus, if the viscosity is known, the thermal conductivity may be calculated using the definition of the Prandtl number. The viscosity of the plasma is primarily due to the heavy particles. Since the electrons have a significantly smaller mass than the ions and neutrals, their contribution to the viscosity is negligible[49]. The heavy particle dynamic viscosity is the sum of the ion viscosity, and the neutral viscosity. Since the mass of the ion differs from that of a neutral only by the mass of the electron, the ions and neutrals will be treated as having the same mass in this two-temperature theory. Therefore, at a given heavy particle temperature, the mean thermal speed of the ions is approximately the same as that of the neutrals. The viscosity may then be obtained from kinetic theory[18, 49], as:

$$\eta_H = \eta_i + \eta_A = m_A <C_H> (n_e L_{iH} + n_A L_{AH})$$ (4.4.1)

where $<C_H>$ is the mean thermal speed of the heavy particles, L_{iH} is the mean free path for an ion colliding with other heavy particles, and L_{AH} is the mean free path for a neutral colliding with other heavy particles. The mean free paths for the ions and neutrals are given by[49]:

$$L_{iH} = \frac{1}{n_e Q_{ii} + n_A Q_{iA}}$$

$$L_{AH} = \frac{1}{n_A Q_{AA} + n_e Q_{iA}}$$

where the Q's denote energy-averaged momentum transfer collision cross sections between various species. Using these, the definition of the ionization fraction $\alpha = n_i/(n_i + n_A)$, and quasi-neutrality $n_i = n_e$ gives the following expression for viscosity in terms of the ionization fraction:

$$\eta_H = m_A <C_H> \left(\frac{\alpha}{\alpha Q_{ii} + (1-\alpha)Q_{iA}} + \frac{1-\alpha}{(1-\alpha)Q_{AA} + \alpha Q_{iA}} \right)$$ (4.4.2)

where Q_{ii} denotes the coulombic ion-ion cross section, Q_{iA} denotes the ion-neutral cross section, and Q_{AA} denotes the neutral-neutral cross section. Typically for argon, $Q_{AA} \approx 10^{-19} m^2$, $Q_{iA} \approx 10^{-18} m^2$, and $Q_{ii} \approx 10^{-16} m^2$. It can be seen from (4.4.2) that when $\alpha = 0$, the viscosity is determined by Q_{AA}. If $\alpha = 1$, then the viscosity is determined by Q_{ii}, which is three orders of magnitude bigger than Q_{AA}. Further, if $\alpha < 0.9$, the viscosity is primarily determined by Q_{iA}, which is only about an order of magnitude bigger than Q_{AA}. This indicates that in order to have very small boundary layer thicknesses, the boundary layer flow must be very nearly fully ionized. In fact, it is this dependence of the viscosity on the degree of ionization that has resulted in

the relatively large boundary layer thicknesses that have been computed. This explains why the non-equilibrium boundary layer grew so quickly as to merge in the middle of the thruster. The straight coaxial thruster of King[23] has been described as being "lossy" compared to the shorter "benchmark" thruster (the "benchmark" thruster was less than 10 cm. long whereas King's coaxial thruster was 20 cm. long). The non-equilibrium boundary layer theory appears to explain why this is so. The resulting dependence of the viscosity on the ionization fraction also causes the heavy particle thermal conductivity to depend on the ionization fraction as well (this is because the heavy particle Prandtl number is roughly constant). Consequently, this is expected to affect the heat transfer to the electrode.

Thus far, MPD boundary layer flow has been considered under the assumptions of non-equilibrium, frozen, and fully ionized flow, for a uniform mass flow of 3 g/sec. A calculation of the non-equilibrium boundary layer has also been performed for a uniform mass flow of 6 g/sec. For this mass flow, the boundary layers merged at approximately 6 cm., as opposed to 4 cm. from the leading edge for a mass flow of 3 g/sec. This is to be expected, since the density is higher in the higher mass flow case which should in turn, give smaller boundary layer thicknesses.

The boundary layer theory solutions presented in this section may be used to estimate the drag, as well as the heat transfer. The heavy particle heat flux that has been calculated in this section, gives an idea of how much heat is transferred from the hot, flowing plasma to the wall by thermal conduction. A constant wall temperature of 3000 K was assumed for this calculation. In the next section, a methodology for determining the cathode surface temperature will be given. This electrode surface temperature may then be used to estimate the erosion rate due to evaporation.

4.5. THE CATHODE SHEATH

The previous chapters and the previous sections of this chapter have focused on the development of a new theory of onset, and a means of estimating the heat transfer to the electrodes. In this section, a methodology for calculating the steady state cathode surface temperature using the results of Sec.4.4 will be given. The heat fluxes due to heavy particle heat conduction, electron bombardment, ion bombardment, electrode heating due to ion recombination at the electrode, cathode evaporation, thermionic emission, radiant exchange with an anode at constant temperature, and heat transfer to an externally supplied coolant will be considered. Existing vapour pressure data for tungsten[51] may then be used to determine the evaporation rate.

Near the cathode, there exists a layer where the quasi-neutrality condition, $n_i \approx n_e$ is no longer valid. This layer known as a sheath, is of the order of a few Debye lengths which is much smaller than the mean free path. Consequently, the sheaths may be treated as being collisionless. In this section, an electron retaining sheath is assumed so that incoming electrons are repelled, and incoming ions are accelerated through the cathode fall. Such a model is necessary in order to determine the number densities of ions and electrons in the sheath. These may then be used in the subsequent cathode heat balance. This will be discussed next.

At steady state, the total energy into the cathode surface must equal the total energy out. Any effects at the root of the cathode or at its tip are ignored. Thus, only heat flow transverse to the cathode surface is considered. The total energy into the cathode surface consists of heavy particle heat conduction, electron bombardment, ion bombardment, and ion recombination at the electrode. The energy out of the surface is due to thermionic emission, evaporation, radiative heat transfer to the anode, and any heat that may be

transferred to an externally supplied coolant. For the purposes of this analysis, the cathode is assumed to be made of tungsten, the anode temperature is taken to be a constant 2000 K, and additional heat is assumed to be removed from the cathode surface by a coolant whose temperature is taken as 1000 K. The radiant exchange between the cathode and the anode may be modelled as that between two long, coaxial, grey cylindrical surfaces whose emissivities are assumed to be 0.4. Thus, the heat balance at steady state for the cathode is:

$$
- q_{wH} + \frac{enC_e}{4} \left(\phi_c + \frac{2kT_\infty}{e} \right) exp(-eV_c/kT_\infty) + \frac{enC_iV_c}{4}
$$

$$
+ \frac{nC_i(\phi_i - \phi_c)}{4} = j_{TE} \left(\phi_c + \frac{2kT_{EC}}{e} \right) + \Gamma\Lambda
$$

$$
+ \frac{5\sigma_{SB}(T_{EC}^4 - 2000^4)}{14}
$$

$$
+ h_{EFF}(T_{EC} - 1000) \tag{4.5.1}
$$

where q_{wH} is the heavy particle conductive heat flux given by (4.3.8), V_c is the cathode sheath voltage drop, n is the electron or ion number density at the sheath-boundary layer edge, C_i is the ion mean thermal speed, C_e is the electron mean thermal speed, j_{TE} is the thermionic electron emission current density, ϕ_c is the cathode work function, T_{EC} is the cathode surface temperature, Γ is the evaporative mass flux, Λ is the heat of sublimation of the cathode, σ_{SB} is the Stefan-Boltzmann constant, and h_{EFF} is the effective heat transfer coefficient between the cathode surface and an external coolant. The exponential boltzmann factor which appears in the electron bombardment term (second term on the left hand side of (4.5.1)) displays the tendency of the sheath to repel most incoming electrons. The cathode sheath voltage drop, V_c is calculated from the overall current conservation:

$$j_\infty = \left\{ \frac{enC_i}{4} + j_{TE} - \frac{enC_e}{4} exp(-eV_c/kT_\infty) \right. \tag{4.5.2}$$

where j_∞ is the free stream current density. The second term on the left hand side of (4.5.1) represents energy addition due to electron bombardment, the third term represents ion bombardment, and the fourth term represents energy deposition at the cathode due to ion recombination at the cathode. The four terms on the right hand side of (4.5.1) represent heat loss due to thermionic emission, evaporation, radiant exchange with the anode, and heat exchange with an externally supplied coolant. Consequently, (4.5.1) is an equation for the unknown T_{EC} given the heavy particle wall heat flux, the electron temperature, the total current density, the electron number density at the edge of the sheath, and the heat transfer coefficient between the surface and the external coolant. Once the cathode surface temperature is known, the evaporation rate can be determined from vapour pressure data for tungsten[51].

For the purposes of illustration, equation (4.5.1) is solved for the various boundary layer assumptions already discussed earlier in this thesis. For present purposes, the cathode is assumed to be made of tungsten which has a work function of 4.52 eV. The choice of the heat transfer coefficient between the surface and the external coolant is chosen to be whatever permits the existence of a steady solution. Four cases are considered. The first is a cathode subjected to a non-equilibrium boundary layer with ionization slip for a mass flow of 3 g/sec. The second is that of a cathode subjected to a frozen boundary layer with a non-equilibrium ionizing free stream, for a mass flow of 3 g/sec. The third case is that of a fully ionized, frozen boundary layer with a fully ionized and frozen free stream for a mass flow of 3 g/sec. The fourth and final case is that of a non-equilibrium boundary layer with ionization slip for a mass flow of 6 g/sec. These will be discussed in the subsequent paragraphs.

An interesting feature of equation (4.5.1) is the existence of two steady state solutions for the cathode surface temperature, one of which is a stable operating point. The other point is an unstable thermal runaway point. Fig.31 shows the variation of the heat defect (i.e. the net heat *into* the cathode) versus the cathode surface temperature. It is apparent that the unstable root gives thermal runaway temperatures. Physically, this means that if the surface temperature increases just above the value given by the second root, the steady state energy balance (4.5.1) indicates a further increase in temperature since the only possible way of losing energy is through radiation, thermionic emission, evaporation, and heat transfer to an external coolant, all of which increase with increasing temperature. This results in a thermal runaway with eventual melting of the cathode.

For the first and fourth cases (i.e 3 g/s with slip and 6 g/s with slip respectively) with external cooling, a stable steady state solution that satisfies (4.5.1) and (4.5.2) simultaneously, could not be found. However, with external heating (i.e. $h_{EFF} < 0$) a stable steady state solution was found in some cases. A lower work function did not resolve this problem and did not yield stable solutions. The variation of the cathode surface temperature for the second case for a heat transfer coefficient of $h_{EFF} = 500 \ W/m^2/K$ is shown in Fig.32. The surface temperature variation for this case for a lower value of $h_{EFF} = 250 \ W/m^2/K$ is shown in Fig.33. In the third case of the fully ionized, frozen boundary layer, a much higher cooling rate is required (corresponding to $h_{EFF} = 3000 \ W/m^2/K$) due to the large rate of ion and electron bombardments. The surface temperature variation for this case is shown in Fig.34. The relative importance of each of the terms in (4.5.1) can be seen from Fig.35 through Fig.37 for the cases that have been studied. From these, it can be seen that only the evaporation heat flux is negligible, but that all other terms are significant in determining the cathode surface temperature. Using the

vapour pressure data for tungsten[-1], the evaporative erosion rate has been calculated and is shown in Fig.38. The erosion rate has been expressed in terms of micrograms per coulomb, which is obtained by dividing the evaporative mass flux by the current density.

It is evident from these results for a tungsten cathode that a significant amount of external cooling may be required in order to operate the MPD thruster at steady state with minimal erosion. In reality cathodes may be made of thoriated tungsten or coated with other substances. Thoriated tungsten cathodes would have a lower work function and thus a higher rate of thermionic cooling. However, judging from the high heating rates observed from the results of the analysis in this section, it appears that external cooling may be necessary even in the case of a thoriated tungsten cathode at steady state.

The approximate analysis of this section is deficient in several areas. Two such areas may be mentioned. Firstly, the effect of the sheath electric field in lowering the work function (Shottky effect) has not been taken into account. This would tend to increase the cooling due to thermionic emission. Secondly, the transfer of heat by radiation to a 0 K ambient through the exit, may be important in determining the surface temperature near the exit. This is of major importance since the bulk of the observed erosion in experiments has been near the inlet and the exit.

From the theory presented in this thesis, we may attempt to explain the major causes of the erosion in the inlet and exit regions. Near the inlet, the boundary layer thickness is small and therefore the heavy particle conductive heat flux is high. Also, the current density and ionization slip are large in this region. Consequently, the sheath voltage drop and the charged particle number densities are large leading to heavy ion and electron bombardment. Near the

exit, the free stream temperature and current density are largest. This leads of course to heavy electron and ion bombardment with a subsequent rise in the surface temperature and evaporation rate.

The simple heat balance given in this section may thus be used to determine the erosion rate due to evaporation. Radiation from the plasma, which has been neglected in (4.5.1) may increase the erosion rate further. In addition to this evaporation rate, there is erosion by sputtering. The boundary layer theory presented in the earlier part of this chapter may also be used to determine sputtering rates. A calculation such as the one presented here may be ultimately used to predict thruster lifetimes.

This chapter has focused on the development of a boundary layer theory for MPD thrusters, and has culminated in an approximate semi-empirical model that may be used in estimating erosion rates due to evaporation. The theory presented in chapters 2 and 3 has provided an understanding of onset. This theory, together with the boundary layer theory of this chapter provides a means of quantifying onset. The next chapter will provide a summary of the findings in this thesis, critique some of the assumptions that have been made, and present recommendations for further work.

CHAPTER 5

SUMMARY AND CONCLUSIONS

This chapter will discuss overall the research that has been performed. A summary of the work described in chapters 1, 2, 3, and 4 will be provided, followed by an outline of the contributions of this thesis to research in magnetoplasmadynamics. Next, a critique of the assumptions that have been made will be given, and this chapter will then conclude with recommendations for further work.

This thesis has attempted to explain and quantify the life-limiting phenomenon of onset in MPD thrusters. Onset refers to the severe electrode erosion accompanied by voltage oscillations that occurs at a critical value of the total current, for a fixed mass flow during quasi-steady operation. For the first time, fully ionized, chemically frozen MPD flow has been considered in chapter 1. This has revealed several interesting points. Firstly, it has been found that the MPD flow is parametrized by a non-dimensional quantity S, the magnetic force number. Secondly, it has been shown that S is related to the onset parameter $J^2/\dot{m}$ which is used to characterize onset experimentally. Examination of the quasi-1D MPD equations has yielded the result that the electric field necessary for a smooth transition from subsonic to supersonic flow is determined by a choking condition (Sec.2.3). Further study of the equations has yielded a limit on S based on Ohm's law. This is the requirement that the electric field be sufficient to draw all the applied current. Thus for steady flow, it has been found that the electric field must simultaneously satisfy the choking condition and Ohm's law. It has been

found that this could be satisfied for steady flow, only for S^* below a certain value. This limit of S^* corresponds to the operating point where the back-EMF becomes comparable to the electric field. For a fixed mass flow, this can be translated to a critical value of the total current. This limit is referred to as back-EMF onset, and has been further explained in terms of the length constraint from Ampere's law, in Sec.2.5. This new mechanism of onset is different from existing anode starvation theories, because it has been shown in recent experiments[15] that mass injection at the anode has a major effect on the predictions of these theories. However, such mass injection would have no effect on the back-EMF onset theory. Furthermore, the back-EMF onset appears in the steady state, as opposed to other existing unsteady theories[13, 14]. The onset condition obtained from the frozen flow theory has been shown to correlate well with the experimental data of Malliaris et al[5]. The back-EMF onset has also been shown to affect the efficiency. For efficient thruster operation, it has been shown that it is necessary to operate in a regime where back-EMF onset is important.

Quasi-one dimensional MPD channel flow has been considered under the equilibrium and non-equilibrium assumptions, in chapter 3. This has been done in order to examine the effects of non-zero ionization rates on back-EMF onset. The equilibrium flow theory of King et al.[7] has been qualitatively studied using a piecewise linear model. The results of this analysis show that the electric field is strongly dependent on the ionization rate at the sonic point. The ionization rate is highest for equilibrium flow, and therefore this yields significantly higher electric fields than for frozen flow. This higher electric field permits a higher back-EMF, and thereby delays back-EMF onset. This explains why King et al. did not find any evidence of back-EMF onset in their equilibrium flow theory over the range of parameters they studied. The electric field dependence on the ionization rate (see Sec.3.3) prompted the
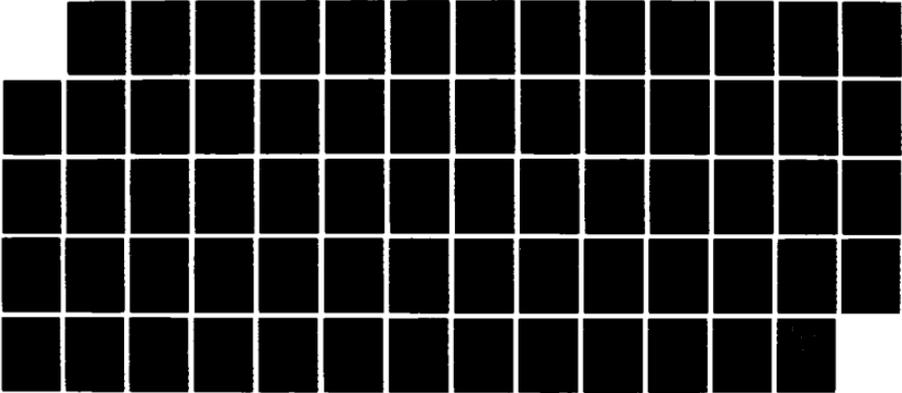
consideration of more realistic ionization rates, under the non-equilibrium assumption. The non-equilibrium theory has not only predicted the onset limit, but has also predicted current versus voltage characteristics in agreement with the experiments of King[23], within the limits of quasi-one dimensionality. Back-EMF onset appears as the failure of a steady solution to exist at a critical value of the current, for a fixed mass flow. This is due to the conflict between the electric field required to sustain a supersonic flow in the thruster, and the electric field necessary to draw all the applied current. Finally, the quasi-1D flow has been considered by partially including the effects of wall friction, and heat transfer. It has been shown by examining the magnetoplasmadynamic choking condition, that heat transfer may delay back-EMF onset while wall friction may cause it to occur sooner.

The quasi-1D MPD channel flow theory developed in chapters 2 and 3, have been utilized to obtain the free stream boundary conditions for an analysis of the *electrode-adjacent boundary layer.* The governing equations of the boundary layer in a two temperature plasma, have been rigorously derived from non-equilibrium kinetic theory. Following the approach of Kalikhman[45] these have been obtained by taking successive moments of the Boltzmann equation. The boundary layer equations have been solved using an approximate momentum and energy integral method, neglecting the electrode sheaths. This has enabled an approximate calculation of the wall shear and the heat transfer to the electrode. The most significant result of the boundary layer research has been to show the strong dependence of the viscosity on the ionization fraction at the wall. This affects such relevant quantities as boundary layer thickness, wall shear, and wall heat flux. This calculation has then been used to estimate the erosion rate due to evaporation . The work in this thesis has thus provided the outline of a systematic method for predicting thruster lifetimes. Though only the erosion due to evaporation has been

addressed here, erosion due to sputtering may be estimated by using existing semi-empirical models[52, 53] in conjunction with the boundary layer theory developed here.

The accomplishments of this thesis may be summarized as follows:

- The first non-equilibrium self-field MPD theory to predict onset due to an excessive back-EMF at high currents, has been developed.

- For the first time, the electrode-adjacent boundary layer in MPD flow has been studied. The governing equations for a two-temperature non-equilibrium plasma boundary layer have been derived from first principles. The effects of wall friction and heat transfer to the wall, have been quantified through the boundary layer analysis for the MPD thruster. These may be used to refine the quasi-1D theory that has been developed.

- The importance of considering detailed thermodynamics (Ionization and recombination) has been firmly established. The importance of non-equilibrium ionization in determining the appearance of back-EMF onset, and in determining boundary layer growth has been established. This work, like King et al.[7] shows the significance of considering conservation of energy.

- The Howarth-Dorodnitsyn integral method has been applied for the first time in the case of a two temperature non-equilibrium plasma boundary layer. The approximate solution has been used to compute the wall shear and the wall heat flux.

The complexity of MPD flow has prompted the use of simplifying assumptions. As a result, some of the effects that have been left out in the present theory, ought to be included in a more detailed calculation. These will be addressed next, and a critique of the assumptions that have been made in the present theory will be discussed.

The theory presented in this thesis is a steady theory that enables a calculation of the erosion rates, in order to quantify MPD thruster lifetimes. However, onset is not only characterized by high erosion rates, but also by large voltage oscillations. This steady theory does not even attempt to study the conditions beyond onset. Therefore, if one is interested in predicting

either the frequency of the voltage oscillations or the nature of the flow beyond onset, then the unsteady behaviour must be incorporated into the theory. This of course, would significantly complicate the relatively simple method of solution proposed in this thesis.

Another weakness of the boundary layer theory presented here, is the assumption of laminar flow. It is not clear at this time whether the MPD boundary layer is laminar or turbulent. Nor is it clear at what Reynold's number the MPD flow would become turbulent. This is of course assuming that the concept of a critical Reynold's number, and a continuum boundary layer, are valid. These will be addressed in greater detail shortly.

Perhaps two of the weakest assumptions made here, have been those of a scalar conductivity, and the neglect of radiative heat transfer. Both effects have been neglected in order to simplify an otherwise complicated problem. According to King[23], the Hall effect may not be negligible in some regions of the thruster. Inclusion of the full Hall effect would render the free stream flow two-dimensional. It is possible however, to partially include the Hall effect in a quasi-1D theory for a long, slender channel, by means of a tensor conductivity[23, 1, 49]. Inclusion of the Hall effect would also render the assumption of negligible ion ohmic heating in the heavy particle sensible energy equation, to be invalid. Radiation from the hot plasma to the wall may also be important for determining the heat transfer to the electrodes. It is not clear whether the plasma is optically thin or thick. It is most likely in a region between optically thin and thick, which makes the incorporation of radiation into the flow equations rather difficult. However, the method that has been presented in this thesis is sufficiently robust, that the radiation effects may be partially modelled by assuming an optically thick gas with an effective radiative conductivity. The inclusion of radiation would most likely lead to increased ionization fractions near the walls, and thereby reduce the

wall shear and wall conductive heat flux by reducing the viscosity and the thermal conductivity. However, there would be an additional heat transfer to the wall because of the radiative interaction between the plasma and the walls. It may therefore enhance the overall erosion rate.

The assumption of a two temperature plasma is perhaps the most realistic of all the assumptions. There is however, a possibility that the plasma is a three temperature fluid near the entrance to the thruster. This could affect the simple theory presented here. The assumption of a uniform electron temperature across the boundary layer is realistic and is supported by the work of Liu *et al.*[38]. Inclusion of the electron sensible energy equation with a varying electron temperature, is not expected to alter the results in this thesis significantly. Furthermore, the plasma in the free stream and the boundary layer, has been assumed to consist of electrons, neutral atoms, and single ions only. The presence of second ions (or doubly ionized atoms) could have a major effect on the erosion rate by sputtering. Since double ions have twice the charge of single ions, they would be acted upon by twice the electromagnetic force (which is proportional to the charge). Any appreciable number of double ions present near the electrodes could therefore contribute significantly to erosion by sputtering.

Since this is the first time that the Howarth-Dorodnitsyn integral method has been applied to the case of a compressible, non-equilibrium, two temperature plasma boundary layer with electromagnetic effects, the accuracy of the results may be questionable. This is because no extensive direct comparison has yet been made between the approximate solution given here and existing numerical solutions, for various situations.

Finally, the boundary layer itself may or may not exist as a continuum. From the free stream to the wall, the nature of the flow may change from a

continuum flow to either a rarefied flow or to one that is in transition. This is evident upon examination of the heavy particle mean free paths given in Sec.4.4. For fully ionized flow ($a = 1$), the ion-heavy particle mean free path is of the order of $10^{-6} m$, which is significantly smaller than any characteristic length. The fluid therefore behaves as a continuum. However, if the flow is weakly ionized ($a \sim 0$), the neutral-heavy particle mean free path is of the order of millimeters. This is only about one-fiftieth of the MPD channel height, and comparable to the boundary layer thickness. The fluid in this case, may either be in a transition regime or in a rarefied free-molecular regime. The flow in the MPD thruster could thus involve continuum, transition, and free-molecular behaviour.

The critique of the present work which has just been outlined, naturally leads to some prospects for future work. Some of the effects which have just been described that have been left out in the current theory, may be incorporated rather easily. Some others may not. However, there may be ways to partially account for these effects. The recommendations for future work, whether or not as an extention of this work, will be discussed next.

The presence of double ions in the quasi-1D MPD flow, may be modelled in a rather straightforward manner. This would merely involve the introduction of a second ionization fraction, a_{++}, and a corresponding rate equation to describe the production and depletion of double ions from single ions. The equation of state would also have to be modified to include second ions. This is a relatively direct extension of the theory described in Sec.3.5 and Sec.3.6. The method of solution would also be identical to the one already described in Sec.3.6. The inclusion of second ions would provide more realistic exit temperatures and velocities.

The effects of wall friction and heat transfer may also be approximately

studied, by solving the governing equations of Sec.3.7. As a first approach, the drag coefficient C_D, and the heat transfer coefficient h_c may be treated as parameters. The present boundary layer theory results have indicated that the wall friction may have a significant effect on the quasi-1D MPD flow. This effect could be approximately quantified using such a parametric analysis. Of course, the equations of Sec.3.7 cannot be reduced to algebraic form as in Sec.3.5 and Sec.3.6. This is because the presence of the wall friction and heat transfer terms necessitates a numerical integration of the momentum and energy equations, as well as the rate equation.

The effect of varying channel geometry is another extension of the quasi-1D theory presented in this thesis. The solution of the quasi-1D equations with varying area, should be no more difficult than solving the quasi-1D MPD flow with wall friction and heat transfer. This would be useful for designers to determine which channel geometry may provide the best acceleration characteristics.

Once the effects of wall friction, heat transfer, and varying channel geometry have been investigated and understood, the boundary layer solution presented here should be extended to partially include the effect of plasma radiation. This may be done by considering the assumptions of an optically thin and an optically thick plasma. A proper study of the plasma radiation problem is however extremely complicated, and may require the approach of Holstein[54, 55] if the plasma is neither optically thin, nor optically thick. However, the coefficients in the optically thin and thick cases may be varied as parameters, in order to estimate the importance of radiation. Plasma radiation may affect not only the heat transfer to the walls, but also the wall friction since the ionization fraction at the wall may increase due to additional heating from the hot plasma. The approximate methods of Sec.4.3 may still be applied in the case of an optically thin or thick plsama, but its accuracy would have to be checked against any existing numerical solutions.

An effect that complicates the theoretical calculations, but may nevertheless be important in MPD thrusters, is the Hall effect. The Hall effect causes the electromagnetic part of the problem to be two-dimensional, and introduces the notion that the electrical conductivity is a tensor. Thus, the current density and electric field vectors cease to be colinear. However, the Hall effect should not be incorporated *at the expense of the detailed thermodynamics*, as has been done by several authors[8, 13, 16]. It is this author's belief that had the detailed thermodynamics been included in these partial Hall effect theories, they would have resulted in the prediction of the back-EMF onset that has been described here. However, the inclusion of the Hall effect is expected to destroy the simplicity of the solution procedures outlined in this thesis.

A major phenomenon not included in the boundary layer analysis presented here, is the effect of electrode sheaths. *The inclusion of sheaths* would be of prime importance in a calculation of electrode erosion by sputtering. This is because the analysis of the sheaths would provide the voltage drop in this region close to the electrode. The sign of this voltage drop would determine to what extent the ions would bombard the electrode material. For an estimate of the erosion rate due to evaporation however, this may not be that important. The omission of sheaths may not be that important at high power since the voltage drop is typically less than 20% of the terminal voltage.

Once the above effects are at least qualitatively understood, the more difficult problem of the entrance region of the thruster should be studied. Virtually nothing is known about this region. The injection of different amounts of mass at the cathode and anode[15] has been shown to have a major impact on the anode sheath reversal theories. This will not have any impact on the back-EMF theory presented here. However, in order to verify the

assumptions and predictions of the back-EMF theory, some detailed diagnostics or analysis of the inlet is necessary. The entrance region for the present designs is very much two-dimensional, which complicates the analysis. The study of the entrance region would not only provide useful verification of back-EMF onset, but may also provide some information on the erosion of the insulator back plate. At present, there is not much understanding of why this occurs.

This work has indicated that though several phenomena may be important in the MPD thruster, the thermodynamics of ionization is perhaps one of the . most important. An improvement over the current state of the art should therefore not be made at the expense of ignoring the importance of ionization. It is also clear, that some more carefully designed experiments are necessary to enable a more positive comparison between the back-EMF theory and experiment. Firstly, it would be useful to repeat the experiments of Barnett[15] on King's straight coaxial thruster, or on another smooth geometry. Secondly, a better comparison between the quasi-1D theories and experiment could be made if the mass flow to the thruster were more uniform[56]. Finally, more experimental information on the entrance and choking regions would be invaluable.

REFERENCES

1. R.G. Jahn, *Physics of Electric Propulsion*, McGraw-Hill Book Company, New York, 1968.

2. A. Sherman, "Theoretical Performance of a Crossed Field MHD Accelerator", *A.R.S. Journal*, Vol. 32, March, 1962, pp. 414-420.

3. J. B. Workman, "Arc Structure in a Magnetic Annular Discharge", *AIAA Journal*, Vol. 7, No. 3, 1969, pp. 512-519.

4. D.L. Chubb, "Fully Ionized Quasi-One-Dimensional Magnetic Nozzle Flow", *AIAA Journal*, Vol. 10, No. 2, 1972, pp. 113-114.

5. A. C. Malliaris, R. R. John, R. L. Garrison, and D. R. Libby, "Performance of Quasi-Steady MPD Thrusters at High Powers", *AIAA Journal*, Vol. 10, No. 2, February, 1972.

6. D.Q. King, W.W. Smith, R.G. Jahn and K.E. Clark, "Effect of Thrust Chamber Configuration on MPD Arcjet Performance", Proceedings of the Princeton/AIAA/DGLR 14th International Electric Propulsion Conference.

7. D. Q. King, K. E. Clark, and R. G. Jahn, "Effect of Choked Flow on Terminal Characteristics of MPD Thrusters", AIAA-81-0686, 15th International Electric Propulsion Conference, April 1981, Las Vegas, Nevada.

8. F.G. Baksht, B. Ya. Moizhes, and A.B. Rybakov, "Critical Regime of a Plasma Accelerator", *Sov. Phys. Tech. Phys.*, Vol. 18, No. 12, 1974, pp. 1613-1616.

9. D. J. Heimerdinger, "An Approximate Two-Dimensional Analysis of an MPD Thruster", Master's thesis, Massachusetts Institute of Technology, June 1984.

10. A.G. Korsun, "Current Limiting by Self Magnetic Field in a Plasma Accelerator", *Sov. Phys. Tech. Phys.*, Vol. 19, No. 1, 1974, pp. 124-126.

11. H. Hugel, "Effect of Self-Magnetic Forces on the Anode Mechanism of a High Current Discharge", *IEEE Transactions on Plasma Science*, Vol. PS-8, No. 4, 1980, pp. 437-442.

12. K. Kuriki and M. Onishi, "Thrust Measurement of KIII MPD Arcjet", *AIAA Journal*, Vol. 20, 1982, pp. 1414-1419.

13. A.P. Shubin, "Dynamic Nature of Critical Regimes in Steady-State High-Current Plasma Accelerators", *Sov. J. Plasma Phys.*, Vol. 2, No. 1, 1976, pp. 18-21.

14. H. O. Schrade, M. Auweter-Kurtz, and H. L. Kurtz, "Stability Problems in

Magnetoplasmadynamic Arc Thrusters", AIAA 18th Fluid Dynamics and Plasmadynamics and Laser Conference, Cincinnati, Ohio, (1985).

15. J. Barnett, *Operation of the MPD Thruster with Stepped Current Input*, PhD dissertation, Princeton University, 1985.

16. M. Martinez-Sanchez, D. J. Heimerdinger, "Analysis of Performance Limiting Factors in MPD Thrusters", IEEE International Conference on Plasma Science, Pittsburgh, Pennsylvania (1985).

17. A. H. Shapiro, *The Dynamics and Thermodynamics of Compressible Fluid Flow*, Ronald Press, New York, 1953.

18. W. G. Vincenti and C. H. Kruger, *Introduction to Physical Gas Dynamics*, John Wiley and Sons, New York, 1967.

19. E.L. Resler, Jr., and W.R. Sears, "The Prospects for Magneto-Aerodynamics", *Journal of the Aeronautical Sciences*, Vol. April, 1958, pp. 235-245.

20. E.L. Resler, Jr., and W.R. Sears, "Magneto-Gasdynamic Channel Flow", *ZAMP*, Vol. IXb, 1958, pp. 509-519.

21. G. W. Sutton and A. Sherman, *Engineering Magnetohydrodynamics*, McGraw-Hill, New York, 1965.

22. W.F. Hughes and F.J. Young, *The Electromagnetodynamics of Fluids*, John Wiley & Sons, Inc, New York, 1966.

23. D. Q. King, *Magnetoplasmadynamic Channel Flow for Design of Coaxial MPD Thrusters*, PhD dissertation, Princeton University, December 1981.

24. P. Mansbach and J. Keck, "Monte Carlo Trajectory Calculations of Atomic Excitation and Ionization by Thermal Electrons", *Physical Review*, Vol. 181, 1969, pp. 275.

25. C. L. Tien, and J. H. Lienhard, *Statistical Thermodynamics*, Holt, Rinehart, and Winston, Inc., New York, 1971.

26. E. S. R. Gopal, *Statistical Mechanics and Properties of Matter*, Ellis Horwood Ltd., Chichester, England, 1974.

27. C. E. Moore, *Atomic Energy Levels*, U. S. Department of Commerce, Washington, D. C., National Bureau of Standards circular #467, Vol. I, 1949.

28. J. Hilsenrath, M. Klein, and D. Y. Sumida, "The Calculation of the Equilibrium Compositions and Thermodynamic Properties of Dissociated and Ionized Gaseous Systems", Tech. report, National Bureau of Standards, 1959.

29. R. K. Seals Jr., and H. A. Hassan, "Analysis of MPD Arcs with Nonequilibrium Ionization", *AIAA Journal*, Vol. 6, No. 12, December, 1968, pp. 2273-2278.

30. D. Q. King, "private communication".

31. J. L. Lawless, and V. V. Subramaniam, "A Theory of Onset in Magnetoplasmadynamic Thrusters", AIAA/DGLR/JSASS 18th International

Electric Propulsion Conference, Alexandria, Virginia (1985). To be published in AIAA Journal of Propulsion & Power.

32. V. V. Subramaniam, and J. L. Lawless, "The Electrical Characteristics of Magnetoplasmadynamic Thrusters", IEEE International Conference on Plasma Science,Pittsburgh, Pennsylvania (1985).

33. H. Schlichting, *Boundary-Layer Theory*, McGraw-Hill,Inc., New York, NY, 1968.

34. N. Curle, "Heat Transfer Through a Compressible Laminar Boundary Layer", *The Aeronautical Quarterly*, Vol. none, No. none, May, 1962, pp. 255-270.

35. G. Poots, "A Solution of the Compressible Laminar Boundary Layer Equations with Heat Transfer and Adverse Pressure Gradient", *Quart. Journ. Mech. and Applied Math.*, Vol. XIII, No. 1, 1960, pp. 57-84.

36. Y. Y. Chan, "Integral Method in Compressible Laminar Boundary Layers and its Application", *The Physics of Fluids*, Vol. 9, No. 2, February, 1966, pp. 350-358.

37. H. W. Emmons, and J. G. Brainerd, "Temperature Effects in a Laminar Compressible-Fluid Boundary Layer Along a Flat Plate", *Journal of Applied Mechanics*, Vol. none, No. A, September, 1941, pp. 105-110.

38. H. Blasius, "Grenzschichten in Flussigkeiten mit kleiner Reibung", Z. Math. u. Phys. 56, 1-37 (1908). Engl. transl. NACA TM 1256..

39. W. S. Liu, B. T. Whitten, and I. I. Glass, "Ionizing argon boundary layers.Part 1. Quasi-steady flat-plate laminar boundary-layer flows", *J. Fluid Mech.*, Vol. 87, No. 4, 1978, pp. 609-642.

40. E. D. Doss, H. A. Dwyer, and M. A. Hoffman, "Influence of Segmentation and Ambipolar Diffusion on MHD Nonequilibrium Boundary Layers", *AIAA Journal*, Vol. 12, No. 2, February, 1974, pp. 155-162.

41. B. Nageswara Rao, "Boundary-layer flow in a magnetohydrodynamic channel", *J.Appl.Phys.*, Vol. 58, No. 7, October, 1985, pp. 2516-2518.

42. Th. von Karman, "Uber laminare und turbulente Reibung", ZAMM 1, 233-253 (1912). Engl. transl. in NACA TM 1092. Also Coll. Works vol.2. 70-97 London 1956..

43. E. Gruschwitz, "Die tubulente Reibungsschicht in ebener Stroemung bei Druckabfall und Druckanstieg", Ing. Arch. 2, 321-346 (1931).

44. K. Wieghardt, "Ueber einen Energiesatz zur Berechnung laminarer Grenzschichten", Ing. Arch. 16, 231-242 (1948).

45. L. E. Kalikhman, *Elements of Magnetogasdynamics*, W. B. Saunders Co., Philadelphia, PA, 1967.

46. V. V. Subramaniam, "The compressible boundary layer equations of a two-temperature plasma", Departmental report, Dept. of Mech. Eng., Carnegie-Mellon University, Pittsburgh, Pennsylvania, February 1986..

47. S. Chapman, and T. G. Cowling, *The Mathematical Theory of Non-Uniform Gases*, Cambridge University Press, Cambridge, England., 1952.

48. F. A. Williams, *Combustion Theory*, Addison-Wesley, 1965.

49. M. Mitchner and C.H. Kruger, Jr., *Partially Ionized Gases*, John Wiley & Sons, New York, 1973.

50. F. D. Hains, "Heat Transfer and Skin Friction in Magneto-Gas Dynamic Channel Flow", Tech. report D1-82-0047, No. 26, Boeing Scientific Research Laboratories, May 1960.

51. R. C. Weast, editor, *Handbook of Chemistry and Physics*, CRC Press, 18901 Cranwood Pkwy, Cleveland, Ohio 44128, 1975-1976, 56th edition

52. J. Bohdansky, J. Roth, and H. L. Bay, "An analytical formula and important parameters for low-energy ion sputtering", *J. Appl. Phys.*, Vol. 51, No. 5, May, 1980, pp. 2861-2865.

53. E. P. Vaulin, N. E. Georgieva, T. P. Martynenko, and L. V. Fecktistov, "Erosion of hot refractory metals caused by low-energy ions", *Soviet Journal of Plasma Physics*, Vol. 7, No. 2, March, 1981, pp. 239-242.

54. T. Holstein, "Imprisonment of Resonance Radiation in Gases", *Physical Review*, Vol. 72, 1947, pp. 1212-1233.

55. T. Holstein, "Imprisonment of Resonance Radiation in Gases. II", *Physical Review*, Vol. 83, 1951, pp. 1159-1168.

56. J. L. Lawless, "private communication".
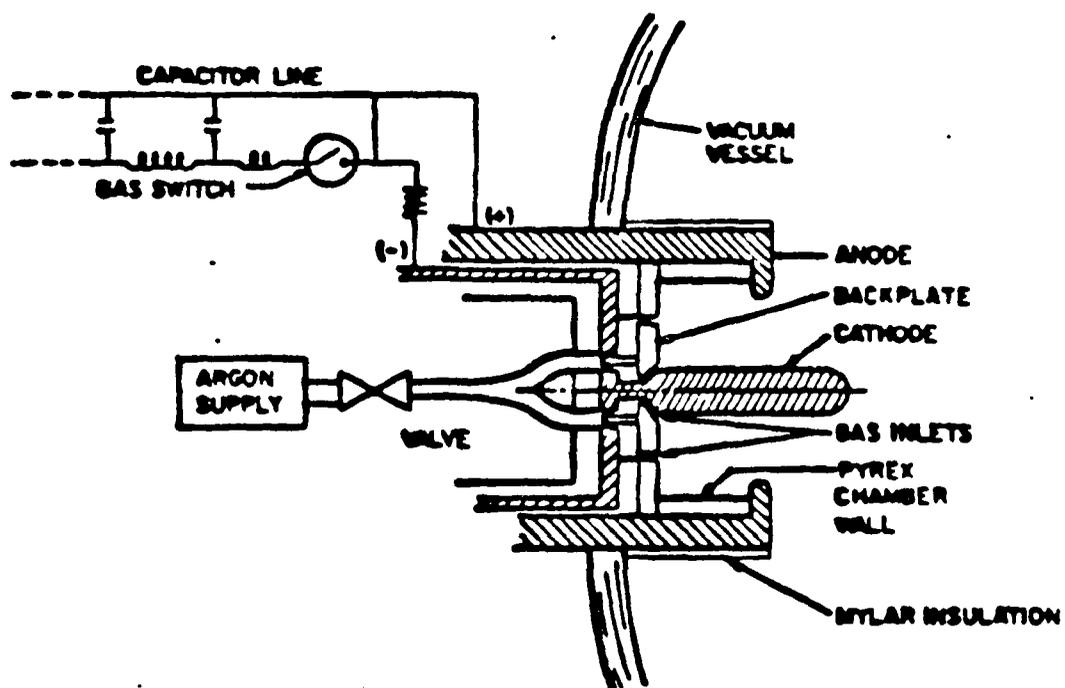
Figure 1: A schematic of an MPD thruster

MPD thruster system schematic
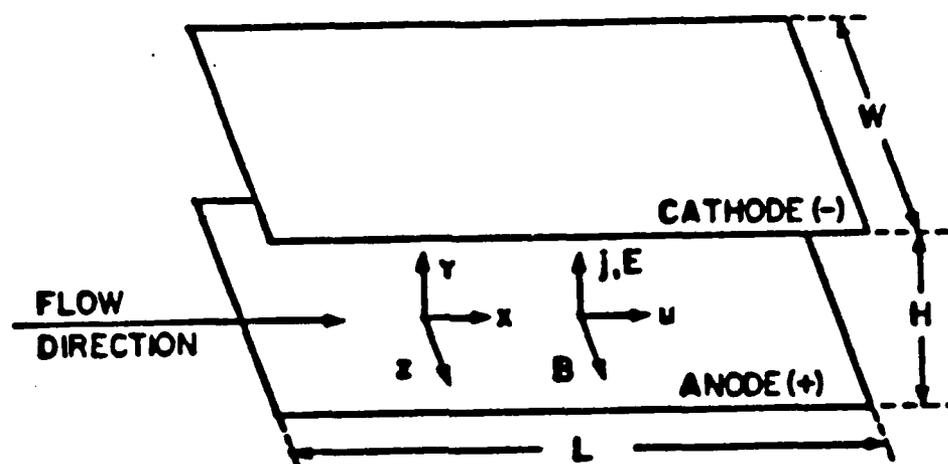
Figure 2: Schematic of plane-parallel geometry

The plane-parallel electrode geometry studied in this paper is analogous to the co-axial geometry used in experiments. The above diagram shows the relative orientation of the flow velocity, u, the current, j, the electric field, E, and the magnetic field, B. The channel has a length L in the flow direction and a width W. The electrodes are separated by a distance H.

APPENDIX F: Unsteady Flow Modeling

This Appendix consists of Chapter 7 from the Ph.D. Thesis of
Ed Richley. This chapter described an unsteady two-temperature
flow simulation of an MPD thruster.

7. MPD (Predictions for a Newer Problem)

7.1 Introduction

This chapter is concerned with the development of another simulation type. The system to be simulated is known as a Magneto-Plasma-Dynamic (MPD) thruster[60]. These thrusters are under development for possible use as space vehicle propulsion units and are of interest because of their high exit velocity.

An MPD thruster is basically an electric discharge in a low pressure fluid. Its operation is based on the interaction of the discharge current with its own self-induced magnetic field. The typical coaxial geometry of an MFD device is shown in Fig. 7.1. The power supply is assumed to be positioned off to the left and configured in such a way as to introduce no asymmetry into the magnetic field. The Lorentz force is able to produce flow velocities much larger than the sonic speeds obtainable with conventional chemical rockets. Since it involves an electric discharge, the governing equations for an MPD device are very similar to those for the previously described wall stabilized arc. However, the boundary conditions, geometry, and operating conditions are all extremely different.

7.2 Modifications to the Equations

As in the case of RadialArc, a one-dimensional non-equilibrium model called "MPD" has been created. In this model, all fluid properties are considered to be uniform with radial position, but are allowed to vary in the axial direction. The non-equilibrium equations considered by simulation type "MPD" are very similar to those of RadialArc. There are, however, several important differences. The most significant difference is the presence of an important magnetic field term. This can be included by modifying the pressure to include the magnetic pressure derived from the self-induced magnetic field. Thus, instead of considering only the gradient of kinetic pressure, the momentum equation now contains a modified term:

$$\frac{\partial}{\partial t}(\rho \vec{v}) + \nabla \circ (\rho \vec{v}\vec{v}) = -\nabla(p + \frac{B^2}{2\mu_o}) \tag{7.1}$$

where B is the magnetic flux density.

This Lorentz force acts directly on the electron gas so as to accelerate electrons downstream. The plasma, however, reacts with an internally generated electric field
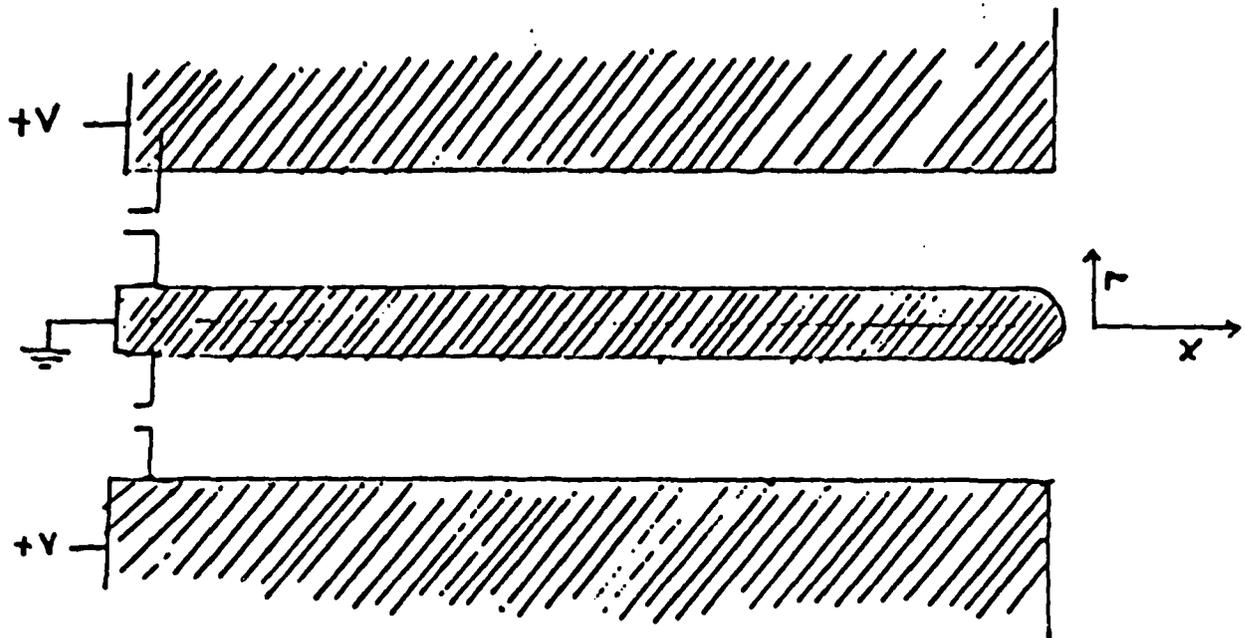
Fig. 7.1: Geometry of a Typical MPD Thruster

so as to prevent any net electric current in the flow direction. Thus, as with the diffusion model used in RadialArc, electrons are retarded by this internally generated field, while ions are accelerated. The Lorentz force, then, must be included in the diffusion model as a body force acting on the electrons. Eq. (2.9) becomes:

$$n_\gamma \sum_{i=1}^{N} m_\gamma n_i \, \omega_{\gamma i} (v_{Di} - v_{D\gamma}) - \frac{\partial}{\partial x} p_\gamma + n_\gamma q_\gamma E_x =$$

(7.2)

$$- \frac{n_\gamma m_\gamma}{\rho} \left(\frac{\partial}{\partial x} p - j_r B \right) + j_{r\gamma} B$$

where j_r is the total transverse electric current, and $j_{r\gamma}$ is the transverse electric current of species γ. $j_{r\gamma}$ is assumed to be only non-zero for electrons. Electrons in

this model are being accelerated in the positive x direction via the Lorentz force, and decelerated by the internally generated electric field (E_x) and collisions with heavy particles.

The Lorentz force always acts perpendicular to the instantaneous direction of motion of electrons and so can contribute no energy to the electron gas. However, the retarding field provides a body force which acts on both the electron and heavy gases and contributes to the energy balance of both. The effects of this body force appear as equal and opposite additional terms in both the electron energy conservation equation and the heavy particle energy conservation equation. This term is:

$$q_e n_e (v + v_{De}) E_x \tag{7.3}$$

where E_x is the axial internally generated electric field. This field is automatically calculated during the diffusion velocity calculation if the model discussed in 2.3.3 is used (with the modifications of Eq. (7.2). The term of Eq. (7.3) is added to the electron energy equation and subtracted from the heavy energy equation. The effect will be to reduce the energy of the electron gas and increase the energy of the heavy gas. Thus, the internally generated electric field provides an additional mechanism for energy exchange between the two fluids.

It has been determined that the energy conservation equations should be cast in a modified form when flow is supersonic. This form is obtained by ignoring the kinetic energy of the electrons, and by using a kinetic energy equation as discussed in appendix B to alter the form of the heavy energy equation. After these steps, the energy conservation equation for the electrons is:

$$\frac{\partial}{\partial t}\left(\frac{3}{2}n_e k T_e\right) + \nabla \circ \left(\frac{5}{2}n_e k T_e\right) \tag{7.4}$$

$$= j_r E_r - \sum_{j=1}^{L} \Delta \epsilon_{je} \frac{d}{dt} \zeta_j - e\dot{x}ch - \nabla \circ \vec{\Gamma}_e + n_e q_e (v + v_{De}) E_z$$

and for the heavy gas:

$$\frac{\partial}{\partial t} \left(\sum_{\gamma \neq e} n_\gamma u_\gamma \right) + \nabla \cdot \left(\sum_{\gamma \neq e} n_\gamma h_\gamma (\vec{v} + \vec{v}_{D\gamma}) \right) = \tag{7.5}$$

$$-\nabla \cdot \vec{\Gamma}_h + e \dot{x} oh + v \left(\nabla (p + \frac{B^2}{2 \mu_o}) \right)$$

$$- \sum_{j=1}^{L} + \Delta \epsilon_{jh} \frac{d}{dt} \ell_j - n_e q_e (v + v_{De}) E_z$$

where the pressure gradient term accounts for the kinetic energy of the heavy gas.

Furthermore, in order to calculate this magnetic field, some form of Ampere's law must be included. In fact, the entire electric and magnetic field situation is quite different in MPD. The voltage across the electrodes can be considered uniform along the axis (although it is allowed to change in time). In reality, for non-planar geometries, the electric field will vary with radial position as well as axial position. However, an approximation is used to retain the one-dimensional nature of the problem by letting the field be uniform between the electrodes. Thus, the *transverse* electric field is assumed to be:

$$E_r(x) = \frac{V}{D(x)} \tag{7.6}$$

where $D(x)$ is the channel width, V is the thruster voltage, and $E_r(x)$ is the local transverse electric field. Once the local electric field has been determined, the transverse electric current density is easily determined from Ohm's law:

$$j_r(x) = \sigma(x) \left(E_r(x) - (v(x) + v_{De}(x)) B(x) \right) \tag{7.7}$$

where $j_r(x)$ is the transverse electric current density, and σ is the local electrical conductivity. In this model the induced EMF is calculated with the total speed of the mobile charges (electrons) and so includes the flow and diffusion velocities. It is assumed that the magnetic field only points in the azimuthal direction (perpendicular to both current and flow) so that Ampere's law takes on a particularly simple form:

$$\frac{\partial B}{\partial x} = -\mu_o j(x) \tag{7.8}$$

This combination of Ohm's law and Ampere's law must then solved as an auxiliary equation in much the same manner as Ohm's law was solved in RadialArc. However, in the MPD context, the diffusion model requires knowledge of the magnetic field, just as the magnetic field model requires knowledge of the diffusion velocities. In order to produce self-consistent magnetic field, diffusion velocities, and axial electric fields both Ampere's law and the diffusion model must be solved together. These laws have been combined in a routine called "MPD__Diffusion" which is called before each flow step. This procedure ensures that as long as electrons are accelerated by the magnetic field, the net energy gain of the electrons due to their interaction with transverse and axial fields is positive. The significance of this approach becomes great in cases where the electric drag is very close to the Lorentz force. Numerical oscillations can result with a less careful approach.

The rest of the equations remain as they were for RadialArc. Thus, the primary difference between the physical description of MPD and that of RadialArc is that MPD must describe a transverse magnetic field, and is not concerned with an axial electric field. This magnetic field then becomes an important part of the momentum transport picture.

7.3 Boundary Conditions

The boundary conditions for MPD are very different than for RadialArc. In the case of RadialArc, there was a symmetry point at one end where fluxes vanish, and constant conditions at the opposite end. Thus, the conditions at the "guard cells" just off the computational mesh were very easy to establish. In the case of MPD, a stagnation point with constant composition and temperature is assumed to exist at some upstream point before the computational mesh. Boundary conditions for the upstream guard cell must then reflect some physically reasonable conditions matching the stagnation point to the thruster inlet. It is important that these conditions remain physically realizable. For example, the guard cell pressure, temperatures, and compositions must all lie between those of the stagnation point and those of the first grid point. Furthermore, the flow velocity must be chosen so as to avoid representing any non-physical condition such as an expansive shock or discontinuity. Following along the lines of techniques reported by Boris, Oran, Fritts and Oswald[61], the following method has been devised which seems to work well under most conditions.

In order to implement these inlet conditions, a characteristic length is needed. This length represents something about the physics of the world outside the thruster. It is an indication of how far away from the inlet the stagnation conditions exist. The

stagnation conditions are given by a constant temperature, composition, and zero momentum. At the inlet guard cell, then, temperatures are assumed to be:

$$T_{guard} = T_{stag} + (T_{inlet} - T_{stag})e^{-dx/InFlowLength} \tag{7.9}$$

where InFlowLength is the characteristic length as specified by the "@InFlowLEngth" command described in the next section and "dx" is the grid spacing. Composition at the guard cell must be chosen to prevent any discontinuities in the pressure distribution. To accomplish this, each species partial pressure is forced to be kink-free. Thus:

$$n_{\gamma guard} = \frac{T_{stag}n_{\gamma stag} + (T_{inlet}n_{\gamma inlet} - T_{stag}n_{\gamma stag})e^{-dx/InFlowLength}}{T_{guard}} \tag{7.10}$$

where the appropriate kinetic temperature is employed if species γ happens to correspond to the electrons. Finally, momentum at the guard cell is related to the flow rate: of the inlet

$$\rho V_{x guard} = FlowRate/Area(0) \tag{7.11}$$

Similarly, the downstream situation requires some kind of outflow boundary condition. The basic problem in modelling outflow conditions is that calculations can not extend spatially to infinity where conditions are known. In the case of MPD, pressure and energy densities are all zero at infinite distance. Since the flow is supersonic at the exit, the conditions chosen must not affect the flow field. A good scheme will be one for which varying some parameter over a significant range does not significantly affect the results of the rest of the modelled region.

The outflow approximation used by MPD is very simple. All that is needed is an approximation for conditions at one point off the computational grid. In order to encourage FCT to flow material into the infinite vacuum, energy density, momentum density, and species concentrations are taken to be zero at the guard cell during the flow process. Furthermore, the last computational cell is treated in a backward difference scheme and so does not directly involve the guard cell. In addition, for the parts of the simulation outside of the flow problem (generation of heat fluxes, diffusion velocities, etc.) the following approximations are used:

$$n_{\gamma W+1} = n_{\gamma W} \tag{7.12}$$

$$T_{W+1} = T_W \tag{7.13}$$

$$T_{eW+1} = T_{eW} \tag{7.14}$$

where W is the index of the last computational grid point. The magnetic field is taken to be zero at the nozzle exit

$$B(W) = 0 \tag{7.15}$$

7.4 The User Interface

As in the case of RadialArc, several commands have been added to the basic list of possible control file entries. Furthermore, some new keywords have been added to the @BoundaryConditions command. Briefly, the new commands are:

@Length	to indicate the length of the thruster
@FlowRate	to indicate a mass flow rate at the inlet
@InFlowLength	to indicate a characteristic length for inflow processes
@Width	to indicate a profile of the channel width
@Area	to indicate a profile of channel area
@Voltage	to indicate the voltage (possibly a function of time)
@Transient	to control the time flow (as in RadialArc)

and are used in addition to the basic THOR commands of @Reactions, @Species, @InitialConditions, and @BoundaryConditions.

As would be expected, the @Length command is used to indicate the length of the thruster. A simple numeric argument is used, and will be interpreted as the length in M. For example:

        @Length(.05)

indicates a 5 cm channel length.

@FlowRate is used to indicate a inlet mass flow rate (kg/s). If not specified, a flow rate of .006 kg/s is assumed. Thus:

```
@FlowRate(.01)
```

indicates a 10 g/s flow rate.

Similarly, @InFlowLEngth is used to indicate a characteristic length for the inlet conditions. Thus:

```
@InFlowLength(.1)
```

indicates a 10cm characteristic inflow length.

@Width allows the specification of a channel width as a function of the x coordinate. Thus, arbitrary profiles can be taken for simulation. All linear dimension units should be M. For example:

```
@Width[.005*(1.0+x**2)]
```

indicates a channel width beginning at 5mm, and increasing quadratically. @Width is a required entry. MPD will not run without it.

@Area is similar to @Width, and is used to indicate the cross-sectional area of the thruster channel. Units are in M^2. For example:

```
@Area[25e-6*(1+x**2)**2]
```

would indicate an area corresponding to a square cross section of the width indicated above. @Area is a required entry.

@Voltage is analogous to the @Current command of RadialArc. Again, the voltage may be a function of time. For example:

```
@Voltage[500*(1-100*time)]
```

Indicates a decreasing voltage ramp. @Voltage is a required entry.

@Transient is identical to the @Transient defined for RadialArc. Again, keywords OutTime, TimeToStop, and Verbose may be used.

Finally, the @BoundaryConditions command has slightly different keywords in MPD than it has for RadialArc. These are "StagTemp" and "StagDensity" and are roughly equivalent to the "WallTemp" and "WallDensity" defined for RadialArc. In the case of MPD, however, a fictitious point upstream from the computational grid is taken to be a stagnation point with constant temperatures and densities as indicated by these keywords.

7.5 An Example In Argon

These equation modifications and boundary equations were employed in a simulation of an MPD thruster in argon. The input control file appeared as follows:

```
@Make(MPD)
@Species(Ar,ArPlus,ELEC)
@Reactions(iAe,iAphoto,iAA)
@AxialPoints(80)
@Voltage[30]
@Length(.2)
@Transient(TimeToStop=10e-6,OutTime=1e-6)
@InitialConditions[Vish80p.out]
@BoundaryConditions(StagTemp=1000.0,StagDensity Ar=1.0e23,
StagDensity ELEC=5.0e19,StagDensity ArPLUS=5.0e19)
@Area[.0078238]
@Width[.0413]
@FlowRate[.006]
@InFlowLength[.04]
@End()
```

This indicates a simulation for a thruster 20cm in length, with 4.13cm between electrodes, and with a cross sectional area of .0078238M^2. These conditions were chosen to roughly correspond to a device investigated by King, Clark, and Jahn[60]. Stagnation conditions are taken to be 10 torr at 1000K, and the applied electric field is 30 volts. Beginning with arbitrary initial conditions, a steady state is reached after several hundred microseconds of simulation. Fig. 7.2 shows the final temperature profiles. This plot indicates the heating of the heavy gas by the electrons as the plasma flows down the channel. Fig. 7.3 shows the plasma flow velocity at various points in the channel. Sonic speed at the exit is roughly 1900 M/s and so the flow has reached supersonic speeds. The current density profile is shown in Fig. 7.4 and indicates the typical droop in the middle where back EMF is significant. At the inlet, back EMF is small because the flow velocity is small. At the

Axial Temperature Profile, 20cm device
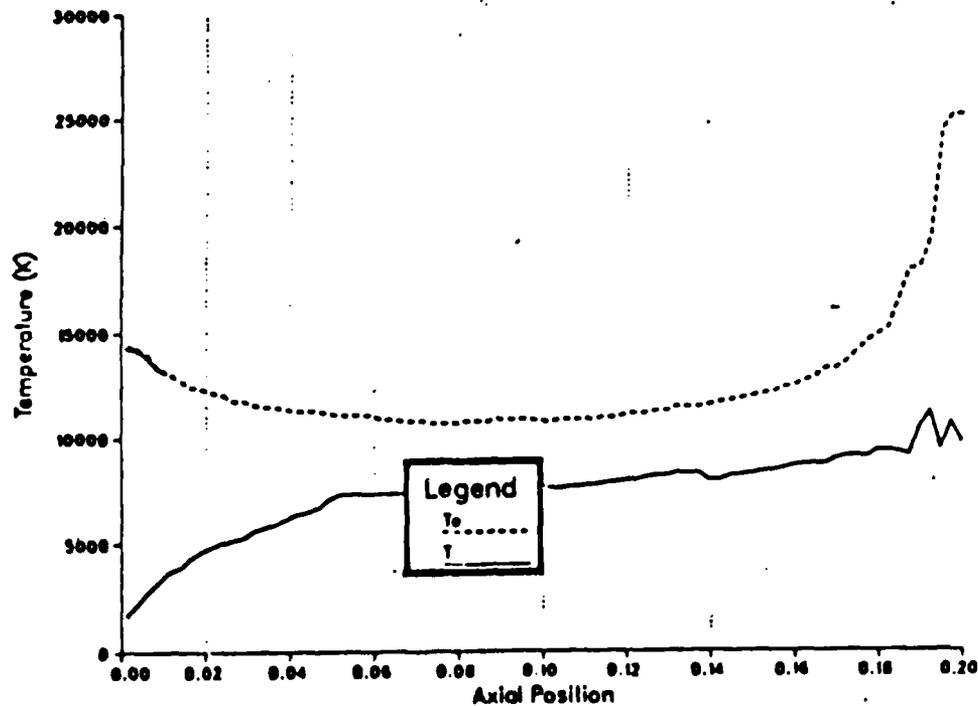
Fig. 7.2: Heavy Particle and Electron Temperatures in 20cm MPD Thruster

exit, the magnetic field is low and back EMF is reduced. In the center, v(x) and B are both large enough to make a significant back EMF. As is shown by Fig. 7.6, species diffusion velocities are only significant in comparison with the flow velocity near the inlet. Finally, Fig. 7.7 shows that the ionization fraction gradually increases as the gas heats on its way downstream.

7.6 Summary

The general computational techniques developed for RadialArc have been shown to be applicable to an MPD problem. Some difficulties were encountered concerning numerical stability and the magnetic-diffusion description. Also, difficulties in the energy conservation model at supersonic speeds were removed by re-casting the energy conservation equations to not include kinetic energy directly. The most significant remaining problem involves the inlet conditions. The chosen model is not entirely satisfactory in representing the mechanisms by which the cold inflowing gas is heated and ionized by the channel plasma. The bulk flow is directed away form

Axial Velocity Profile, 20cm device
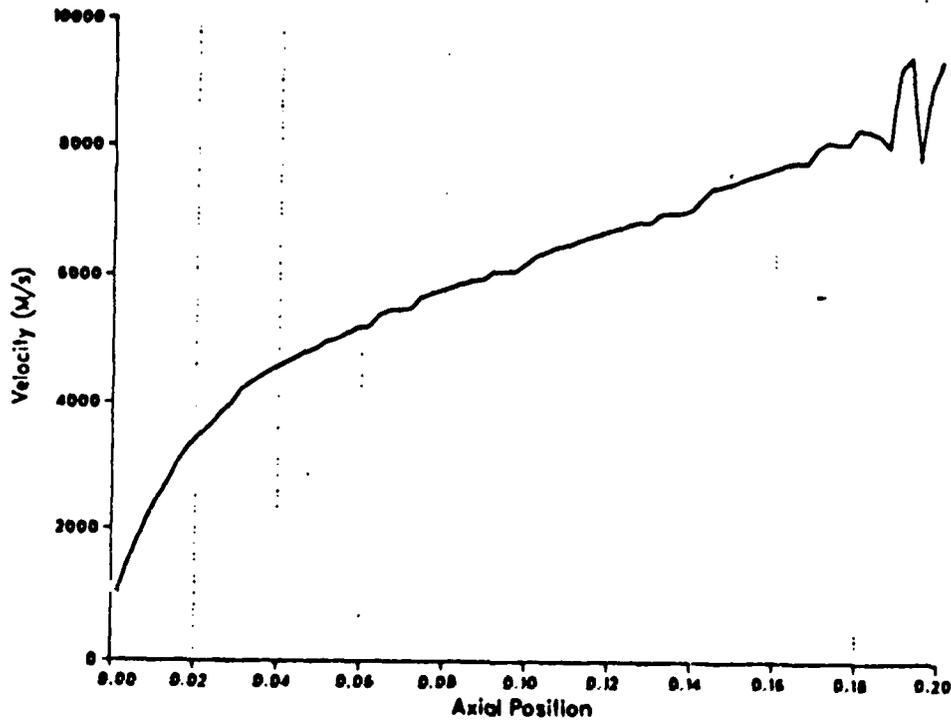
Fig. 7.3: Flow velocity in 20cm MPD thruster

this inlet, indicating that some recirculation zones, such as in a flame holder, are necessary. THis aspect has not been addressed, but a model for these effects could be easily added to MPD.

The results of this SimulationType are expected to be useful as a bulk flow model for future analysis of electrode erosion in MPD thrusters. More work remains to be done on the model itself, but the current results are typical of other investigations, both theoretical and experimental, and have the added advantage of including the non-equilibrium description.

Current Density Profile, 20cm device
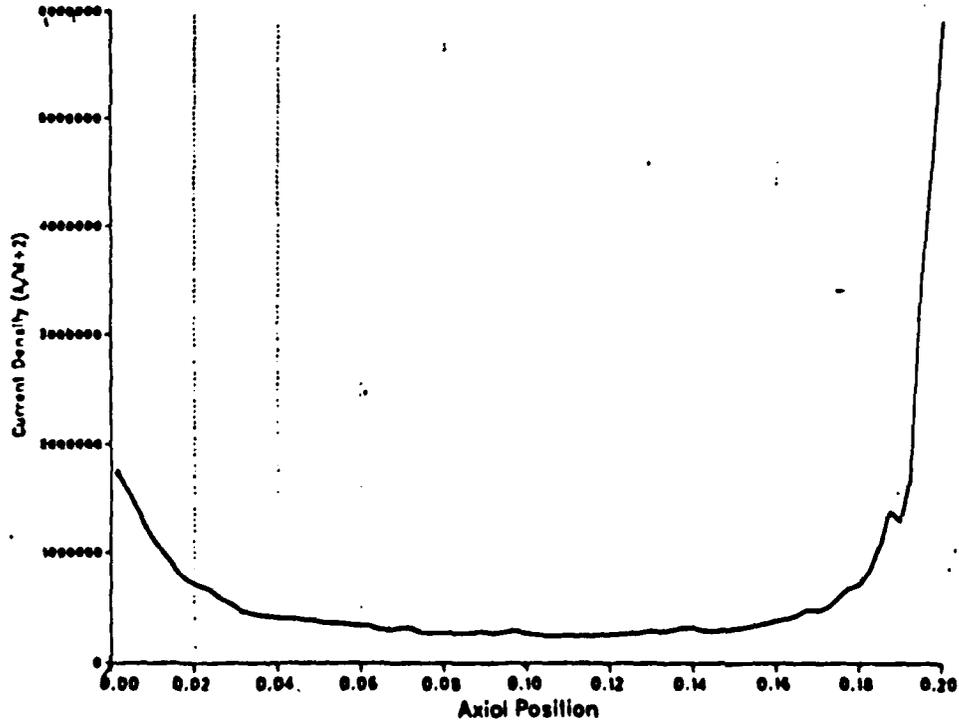
Fig. 7.4: Current Density in 20cm MPD Thruster (voltage = 30v, total current = 26000 amps)
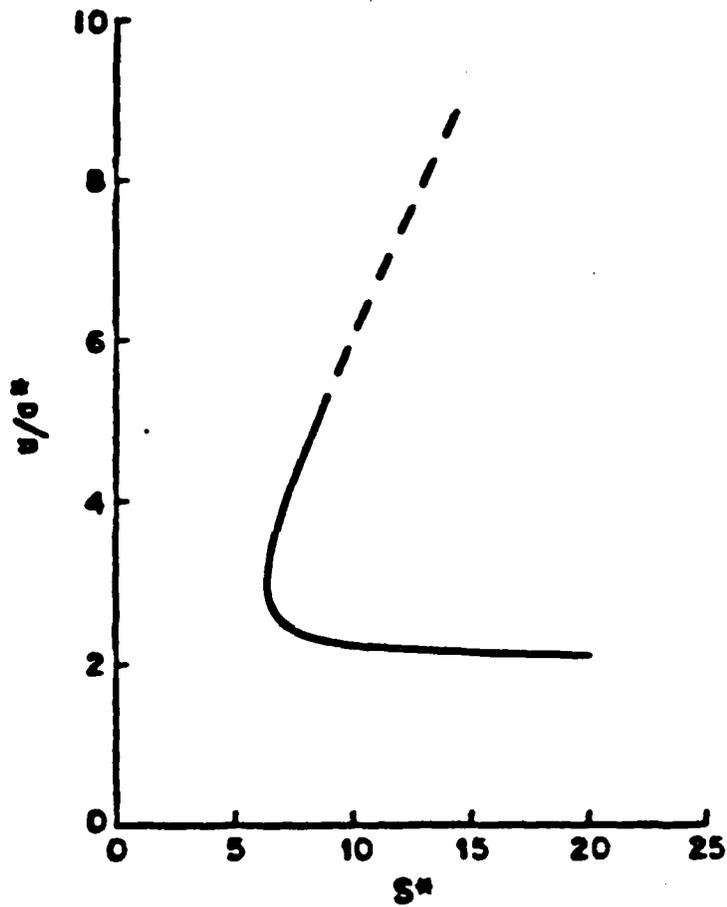
Figure 3: Exit flow speed versus S^*

The exit flow speed, nondimensionalized by the sound speed at the choking point, is plotted against the magnetic force number, S^*. The upper branch represents supersonic flow and the lower represents subsonic flow. The supersonic branch is shown dashed for $S^*>8.52$ since this range violates the onset condition discussed in Sec. 2.5. S^* is defined by (2.4.7) or (2.4.12). This plot was calculated using the frozen-flow model of Sec. 2.4.
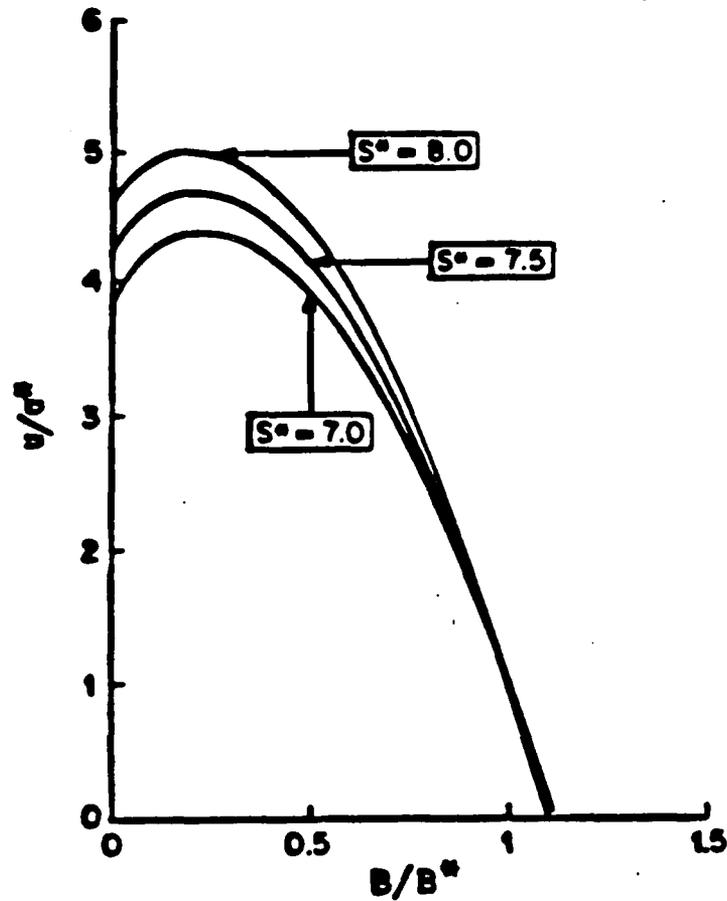
Figure 4: Flow speed versus Magnetic field

The flow speed u is plotted against the magnetic field B for three values of the magnetic force number, S^*. u and B have been nondimensionalized, respectively, by the speed of sound at the choking point a^*, and the magnetic field at the choking point B^*. Near the inlet, the speed is very low. Going downstream, the magnetic field declines. At $B/B^*=1$, the flow has accelerated to $u/a^*=1$ for all S^*. The speed continues to increase until very near the exit. The decline in speed near the exit is because ohmic heating, which decelerates the flow, becomes more important than the Lorentz force, which tends to accelerate the flow, because B is small. See (2.3.1). These curves were calculated using the analytical solution, (2.4.8) of Sec. 2.4.
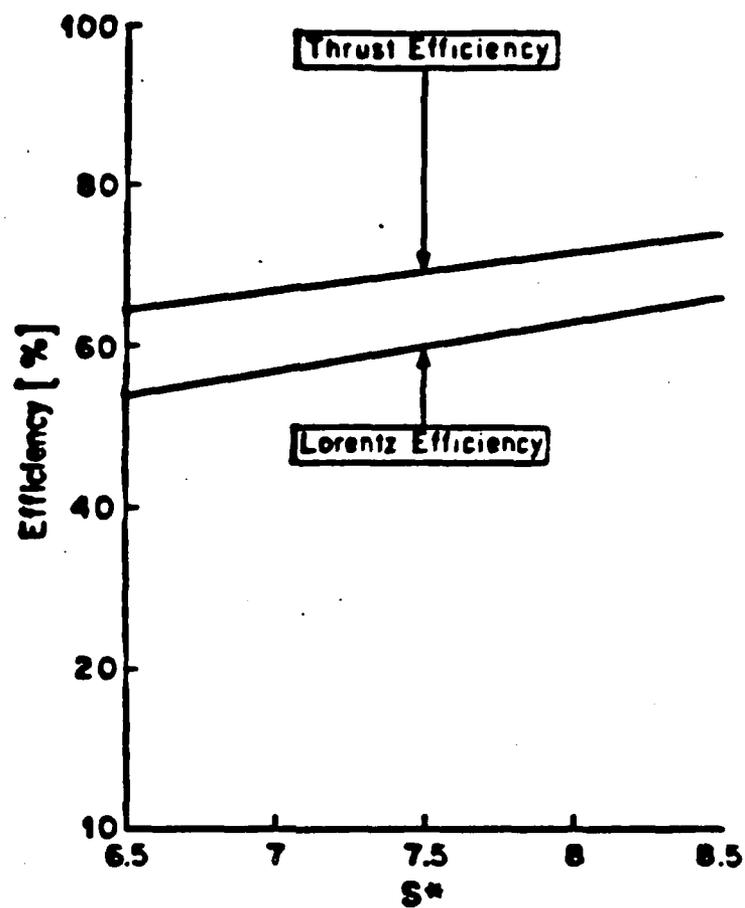
Figure 5: Efficiency versus S^*

The thrust efficiency η, defined in (2.2.14), and the Lorentz efficiency η_L, defined in (2.2.11), are plotted against the magnetic force number S^* for supersonic flow. S^* is defined in (2.4.7) or (2.4.12).
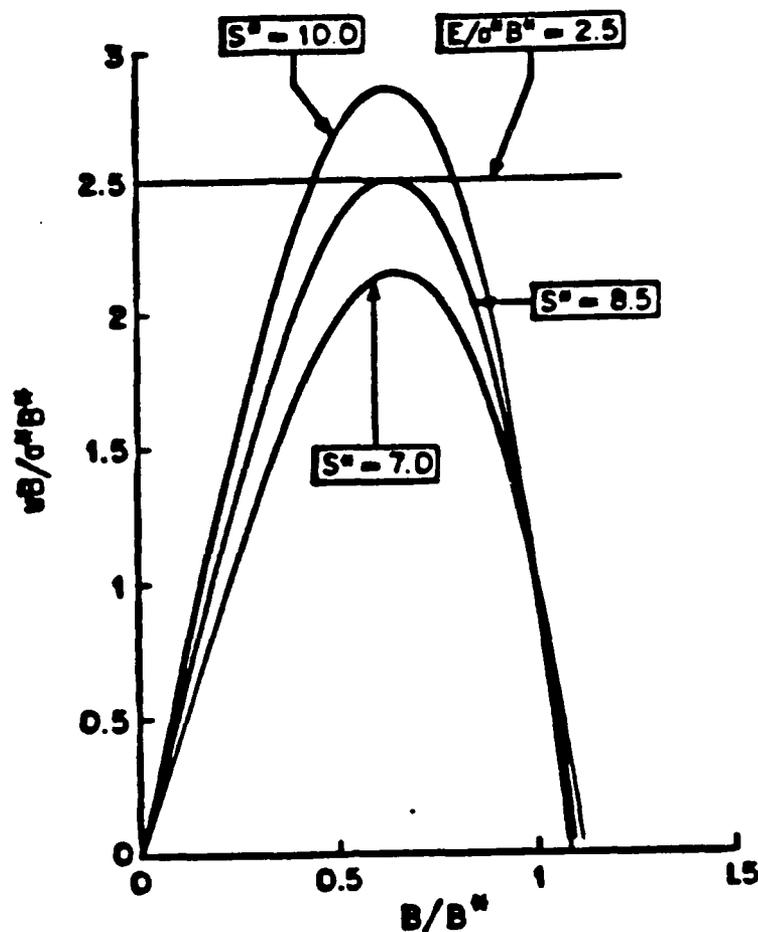
Figure 6: Back-EMF versus Magnetic field

The back-EMF, uB, is plotted against the magnetic field, B, for three values of the magnetic force number, S^*, for supersonic flow. Both the back-EMF and the magnetic field are nondimensionalized by their values at the choking point. These curves were calculated using the frozen-flow solution of (2.4.8). The back-EMF is small near the inlet because u is small. See 4. The back-EMF is small near the exit because B is small. See the discussion of boundary conditions in Sec. 2.2. The back-EMF peaks in the middle of the thruster. Also, the electric field determined by the choking condition, (2.4.2), is shown as a dashed line. For the largest S shown, the back-EMF is larger than the electric field during part of the flow. The implications of this are discussed in Sec. 2.5.
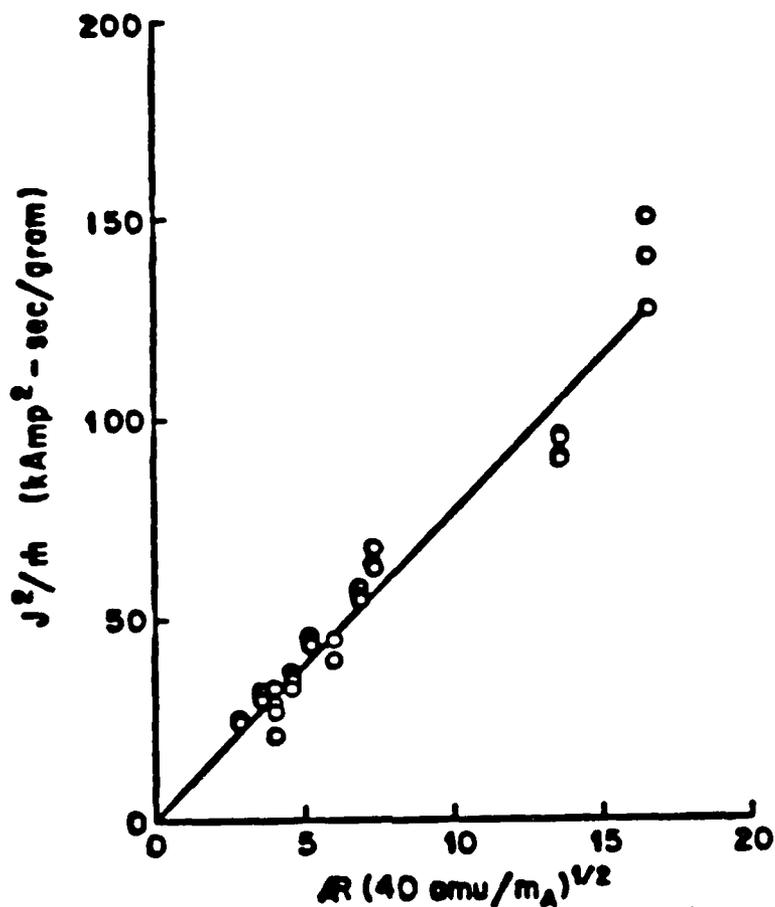
Figure 7: Comparison with experiments of Malliaris *et al.*

The experimental data of Malliaris *et al.*[5] for onset conditions correlate as predicted by back-EMF onset theory. The ordinate is the value of $J^2/\dot{m}$ at which onset was observed to occur. The abscissa is $R(40 \text{ amu}/m_A)^{1/2}$ where R is the thruster aspect ratio and m_A is the propellant's atomic mass. 40 amu is the atomic mass of argon. The data shown cover the range of $R=4.0$ to 13.6 and the propellants used were helium, neon, argon, krypton, and xenon. The solid line is a best fit to the experimental data. The back-EMF theory of onset is discussed in Sec. 2.5.
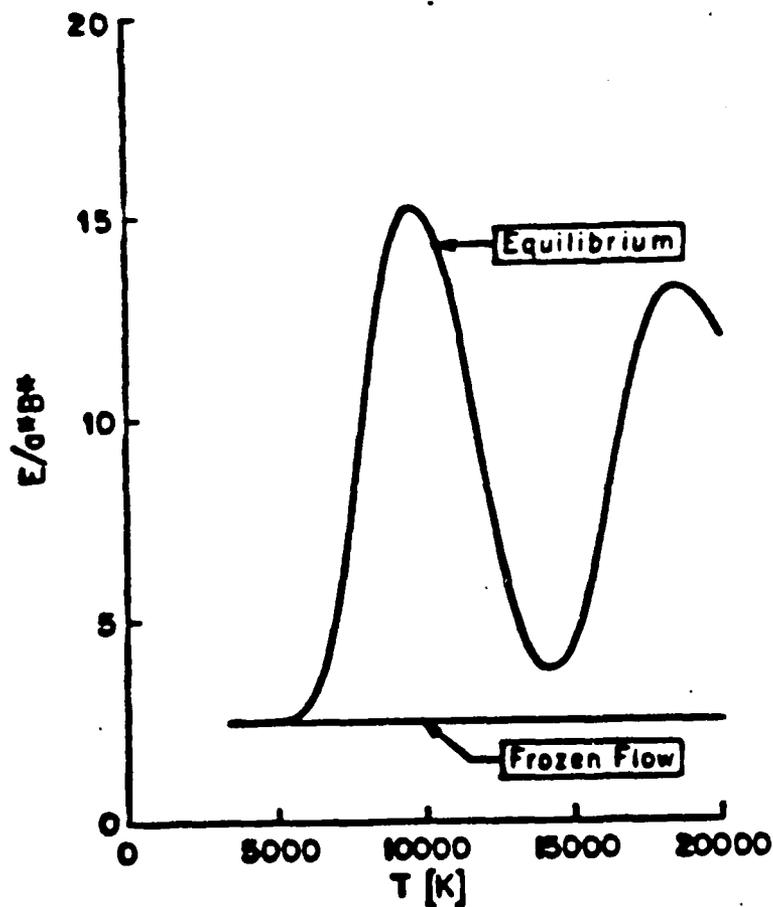
Figure 8: Electric field versus Temperature at the sonic point

The electric field determined by the choking condition, (2.3.3), is plotted against temperature at the choking point for the two cases of equilibrium and frozen flow. The equilibrium curve uses the enthalpy including translational, electronic, and ionizational contributions for an equilibrium composition of argon and its first six ions. The frozen flow curve assumes a constant composition of electrons and once ionized argon with enthalpy as given by (2.5.2). A mass density of 0.0007 kg/m³ was assumed for the equilibrium calculation.
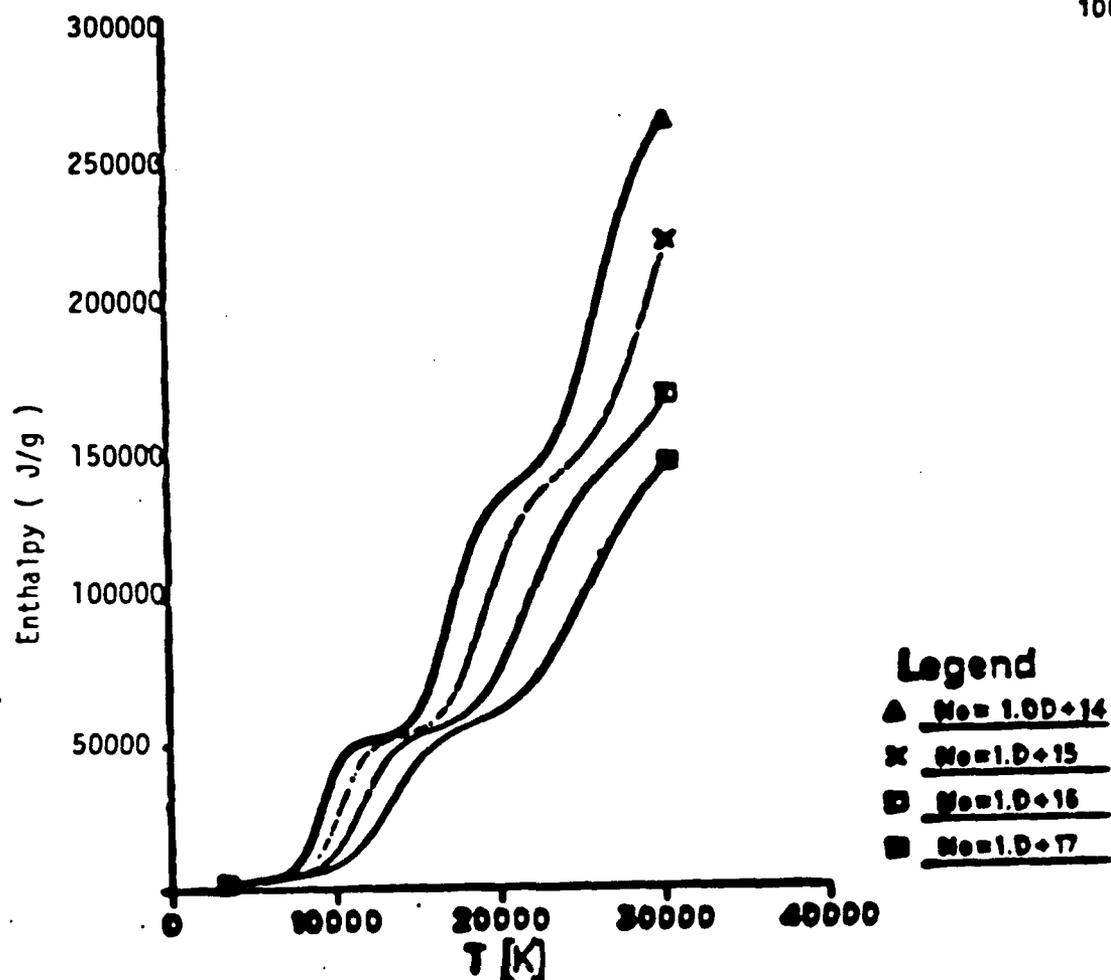
Figure 9: Argon enthalpy at equilibrium versus Temperature

The variation of specific enthalpy versus tempera ure for Argon is shown at various number densities. These results were obtaine by using a detailed statistical thermodynamics. Upto six excited states have been accounted for each of the species A, A+, A++, and A+++. The details of the calculation are given in Sec. 3.4.
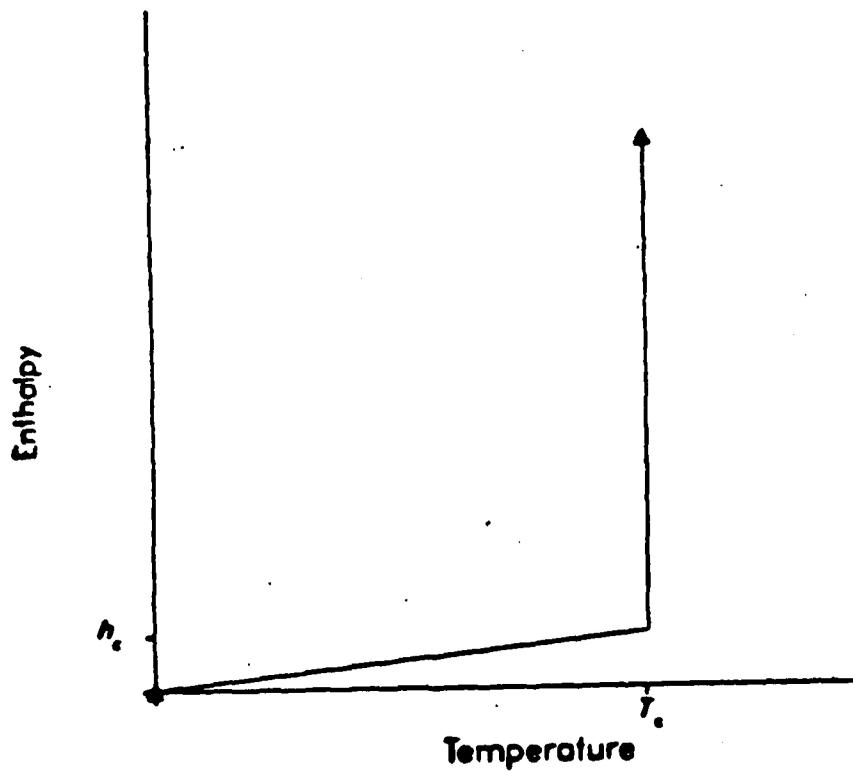
Figure 10: Idealized argon enthalpy versus Temperature

The variation of specific enthalpy versus temperature for argon in thermodynamic equilibrium is approximately modeled using the above piecewise linear form. This graph represents Fig.9 approximately. In this piecewise linear model, the enthalpy varies linearly until a cutoff temperature $T = T_c$ is reached. In this linear region, any energy that is added goes into the translational mode. After this cutoff temperature is reached, the temperature remains at $T = T_c$ and the enthalpy continues to increase. This piecewise linear variation qualitatively simulates the equilibrium behaviour of the enthalpy. See Sec.3.4 for a full discussion.
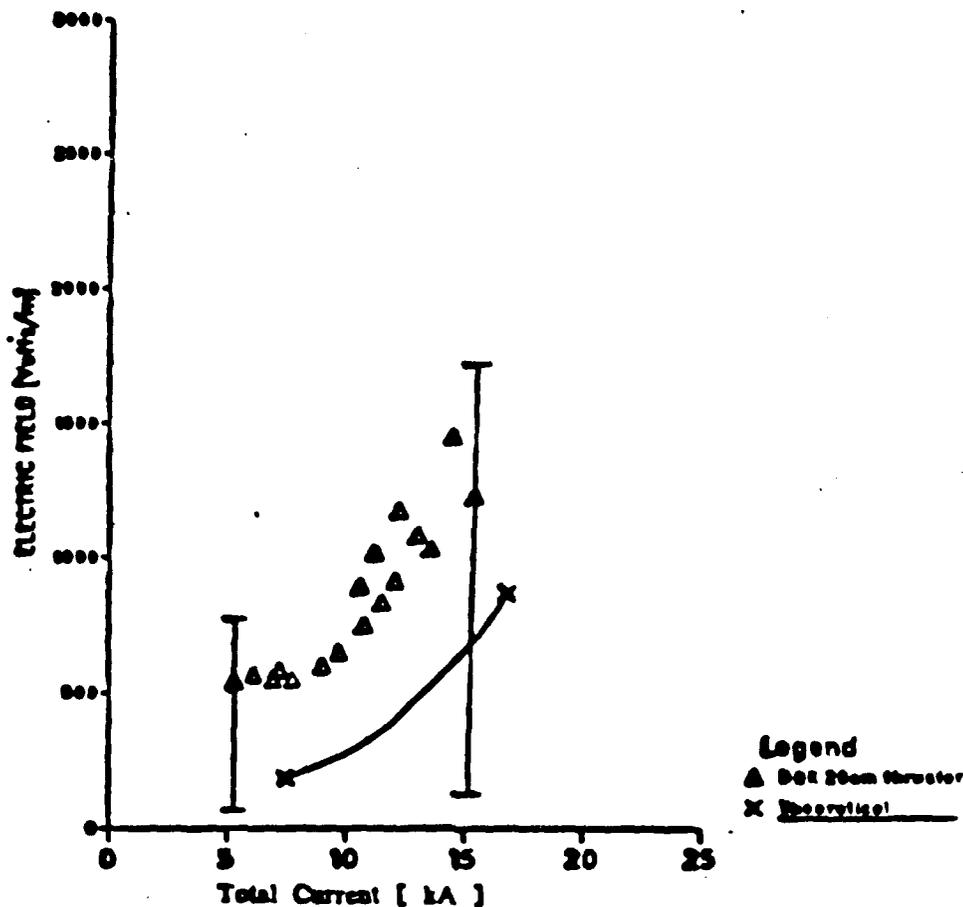
Figure 11: Electric field versus Total current for 3g/sec

The variation of the electric field is shown versus the total current. The experimental data of King[23] for a 20 cm. long straight coaxial thruster are plotted as discrete points, for a total mass flow of 3 g/sec. *The vertical bars do not denote experimental error bars.* These bars have been used to denote the variation of the experiment from quasi-one dimensionality[30]. The solid curve represents the prediction of the non-equilibrium theory of Sec.3.5 corresponding to a uniform mass flow of 3 g/sec. The upper portion of the solid curve ends where no steady solution to the equations of Sec.3.5 was found. This is interpreted as the theoretical onset point. As can be seen, this agrees well with the onset limit observed in the experiment, where the data is seen to be scattered. See Sec.3.5 and Sec.3.6 for a detailed discussion.
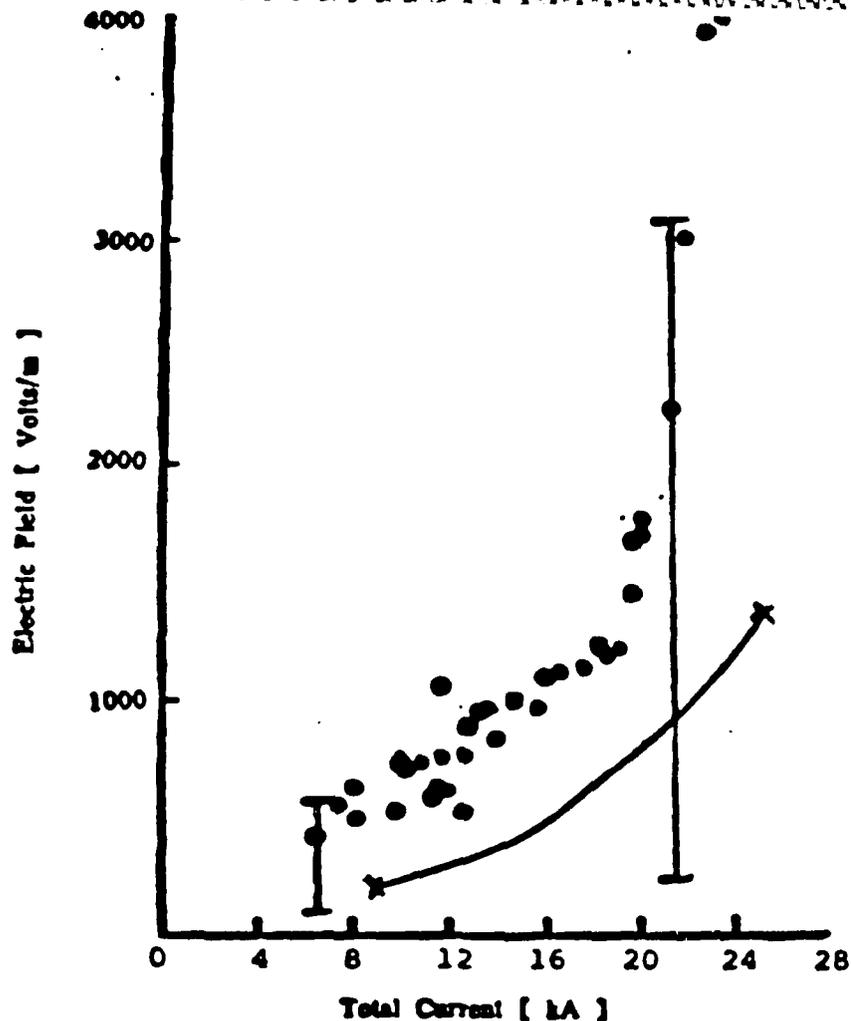
Figure 12: Electric field versus Total current for 6g/sec

The experimental data of King[23] for a 20 cm. long straight coaxial thruster are plotted as discrete points, for a total mass flow of 6 g/sec. *The vertical bars do not denote experimental error bars.* These bars serve to denote the variation of the experiment from quasi-one dimensionality. The solid curve represents the theoretical predictions of the non-equilibrium theory of Sec.3.5 for a uniform mass flow of 6 g/sec. The curve ends at the upper point where no steady solution could be found. This is the theoretical onset limit, which agrees well with the experimental onset limit of $\sim$ 28 kA.
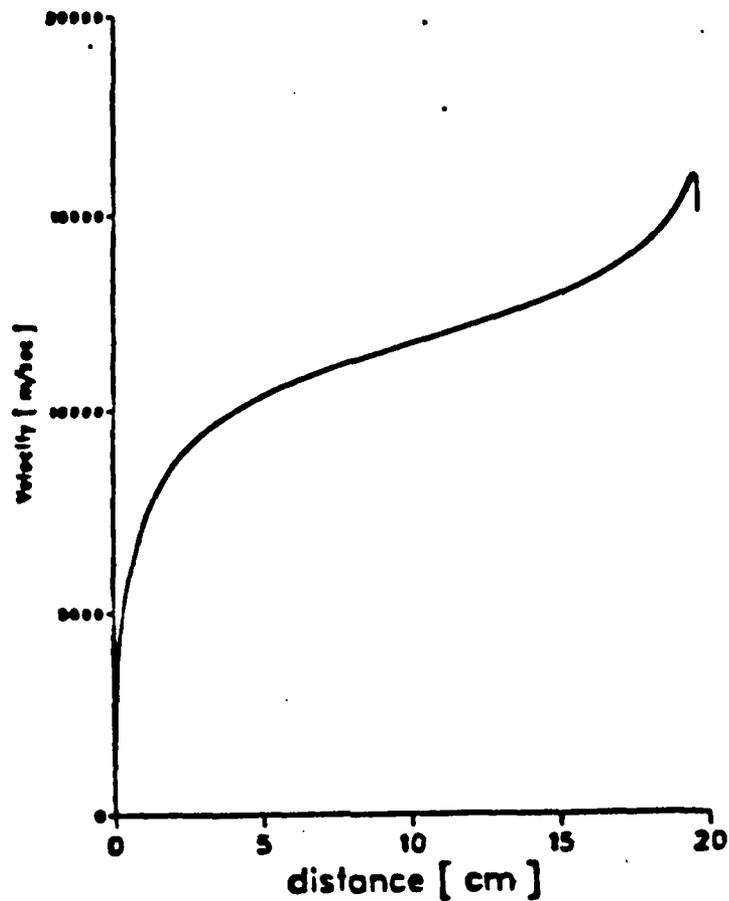
Figure 13: Velocity versus Distance for 3g/sec

The plasma flow speed is shown here as a function of distance along the thruster, for a uniform mass flow of 3 g/sec. This profile was obtained from the solutions to the quasi-1D non-equilibrium equations given in Sec.3.5 and Sec.3.6. It can be seen that the speed increases monotonically until near the exit, where it decreases. This is due to the dominance of ohmic heating near the exit which causes a supersonic flow to decelerate.
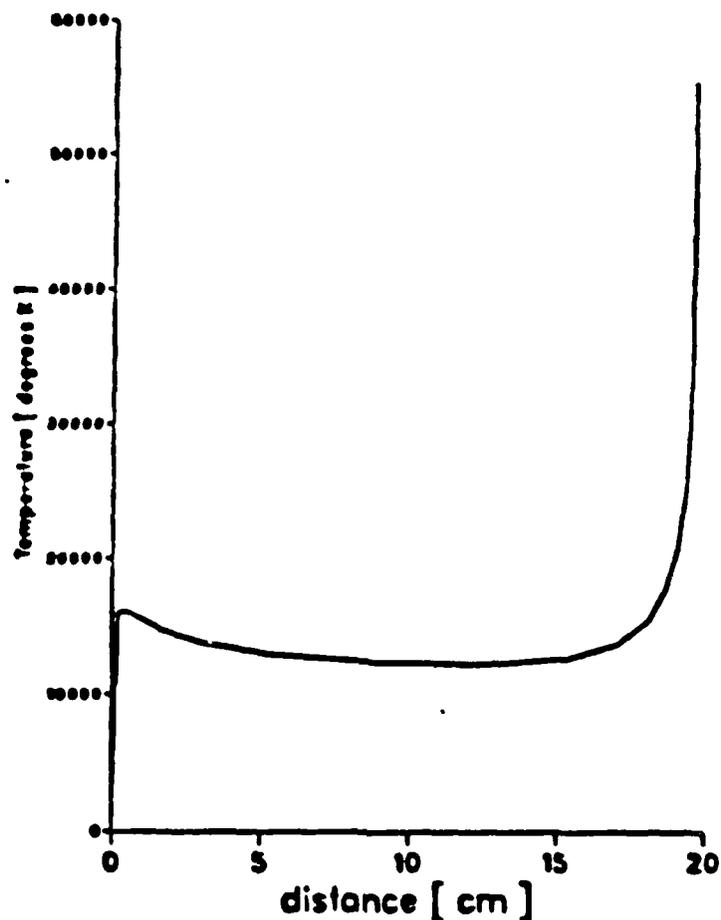
Figure 14: Temperature versus Distance for 3g/sec

The plasma temperature is shown in this figure versus distance along the length of the thruster, for a uniform mass flow of 3 g/sec. See Sec.3.5 and Sec.3.6 for the solutions of the quasi-1D non-equilibrium theory, which were used to obtain the above profile. The temperature increases sharply from the inlet to the sonic point primarily due to ohmic heating. Beyond the sonic point, there is a slight decrease because of the acceleration of the supersonic flow. Near the exit, the temperature rises again because of ohmic heating. This temperature rise near the exit is accompanied by the decreasing velocity shown earlier in Fig.13. The unrealistically high exit temperatures are due to the fact that the presence of second ions were not considered in the non-equilibrium theory. See Sec.3.6 for details.
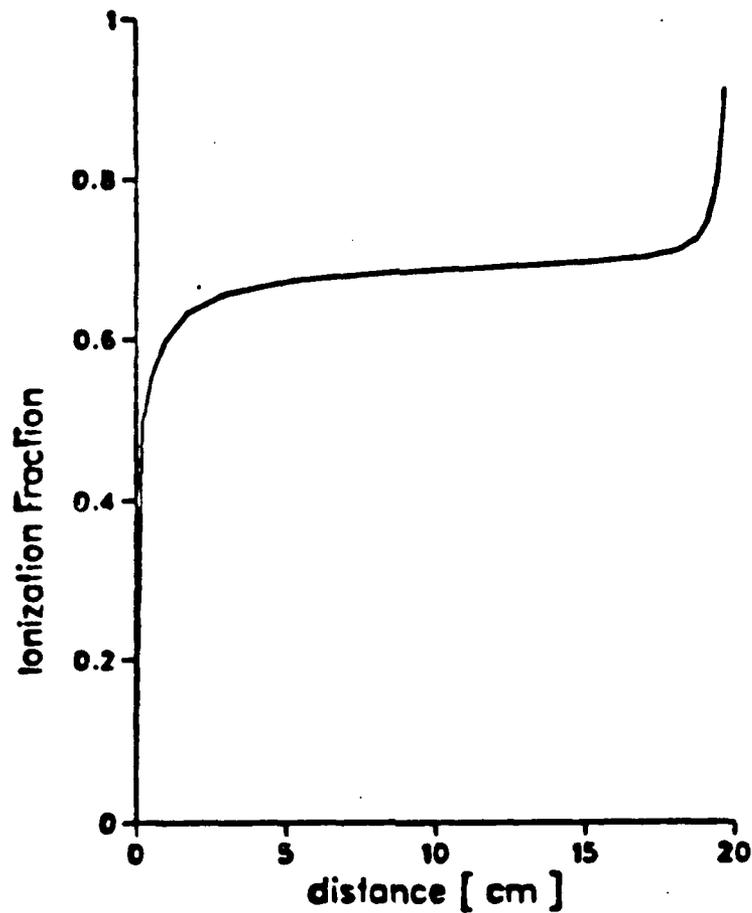
Figure 15: Ionization fraction versus Distance for 3g/sec

The ionization fraction has been plotted here as function of the distance along the thruster. The ionization fraction shows marked increases near the entrance and near the exit, where the most drastic variations in temperature take place. This again, is from the solution of the non-equilibrium equations found in Sec.3.5 and Sec.3.6, for a uniform mass flow of 3 g/sec.
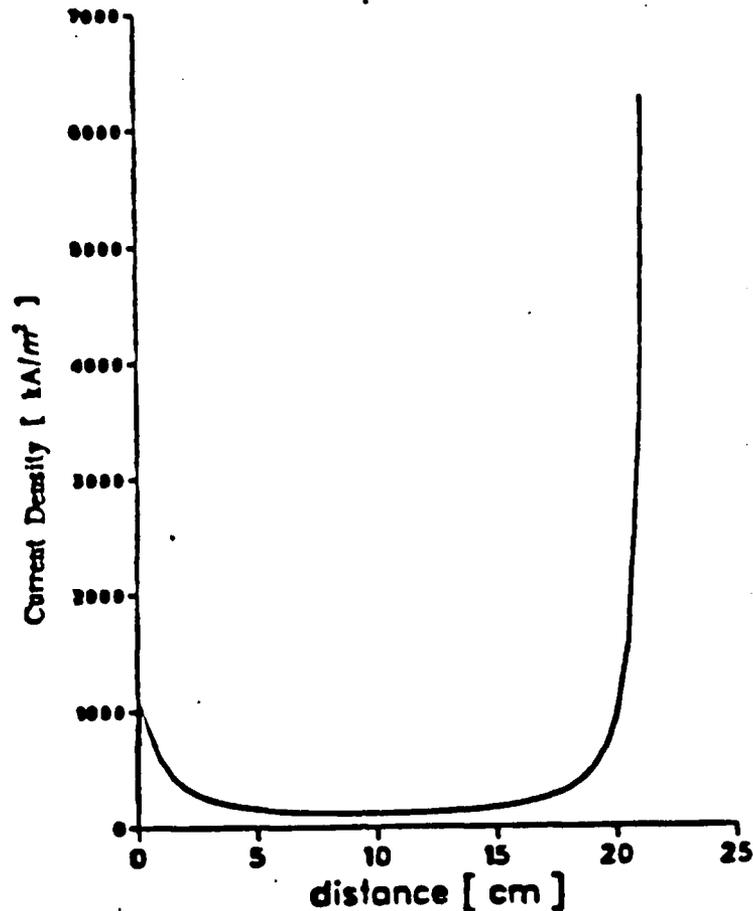
Figure 16: Current density versus Distance for 3g/sec

The current density is shown here versus distance for a uniform mass flow of 3 g/sec. This is from the solutions of the governing equations given in Sec.3.5 and Sec.3.6. The current density is small near the entrance because the temperature is small which makes the conductivity small. Then, it increases as the temperature increases. Next, as the flow speed increases and the magnetic field decreases, the current density drops until a minimum is reached. This minimum current density corresponds to a maximum back-EMF. The current density then rises rapidly toward the exit because the rising temperature causes the conductivity to increase.
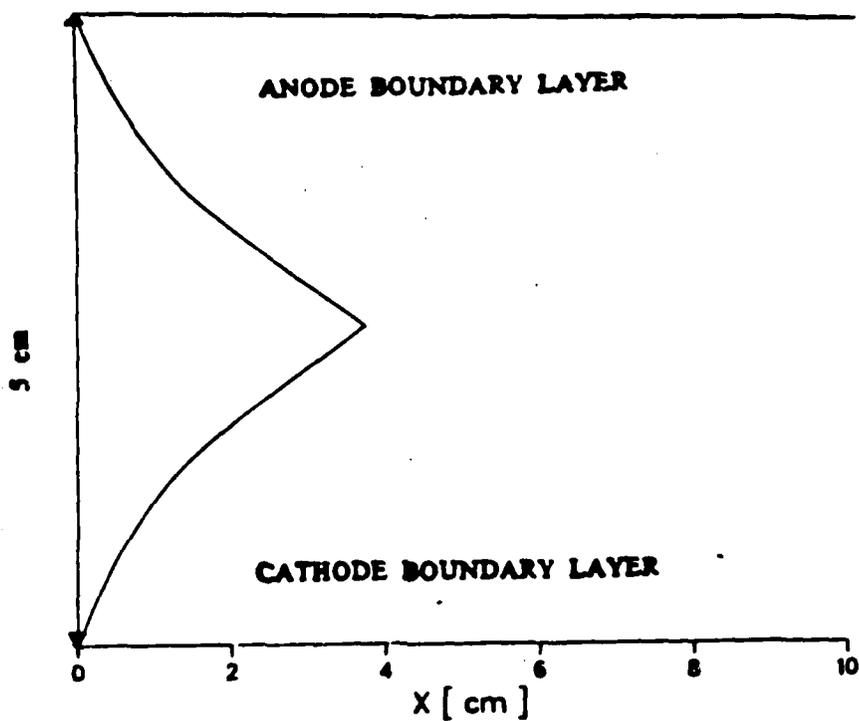
Figure 17: Non-equilibrium boundary layer growth

The growth of the electrode boundary layers is plotted as a function of the distance along the electrode. The non-equilibrium boundary layer calculations of Sec.4.3 and Sec.4.4 have been performed for the cathode, for a total mass flow of 3g/sec to the MPD thruster. The anode boundary layer has been plotted assuming symmetry. This is done to show the approximate location where the boundary layers merge, and the flow in the thruster becomes fully developed. See the discussion of Sec.4.4.
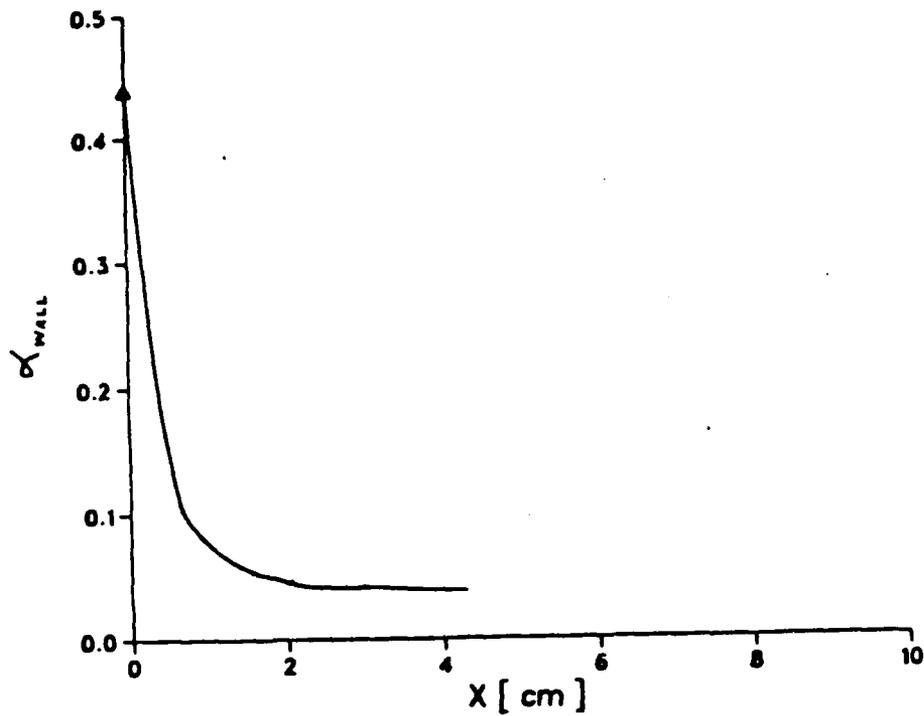
Figure 18: Ionization fraction at the wall versus Distance

The slip ionization fraction at the wall is plotted here as a function of the distance along the electrode. The non-equilibrium boundary layer theory of Sec.4.3 and Sec.4.4 has been used to compute this profile for a total mass flow of 3 g/sec to the thruster. As expected, the slip ionization fraction decreases continuously with increasing distance near the leading edge of the boundary layer.
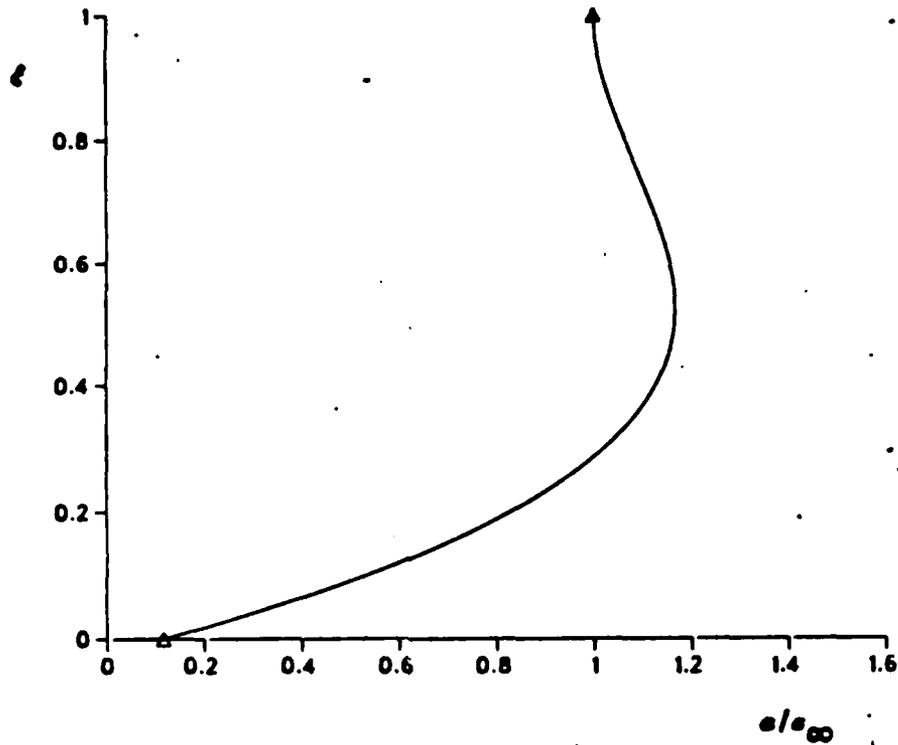
Figure 19: Ionization fraction versus Transverse distance

The ionization fraction non-dimensionalized by the free stream ionization fraction, is plotted here versus the Howarth-Dorodnitsyn transverse coordinate defined in Sec.4.3, at 1 cm. from the leading edge. This calculation has been performed for a total mass flow of 3 g/sec to the thruster. The bulge in the profile is caused by the opposing effects of ionization due to the high electron temperature, and recombination due to the presence of the cold wall.
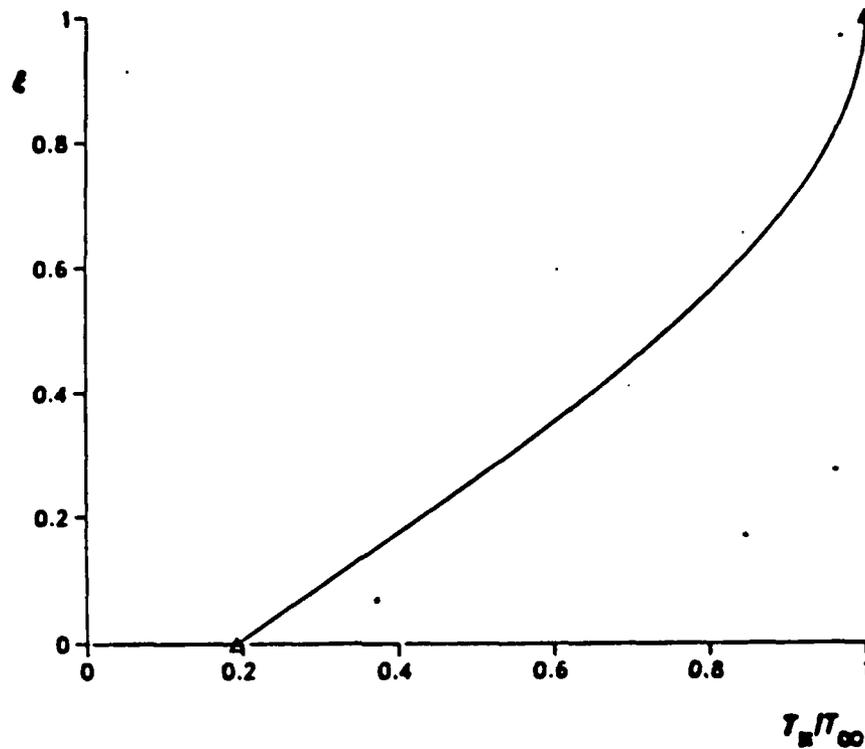
Figure 20: Heavy particle temperature versus Transverse distance

The variation of the heavy particle temperature non-dimensionalized by the free stream temperature, is shown here versus the Howarth-Dorodnitsyn transverse coordinate ℓ. ℓ has been defined in Sec.4.3. This calculation has been performed for a total mass flow of 3 g/sec, and is shown at a location of 1 cm. from the leading edge of the boundary layer. See Sec.4.4 for further discussion.
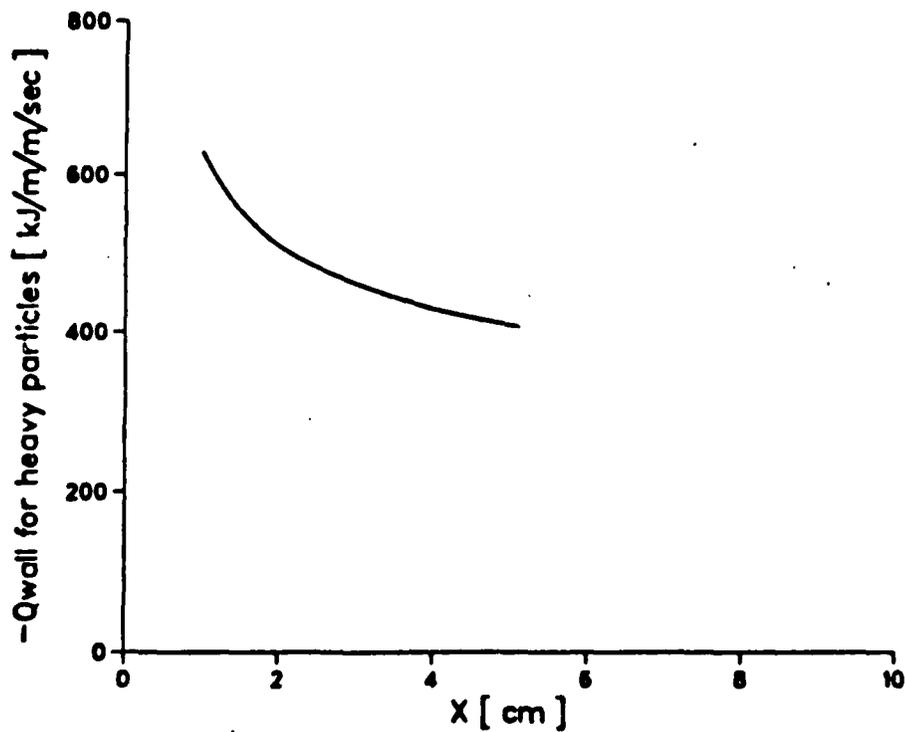
Figure 21: Heavy particle wall heat flux versus Distance

The heavy particle wall heat flux is shown here versus distance along the electrode, for a total mass flow of 3 g/sec. Note the decrease of the heat flux along the electrode, as the boundary layer thickness increases downstream from the leading edge. See Sec.4.4 for further discussion.
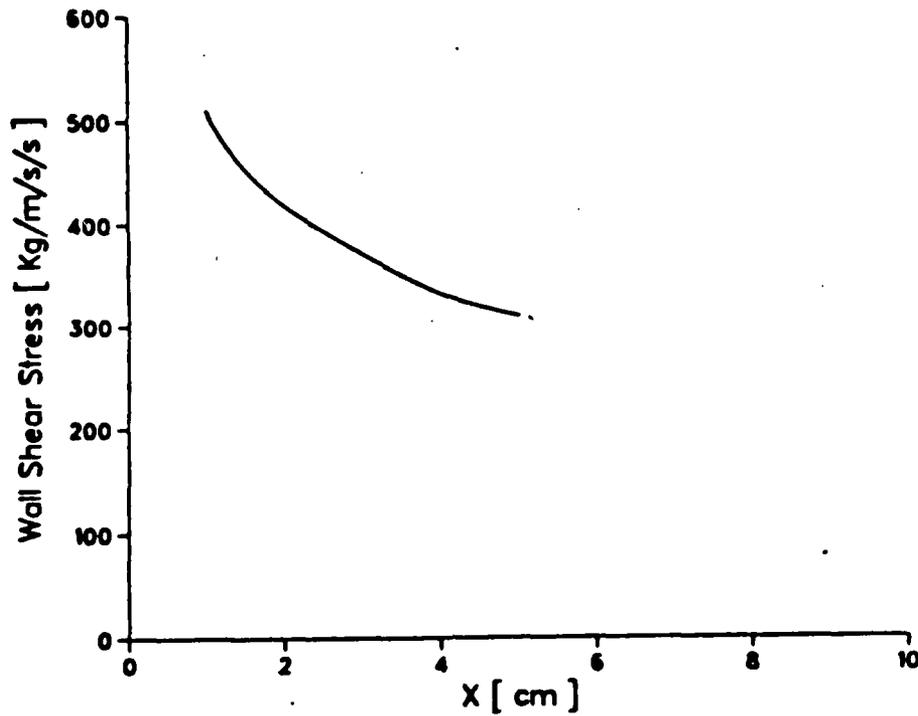
Figure 22: Wall shear versus Distance

The wall shear stress is plotted here as a function of distance along the electrode. Note the decreasing shear, as the boundary layer thickness increases along the length of the electrode. This profile has been calculated near onset for a total mass flow of 3g/sec. See Sec.4.4 for further details.
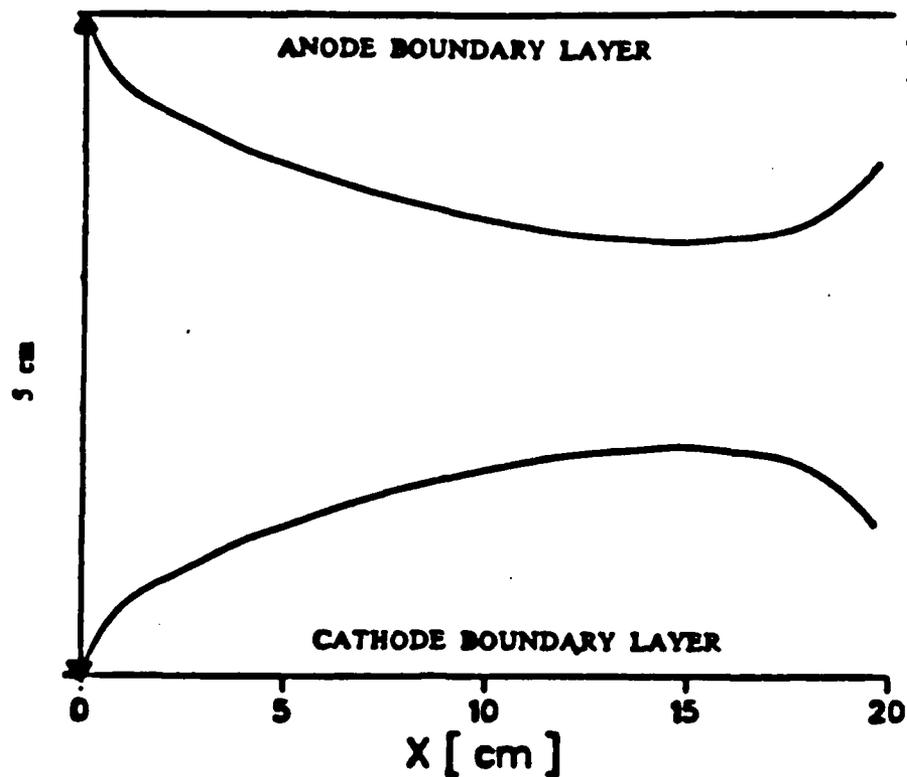
Figure 23: Frozen boundary layer growth

The growth of the cathode and anode boundary layers is shown here versus distance along the electrode. The anode boundary layer has been plotted assuming symmetry, though the frozen boundary layer calculations were performed for the cathode. A total mass flow of 3 g/sec is assumed input to the thruster, the free stream is assumed to follow the non-equilibrium quasi-1D description of Sec.3.5 and Sec.3.6, and the boundary layer is assumed to be chemically frozen. See Sec.4.4 for further discussion.
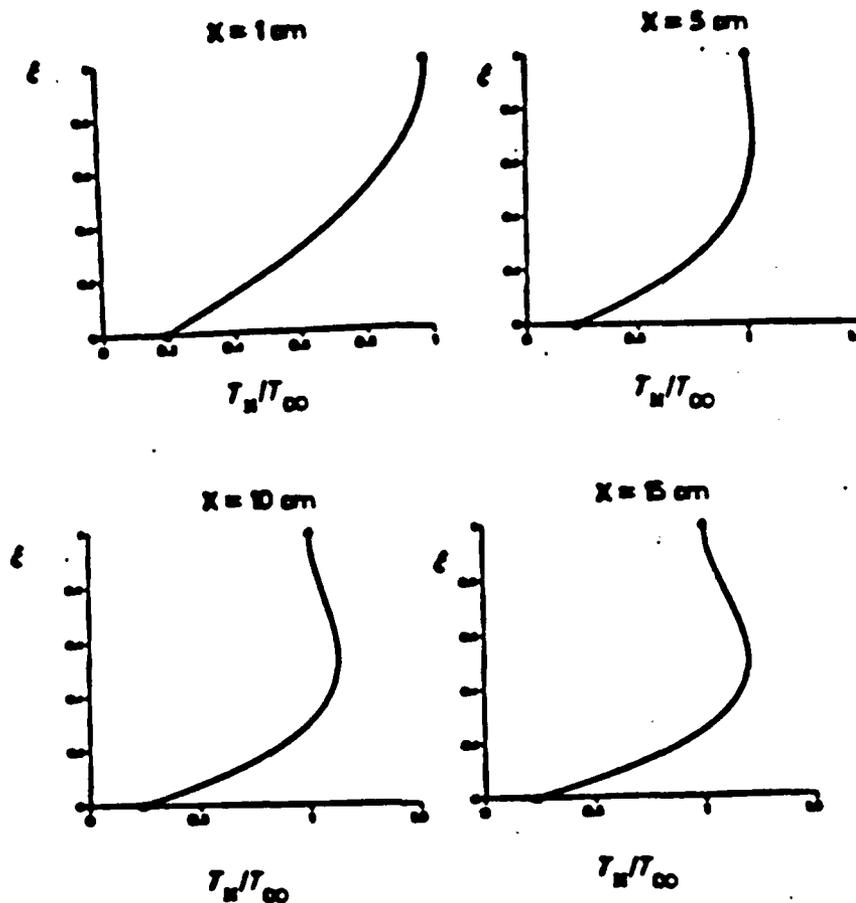
Figure 24: Heavy particle temperature profiles

The heavy particle temperature non-dimensionalized by the free stream temperature, has been plotted versus ξ, the Howarth-Dorodnitsyn transverse coordinate at locations of 1 cm., 5 cm., 10 cm., and 15 cm. from the leading edge. A mass flow of 3 g/sec is assumed, the free stream is ionizing, and the boundary layer is chemically frozen. Notice the bulge in the profiles apparent far downstream of the leading edge, caused by the conflict between viscous dissipation in the boundary layer, and heat transfer to the cold wall. See Sec.4.4 for discussion.
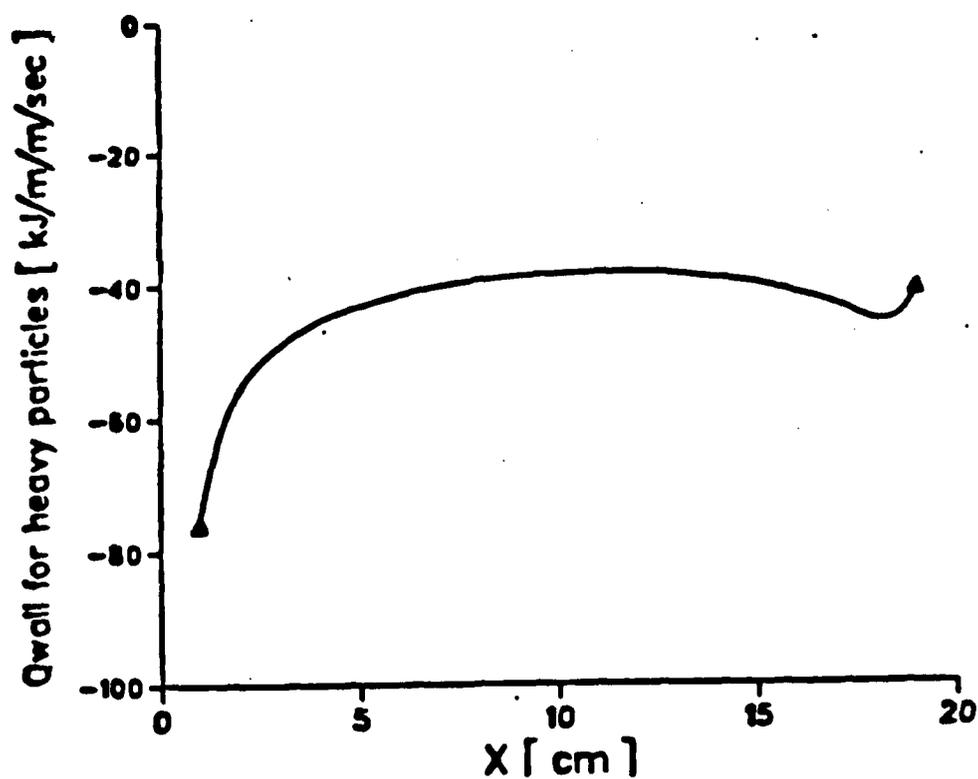
Figure 25: Heavy particle wall heat flux versus Distance

The wall heat flux due to the heavy particles is shown here as a function of the distance along the electrode. This calculation has been performed for a mass flow of 3 g/sec, an ionizing free stream, and a frozen boundary layer. See Sec.4.4 for details.
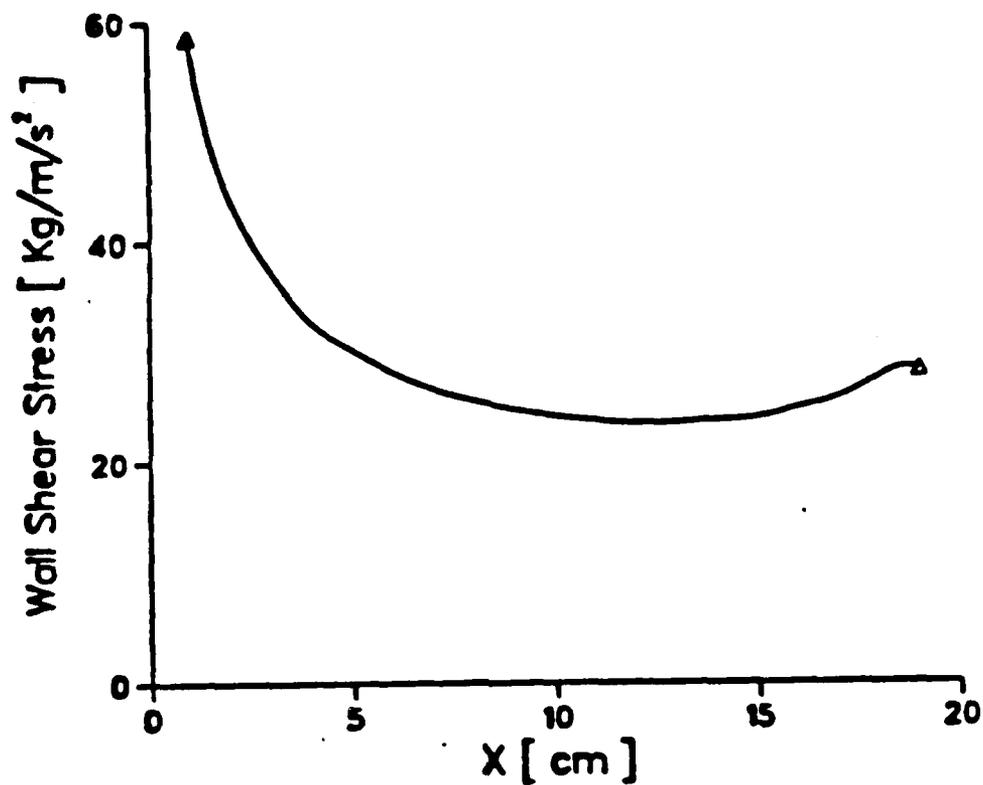
Figure 26: Wall shear versus Distance

The wall shear is shown here as a function of distance from the leading edge of the boundary layer, for a mass flow of 3 g/sec. The free stream flow is assumed to follow the quasi-1D non-equilibrium description of Sec.3.5, while the boundary layer is assumed to be chemically frozen. See Sec.4.4 for discussion.

ANODE BOUNDARY LAYER

CATHODE BOUNDARY LAYER

5 cm

X [cm]
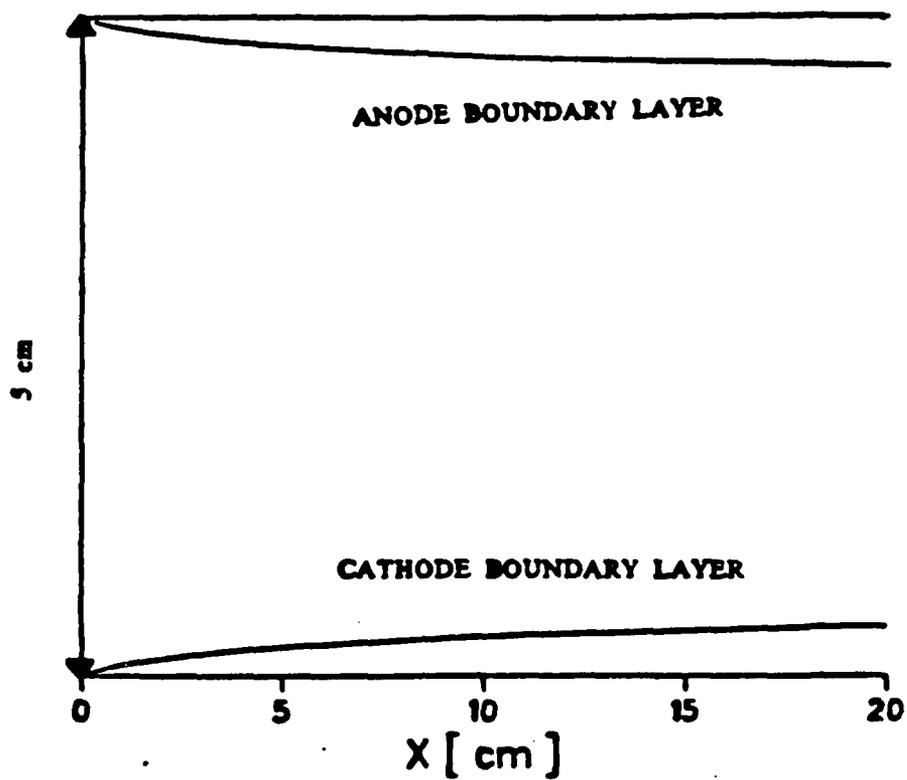
Figure 27: Fully ionized boundary layer growth

The cathode and anode boundary layers are shown for a fully ionized, frozen flow. The calculation has been performed for a mass flow of 3 g/sec, and both the free stream and the boundary layer are assumed to be fully ionized and compositionally frozen. The calculation has been performed for the cathode boundary layer, and the anode boundary layer is plotted assuming symmetry.
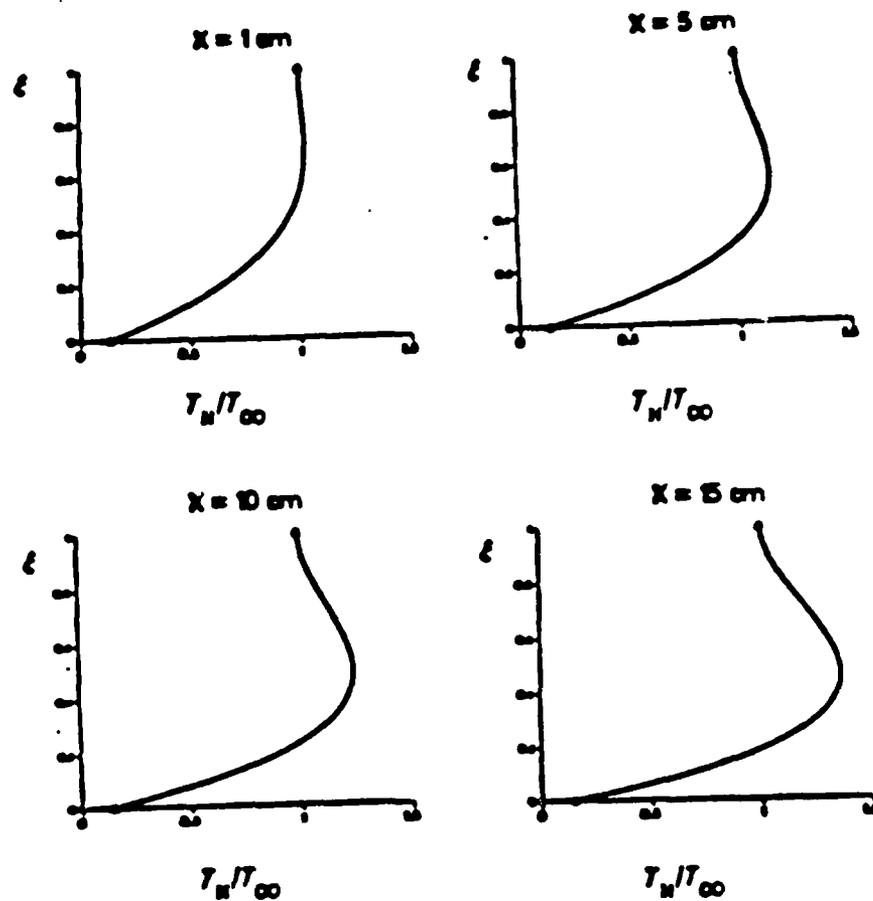
Figure 28: Heavy particle temperature versus Transverse distance

The heavy particle temperature non-dimensionalized by the free stream temperature, is plotted here versus ξ, the Howarth-Dorodnitsyn transverse coordinate. This calculation has been performed for a total mass flow of 3 g/sec, and assuming a fully ionized, frozen free stream and boundary layer. Note the significant bulge in the profiles, due to the conflict between viscous dissipation in the relatively thin boundary layer, and the heat transfer to the wall.
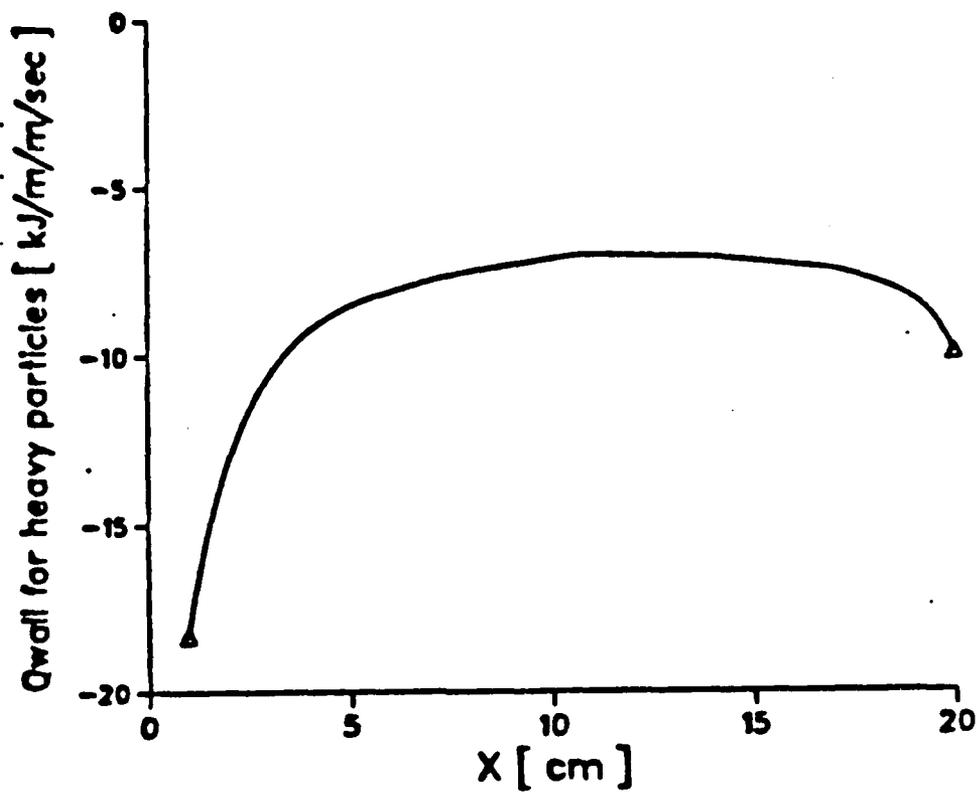
Figure 29:   Heavy particle wall heat flux versus Distance

The heavy particle heat flux profile is shown here for the fully ionized, frozen boundary layer and free stream case.   The calculation has been performed for a total mass flow of 3 g/sec.   See Sec.4.4 for discussion.
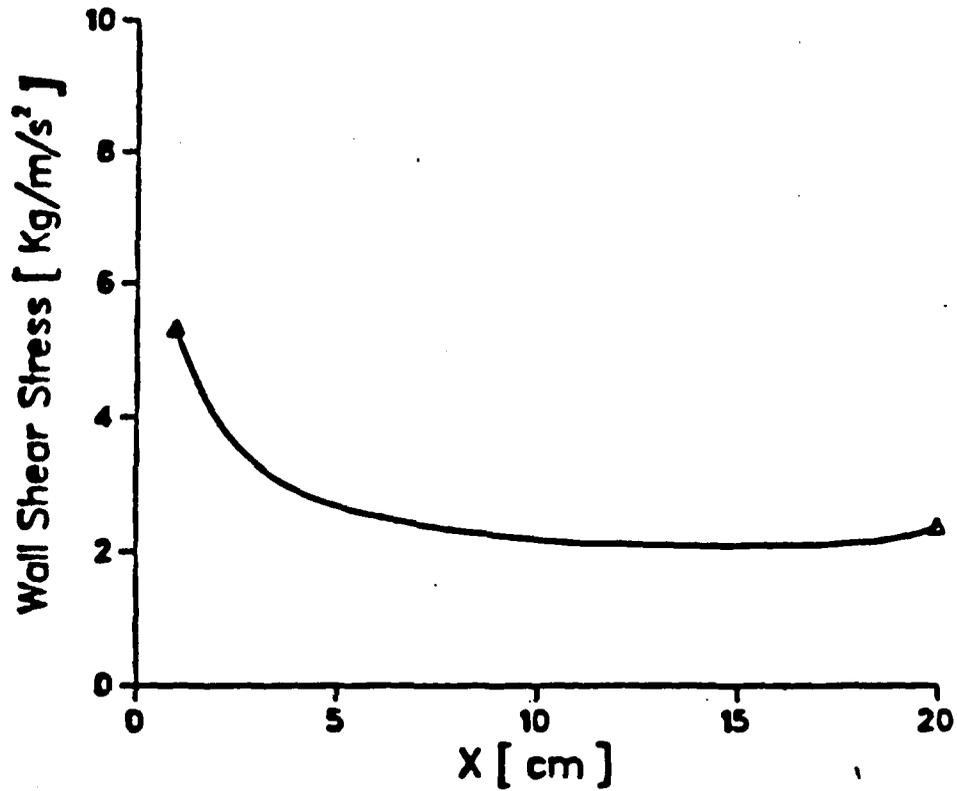
Figure 30: Wall shear versus Distance

The wall shear is shown here versus distance along the electrode, for the fully ionized, frozen flow case. A mass flow of 3 g/sec has been assumed. See Sec.4.4 for details.
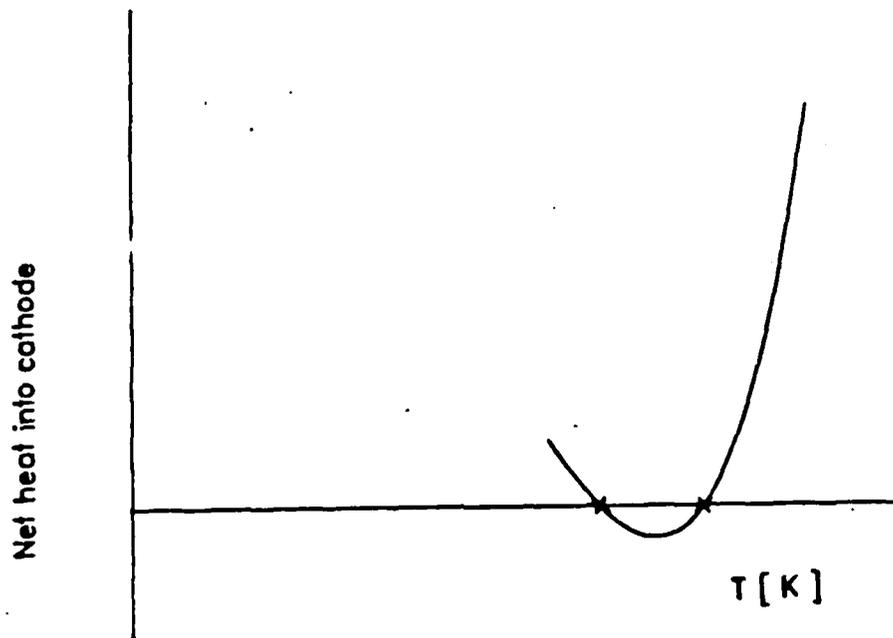
Figure 31: Heat defect versus surface temperature

The net heat into the cathode, i.e. the heat defect is shown here as a function of cathode surface temperature. Intersections with the horizontal axis denote steady state solutions to equation (4.5.1). Note the existence of a stable root and an unstable root. The stable root is the point at which the slope of the curve is negative. See Sec.4.5 for details.
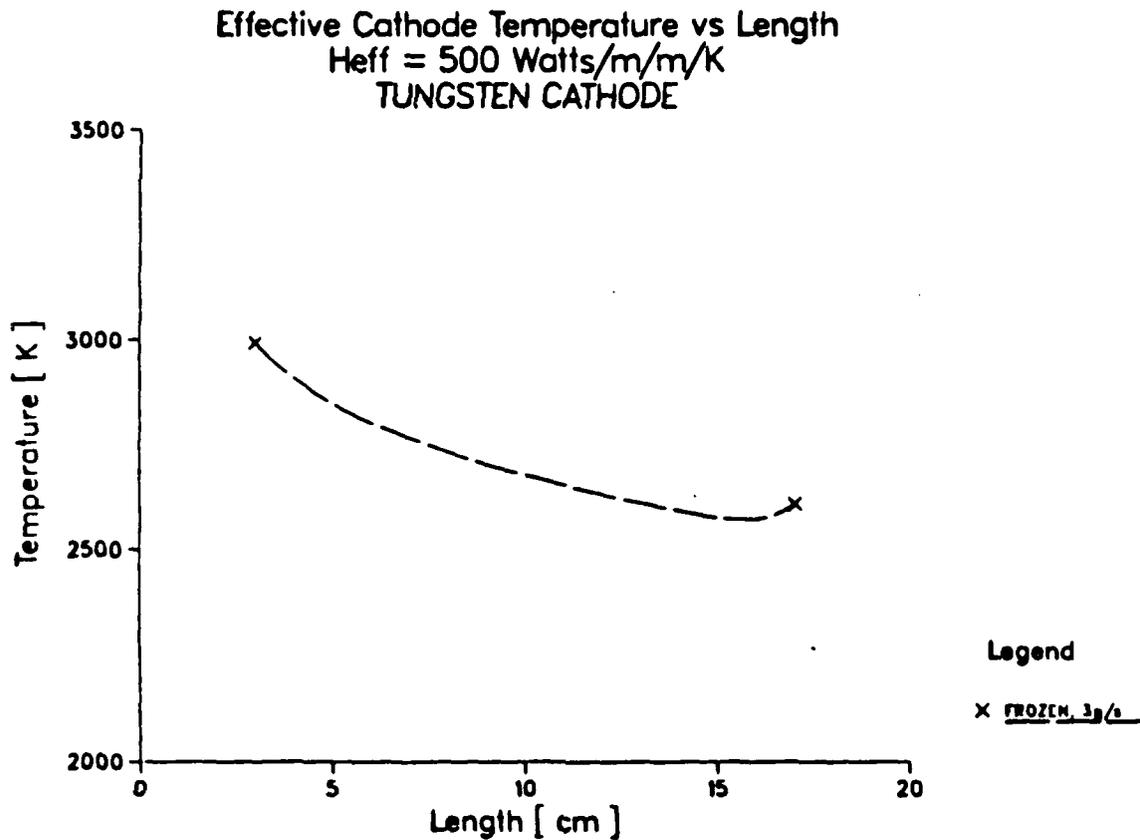
Figure 32: Cathode surface temperature profile

The cathode surface temperature determined by equation (4.5.1) is shown here versus distance along the electrode, for a heat transfer coefficient of 500 $Watts/m^2/K$. This is for the case of a frozen boundary layer with a non-equilibrium free stream, for a mass flow of 3 g/sec. See Sec.4.5 for the discussion.

Effective Cathode Temperature vs Length
Heff = 250 Watts/m/m/K
TUNGSTEN CATHODE
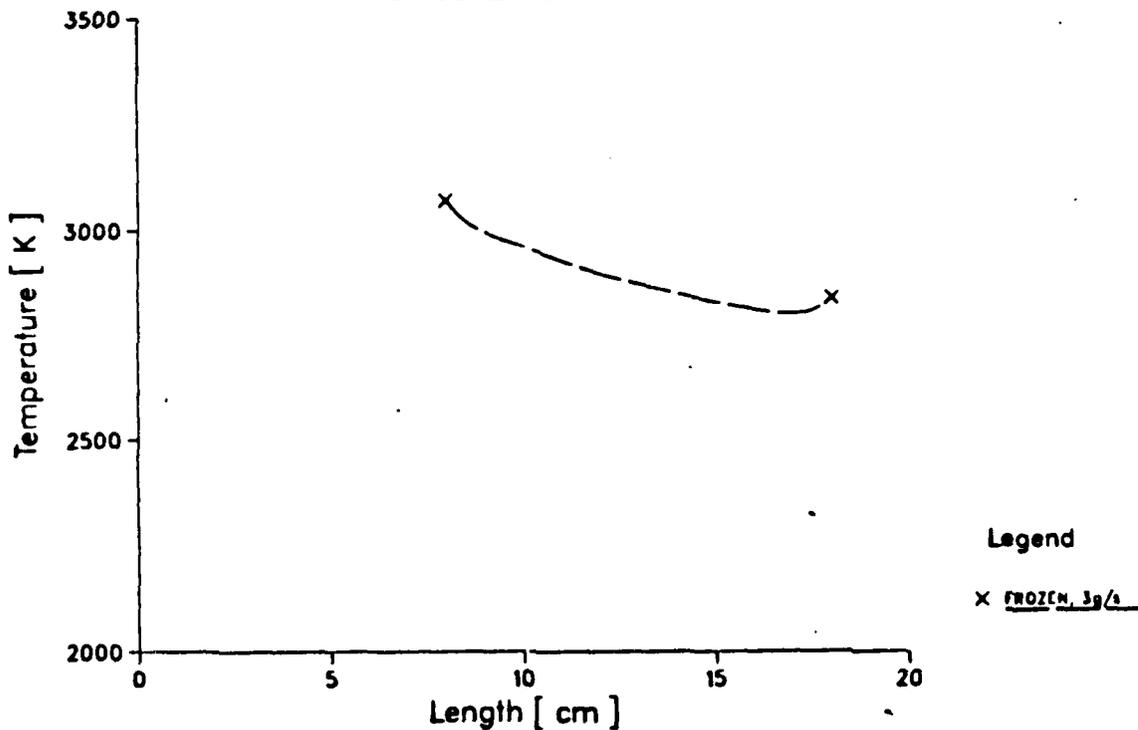
Figure 33: Cathode surface temperature profile

The cathode surface temperature determined by equation (4.5.1) is shown here versus distance along the electrode, for a heat transfer coefficient of 250 $Watts/m^2/K$. This is for the case of a frozen boundary layer with a non-equilibrium free stream, for a mass flow of 3 g/sec. See Sec.4.5 for the discussion.

Cathode Surface Temperature vs Length
Heff = 3000 Watts/m/m/K
TUNGSTEN CATHODE
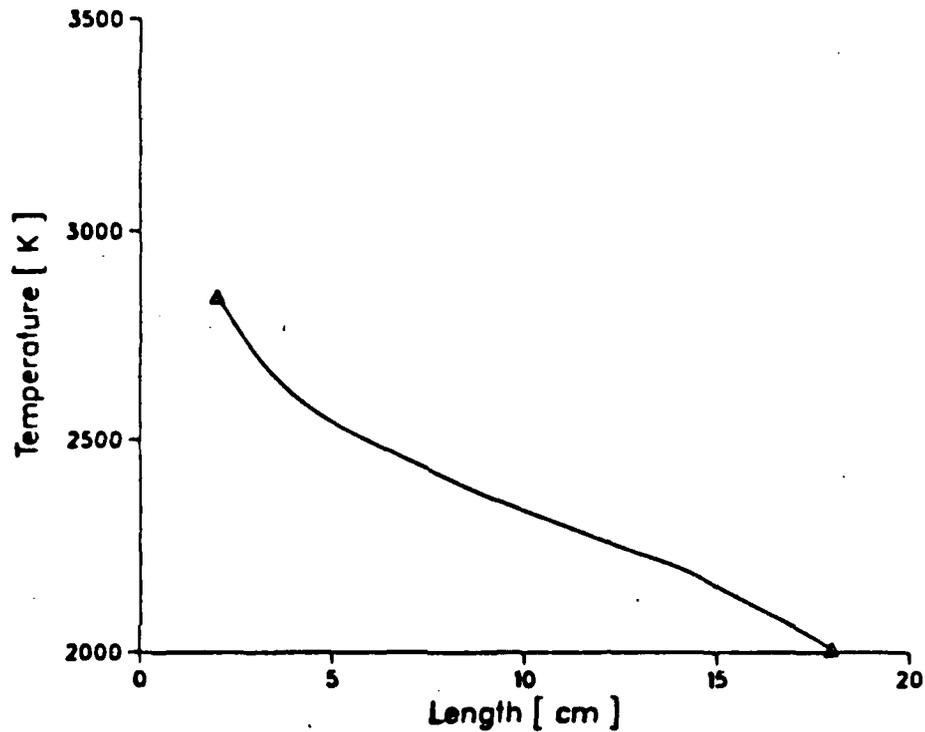
Figure 34: Cathode surface temperature profile

The cathode surface temperature determined by equation (4.5.1) is shown here versus distance along the electrode, for a heat transfer coefficient of 3000 $Watts/m^2/K$. This case is that of a cathode subjected to a fully ionized, frozen boundary layer with a fully ionized, frozen free stream. See Sec.4.5 for further details.

Heat Fluxes vs Length
Frozen Boundary Layer, 3g/s at Onset
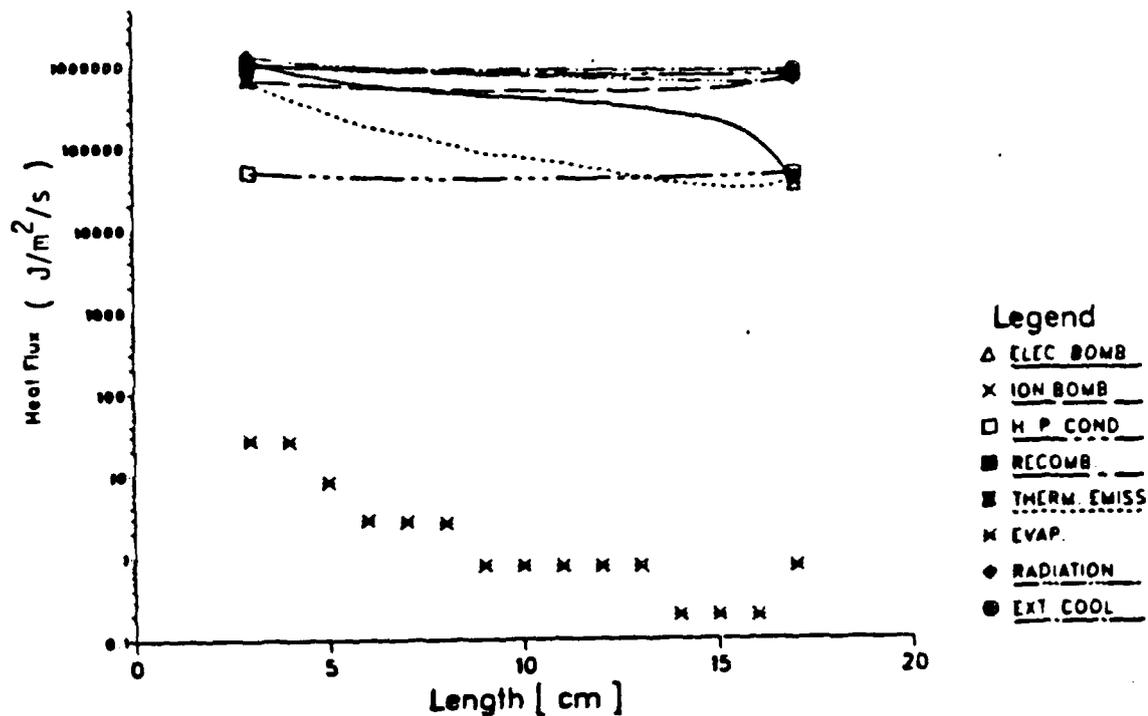
Figure 35: Heat fluxes versus distance

The various heat fluxes that contribute to the cathode energy balance given by (4.5.1) are plotted here versus distance. The case shown here is that of a frozen boundary layer with a non-equilibrium free stream for a mass flow of 3 g/sec at onset. This case considers heat transfer to an externally supplied coolant with an effective heat transfer coefficient of 500 $Watts/m^2/K$. See Sec.4.5 for details of the erosion calculation.

Heat Fluxes vs Length
Frozen Boundary Layer, 3g/s at Onset
Heff = 250 Watts/m/m/K
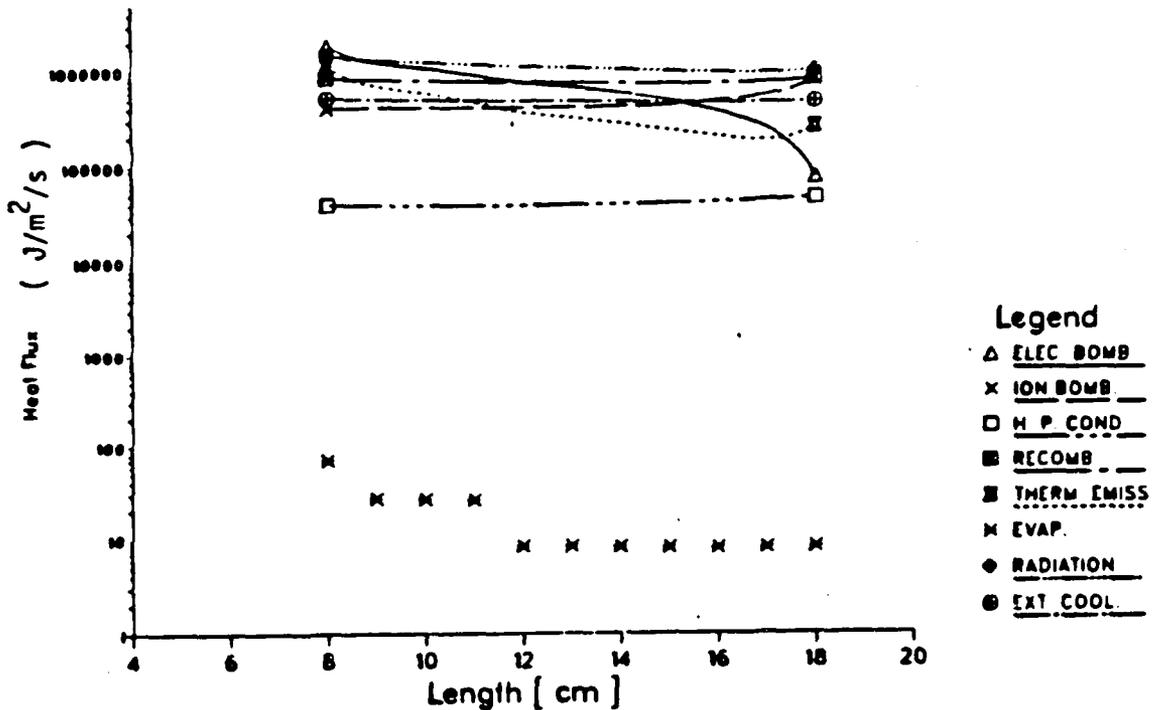
Legend
- △ ELEC BOMB
- ✕ ION BOMB
- □ H P COND
- ▣ RECOMB
- ▦ THERM EMISS
- ✖ EVAP.
- ◆ RADIATION
- ⊕ EXT COOL

Figure 36: Heat fluxes versus distance

The various heat fluxes that contribute to the cathode energy balance given by (4.5.1) are plotted here versus distance. The case shown here is that of a frozen boundary layer with a non-equilibrium free stream for a mass flow of 3 g/sec at onset. This case considers heat transfer to an externally supplied coolant with an effective heat transfer coefficient of 250 $Watts/m^2/K$. See Sec.4.5 for details of the erosion calculation.

Heat Fluxes vs Length
Frozen, Fully Ionized Boundary Layer
3g/s at Onset, Heff = 3000 Watts/m/m/s

Legend
△ ELEC BOMB
✕ ION BOMB
☐ H. P COND
▦ RECOMB
▧ THERM EMISS
✕ RADIATION
◆ EXT. COOL
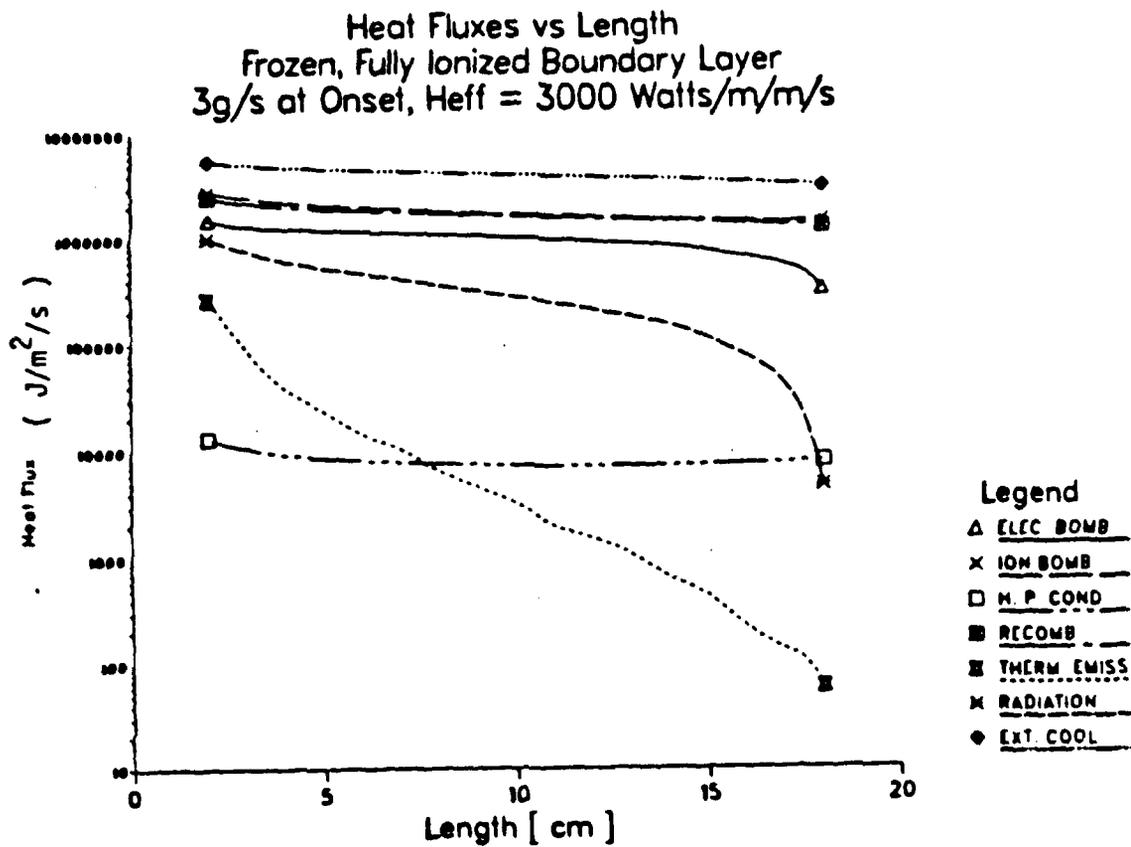
Figure 37:   Heat fluxes versus distance

The various heat fluxes that contribute to the cathode energy balance given by (4.5.1) are plotted here versus distance. The case shown here is that of a fully ionized, frozen boundary layer with a fully ionized, frozen free stream for a mass flow of 3 g/sec at onset. This case considers heat transfer to an externally supplied coolant with an effective heat transfer coefficient of 3000 Watts/m^2/K.

Evaporative Erosion vs Length
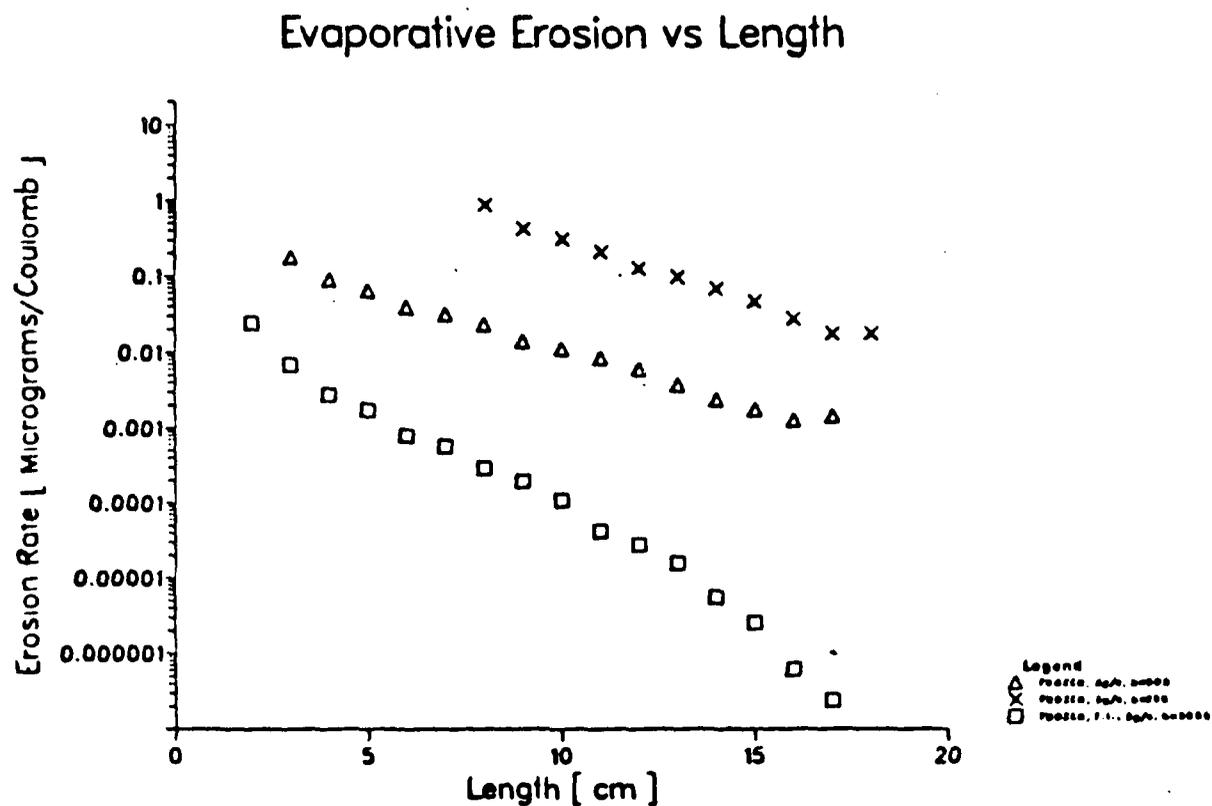
Figure 38: Evaporative Erosion versus distance

The erosion rate expressed in units of micrograms per coulomb is shown here as a function of distance. This erosion rate is the evaporation mass flux divided by the current density. This figure when viewed in conjunction with Fig.16 shows the higher evaporation rates near the entrance and exit regions, as opposed to the middle region of the thruster. See Sec.4.5 for the discussion.

TABLE 1

$n_o = 2.6888E+19 \text{ cm}^{-3}$

TEMPERATURE	S (J/g/°K)		U (J/g)		H (J/g)		c_v (J/g/°K)		n_e (#/cm³)	
	ANEC.FOR(1)	DATA(2)	ANEC.FOR(1)	DATA(2)	ANEC.FOR(1)	DATA(2)	ANEC.FOR(1)	DATA(2)	ANEC.FOR(1)	DATA(2)
4000	4.67	4.67	1249	1249	2082	2082	0.312	0.312	4.89E+10	4.90E+10
6000	4.79	4.79	1874	1874	3123	3124	0.313	0.313	1.38E+14	1.39E+14
8000	4.88	4.88	2510	2510	4175	4178	0.331	0.331	7.83E+15	7.99E+15
10000	4.97	4.97	3263	3271	5352	5362	0.503	0.462	9.15E+16	9.64E+16
12000	5.08	5.09	4501	4576	7044	7122	0.708	0.905	4.80E+17	5.27E+17
14000	5.26	5.29	6888	7260	9973	10353	1.477	1.840	1.57E+18	1.79E+18
16000	5.54	5.62	11150	12260	14925	16073	2.685	3.160	3.76E+18	4.40E+18

(1) ANEC.FOR results were obtained using the methods of statistical thermodynamics outlined in chapter 3.

(2) This is the published data of Hilsenrath et al.

The methods of equilibrium statistical thermodynamics outlined in chapter 3, have been compared with the published data of Hilsenrath et al. This statistical thermodynamics calculation has been used as the basis for approximating the equilibrium variation of enthalpy, with the piecewise linear model also described in chapter 3.

TABLE 2

$$n_o = 2.6885E+16 \text{ cm}^{-3}$$

TEMPERATURE (°K)	S (J/g/°K)		U (J/g)		H (J/g)		C_v (J/g/°K)		n_e (#/cm³)	
	ANEC.FOR(1)	DATA(2)	ANEC.FOR(1)	DATA(2)	ANEC.FOR(1)	DATA(2)	ANEC.FOR(1)	DATA(2)	ANEC.FOR(1)	DATA(2)
4000	6.10	6.10	1249	1249	2081.5	2081.5	0.312	0.312	1.55E+9	1.54E+9
6000	6.23	6.23	1880	1880	3129	3129	0.330	0.330	4.37E+12	4.35E+12
8000	6.37	6.37	2871	2871	4551	4551	0.882	0.882	2.47E+14	2.46E+14
10000	6.86	6.86	7341	7362	9635	9656	4.304	4.328	2.75E+15	2.76E+15
12000	8.16	8.17	21780	21914	25357	25485	9.614	9.654	1.16E+16	1.17E+16
14000	9.50	9.51	39120	39203	44414	44481	6.205	6.132	2.20E+16	2.20E+16
16000	10.00	10.00	46530	46494	53056	52997	1.894	2.022	2.58E+16	2.58E+16

(1) ANEC.FOR results were obtained using the methods of statistical thermodynamics outlined in chapter 3.

(2) This is the published data of Hilsenrath et al.

The methods of equilibrium statistical thermodynamics outlined in chapter 3 have been compared with the published data of Hilsenrath et al. This statistical thermodynamics calculation has been used as the basis for approximating the equilibrium variation of enthalpy, with the piecewise linear model also described in chapter 3.

TABLE 3

$E/a^*\beta^*$	Lower limit on S^*	Upper limit on S^* (from Ohm's law)
2.5	1.66	8.60
5.0	2.00	23.10
10.0	2.00	52.60
15.0	2.00	81.60
20.0	5.10	110.70
25.0	8.10	139.70
27.12	9.30	147.40

This table shows how the limits on the magnetic force number, S^*, vary with the non-dimensional electric field. This occurs as the current is increased. The above table has been compiled for $h^*/h_c = 1$, and is the result predicted by the piecewise linear model of chapter 5.

END
DATE
FILMED
4-88
DTIC